Driftwood Transport and Fate in Coastal Waters

Enda Murphy

Thesis submitted in partial fulfillment of the requirements for the degree of

Doctorate in Philosophy Civil Engineering

Academic advisors: Prof. Ioan Nistor and Prof. Andrew Cornett

University of Ottawa
Ottawa, Ontario, Canada

Abstract

Driftwood, which consists of fragments of wood transported by water, is abundant in many of the world's coastal zones. The origins of coastal driftwood include inland and coastal forests, and industry (e.g., forestry and construction). Wood is thought to provide a number of ecosystem services in coastal zones and estuaries, including habitat, structure, nutrients, and carbon storage. These perceived benefits have led to the increasing utilization of wood in so-called nature-based shore protection and coastal restoration schemes. However, the evidence to support this practice is limited. Large quantities and accumulations of driftwood are known to be detrimental to the health and performance of some sensitive coastal ecosystems and nature-based features, such as newly establishing or restored salt marshes. Moreover, buoyant coastal driftwood (or "woody debris" when referring to negative impacts) mobilized by natural disturbances, such as tsunami or storm waves, poses hazards to communities, the environment, infrastructure, and other valued assets; and can incur substantial cleanup or mitigation costs. While the fate and transport of wood in fluvial systems or debris mobilized by tsunami has received substantial attention in the literature, comparatively few studies have investigated coastal driftwood transport and mobility in open-coast settings, where wind waves are an important driver. A thorough understanding of coastal driftwood fate and transport mechanisms and pathways is needed to inform risk management practice, and to weigh the risks and benefits of using wood in nature-based solutions, and implications for coastal structures.

This study characterized physical processes governing the transport and fate of coastal driftwood. Scale physical model experiments and optical tracking of model driftwood were conducted to quantify wave-driven transport and dispersion on a sandy shoreline with fringing reefs and various coastal structures. A numerical, Lagrangian particle-tracking model was developed to simulate driftwood transport in wave-dominated environments, and was validated using the experimental data. The physical and numerical modelling results provided unique insights to factors affecting coastal driftwood mobility, pertaining to driftwood characteristics (e.g., length, roughness, buoyancy), hydrodynamics (e.g., sea state parameters, wave-induced circulation, surf zone and swash zone dynamics), and coastal structures (e.g., length of groynes at the water line). The results highlighted the sensitivity of driftwood dynamics to surf zone and swash zone hydrodynamics, and the capabilities and limitations of two "state-of-the-art" nonlinear shallow water equations wave models (the reduced 2-layer XBeach non-hydrostatic model, and SWASH) as tools for simulating these processes were assessed. The numerical driftwood transport model (WOODRIFTSIM) incorporated a novel, physics-based beaching and washoff algorithm, which was used to assess the suitability of probabilistic formulae incorporated in several existing marine debris models, which typically assume an exponential decay in the probability of driftwood remobilization following a beaching event.

The findings from the study were synthesized to describe practical implications for the use of coastal driftwood in nature-based shore protection with respect to service life, quantity, stability, and effects on wave run-up and morphodynamics. Considerations for coastal structure design in regions with mobile driftwood were also discussed. Limitations of the work, and needs for further research to develop a more comprehensive understanding of coastal driftwood fate and transport were identified.

Acknowledgements

I am grateful to my supervisors, Ioan Nistor and Andrew Cornett, for their mentorship, guidance, and humour. They offered encouragement, advice, patience, inspiration, and insight that went well beyond academics. They afforded me numerous opportunities for growth and learning. I could not have found better role models.

Thanks to the many people that have contributed in some way to my doctoral research. Thanks to Alistair Rayner for playing "Pooh sticks" with me in the lab, Jacob Stolle for sharing his optical tracking scripts, Vahid Pilechi for providing insights on particle-tracking models and life, Jessica Wilson for sharing data and insights on large wood installations on the west coast, Colin Rennie and Abdolmajid Mohammadian for their constructive review of my thesis proposal, Scott Baker and Mitch Provan for their input and advice on physical modelling, Michelle Côté and Gwyn Lintern for sharing data from driftwood surveys in British Columbia, Scott Dallimore for sharing his thoughts on driftwood at Tuktoyaktuk, Phil Osborne for his mentorship and for introducing me to the work that motivated this research, reviewers of my journal articles – particularly Michael Grilliot, who provided thorough, constructive input that helped to improve my work. Thanks to Ivana Kubat and Dave Murrin at the National Research Council (NRC) of Canada for providing the opportunity to pursue a PhD.

Mom and Dad, thanks for always supporting and encouraging me. Jess, wish you were here to slag me about why it took me so long. Cathy, thanks for putting up with all the moaning – there'll be something else now. Doris, I'll try to make up for all the missed walks.

Lastly, I would like to acknowledge the Alexander Graham Bell Canada Graduate Doctoral Scholarship (CGS D) provided by the Natural Sciences and Engineering Research Council of Canada (NSERC), and the NRC for their financial support throughout my graduate studies. Furthermore, I would like to acknowledge the financial support provided by my supervisors through their research funds, particularly the NSERC Discovery Grant of Professor Nistor.

Table of Contents

List of Figures

List of Tables

List of Acronyms

2D	Two-dimensional
3D	Three-dimensional
CFL	Courant-Friedrichs-Lewy
FOV	Field of view
GPU	Graphics processing units
HD	High definition
HFA	Hydrostatic front approximation
HSV	Hue-saturation-value
ID	Alphanumeric identification code
JONSWAP	JOint North Sea WAve Project
LiDAR	Light detection and ranging
MSL	Mean sea level
NLSW	Nonlinear shallow water
RAM	Random-access memory
RMSE	Root-mean-square error
SI	Scatter Index
SPH	Smoothed particle hydrodynamics
SWASH	Simulating WAves till SHore
XB-NH+	XBeach Non-hydrostatic (reduced two-layer version)

List of Symbols

$\boldsymbol{a}$	Wave amplitude [m]
$\boldsymbol{Adv}$	Deterministic particle advection vector [m s^{-1}]
$\boldsymbol{a_{mob}}$	Specific rate of driftwood mobilization [s^{-1}]
$\boldsymbol{\alpha}$	Significance level of two-tailed *t*-test [-]
$\boldsymbol{\alpha_P}$	Angle between orbital velocity vector and long axis of driftwood [°]
$\boldsymbol{A_s}$	Submerged cross-sectional area of driftwood [m^2]
$\boldsymbol{B}$	Cross-shore length scale for driftwood diffusion [m]
$\boldsymbol{C_D}$	Drag coefficient [-]
$\boldsymbol{C_L}$	Lift coefficient [-]
$\boldsymbol{C_M}$	Inertia coefficient [-]
CM1, CM2, CM3	Electromagnetic current meter IDs [-]
$\boldsymbol{\partial}$	Partial differential operator [-]
$\boldsymbol{D}$	Horizontal diffusion coefficient [m^2 s^{-1}]
$\boldsymbol{Disp}$	Stochastic particle dispersion vector [m s^{-1}]
$\boldsymbol{d_p}$	Theoretical open-water draft at driftwood centroid [m]
$\boldsymbol{D_p}$	Mean driftwood stem diameter [m]
$\boldsymbol{D_{RW}}$	Root wad cone diameter [m]
$\boldsymbol{D_z}$	Vertical diffusion coefficient [m^2 s^{-1}]
$\boldsymbol{\Delta t}$	Time step [s]
$\boldsymbol{\Delta U}$	Velocity difference between upper and lower layers of XB-NH+ [m s^{-1}]
$\boldsymbol{F_B}$	Archimedean buoyancy force on driftwood [N]
$\boldsymbol{F_D}$	Wave-induced drag force on driftwood [N]
$\boldsymbol{F_g}$	Gravity force on driftwood [N]
$\boldsymbol{F_H}$	In-line wave-induced forces on driftwood [N]
$\boldsymbol{F_I}$	Wave-induced inertia force on driftwood [N]
$\boldsymbol{F_L}$	Wave-induced lift force on driftwood [N]
$\boldsymbol{F_\mu}$	Stabilizing friction force at the wood-bed interface [N]
$\boldsymbol{F_N}$	Normal force at the wood-bed interface [N]
$\boldsymbol{g}$	Gravitational acceleration [m s^{-2}]
$\boldsymbol{h}$	Water depth [m]
$\boldsymbol{h_p}$	Water depth at driftwood centroid [m]
$\boldsymbol{H}$	Wave height [m]
$\boldsymbol{H_b}$	Breaking wave height [m]
$\boldsymbol{H_{m0}}$	Spectral (zeroth moment) significant wave height [m]
$\boldsymbol{H_{rms}}$	Root-mean-square wave height [m]
$\boldsymbol{H_s}$	Significant wave height [m]

$\boldsymbol{k}$	Wave number [m^{-1}]
$\boldsymbol{K}$	Horizontal dispersion coefficient (isotropic) [$m^2\ s^{-1}$]
$\boldsymbol{KC}$	Keulegan-Carpenter number [-]
$\boldsymbol{K_x}$, $\boldsymbol{K_y}$	Horizontal dispersion coefficient (cross-shore, alongshore) [$m^2\ s^{-1}$]
$\boldsymbol{L_P}$	Driftwood length [m]
$\boldsymbol{L}$	Driftwood stem length [m]
$\boldsymbol{L_{RW}}$	Root wad cone length [m]
$\boldsymbol{\lambda}$	Wavelength [m]
L1, L2, L3, L4	Shore configuration / layout IDs [-]
$\boldsymbol{\mu}$	Coefficient of (static or dynamic) friction [-]
$\boldsymbol{\eta}$	Water level above mean sea level [m]
$\boldsymbol{N_d}$, $\boldsymbol{N_P}$	Number of driftwood pieces (detected, released) [-]
$\boldsymbol{N_{events}}$	Number of driftwood beaching events [-]
$\boldsymbol{\omega}$	Radian frequency of waves [rad s^{-1}]
$\boldsymbol{P}$	Probability of driftwood remobilization [-]
$\boldsymbol{p}$	Void ratio of root wad [-]
$\boldsymbol{Pe}$	Péclet number [-]
$\boldsymbol{\rho}$	Density of water [kg m^{-3}]
$\boldsymbol{\rho_D}$	Density of wood [kg m^{-3}]
$\boldsymbol{R}$	Rational number selected randomly from a standard normal distribution [-]
$\boldsymbol{r}$	Pearson correlation coefficient [-]
$\boldsymbol{R^2}$	Coefficient of determination [-]
$\boldsymbol{S_G}$	Specific gravity of wood [-]
$\boldsymbol{Sc_t}$	Turbulent Schmidt number [-]
$\boldsymbol{\sigma_x^2}$, $\boldsymbol{\sigma_y^2}$	Variance (cross-shore, alongshore) [m^2]
$\boldsymbol{t}$	Time [s]
$\boldsymbol{t_B}$	Time since driftwood beaching event [s]
$\boldsymbol{T}$	Wave period [s]
$\boldsymbol{T_b}$	Breaking wave period [s]
$\boldsymbol{T_m}$	Mean wave period [s]
$\boldsymbol{T_p}$	Peak wave period [s]
$\boldsymbol{T_d}$	$t(\langle N_d \rangle / \langle N_P \rangle < 0.67)$ for at least 50 consecutive image captures [s]
$\boldsymbol{T_{50}}$	Half-life for driftwood remobilization [s]
$\boldsymbol{T_R}$	Mean driftwood retention (or residence) time [s]
$\boldsymbol{T_{stg}}$	Duration for driftwood immobilization [s]
TS1, TS2, …TS19	Test series IDs **[-]**
$\boldsymbol{\theta}$	Bed slope [°]
$\boldsymbol{\theta_P}$	Driftwood orientation (0° = shore-parallel, ±90° = shore-perpendicular) [°]
$\boldsymbol{U = u, v}$	Depth average wave-induced horizontal velocity vector (in x, y) [m s^{-1}]

$\boldsymbol{U_{CM2}}, \boldsymbol{U_{CM3}}$	Mean (low-pass filtered) current speed at CM2 and CM3 [m s^{-1}]
$\boldsymbol{U_p = u_p, v_p, w_p}$	Particle velocity vector (in x, y, z) [m s^{-1}]
$\boldsymbol{U_P}$	Mean driftwood centroid velocity – cross-shore component [m s^{-1}]
$\boldsymbol{u'_p}$	$u_{p,n-1} + 0.5 u_{pt} \Delta t$ [m s^{-1}]
$\boldsymbol{u_{pt}}$	Temporal gradient in cross-shore velocity component [m s^{-2}]
$\boldsymbol{u_{px,n}, u_{py,n}}$	Spatial gradients in cross-shore particle velocity at time step n [s^{-1}]
$\boldsymbol{U_S}$	Stokes drift velocity [m s^{-1}]
$\boldsymbol{U_{surf} = u_{surf}, v_{surf}}$	Surface horizontal velocity vector (cross-shore, alongshore) [m s^{-1}]
$\boldsymbol{V_P}$	Mean driftwood centroid velocity – alongshore component [m s^{-1}]
$\boldsymbol{v'_p}$	$v_{p,n-1} + 0.5 v_{pt} \Delta t$ [m s^{-1}]
$\boldsymbol{v_{pt}}$	Temporal gradient in alongshore velocity component [m s^{-2}]
$\boldsymbol{v_{px,n}, v_{py,n}}$	Spatial gradients in alongshore particle velocity at time step n [s^{-1}]
$\boldsymbol{\nu_h}$	Horizontal eddy diffusivity [m^2 s^{-1}]
$\boldsymbol{w}$	Fall velocity of driftwood [m s^{-1}]
WP1, …, WP19	Capacitance wave probe IDs [-]
$\boldsymbol{x, y, z}$	Cross-shore, alongshore, and vertical co-ordinates [-]
$\boldsymbol{X_{p,n} = x_{p,n}, y_{p,n}, z_{p,n}}$	Particle position at time step n [m]
$\boldsymbol{X}$, $\boldsymbol{Y}$	Mean centroid travel distance (cross-shore, alongshore) [m]
$\boldsymbol{X_B}, \boldsymbol{Y_B}$	Camera field-of-view length (cross-shore, alongshore) [m]
$\boldsymbol{x_j}$, $\boldsymbol{y_j}$	Travel distance of driftwood j centroid (cross-shore, alongshore) [m]
$\langle \square \rangle$	Ensemble average [-]
$\sum \square$	Ensemble sum [-]
$\lvert \square \rvert$	Absolute value [-]

Chapter 1. Introduction

1.1 Background and Motivation

Wood (i.e., logs, trees, processed timber, and fragments thereof) originating from natural and anthropogenic sources is ubiquitous in coastal waters and on shorelines. These materials are thought to play an important role in supporting healthy coastal and global ecosystems, providing habitat, structure, nutrients and carbon storage (Gonor et al., 1988; Grilliot, 2019; Krauss et al., 2005; Storry et al., 2006; Rich et al., 2014). The purported benefits of wood in coastal zones and estuaries include the provision of critical links between aquatic and terrestrial ecosystems (Grilliot, 2019), substrate and nurse sites for seeds and vegetation (Hood, 2007; Gonor et al., 1988), nesting and perches for birds (Gonor et al., 1988), shade and habitat for a variety of flora and fauna (Storry et al., 2006; Simenstad et al., 2003), structural heterogeneity (Dayton, 1971), nutrients (Storry et al., 2006), carbon and water storage (Kramer, 2016), solid substrate for fish spawn (Gonor et al., 1988), refuge from predation (Everett & Ruiz, 1993; Storry et al., 2006), and resting areas for marine mammals (Gonor et al., 1988). Under certain circumstances, wood can trap and stabilize beach and dune sediments (Grilliot, 2019; Davidson et al., 2020; Heathfield & Walker, 2011; Kramer, 2016; Simenstad et al., 2003; Kennedy & Woods, 2012; Wilson, 2020). Driftwood, i.e., wood transported by water, can act as an "agent of dispersion" or "raft" (Thiel & Gutow, 2005; Gracia et al., 2018; Gonor et al., 1988), supporting transport and dispersal of a variety of less mobile or non-swimming entities such as boring invertebrates, plants, seeds, and carbon.

Driftwood is of interest to researchers in a variety of fields, providing data to support studies of oceanography, geomorphology, ecology, human occupation, and climate change (Steelandt et al., 2015; Kim et al., 2020; Grilliot, 2019; Dalaiden et al., 2018). The natural sorting of driftwood by size and age along shorelines can provide valuable insight to historical water levels at sites where conventional water level measurements are sparse or non-existent (Harper et al., 1988; Kim et al., 2020; Ferguson et al., 2022), and to historical or changing oceanographic conditions (Giddings, 1952; Dyke et al., 1997). In seas prone to seasonal ice cover, driftwood is a useful indicator of trends and changes in sea ice dynamics (Häggblom, 1982; Johansen, 1999; Dalaiden et al., 2018). Driftwood, acting as natural drogues or drifters, can also provide insight to the fate and transport of marine pollutants (Johansen, 1999) and litter, including plastics. Lepofsky et al. (2003), Alix (2005), and Shaw (2012) describe extensive and varied use of driftwood by Indigenous people in North America, e.g., as fuel and construction materials. More recently, the potential for logs and wood to provide or contribute to a variety of valuable estuarine and coastal ecosystem services (Barbier et al., 2011) has been established, including sustainable energy (Bartocci et al., 2017; Cotana et al., 2016) and nature-based coastal engineering solutions (Wilson

et al., 2020; Kennedy & Woods, 2012; Kaminsky et al., 2020; Murphy et al., 2024a; Bridges et al., 2021).

On the other hand, driftwood, particularly in excessive quantities, can negatively impact ecosystems and human activities in coastal zones. Large accumulations of wood can smother vegetation and benthic ecosystems, reduce biodiversity, inhibit photosynthesis in submerged aquatic vegetation beds, leach toxic compounds, trap anthropogenic litter, and de-oxygenate coastal waters (Edgell & Ross, 1983; Rangel-Buitrago et al., 2021; Viehman et al., 2011). As agents of dispersion, driftwood can contribute to the spread of invasive species (Convey et al., 2002; Gracia et al., 2018) and increase the risk of timber infrastructure degradation by marine borers (Crossman & Simm, 2004). Driftwood can pose significant hazards in coastal waters, clogging harbours and impacting navigation (Doong et al., 2011), causing damage to boats and infrastructure during storm or tsunami events (Nistor et al., 2017; Edgell & Ross, 1983; Mori et al., 2019), impeding beach access for tourists and recreational users (Edgell & Ross, 1983; Rangel-Buitrago et al., 2021), and negatively affecting the hydraulic performance and operation of intakes and marine renewable energy devices (Brown & Niedzwecki, 2018; Cornett et al., 2018). The direct and indirect societal costs of managing these risks are significant (Edgell & Ross, 1983; Bartocci et al., 2017; Doong et al., 2011). A complicating factor is that the abundance and distribution of wood in coastal regions is non-stationary (Steelandt et al., 2013; Gonor et al., 1988; Alix, 2005; Rich et al., 2014; Simenstad et al., 2003), and the potential impacts of changes in wood supply (e.g., due to climate change, changes in forest management, or removal of dams) are largely unknown.

An improved understanding of, and ability to predict, driftwood transport and fate in coastal regions, particularly hotspots for accumulation, is needed to inform sustainable management practices and risk reduction (Brown & Niedzwecki, 2018). For example, the dynamics and mobility of driftwood have significant implications for its potential role in: supporting colonization by different plant species (Hood, 2007); providing habitat for fish species (Simenstad et al., 2003); influencing the efficacy of nature-based shore protection solutions (Elliott et al., 2016); and in contributing to hazards to coastal infrastructure and communities.

1.2 Objectives

The objectives of this thesis are to:

- Investigate and characterize the physical processes driving the transport and fate of driftwood in coastal waters;
- Develop a predictive (numerical) model to simulate driftwood transport in nearshore, wave-dominated environments; and
- Inform best practices for managing driftwood in coastal regions, particularly with regard to its use in nature-based coastal engineering schemes.

1.3 Scope

A state-of-the-art critical review of literature (Chapter 2), and experimental and numerical methods were employed to address the objectives described in Section 1.2. The experimental research involved driftwood release experiments in a scale physical model of a sandy coast with fringing reefs and various coastal structures exposed to oblique waves (Chapter 3), and the use of optical tracking techniques to quantify driftwood transport and dispersion (Chapter 4). A Lagrangian driftwood transport model was developed to incorporate a novel, computationally-efficient beaching and remobilization algorithm, and used to numerically replicate the physical model experiments. The driftwood transport model was driven by two "state-of-the-art" nonlinear shallow water wave equations hydrodynamic solvers (the reduced two-layer version of XBeach Non-hydrostatic, and SWASH with four sigma layers) to investigate the influence of different aspects of nearshore wave-driven hydrodynamics and circulation on driftwood transport, and to examine the capabilities of the models in providing hydrodynamic input to drive driftwood transport simulations (Chapter 5).

1.4 Contributions and Novelty of the Study

There is a dearth of scientific literature pertaining to the transport and fate of driftwood in coastal and estuarine environments (Doong et al., 2011; Simenstad et al., 2003), and the factors underlying many observed characteristics of coastal driftwood (e.g., patchiness) and associated transport processes (e.g., beaching and washoff/mobilization) remain poorly understood. The majority of research on physical transport of driftwood and woody debris has thus far been limited to tsunami-driven transport (Nistor et al., 2017) and transport in inland (riverine) environments (see, e.g., Kramer (2016) and references therein), where spatio-temporal scales and driving processes are significantly different from typical climatic or even extreme (storm) conditions in coastal waters. This study address some of these gaps and is believed to be the first to:

- Apply physical model testing to characterize wave-driven transport of driftwood in coastal waters;
- Analyse the key factors driving transport and accumulation of driftwood on wave-dominated shorelines; and
- Develop and validate a predictive (numerical) model for driftwood transport in coastal waters.

The novel research program described here translates into: (1) an improved understanding of driftwood transport processes, and driftwood interactions with shoreline features; (2) valuable insight to the role and behaviour of driftwood in coastal environments, and its effects on shorelines, infrastructure, habitats, natural hazard risks and community resilience; (3) a fully-documented experimental dataset concerning driftwood transport in a nearshore environment; (4) a predictive

model of driftwood fate in coastal waters; and (5) insight to best practices for managing driftwood in coastal regions, and the utility of wood in nature-based coastal engineering schemes.

1.5 Publications and Presentations

1.5.1 Journal Articles

1) **Murphy, E.**, Cornett, A., Nistor, I., Pilechi, A. (2024). Development and experimental validation of a Langrangian particle-tracking model to simulate wave-driven transport of driftwood in the nearshore. Manuscript submitted for publication (under review by the Journal of Waterway, Port, Coastal, and Ocean Engineering – American Society of Civil Engineers).
    - The first author (Enda Murphy) was responsible for conceptualization, methodology, software, validation, formal analysis, investigation, data curation, writing (original draft, review and editing), and visualization. A modified preprint of the manuscript is included in Chapter 5 of this thesis.
2) **Murphy, E.**, Nistor, I., Cornett, A., Rayner, A., Baker, S., & Stolle, J. (2024). Application of an optical tracking technique to characterize nearshore wave-driven transport and dispersion of model driftwood. *Coastal Engineering*, 104481. https://doi.org/10.1016/j.coastaleng.2024.104481
    - The first author (Enda Murphy) was responsible for conceptualization, methodology, software, validation, formal analysis, investigation, data curation, writing (original draft, review and editing), and visualization. A modified preprint of the manuscript is included in Chapter 4 of this thesis.
3) **Murphy, E.**, Nistor, I., Cornett, A., Wilson, J., & Pilechi, A. (2021). Fate and transport of coastal driftwood: A critical review. *Marine Pollution Bulletin*, 170, 112649.
    - The first author (Enda Murphy) was responsible for conceptualization, methodology, writing (original draft, review, and editing). A modified preprint of the manuscript is included in Chapter 2 of this thesis.

1.5.2 Conference, Symposium and Workshop Proceedings

1) **Murphy, E.**, Nistor, I., & Cornett, A. (2024). Buoyant driftwood dynamics in the surf zone. Extended abstract accepted for oral presentation at the *38th International Conference on Coastal Engineering (ICCE2024)*, Rome.
    - The first author (Enda Murphy) is responsible for conceptualization, methodology, software, validation, formal analysis, investigation, data curation, writing (original draft, review and editing), visualization, and delivery of the oral presentation at the conference. The extended abstract is not included in this thesis.
2) **Murphy, E.**, Nistor, I., & Cornett, A. (2024). Coastal driftwood fate and transport. Oral presentation at *Graduate Research on Water Technology and Hydraulics (GROWTH) Symposium 2024*, Kitchener.

- The first author (Enda Murphy) was responsible for delivery of the oral presentation at the symposium.

3) **Murphy, E.**, Cornett, A., & Nistor, I. (2023). Numerical simulation of driftwood transport by waves in a laboratory basin. Extended abstract in *Proceedings 37th International Conference on Coastal Engineering (ICCE2022)*, Sydney. https://doi.org/10.9753/icce.v37.management.7
    - The first author (Enda Murphy) was responsible for conceptualization, methodology, software, validation, formal analysis, investigation, data curation, writing (original draft, review and editing), visualization, and delivery of the oral presentation at the conference. The extended abstract is not included in this thesis.
    - Awarded Outstanding Student Abstract by the Coastal Engineering Research Council of the Coastal Ocean Port and River Institute and the Local Organizing Committee. Ranked among the top 5% of all abstracts and one of nine student awards.
4) **Murphy, E.**, Nistor, I., & Cornett, A. (2023). Coastal driftwood and woody debris – new insights on fate and transport to inform nature-based solutions design. Oral presentation at *Coastal Zone Canada 2023* conference, Victoria, 12 June 2023.
    - The first author (Enda Murphy) was responsible for delivery of the oral presentation at the conference. The abstract is not included in this thesis.
5) **Murphy, E.**, Cornett, A., Nistor, I., and Baker, S. (2020). Modeling Transport and Fate of Woody Debris in Coastal Waters. In *Proceedings of the virtual Conference on Coastal Engineering (vICCE)*, 36, https://doi.org/10.9753/icce.v36v.papers.1
    - The first author (Enda Murphy) was responsible for conceptualization, methodology, software, validation, formal analysis, investigation, data curation, writing (original draft, review and editing), visualization, and delivery of the oral presentation at the conference. A modified preprint of the manuscript is included in Chapter 3 of this manuscript.

1.6 Research Impacts

The following is a list of publications the author (Enda Murphy) led or contributed to, which have been informed by or supported the research described in this thesis:

1.6.1 Journal Articles

1) Bridges, T., Smith, J. M., King, J., Simm, J., Dillard, M., de Vries, J., Reed, D., Piercy, C.D., van Zanten, B., Arkema, K., Swannack, T., de Looff, H., Lodder, Q., Jeuken, C., Pontee, N., Gailani, J.Z., Whitfield, P., **Murphy, E.**, Lowe, R.J., McLeod, E., Altman, S., Cairns, C., Suedel, B.C., & Naylor, L.A. (2022). Coastal Natural and Nature-Based Features: International Guidelines for Flood Risk Management. *Frontiers in Built Environment*, 8, 904483.

- The eighteenth author (Enda Murphy) was responsible for contributing to sections of the manuscript, and contributing to the manuscript revision. The manuscript is not included in this thesis.

2) Ferguson, S., Provan, M., **Murphy, E.**, Bérubé, D., Desrosiers, M., Robichaud, A., & Kim, J. (2022). Assessing numerical model skill at simulating coastal flooding using field observations of deposited debris and photographic evidence. *Water*, 14(4), 589.
    - The third author (Enda Murphy) was responsible for contributing to conceptualization, methodology, and writing (review and editing). The manuscript is not included in this thesis.
3) Pilechi, A., Mohammadian, A., & **Murphy, E.** (2022). A numerical framework for modeling fate and transport of microplastics in inland and coastal waters. *Marine Pollution Bulletin*, 184, 114119.
    - The third author (Enda Murphy) was responsible for conceptualization, methodology, and writing (review and editing). The manuscript is not included in this thesis.
4) Kim, J., **Murphy, E.**, Nistor, I., Ferguson, S., & Provan, M. (2021). Numerical analysis of storm surges on Canada's western Arctic coastline. *Journal of Marine Science and Engineering*, 9(3), 326.
    - The second author (Enda Murphy) was responsible for contributing to conceptualization, investigation, methodology, supervision, and writing (review and editing). The manuscript is not included in this thesis.

1.6.2 Conference, Symposium and Workshop Proceedings

1) **Murphy, E.**, Cornett, A., van Proosdij, D., Mulligan, R.P., & Osborne, P.D. (2024). Evidence-based guidance for nature-based coastal infrastructure in Canada. Abstract accepted for oral presentation at the *Nature Based Coastal Solutions and Ecological Restoration Symposium 2024*, Halifax, 24 June 2024.
    - The first author (Enda Murphy) was responsible for conceptualization, methodology, formal analysis, and writing (review, and editing). The abstract is not included in this thesis.
2) Provan, M., **Murphy, E.**, Rahman, A., Morris, E., & Matfin, A. (2024). Large-scale experimental model of edge treatments for constructed salt marshes. Extended abstract in *Proceedings of CoastLab24, 9th Conference on Physical Modelling in Coastal Engineering*, Delft. https://doi.org/10.59490/coastlab.2024.748
    - The second author (Enda Murphy) was responsible for conceptualization, methodology, formal analysis, and writing (review, and editing). The abstract is not included in this thesis.
3) Provan, M., **Murphy, E.**, Rahman, A., Morris, E., & Matfin, A. (2023). Experimental study of edge stabilization features and interactions with sediments and debris on a Living Dyke. In *Proceedings Coastal Sediments 2023 Conference*, New Orleans. https://doi.org/10.1142/9789811275135_0199

- The second author (Enda Murphy) was responsible for conceptualization, methodology, formal analysis, and writing (review, and editing). The manuscript is not included in this thesis.

4) Fusina, G., **Murphy, E.**, and King, J. (2023) Nature-Based Infrastructure for Coastal Erosion: a dual-impact technology? In *Proceedings NATO Climate Change & Security Workshop 2023*, Lerici. [In Press]
    - The second author (Enda Murphy) was responsible for contributing to conceptualization, methodology, literature review, writing (original draft, review, and editing). The manuscript is not included in this thesis.
5) **Murphy, E.** (2023). Leveraging Applied Research to Guide Nature-based Coastal Solutions in Canada's Cold Regions. Invited oral presentation at *Collaborative Development of Natural and Nature-based Solutions for Coastal Resiliency in the Arctic and Adjacent Regions: A Workshop*, American Society of Civil Engineers Headquarters, Reston, 24-25 October 2023. https://ewn.erdc.dren.mil/wp-content/uploads/2024/03/Arctic-NNBS-Workshop-Report-Pre-Publication-Version.pdf
    - The author (Enda Murphy) delivered the oral presentation.
6) Provan, M., **Murphy, E.**, Rahman, A., Matfin, A., & Morris, E. (2023). Flume experiments on the performance of marsh edge treatments for a living dyke pilot project, Boundary Bay, British Columbia. Oral presentation at *Coastal Zone Canada 2023 conference*, Victoria, 14 June 2023.
    - The second author (Enda Murphy) delivered the oral presentation.
7) van Proosdij, D., **Murphy, E.**, Cornett, A., Nistor, I., Mulligan, R., Côté, M., Stolle, J., Knox, P., & Baker, S. (2023). Collaborative living laboratories to inform Canadian design guidance for coastal nature-based solutions. Extended abstract in *Proceedings 37th International Conference on Coastal Engineering (ICCE2022)*, Sydney. https://doi.org/10.9753/icce.v37.management.74
    - The second author (Enda Murphy) was responsible for conceptualization, methodology, software, validation, formal analysis, investigation, data curation, writing (original draft, review and editing), visualization, and delivery of the oral presentation at the conference. The extended abstract is not included in this thesis.
8) **Murphy, E.**, & Baker, S. (2023). Applied research to guide Engineering With Nature on the Great Lakes, invited talk at *Engineering With Nature Great Lakes Playbook Workshop*, virtual, 24 January 2023.
    - The first author (Enda Murphy) delivered the oral presentation.
9) **Murphy, E.**, Baron, B., Cornett, A., van Proosdij, D., Nistor, I., Mulligan, R., Côté, M., Manson G., Duncan, T., Knox, P., & Baker, S. (2022). Applied research to inform Canadian design guidance for nature-based coastal infrastructure. Abstract in *Proceedings Climate-Resilient Coastal Nature-based Infrastructure Workshop 2022*,

Halifax, 29 June 2022. https://www.transcoastaladaptations.com/news/workshop-series-2022

- The first author (Enda Murphy) was responsible for conceptualization, methodology, supervision, investigation, data curation, writing (original draft, review and editing), visualization, and delivery of the oral presentation at the workshop. The abstract is not included in this thesis.

10) Ferguson, S., Provan, M., **Murphy, E.**, Bérubé, D., Desrosiers, M., Robichaud, A., & Kim, J. (2021). Assessing numerical model skill at simulating coastal flooding using field observations of deposited debris and photographic evidence. Abstract in *Proceedings of the 8th International Conference on Flood Management*, online, https://www.icfm.world/ICFM-Conferences/ICFM8/730/Book-of-abstracts
    - The third author (Enda Murphy) was responsible for conceptualization, methodology, supervision, writing (review and editing). The abstract is not included in this thesis.
11) **Murphy, E.**, & Cornett, A. (2021). Towards Canadian Guidelines on the Use of Nature-Based Features in Coastal Flood and Erosion Risk Management. Invited oral presentation at *PIANC Workshop on Working with Nature for Climate-Resilient Ports and Waterways*, virtual, https://www.pianc.org/working-with-nature/
    - The first author (Enda Murphy) delivered the oral presentation.
12) Kim, J., **Murphy, E.**, Nistor, I., Ferguson, S., & Provan, M. (2020). Numerical investigation of storm surges in the Beaufort Sea considering the ERA5 reanalysis, sea ice, and driftwood lines. Abstract and oral presentation at *Arctic Change 2020*, virtual, https://doi.org/10.1139/as-2021-0018.
    - The second author (Enda Murphy) was responsible for conceptualization, methodology, supervision, and writing (review and editing). The abstract is not included in this thesis.

1.6.3 Books

1) **Murphy, E.**, Cornett, A., van Proosdij, D., & Mulligan, R. (Eds.) (2024). *Nature-based Infrastructure for Coastal Flood and Erosion Risk Management – A Canadian Design Guide.* National Research Council of Canada, Ottawa. 336 pp. https://doi.org/10.4224/40003325
    - The lead editor (Enda Murphy) was responsible for conceptualization, literature review, project administration, writing (original draft, review, and editing). The manuscript is not included in this thesis. However, some of the recommendations in the guide pertaining to driftwood are reproduced in Chapter 6 of this thesis.

1.6.4 Book Chapters

1) **Murphy, E.**, Cornett, A., Fusina, G., & van Proosdij, D. (2024). "Chapter 1 – Introduction." In Murphy, E., Cornett, A., van Proosdij, D., & Mulligan, R.P. (Eds.)

Nature-Based Infrastructure for Coastal Flood and Erosion Risk Management – A Canadian Design Guide. pp. 18-26. National Research Council of Canada, Ottawa. https://doi.org/10.4224/40003325

- The first author (Enda Murphy) was responsible for conceptualization, literature review, and writing (original draft, revision, and editing). The manuscript is not included in this thesis.

2) **Murphy, E.**, van Proosdij, D., & Eyquem, J.L. (2024). "Chapter 2 – Principles, Key Concepts, Framework." In Murphy, E., Cornett, A., van Proosdij, D., & Mulligan, R.P. (Eds.) *Nature-Based Infrastructure for Coastal Flood and Erosion Risk Management – A Canadian Design Guide.* pp. 27-43. National Research Council of Canada, Ottawa. https://doi.org/10.4224/40003325
    - The first author (Enda Murphy) was responsible for conceptualization, literature review, and writing (original draft, revision, and editing). The manuscript is not included in this thesis.
3) Cornett, A., Osborne, P.D., van Proosdij, D., Manson, G., & **Murphy, E.** (2024). "Chapter 6 – Regional Considerations for Nature-Based Coastal Infrastructure." In Murphy, E., Cornett, A., van Proosdij, D., & Mulligan, R.P. (Eds.) *Nature-Based Infrastructure for Coastal Flood and Erosion Risk Management – A Canadian Design Guide.* pp. 107-142. National Research Council of Canada, Ottawa. https://doi.org/10.4224/40003325
    - The fifth author (Enda Murphy) was responsible for conceptualization, and contributing to literature review, and writing (revision, and editing). The manuscript is not included in this thesis.
4) Osborne, P. D., van Proosdij, D., Camarena, A., Cornett, A., & **Murphy, E.** (2024). "Chapter 7 – System Analysis and Design." In Murphy, E., Cornett, A., van Proosdij, D., & Mulligan, R.P. (Eds.) *Nature-Based Infrastructure for Coastal Flood and Erosion Risk Management - A Canadian Design Guide.* pp. 143-160. National Research Council of Canada, Ottawa. https://doi.org/10.4224/40003325
    - The fifth author (Enda Murphy) was responsible for conceptualization, and contributing to literature review, and writing (original draft, revision, and editing). The manuscript is not included in this thesis.
5) Baker, S., **Murphy, E.**, van Proosdij, D., Wilson, J., & Logan, S. (2024). "Chapter 10 – Hybrid Solutions." In Murphy, E., Cornett, A., van Proosdij, D., & Mulligan, R.P. (Eds.) *Nature-Based Infrastructure for Coastal Flood and Erosion Risk Management - A Canadian Design Guide.* pp. 245-269. National Research Council of Canada, Ottawa. https://doi.org/10.4224/40003325
    - The second author (Enda Murphy) was responsible for conceptualization, and contributing to literature review, and writing (original draft, revision, and editing). The manuscript is not included in this thesis. However,

aspects of the guidance related to driftwood is reproduced in Chapter 6 of this thesis.

6) **Murphy, E.**, Cornett, A., van Proosdij, D., & Mulligan, R. (2024). "Chapter 14 – Conclusion." In Murphy, E., Cornett, A., van Proosdij, D., & Mulligan, R.P. (Eds.) *Nature-Based Infrastructure for Coastal Flood and Erosion Risk Management - A Canadian Design Guide.* pp. 334-336. National Research Council of Canada, Ottawa. https://doi.org/10.4224/40003325]
    - The first author (Enda Murphy) was responsible for conceptualization, literature review, writing (original draft, review, and editing). The manuscript is not included in this thesis.
7) **Murphy, E.**, and Osler, M. (2022). "Coastal Floods." In S. Safaie, S. Johnstone, & N.L. Hastings (Eds.), *Resilient Pathways Report: Co-creating new Knowledge for Understanding Risk and Resilience in BC* (pp. 130-149), Geological Survey of Canada, Open File 8910. https://doi.org/10.4095/330531
    - The first author (Enda Murphy) was responsible for conceptualization, literature review, writing (original draft, review, and editing). The manuscript is not included in this thesis.
8) Gailani, J., Whitfield, P., **Murphy, E.**, de Vries, J., Thomson, G., Mears, W., & Szimanski, D. (2021). "Chapter 11 – Islands." In T.S. Bridges, J.K. King, J.D. Simm, M.W. Beck, G. Collins, Q. Lodder, & R.K. Mohan (Eds.), *International Guidelines on Natural and Nature-Based Features for Flood Risk Management* (pp. 501-558), U.S. Army Research and Development Centre. http://dx.doi.org/10.21079/11681/41946
    - The third author (Enda Murphy) was responsible for conceptualization, literature review, and writing (original draft, review, and editing). The manuscript is not included in this thesis.

1.6.5 Technical Reports

1) Kim, J., **Murphy, E.**, Ferguson, S., Provan, M., & Nistor, I. (2024). Numerical simulation of coastal flood hazard in the Beaufort Sea and the Hamlet of Tuktoyaktuk, Northwest Territories. Technical Report No. OCRE-2022-TR-015, National Research Council Canada, Ottawa. https://doi.org/10.4224/40003267
    - The second author (Enda Murphy) was responsible for conceptualization, methodology, supervision, writing (review, and editing). The manuscript is not included in this thesis.
2) Provan, M., **Murphy, E.**, & Rahman, A. (2023). Experimental testing of edge stabilization features for a Living Dyke. Technical Report No. OCRE-2022-TR-051, National Research Council Canada, Ottawa. https://doi.org/10.4224/40002987
    - The second author (Enda Murphy) was responsible for conceptualization, methodology, formal analysis, and writing (review, and editing). The manuscript is not included in this thesis.

3) Vouk, I., Pilechi, V., Provan, M., & **Murphy, E.** (2021). Nature-Based Solutions for Coastal and Riverine Flood and Erosion Risk Management. Canadian Standards Association, Toronto.
    - The fourth author (Enda Murphy) was responsible for conceptualization, literature review, writing (original draft, review, and editing), and supervision. The manuscript is not included in this thesis.

1.7 Outline of the Thesis

This thesis is organized as follows:

- Chapter 2 (Literature Review) consists of a critical review of literature to frame the current state of research on fate and transport of driftwood in coastal waters, and to identify research needs and opportunities to address challenges and knowledge gaps. The chapter is based on a review paper published in *Marine Pollution Bulletin*.
- Chapter 3 (Physical Modelling Experiments) describes a series of reduced-scale physical modelling experiments conducted in a wave basin to investigate wave-driven driftwood transport and mobility in a sandy, coastal reach with various structures (groynes and breakwaters). It includes a qualitative analysis and discussion of the key factors controlling driftwood mobility. This chapter is based on a paper published in the proceedings of the *International Conference on Coastal Engineering*.
- Chapter 4 (Optical Tracking Analysis) presents a quantitative analysis of the experiments described in Chapter 3, applying an optical tracking technique to characterize driftwood mean transport and dispersion under different wave and water level conditions. The results provide additional insight to drivers of, and constraints on, driftwood mobility in nearshore, wave-dominated settings. This chapter is based on an article published in *Coastal Engineering (Elsevier)*.
- Chapter 5 (Numerical Driftwood Model) describes the development and application of a numerical model to reproduce, at prototype scale, the physical model experiments described in Chapters 3 and 4. The Lagrangian (particle-tracking) numerical model was developed in MATLAB, and driven by two different non-linear shallow water equations solvers (XBeach Non-Hydrostatic reduced 2-layer model, and SWASH) to investigate the importance of resolving three-dimensional surf zone processes to accurately simulate coastal driftwood transport. The Lagrangian driftwood model incorporated a computationally efficient, dynamics-based beaching and washoff algorithm, developed to address the observed importance of these processes in controlling driftwood transport, as described in Chapters 3 and 4. This chapter is based on a draft manuscript that is presently under review by the *Journal of Waterway, Port, Coastal, and Ocean Engineering (American Society of Civil Engineers)*.
- Chapter 6 (Synthesis and Discussion) synthesizes the findings of the literature review, and the experimental and numerical analyses to provide recommendations for best practices to

manage driftwood in coastal regions, and the design of nature-based coastal engineering schemes incorporating or affected by logs or woody debris.

- Chapter 7 (Conclusion).
- Supplementary information is provided in the Appendices.

Chapter 2. Literature Review

This chapter is a preprint of a modified version of the following published article:

Murphy, E., Nistor, I., Cornett, A., Wilson, J., & Pilechi, A. (2021). Fate and transport of coastal driftwood: A critical review. *Marine Pollution Bulletin*, 170, 112649.

Abstract:

Driftwood originating from natural and anthropogenic sources is abundant in coastal regions and plays an important role in ecosystems, providing habitat, structure, nutrients, and carbon storage. Conversely, large accumulations of driftwood can litter coastal zones, negatively impact coastal ecosystems and pose hazards to navigation, infrastructure and communities. Knowledge of the processes underlying the fate and transport of coastal driftwood is therefore needed to inform sustainable management practices. The present state of understanding is limited, and predominantly founded on studies of rivers and tsunamis, where the spatio-temporal scales and driving processes are significantly different from typical climatic or storm conditions in coastal waters. The authors critically review research on fate and transport of driftwood in coastal waters, and identify research needs and opportunities. Key knowledge gaps relate to: interactions between driftwood, littoral zone hydrodynamics and geomorphology; mechanisms of driftwood rafting and accumulation; and influence of weathering and degradation on mobility.

Keywords: Driftwood, woody debris, fate and transport, coastal engineering, coastal hydrodynamics

2.1 Introduction

Driftwood originating from natural and anthropogenic sources is ubiquitous in coastal waters and on shorelines. The term “woody debris” is often used synonymously with driftwood, or “large/coarse woody debris” when length scales exceed certain thresholds (Wilson et al., 2020; Rich et al., 2014; Everett & Ruiz, 1993; Abbe & Montgomery, 2003; Braudrick & Grant, 2001; Rangel-Buitrago et al., 2021; Kennedy & Woods, 2012; Perry et al., 2018). However, not all woody debris is driftwood, the latter being reserved for trees, logs, or wood fragments transported in or over water by wind, waves, currents and/or ice. Though sometimes perceived as litter or debris (Gall & Thompson, 2015), with associated negative connotations, driftwood plays an important role in supporting healthy coastal and global ecosystems, providing habitat, structure, nutrients and carbon storage (Gonor et al., 1988; Grilliot, 2019; Krauss et al., 2005; Storry et al., 2006; Rich et al., 2014). It provides a critical link between aquatic and terrestrial ecosystems (Grilliot, 2019), substrate and nurse sites for seeds and vegetation (Hood, 2007; Gonor et al., 1988), nesting and perches for birds (Gonor et al., 1988), shade and habitat for a variety of flora and fauna (Storry et al., 2006; Simenstad et al., 2003), structural heterogeneity (Dayton, 1971), nutrients

(Storry et al., 2006), carbon and water storage (Kramer, 2016), solid substrate for fish spawn (Gonor et al., 1988), refuge from predation (Everett & Ruiz, 1993; Storry et al., 2006), and resting areas for marine mammals (Gonor et al., 1988). Under certain circumstances, driftwood can trap and stabilize beach and dune sediments (Grilliot, 2019; Davidson et al., 2020; Heathfield & Walker, 2011; Kramer, 2016; Simenstad et al., 2003; Kennedy & Woods, 2012; Wilson, 2020). Because of its mobility, driftwood can act as an "agent of dispersion" or "raft" (Thiel & Gutow, 2005; Gracia et al., 2018; Gonor et al., 1988), supporting transport and dispersal of a variety of less mobile or non-swimming entities such as boring invertebrates, plants, seeds, and carbon. The dynamics and distribution of driftwood have implications for its role within coastal ecosystems. For example, the mobility of driftwood affects its suitability for supporting colonization by different plant species (Hood, 2007), and heterogeneous distributions of driftwood can provide refuge and habitat for certain juvenile fish species (Simenstad et al., 2003).

Driftwood has been of interest and use to Indigenous peoples for millennia (Lepofsky et al., 2003; Tipa, 2009; Alix, 2005; Shaw, 2012; Steelandt et al., 2013). Lepofsky et al. (2003), Alix (2005), Steelandt et al. (2013) and Shaw (2012) describe extensive and varied use of driftwood by Indigenous people in North America, e.g., as fuel and construction materials. Tipa (2009) recounts how Maori people used driftwood to inform the design of weirs for eel harvesting in New Zealand. More recently, the potential for logs and wood to provide or contribute to a variety of valuable estuarine and coastal ecosystem services (Barbier et al., 2011) has been established, including sustainable energy (Bartocci et al., 2017; Cotana et al., 2016) and nature-based coastal engineering solutions (Wilson et al., 2020; Kennedy & Woods, 2012; Kaminsky et al., 2020). The dynamics and mobility of driftwood in coastal and estuarine systems are considerations for its effective integration in restoration works or nature-based shore protection solutions (Elliott et al., 2016; Rich et al., 2014). The presence, characteristics, movement and fate of driftwood are of interest to researchers in a variety of fields, providing data to support studies of oceanography, geomorphology, ecology, human occupation, and climate change (Steelandt et al., 2015; Kim et al., 2020; Grilliot, 2019; Dalaiden et al., 2018; Kim et al., 2021). The natural sorting of driftwood by size and age along shorelines can provide valuable insight to historical water levels at sites where conventional water level measurements are sparse or non-existent (Harper et al., 1988; Kim et al., 2020; Kim et al., 2021), and to historical or changing oceanographic conditions (Giddings, 1952; Dyke et al., 1997). In seas prone to seasonal ice cover, driftwood is a useful indicator of trends and changes in sea ice dynamics (Häggblom, 1982; Johansen, 1999; Dalaiden et al., 2018). Driftwood, acting as natural drogues or drifters, can also provide insight to the fate and transport of marine pollutants (Johansen, 1999) and litter, including plastics.

On the other hand, driftwood, particularly in excessive quantities, can negatively impact ecosystems and human activities in coastal zones. Manufactured or processed wood is frequently amongst the most abundant anthropogenic litter type observed on beaches and coastal waters around the world (Thiel et al., 2013; Rangel-Buitrago et al., 2017; Rangel-Buitrago et al., 2021; Rech et al., 2014; Williams & Simmons, 1997; Golik & Gertner, 1992; Willis et al., 2017; Rosevelt

et al., 2013; Ryan, 2013). Large accumulations of wood can smother benthic ecosystems, reduce biodiversity, inhibit photosynthesis in submerged aquatic vegetation beds, leach toxic compounds, trap other types of anthropogenic litter, and de-oxygenate coastal waters (Edgell & Ross, 1983; Rangel-Buitrago et al., 2021). As an agent of dispersion, driftwood can contribute to the spread of invasive species (Convey et al., 2002; Gracia et al., 2018) and increase the risk of timber infrastructure degradation by marine borers (Crossman & Simm, 2004). Accumulations of driftwood on the shore can be perceived as litter, incite negative public responses, and deter or pose hazards to beach users (Rangel-Buitrago et al., 2021). Driftwood poses hazards in coastal waters, clogging harbours and impacting navigation (Doong et al., 2011), causing damage to boats and infrastructure during storm or tsunami events (Nistor et al., 2017; Edgell & Ross, 1983; Mori et al., 2019), impeding beach access for tourists and recreational users (Edgell & Ross, 1983; Rangel-Buitrago et al., 2021), and negatively affecting the hydraulic performance and operation of intakes and marine renewable energy devices (Brown & Niedzwecki, 2018; Cornett et al., 2018). The direct and indirect societal costs of managing these risks are substantial (Edgell & Ross, 1983; Bartocci et al., 2017; Doong et al., 2011). A complicating factor is that the abundance and distribution of driftwood in coastal regions is non-stationary (Steelandt et al., 2013; Gonor et al., 1988; Alix, 2005; Rich et al., 2014; Simenstad et al., 2003), and the potential impacts of changes in wood supply (e.g., due to climate change, changes in forest management, or removal of dams) are largely unknown.

An improved understanding of, and ability to predict, driftwood transport and fate in coastal regions, particularly hotspots for accumulation, is needed to inform sustainable management practices and mitigate risks (Brown & Niedzwecki, 2018). In this chapter, the current state of research on fate and transport of driftwood in coastal waters is reviewed, and research needs and opportunities to address challenges and knowledge gaps are identified.

2.2 Literature Review

2.2.1 Abundance and distribution of coastal driftwood

Driftwood is present in many of the world's oceans and coastal ecosystems (Kennedy & Woods, 2012; Thiel & Gutow, 2005). The highest abundance of natural wood is in northern oceans (Arctic and North Pacific) proximate to the large, boreal forests of North America and Asia (Thiel & Gutow, 2005). However, driftwood is also found at mid-latitudes in the Atlantic and Pacific Oceans (Thiel & Gutow, 2005; Gracia et al., 2018; Rangel-Buitrago et al., 2017; Wolff, 1979), semi-enclosed European seas (Cotana et al., 2016; Thiel et al., 2011), in sub-tropical coastal wetlands (Krauss et al., 2005), and on beaches adjacent to steep, forested watersheds (Kennedy & Woods, 2012). Owing to the complete absence of trees in Antarctica and limited human activities, driftwood is relatively scarce in, though not absent from, the southernmost latitudes of the planetary ocean (Convey et al., 2002; Björdal & Dayton, 2020; Glover & Dahlgren, 2013).

Coastal driftwood is of natural and anthropogenic origins. Driftwood from natural sources consists of trees, branches, bark, and root systems (and fragments thereof), which has generally migrated through the four distinct stages of a "driftwood cycle", as described by Alix (2005): treefall, river transport, ocean circulation, and coastal delivery. In this context, the term treefall encompasses a variety of processes leading to recruitment of driftwood to rivers, including riverbank and floodplain erosion, hillslope failure (including landslides, avalanches and debris flows), wind throw, fire, lightning strikes, beaver activity, and plucking by ice in cold regions (Alix, 2005; Kasprak et al., 2012; Wohl, 2017; Doong et al., 2011; Krauss et al., 2005). Coastal erosion, storm events, and landslides can also deliver wood directly to the oceans (Thiel & Gutow, 2005) or coastal ecosystems (Krauss et al., 2005; Heathfield & Walker, 2011), bypassing the second stage of the cycle described above. In addition to escape logs from forestry activities (Eamer & Walker, 2010; Steelandt et al., 2015; Edgell & Ross, 1983), coastal driftwood of anthropogenic origin can include vessel fragments (Häggblom, 1982; Björdal & Dayton, 2020), wood pilings from marine structures (Gonor et al., 1988), and processed/manufactured wood such as planks, boards and pallets (Thiel & Gutow, 2005; Steelandt et al., 2013; Steelandt et al., 2015; Rangel-Buitrago et al., 2017).

The proportion of coastal driftwood of natural and anthropogenic origin varies by region and in time. Driftwood on Arctic coastlines typically consists of trees or tree fragments uprooted by disturbances such as storms, floods, fires, landslides and erosion events, and delivered to the coast by rivers, or by sea ice from distant shores (Alix, 2005; Steelandt et al., 2015; Dyke et al., 1997). However, the increasing widespread use and availability of commercially processed wood has led to it becoming increasingly abundant on Low Arctic and subarctic shores of North America (Steelandt et al., 2013). The proportions of driftwood originating from natural and anthropogenic (e.g., logging) sources on the Pacific Northwest coast of North America is difficult to determine, owing to changes in forestry practices, spatial variability, and degradation processes that obscure clues as to the origins, such as cut ends and root systems (Dayton, 1971). According to Thonon (2006), the majority of driftwood transported to the Fraser River estuary, likely a significant regional source, is of natural origin. Dayton (1971) reported that at least 50% of beached logs on an island in the Salish Sea were from logging origins, compared to less than 15% at sites on the outer coast of the Olympic Peninsula. Walker & Barrie (2006), Eamer & Walker (2010), and Heathfield & Walker (2011) contended that driftwood deposits on Canada's west coast are primarily attributable to historical escape logs from the coastal logging industry. From surveys of five island coastal sites in the Antarctic, Convey et al. (2002) recorded 43 natural wood items compared to 70 of anthropogenic origin. The latter example suggests that in naturally "wood-poor" regions, such as the Southern Ocean, human activities are the main sources of driftwood.

A key characteristic of driftwood distributions in coastal regions is patchiness (Thiel & Gutow, 2005; Kramer, 2016; Steelandt et al., 2013), i.e., it is predominantly concentrated in zones of significant accumulation, or hotspots (Figure 2-1). This characteristic, which is applicable to most types of floating marine debris including anthropogenic litter, is perhaps most famously

exemplified by the “Pacific Garbage Patch” (Lebreton et al., 2012), which has attracted global media and public interest. Kramer (2016) used the term “driftcretions” to describe large, stable concentrations of driftwood on shorelines of Great Slave Lake in Canada, and suggested that the patchiness exhibited by driftwood in coastal regions is an important factor defining its role in promoting habitat diversity. Harvesters of driftwood (e.g., for fuel) have also taken advantage of this tendency to accumulate in large patches (Shaw, 2012). However, the patchy distribution of driftwood in coastal regions makes it challenging to extrapolate broad spatial distributions from site-specific field data (Thiel & Gutow, 2005), and to predict impacts on shorelines and coastal structures.

Figure 2-1. Accumulation of driftwood on the Beaufort Sea coast of Canada. Photo credit: Enda Murphy.

The abundance and distribution of coastal driftwood changes over time in response to a variety of drivers including: climate; seasonal meteorology, hydrology and oceanography; and human activity (Alix, 2005; Kramer, 2016). Kramer (2016) suggested that wood is now less abundant on global shorelines compared to the period before intensive human settlement. For the Pacific Northwest and Arctic coasts of North America, there is no clear agreement in the literature on the dominant drivers of change in driftwood abundance. Benda & Sias (2003) and MacVicar & Piégay (2012) present frameworks for evaluating wood budgets in river watersheds, which provide a useful basis for evaluating coastal driftwood supply from riverine sources, and to develop analogous frameworks for coastal reaches. Using monitoring data from 131 reservoirs in Japan, Seo et al. (2008) identified a variety of factors controlling fluvial export of large wood, with watershed area and annual precipitation being the strongest indicators. The majority of publications suggest there has been an overall decline in supply to the Pacific Northwest coast

since the late 20th century, purportedly due to: deforestation, the decline in and regulation of forestry activities, and more efficient felling, transportation and recovery practices (Gonor et al., 1988; Heathfield & Walker, 2011; Rich et al., 2014). Gonor et al. (1988) contend that harvesting of driftwood for energy (i.e., firewood) has also reduced the quantity of wood on Pacific shores of North America, although Indigenous peoples have been collecting firewood from beaches for thousands of years (Grilliot, 2019; Shaw, 2012) and beachcombers have been capturing escape logs since the expansion of industrial logging in the 1950s (Edgell & Ross, 1983). Kramer (2016) suggested there has been a decline in supply of driftwood to Arctic coasts (e.g., resulting from deforestation, hydropower exploitation, proliferation of dams, land use change, or climate-induced migration of forest cover). This appears to conflict with findings from interviews with Inuit elders in coastal Nunavik, northern Canada, which indicated that driftwood accumulation on beaches has increased due to a decline in harvesting practices (Steelandt et al., 2013).

2.2.2 Transport drivers and processes

The majority of scientific literature describing driftwood transport processes is focussed on riverine environments. Driftwood transport in coastal waters is less constrained than in rivers, where wood mobility is limited by hydraulic conditions, and geometric scales (e.g., channel widths and depths) (Kramer, 2016; Bertoldi et al., 2014). Indeed, driftwood can traverse entire ocean basins, particularly in northern oceans where sea ice can inhibit loss of buoyancy and settling (Dalaiden et al., 2018; Johansen, 1999). Driftwood of Caribbean origin has been found in regions as distant as northwest Europe (Thiel & Gutow, 2005), driftwood from Siberia in Norway (Johansen, 1999; Dyke et al., 1997), and trees on Hawaiian beaches from North America, the Philippines, Japan, and Malaysia (Gonor et al., 1988). Mean drift rates reportedly range from less than 0.1 km/h in parts of the Arctic Ocean to 7 km/h in the Ariake Sea, Japan (Thiel & Gutow, 2005). However, fluctuations in coastal driftwood supply and transport rates can occur over multiple time scales, in response to natural system dynamics and human influences (see, e.g., Figure 2-2) (Wohl, 2017; Dyke et al., 1997; Häggblom, 1982).

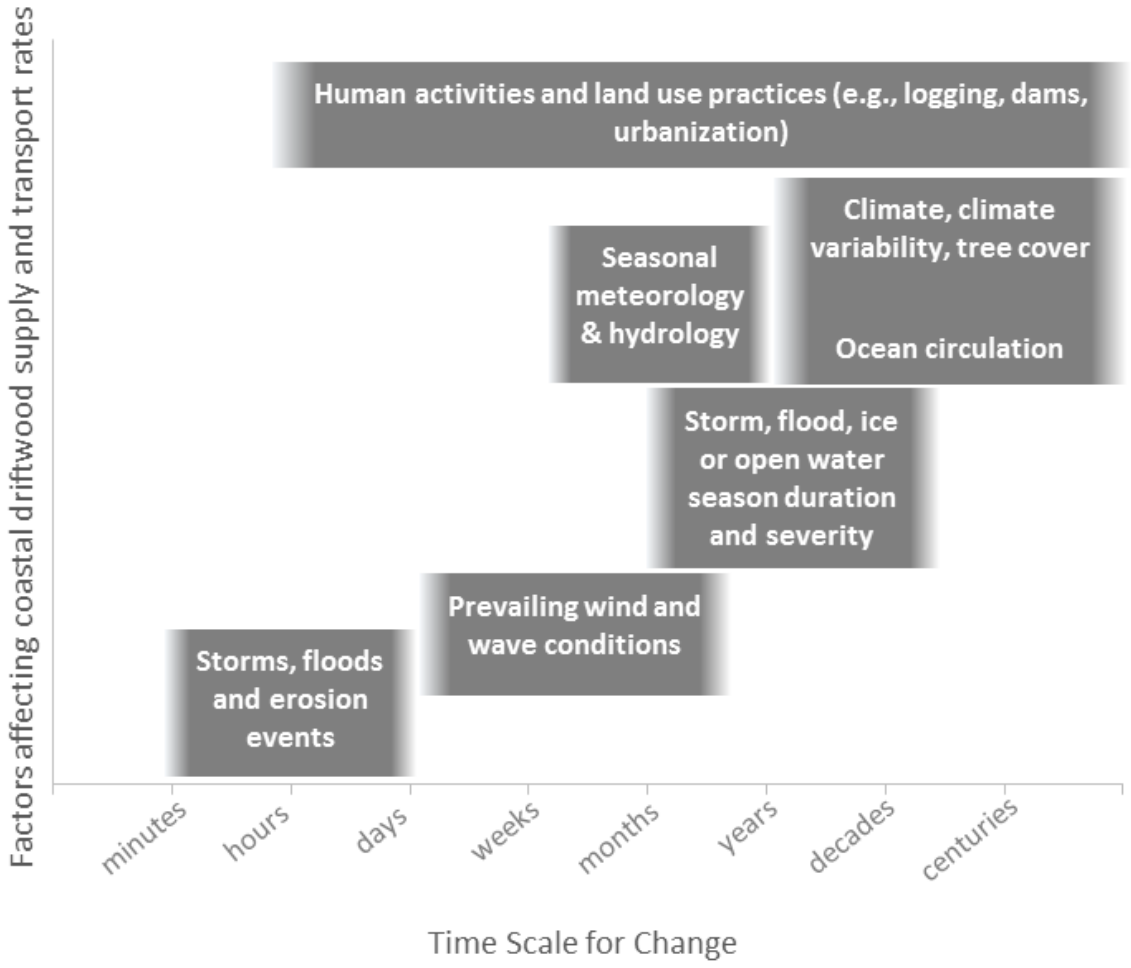

Figure 2-2. Time scales and factors driving changes in coastal driftwood supply and transport rates.

Once released into coastal waters, driftwood transport is influenced by a variety of driving physical transport processes, including (Figure 2-3):

- Ocean currents (e.g., driven by tides, wind, baroclinic effects, waves, global and regional circulation, and fluvial discharges);
- Wind;
- Waves;
- Buoyancy (including settling) effects; and
- Sea ice dynamics.

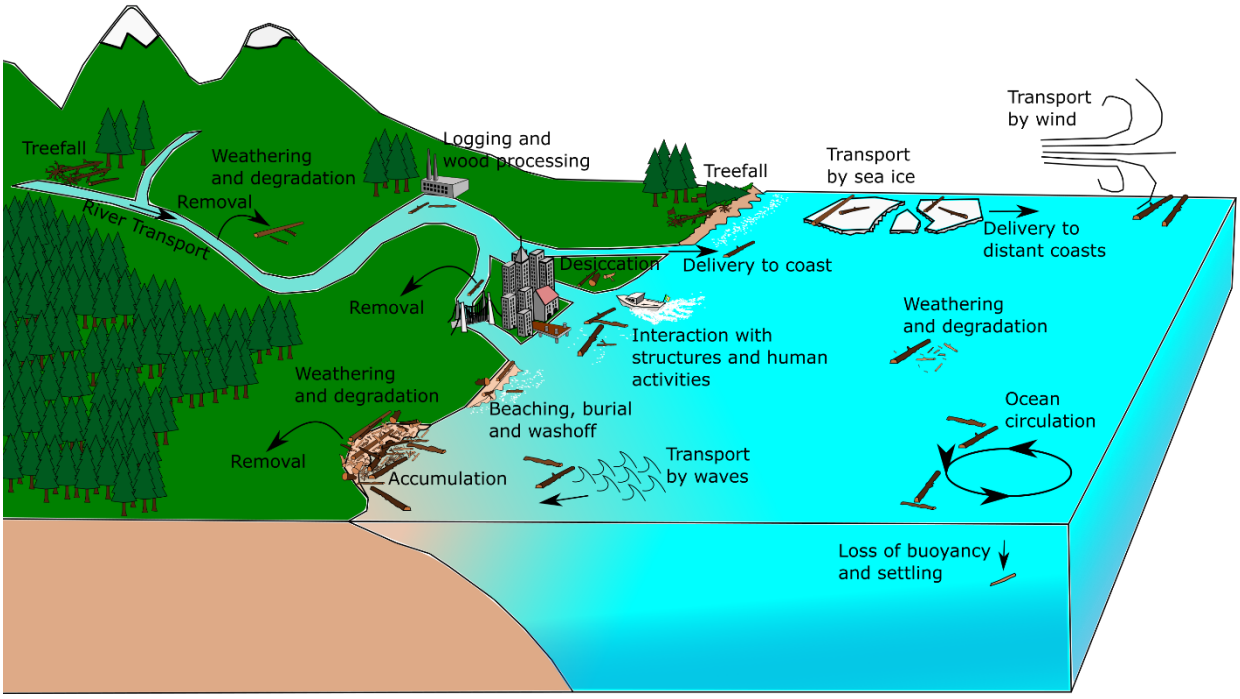

Figure 2-3. Conceptual framework of driftwood transport processes.

The strong correlation between observed debris drift rates and mean ocean current speeds suggests that ocean currents and circulation are major drivers of driftwood transport in the open ocean (Thiel & Gutow, 2005; Grilliot, 2019). The surface currents to which floating debris and driftwood are exposed are strongly influenced in open ocean settings by the combined effects of wind stress acting on the ocean surface and Coriolis forces (i.e., resulting in Ekman transport and Langmuir circulation). In coastal and estuarine regions, currents and circulation are strongly influenced by tides, wave-current interactions, storm surges, hydrodynamic interactions with shoreline features and geomorphology, fluvial discharges and baroclinic effects.

Waves are a significant driver of transport in oceans (Kubota, 1994), particularly near coasts, where littoral processes can transport material alongshore, and strong wave events can push driftwood up the shore or erode beaches and mobilize beached wood (Grilliot et al., 2019). Wave-induced rip currents can extend well seaward of the surf zone, providing a conduit for offshore transport of debris or driftwood (Castelle et al., 2016; Murphy et al., 2020; Johnson & Pattiaratchi, 2004a). In open waters, Stokes drift and secondary drift forces play a role in transporting floating debris (Pattiaratchi & Wijeratne, 2019; Newman, 1965; Iwasaki et al., 2017; Kubota, 1994).

Direct wind action ("windage") is an important transport driver for buoyant marine debris in both coastal and open ocean environments (Critchell et al., 2015; Neumann et al., 2014; Thiel & Gutow, 2005; Jalón-Rojas et al., 2019). For marine driftwood, these effects are relevant during the buoyant phase before waterlogging. The primary direct effects of wind are to exert drag forces on the emergent portion(s) of driftwood. In particular, onshore winds can play an important role in delivery of driftwood to the shore and subsequent beaching and burial (Alix, 2005; Thiel & Gutow,

2005; Gonor et al., 1988; Grilliot, 2019), whereas offshore winds can transport driftwood away from land (Alix, 2005). However, because wind influences are intrinsically linked to the buoyancy of the driftwood, which is often a source of uncertainty or varying in time (Häggblom, 1982; Thiel & Gutow, 2005), wind effects on transport remain difficult to accurately predict for driftwood and other types of marine debris (Critchell et al., 2015; Kubota, 1994).

Buoyancy is a major factor determining the capacity for driftwood transport (Häggblom, 1982; Thiel & Gutow, 2005; Steelandt et al., 2015; Alix, 2005; Kramer, 2016; Gracia et al., 2018; Rangel-Buitrago et al., 2021). Over time, saturation tends to reduce the buoyancy of driftwood, causing it to settle on shorelines or the seabed, as evidenced by deep-sea imaging and driftwood capture by bottom trawls (Wolff, 1979; Pailleret et al., 2007; Bernardino et al., 2010). Driftwood deposited on shorelines may dry out and regain its buoyancy. The longer a piece of driftwood can stay afloat, the more likely it is to be transported over large distances. The net buoyancy force, $F_g - F_B$, acting on an idealized piece of wood (with a cylindrical stem and a conical root wad) in water is given by (D'Aoust & Millar, 2000):

$$F_g - F_B = \left(\frac{\pi D_P^2 L}{4} + \frac{1}{3} \frac{\pi D_{RW}^2 L_{RW}}{4} (1 - p) \right) \rho g (1 - S_G) \qquad (2\text{-}1)$$

where L = length of stem, D_P = mean diameter of stem, L_{RW} = length of root wad cone, D_{RW} = mean diameter of root wad cone, p = void ratio of root wad, ρ = density of water, g = gravitational acceleration and S_G = specific gravity of the wood. D'Aoust & Millar (2000) suggest a typical value of p = 0.2 based on surveys in Pacific Northwest river watersheds. In case there is no root wad (i.e., $L_{RW} = D_{RW} = 0$), Equation 2-1 reduces to the buoyancy force exerted on a cylindrical piece of wood. Interestingly, although the presence of a root wad increases the buoyant force on the wood piece (according to Equation 2-1) when water depth is not a limiting factor, in depth-limited conditions the overall buoyancy is reduced because root wad contact with the bed inclines the piece, lifting one end out of the water (Kang & Kimura, 2018; Braudrick & Grant, 2000). The presence or absence of root wads, bark and other irregularities is known to play a significant role in influencing the buoyancy and mobility of driftwood (Knox et al., 2018; Häggblom, 1982; Murphy et al., 2020; Simenstad et al., 2003; Perry et al., 2018; Gonor et al., 1988). Further inspection of Equation 2-1 reveals the three main variables influencing the buoyancy of driftwood:

1. Wood volume;
2. Wood density (ρS_G); and
3. Water density (ρ).

Initial wood volume and specific gravity are to a large extent controlled by the wood species or taxa. In fact, Kramer (2016) described tree species as a "master variable" governing many other mobility predictors, and the best predictor of transport distance variance based on field studies.

However, a variety of factors governing the time-dependent volume and density of driftwood makes it difficult to developed generalized models for driftwood buoyancy rates of change. Häggblom (1982) reviewed reports and field data and attempted to calculate the maximum buoyant period for six tree species commonly found in Arctic seas. He concluded that conifers (spruce, pine and larch) could remain buoyant for 9-17 months, whereas the buoyant period for deciduous trees (birch, aspen and willow) is 6-10 months. However, as pointed out by Alix (2005), Häggblom's suggested maximum durations of buoyancy were based on a limited number of species and very specific conditions of tree growth and condition (e.g., intact bark), which are neither broadly representative of real driftwood nor, presumably, ambient environmental conditions (e.g., water temperature, salinity, ice regime, presence of marine borers) in other regions. As such, care should be taken when extrapolating Häggblom's (1982) findings to other regions, wood species and wood condition. In particular, his hypothesis that wood condition and time history of desiccation (drying or seasoning) are more important than overall volume in determining buoyancy of deciduous driftwood warrants testing over a larger sample of wood species and environments. All else being equal, Häggblom's conclusion that larger pieces of driftwood tend to stay afloat for longer should logically hold, because larger pieces are more buoyant (Equation 2-1), take longer to become fully saturated following contact with water, and take longer to weather/degrade. Other factors related to the wood type or taxa affecting specific gravity (and therefore buoyancy) include the proportion of early to later wood, proportion of heartwood to sapwood, initial moisture content, and resistance to degradation (Bladé et al., 2016; Ruiz-Villanueva et al., 2015; Gonor et al., 1988; Alix, 2005). Specific gravities for various tree types and conditions reported in literature are shown in Table 2-1. The death of colonizing marine organisms after beaching may also contribute to increased buoyancy (Thiel & Gutow, 2005). Water density, which is a function of temperature and salinity, also influences driftwood buoyancy (Häggblom, 1982). Buoyant forces (Equation 2-1) are approximately 2% higher in seawater with ρ = 1,020 kg/m^3 (representative of annual average surface water densities in parts of the North Atlantic Ocean) than in freshwater rivers and lakes.

Table 2-1. Specific gravities of wood for different tree taxa and conditions reported in literature.

Species	S_G	**Conditions**	**Location**	**Reference**
Douglas fir (*Pseudotsuga menziesii*) - coniferous	0.5	"Typical of coniferous species… …with a moisture content of about 15%" "…represents fairly dry conditions prior to submergence"	Pacific Northwest Canada and United States river watersheds	D'Aoust & Millar (2000)
Abies - coniferous	0.59 – 0.89	Fresh cut live wood	Riparian forest of the Ain River watershed, France	Ruiz-Villanueva et al. (2015)
Acer, Alnus, Fraxinus, and *Populus* - deciduous	0.72 – 1.08	Fresh cut live wood		
Populus, Abies, Alnus, Fraxinus and *Quercus* – mixed coniferous / deciduous	0.35 – 0.91	Dead wood samples from reservoir	Genissiat Reservoir, French Rhone	

The upper limits or constraints on driftwood travel distances are not well defined in the literature. As the buoyancy of wood in water is time-limited, it is logical that large expanses of open water are not conducive to transport of driftwood over large distances (Häggblom, 1982; Dyke et al., 1997). Sea ice is therefore a significant agent of driftwood transport in polar regions, particularly in regions with multi-year ice, where driftwood can remain frozen on or in the ice for years (Dyke et al., 1997; Dalaiden et al., 2018). Despite Dyke et al.'s (1997) contention that ice is an "essential" requirement for "far-travelled" driftwood, and the maximum durations of buoyancy noted by Häggblom (1982), driftwood is known to have traversed ice-free ocean basins (Gonor et al., 1988; Barber et al., 1959). Research is needed to better understand buoyancy constraints, rates of change, and mechanisms that could conceivably facilitate transport of driftwood over ice-free oceans.

Coastal driftwood can become "beached" or stranded on the shore (Figure 2-4) in response to wave action and water level fluctuations. The precise mechanisms resulting in beaching (or washoff/mobilization) of driftwood are not well understood. However, most studies suggest that driftwood becomes deposited on beaches or landward dune systems by storm waves, wind and high water level events (Thiel & Gutow, 2005; Gonor et al., 1988; Pattiaratchi & Wijeratne, 2019; Kennedy & Woods, 2012; Grilliot, 2019; Kako et al., 2018), or tsunami (Nistor et al., 2017). Driftwood deposited at higher elevations has a lower probability of being re-mobilized by

subsequent high-water level or wave events (Thiel & Gutow, 2005). Driftwood deposited on sand or gravel beaches can trap wind-blown or wave-driven sediment (and other debris), and promote accretion and vegetation growth, eventually even leading to complete burial (Heathfield & Walker, 2011; Eamer & Walker, 2010; Kennedy & Woods, 2012; Gonor et al., 1988; Grilliot, 2019; Murphy et al., 2020). This process may take months to years depending on wood and sediment budgets, exposure to waves and water levels, and vegetation growth rates (Heathfield & Walker, 2011). The frequency, magnitude and clustering (i.e., inter-event duration) of extreme wave and water level events are therefore expected to be factors affecting marine driftwood beaching and mobilization (Murphy et al., 2020).

Figure 2-4. Driftwood on the upper beach, Sunshine Coast, British Columbia. Photo credit: Enda Murphy.

Although the role of driftwood in influencing coastal geomorphology is an emerging area of research (Grilliot, 2019; Kennedy & Woods, 2012; Wilson et al., 2020; Davidson et al., 2020), there is a dearth of literature pertaining to the effects of coastal landform and geomorphology on trapping of marine debris (Critchell et al., 2015) such as driftwood. It is not always obvious why waterborne debris tends to accumulate on some beaches and not on others nearby (Critchell et al., 2015; Convey et al., 2002). However, it is highly likely that shoreline geomorphology influences the fate of marine debris such as driftwood; since inlets, bays, and marshes are often regions of accumulation (Thiel & Gutow, 2005).

The large accumulations of driftwood that exist at many coastal sites suggest that interactions between individual pieces of wood are potential factors affecting fate. Indeed, driftwood can become entangled and form large floating rafts, which have been observed at significant distances

offshore (Thiel & Gutow, 2005). Studies on driftwood accumulation in rivers indicate that the probability of wood entanglement, rafting and jamming at hydraulic structures increases when one or more pieces becomes trapped (Knox et al., 2018; Cornett et al., 2018; Abbe & Montgomery, 2003). An experimental study by Murphy et al. (2020) (Chapter 3) showed similar findings for driftwood interacting with coastal structures (e.g., groynes and breakwaters) in waves. However, the mechanisms and conditions leading to wood entanglement, rafting and accumulation under typical climatic or storm conditions in coastal waters remain poorly understood, which inhibits implementation of mitigation measures like those applied in river systems (Schmocker & Weitbrecht, 2013).

2.2.3 Weathering and degradation

As wood moves through various stages of the driftwood cycle (Figure 2-3), it is subjected to weathering and degradation by a variety of biological and physico-chemical processes, or by human activities (e.g., burning, vandalism). In addition to the wood source, understanding mechanisms and rates of degradation is therefore important in the context of their influence on wood volume (and therefore, buoyancy, and exposure to wind and hydrodynamic forcing), water content (also influencing buoyancy), and roughness (e.g., the presence or absence or bark and root systems); all potentially important factors controlling driftwood transport in coastal environments. The proportion of natural driftwood retaining root systems at coastal sites varies substantially by location. A summary of observations pertaining to the presence of root systems on driftwood at coastal sites in North America, from published literature and unpublished data, is shown in Table 2-2. Based on this limited sample dataset, the fraction of wood pieces retaining root systems tends to be inversely proportional to travel distance (or time) from origin to the coast. For example, higher percentages of wood pieces with intact root systems are generally observed in exposed, open coast regions proximate to forests, where storms and erosion may deliver trees directly to the shore and coastal waters. The large travel distances from the Arctic treeline to the sea may partly explain the comparatively lower root wad retention by driftwood on Arctic coasts (Steelandt et al., 2015). However, the cause-effect relationship between travel distance and the presence or absence of root systems is unclear, since the absence of root wads and other irregularities contributes to greater mobility (Braudrick & Grant, 2000; Braudrick & Grant, 2001; Bertoldi et al., 2014; Murphy et al., 2020; Cornett et al., 2017) and longer travel times increase the exposure of driftwood to weathering and degradation processes. From observations along two rivers in Alaska, Alix (2005) concluded that “many” trees enter rivers without intact root systems and these specimens are presumably reflected in the data in Table 2-2. It is reasonable to assume that all datasets referenced in Table 2-2 reflect some samples of driftwood that experienced root system damage prior to release into river or coastal systems. Further research is needed on the conditions and factors influencing retention or loss of root systems prior to wood entry into rivers and coastal waters, and on the cause-effect relationships between travel distance, degradation processes and coastal driftwood roughness or morphology.

Table 2-2. Observed percentages of coastal driftwood retaining root systems in published literature.

Location	**Percentage of observed wood pieces retaining root systems***	**Reference**
Ivujivik, Arctic Canada	3% (10)	Steelandt et al. (2015)
Akulivik, Arctic Canada	9% (12)	
Inukjuak, Arctic Canada	6% (49)	
Umiujaq, Arctic Canada	12% (30)	
San Juan Island, Washington, United States	15%	Dayton (1971)
Olympic Peninsula Outer Coast, Washington, United States	85%	
Ediz Hook, Washington, United States	7% (6)	Unpublished data (personal correspondence, I. Miller, University of Washington, 2019)
Nunavak, Alaska, United States	68% (34)	Alix (2005)
Wainwright, Alaska, United States	40% (17)	
Sinaruruk, Alaska, United States	19% (15)	
Lisburne, Alaska, United States	53% (17)	
Nome, Alaska, United States	74% (31)	
Inaghpik, Alaska, United States	51% (22)	

*Note: values in parentheses indicate the number of samples/observations.

Degradation rates can vary substantially depending on wood characteristics and environmental conditions (Harmon & Hua, 1991; Björdal & Dayton, 2020). The susceptibility or resistance of marine driftwood to bio-degradation depends on the presence and species of organisms (Gonor et al., 1988), wood species (Borges et al., 2008), the proportion of heartwood to sapwood (sapwood has no appreciable resistance to bio-degradation), moisture content, density, the condition and age of the wood, and local site conditions. Marine driftwood is colonized by a wide variety of boring organisms (Thiel & Gutow, 2005), fungi (Steelandt et al., 2015; Gonor et al., 1988) and bacteria (Gonor et al., 1988). Where they are active, marine boring organisms are the primary agent causing rapid degradation of wood (Crossman & Simm, 2004), and certain species of marine worms and isopods are capable of causing complete disintegration or waterlogging of driftwood over time scales of days to a few years (Grilliot, 2019; Gonor et al., 1988; Björdal & Dayton, 2020). In regions less conducive to marine microorganism survival, such as the High Arctic, where the alkaline soils and cold, arid climate are limiters, bio-degradation rates are lower and fungi potentially play a more important role (Steelandt et al., 2015). However, evidence of active wood degradation by specialized marine micro-organisms has been found in the cold, coastal waters of Antarctica (Björdal & Dayton, 2020). Wood decay or rotting is a process whereby fungi infect and degrade wood (Williams, 2005), and can only occur at certain temperatures and in the presence of water; i.e., moisture contents in excess of 20% (Crossman & Simm, 2004). The role of marine

bacteria in degrading (i.e., rotting) wood is less clear, although Gonor et al. (1988) suggest it is a minor one, with bacteria decomposing smaller wood particles only after boring organisms have broken up larger pieces. Nevertheless, the presence of wood-degrading bacteria may be indicative of conditions favourable to fungal decay (Crossman & Simm, 2004).

Driftwood is susceptible to abrasion by water, sediment, ice and other debris during transport, leading to fragmentation and break-up. In coastal regions, waves play a significant role in degrading wood (Crossman & Simm, 2004), particularly in intertidal zones and on rocky shorelines (Thiel & Gutow, 2005; Gonor et al., 1988). The presence and type of local sediment influences the rate at which wood is mechanically degraded under hydrodynamic forcing, with sand and gravel being more abrasive than mud or silt (Crossman & Simm, 2004). Driftwood resistance to abrasion is dependent on taxa (denser, harder woods are more resistant than softwoods), moisture content (wood with higher moisture content is more susceptible), and level of fungal decay (Crossman & Simm, 2004). The exterior of driftwood pieces can be damaged or fractured by contact with sea ice (Häggblom, 1982; Alix, 2005).

Wood is susceptible to photodegradation, which is primarily a process whereby ultraviolet (UV) light is absorbed, and, in the presence of oxygen and water, initiates a chain reaction to degrade the polymeric components of the wood (Williams, 2005). However, photodegradation acts only on the surface of wood and is a relatively slow process, taking more than 100 years to degrade a wood surface by 5-6 mm (Williams, 2005). Despite slow rates of photodegradation, it can be a precursor for other wood degradation processes (Crossman & Simm, 2004) because of its role in creating surface irregularities and fissures that facilitate moisture and biota ingress.

Chemical degradation of wood surfaces can occur where it is exposed to highly acidic or alkaline conditions, causing some loss of surface integrity (Crossman & Simm, 2004). However, alkaline soils can also inhibit bio-degradation, for example in the Canadian High Arctic (Steelandt et al., 2015). Salt deposits on the surface of wood (e.g., from seawater) can inhibit fungal attack and act as a preservative (Crossman & Simm, 2004).

2.2.3 Physical modelling

Acquisition of field data that provides statistically meaningful insight to driftwood dynamics in coastal environments is extremely challenging, owing to patchy distributions in the field, the large spatial and temporal scales relevant to driftwood transport, changing rates of supply, the site-specific nature of local transport processes, and the potential for observer and sampling effort bias (Convey et al., 2002). Consequently, experimental studies offer significant potential as alternative or complementary means to investigate physical drivers and transport processes (Nistor et al., 2017; Murphy et al., 2020).

Many recent developments and progress in understanding driftwood transport in river systems have resulted from physical model experiments (Kramer, 2016; Wohl, 2017). Numerous studies have focused on investigating the physical processes and driftwood characteristics leading to entrainment, jamming and accumulation at channel constrictions, bridges, and other hydraulic

structures (Davidson et al., 2015; Knox et al., 2018; Cornett et al., 2018; Perry et al., 2018; Bertoldi et al., 2000; Schmocker & Hager, 2011; Bocchiola et al., 2008). Flume experiments have provided crucial information to support the development of numerical models for predicting driftwood transport in riverine environments (Ruiz-Villanueva et al., 2014b; Kang & Kimura, 2018; Persi et al., 2019; Eaton et al., 2013; Kimura & Kitazono, 2018; Kimura & Kitazono, 2019). Experimental studies have contributed to an improved understanding of driftwood interactions with, and impacts on, infrastructure in river channels and floodplains (Haehnel & Daly, 2004; Schmocker & Hager, 2011; Schmocker & Weitbrecht, 2013; Schalko et al., 2018). Physical models have also informed studies of the efficacy of engineering measures to manage the risks associated with driftwood jamming and accumulation in river systems (Schmocker & Weitbrecht, 2013; Knox et al., 2018; Schmocker & Hager, 2013).

Laboratory experiments have provided important insights to the dynamics and impacts of various types of debris mobilized by tsunami, including shipping containers (Stolle et al., 2016; Rueben et al., 2015; Nistor et al., 2017), disc-shaped objects (Shafiei et al., 2016) and woody debris (Ikeno et al., 2016; Matsutomi, 2009; Nouri et al., 2010). Nistor et al. (2017) present a comprehensive review of tsunami-driven debris motion and loads, citing numerous physical modelling studies, and identify challenges to be overcome to model debris motion in reduced-scale experiments. As discussed by Nistor et al. (2017), these studies have predominantly sought to quantify debris motions in terms of onshore-offshore transport and lateral spreading in response to the propagation and recession of tsunami bores over land, on time scales of minutes to hours.

In contrast to the large number of experimental studies associated with river environments and tsunamis, there is an apparent dearth of physical modelling studies investigating driftwood transport and fate (including beaching and washoff/mobilization) in coastal waters under typical climatic or storm conditions. Wilson et al. (2020) investigated the interaction between pieces of large wood anchored in various configurations on a gravel beach, and waves, wave run-up and beach profile response. Murphy et al. (2020) (Chapter 3) released pieces of wood in a 1/30 scale coastal model, constructed in a 50.4-metre by 29.4-metre wave basin, and tracked the driftwood behaviour in response to waves and wave-driven circulation. Despite limitations including model scale effects, Murphy, et al.'s (2020) experiments provided several insights to factors affecting driftwood mobility in coastal areas, including sea state and wave-induced circulation, the length and roughness/morphology of driftwood pieces, and beaching/washoff processes (Section 3.7).

2.2.4 Numerical modelling

There are few numerical studies of the transport and fate of driftwood in coastal waters. The majority of research on numerical modelling of the transport of buoyant objects in aquatic environments is concentrated on wood transport in rivers (Bladé et al., 2016; Ruiz-Villanueva et al., 2014a; Ruiz-Villanueva et al., 2014b; Kang & Kimura, 2018; Kimura & Kitazono, 2018; Persi et al., 2019), tsunami-driven transport of debris (Nistor et al., 2017), or transport of plastics and anthropogenic marine litter (such as plastics) at global or large regional oceanic scales (Brown & Niedzwecki, 2018; Mansui et al., 2015; Jalón-Rojas et al., 2019; Lebreton et al., 2012; Neumann

et al., 2014; van Sebille et al., 2018). One known numerical investigation of driftwood transport is a study by Dalaiden et al. (2018), which involved simulating transport by sea ice in the Arctic Ocean over multi-decadal time scales.

As explained by Nistor et al. (2017), numerical modelling studies of tsunami-driven debris transport have tended towards dynamic coupling of fluid and solid mechanics equations solvers, typically involving high-fidelity Navier-Stokes equations solvers (Eulerian or smoothed-particle hydrodynamics) coupled with discrete element method (DEM) models to simulate solid body motions. These coupled models show promising abilities to accurately simulate debris motion and fluid-solid interactions under quasi-steady hydrodynamic forcing but are computationally burdensome (Nistor et al., 2017), and impractical for application to driftwood transport by wind waves or other coastal process drivers at oceanic, regional or coastal reach scales.

The majority of numerical studies of driftwood transport in rivers utilize Eulerian, two-dimensional, shallow water Navier-Stokes equations solvers to describe hydrodynamics, coupled with Lagrangian (particle-based) models that describe the driftwood transport and interactions with channel sides or hydraulic structures (Stockstill et al., 2009; Ruiz-Villanueva et al., 2014b; Kang & Kimura, 2018; Persi et al., 2019). Bladé et al. (2016) reviewed a number of considerations and choices for these types of models, such as kinematic versus dynamic formulations, treatment of driftwood motion, driftwood-driftwood interactions, driftwood-boundary interactions, buoyancy effects, and coupling with hydrodynamics and sediment transport. Kimura & Kitazono (2018) showed that coupling with three-dimensional flow models is typically required only when the driftwood Richardson number is less than 10 (i.e., the driftwood is not strongly buoyant).

A variety of techniques can be used to incorporate information about driftwood geometry and orientation in Lagrangian (particle-based) transport models. Ruiz-Villanueva et al. (2014b) used a method whereby each particle represents a single piece of wood with an assumed cylindrical geometry, and the position and orientation of each cylinder is updated based on velocities at the centroid and ends. An acknowledged limitation of this approach is that the effects of root wads or other geometrical irregularities, known to be important factors affecting transport and accumulation, cannot be captured. Stockstill et al. (2009) used a discrete element model approach, which allows for a broader range of driftwood geometries to be modelled, by using multiple particles to capture the basic shape of each piece. The motion of each particle is calculated based on resultant forces, including hydrodynamics, internal forces (interactions between particles comprising a piece of wood), and interactions with other pieces. Kang & Kimura (2018) and Kimura & Kitazono (2018) also used a variant of the discrete element model, whereby multiple particles forming each piece of driftwood are advected independently. The centroid is then re-computed based on the mean position of the advected particles and the particles are re-arranged to capture the original shape of the piece. A key consideration for these Eulerian(flow)-Lagrangian(driftwood) models is whether to utilize kinematic or dynamic approaches for simulating wood transport. Kinematic models assign driftwood velocities based on the fluid flow velocity, whereas dynamic models take into account forces acting on the driftwood (and also

potentially on the fluid). Although the latter approach is expected to be more consistent with the physics of driftwood transport, Bladé et al. (2016) identified advantages and disadvantages of both kinematic and dynamic models, and concluded that simpler, kinematic approaches can accurately capture log transport in rivers. An inherent challenge with dynamics-based models is the selection of appropriate force coefficients (e.g., drag coefficients), which can introduce significant uncertainty.

Brown & Niedzwecki (2018) summarize numerical modelling studies of debris transport in the marine environment, which generally focus on anthropogenic litter with long-lived buoyancy, most commonly plastics, rather than driftwood. Nevertheless, these models have potential to provide insight to driftwood transport. Most studies, particularly those focussed on transport at global oceanic scales, make use of Eulerian global circulation models to provide hydrodynamic and meteorological data, which are then used as forcing inputs to evaluate debris transport using off-line, Lagrangian techniques (Lebreton et al., 2012; Mansui et al., 2015; Jalón-Rojas et al., 2019). In some cases, dedicated regional models are used to provide higher resolution hydrodynamic forcing (Critchell et al., 2015; Kako et al., 2011; Neumann et al., 2014), which is important to capture the transport and fate of waterborne agents in response to complex topographies and bathymetries in coastal waters (Grech et al., 2016).

By contrast to many numerical modelling studies of driftwood transport in rivers that incorporate force dynamics and piece geometries, Lagrangian analyses of flotsam and debris transport in oceans and seas more typically utilize a kinematics-based approach to simulate the passive advection and diffusion of particles, as proxies for debris. The horizontal positions of particles (proxies for debris pieces), $X_p = (x_p, y_p)$, are evaluated at each model time step, n (in increments, Δt), using an equation of the general form (Yoon et al., 2010; Pattiaratchi & Wijeratne, 2019):

$$X_{p,n+1} = X_{p,n} + U_{surf}\Delta t + R\sqrt{2D\Delta t} \qquad (2\text{-}2)$$

where t is time, $U_{surf} = (u_{surf}, v_{surf})$ is the surface water velocity vector, R is a rational number between -1 and +1 selected randomly from a specified (usually normal) probability distribution, and D is a horizontal diffusion coefficient (assumed constant and homogeneous in the example in Equation 2-2 above). The second term on the right-hand side of Equation 2-2 describes advection of debris particles by currents, using the commonly applied first order (Euler) explicit time stepping scheme. However, the growing realization that higher order numerical schemes can provide more accurate results (van Sebille et al., 2018), and even reduce computational cost through efficiencies (Gräwe et al., 2012; Lee et al., 2005), has led to them being increasingly adopted for practical applications (Jalón-Rojas et al., 2019; Kako et al., 2011; Lebreton et al., 2012). In some studies, the advection terms are modified to include wind effects (i.e., windage) (Jalón-Rojas et al., 2019), and wave effects (Iwasaki et al., 2017). For example, Pattiaratchi & Wijeratne (2019) include an additional term in Equation 2-2 representing Stokes drift contributions to advection:

$$U_S \Delta t = \frac{1}{8} \omega k H^2 \frac{cosh(-2kz)}{sinh^2(kh)} \Delta t \quad (2\text{-}3)$$

where U_S is the Stokes drift velocity, ω is the radian frequency of waves, k is the wave number, H is the wave height, h is the water depth and z is the vertical co-ordinate. Since the Stokes drift term of the form shown in Equation 2-3 is depth-dependent, a three-dimensional approach is required to track the vertical position of particles, z_p, as follows:

$$z_{p,n+1} = z_{p,n} + w\Delta t + R\sqrt{2D_z \Delta t} \quad (2\text{-}4)$$

Here, w is the fall velocity of debris (based on debris characteristics, including relative buoyancy, which may change over time in the case of driftwood), and D_z is a vertical diffusion coefficient. The last terms on the right-hand side of Eqs. 2-2 and 2-4 are stochastic terms, which describe diffusion of particles as a random walk process, assuming spatially uniform diffusion coefficients (D and D_z). However, turbulent diffusion in coastal environments is inherently non-uniform, owing to gradients induced by wind, waves, shore and bottom boundaries, vegetation, and density stratification. Hunter et al. (1993), Visser (1997), Spagnol et al. (2002), Ross & Sharples (2004), and Nordam et al. (2019) describe correction techniques and consistent numerical schemes to capture the effects of spatially and temporally varying diffusivity in random walk models, and eliminate errors (e.g., unrealistic accumulation of particles in zones of low diffusivity).

Critchell & Lambrechts (2016) and Jalón-Rojas et al. (2019) both describe techniques for simulating mobilization (washing off) of plastic debris that has become beached, using stochastic processes. Jalón-Rojas et al.'s (2019) model used a time scale-dependent approach (i.e., half-life). Both approaches require subjective assumptions (or data for calibration) to implement, and do not necessarily capture the physics of debris-shore interactions. Neither Critchell & Lambrechts (2016) nor Jalón-Rojas et al. (2019) clearly articulate how beaching is initiated in the models. Pattiaratchi & Wijeratne (2019) used a three-dimensional particle-tracking approach coupled with hydrodynamic models that incorporated wetting and drying, a Stokes drift formulation for wave-driven transport based on linear wave theory, bed shear stress considerations and time-dependent buoyancy to simulate deposition and resuspension of seagrass wrack on beaches.

2.2.5 Summary

Key findings, knowledge gaps, challenges and limitations identified by the literature review are summarized in Table 2-3.

Table 2-3. Summary of literature review.

Topic	Key Findings in Literature	Knowledge Gaps, Challenges and Limitations
Abundance and Distribution	• Driftwood is present in all oceans • Natural and anthropogenic sources (e.g., rivers, coastal forests, logging, wood manufacturing, shipping) • Abundance and distribution varies spatially and temporally in response to climate; seasonal meteorology, hydrology and oceanography; and human activity • Highest concentrations in northern oceans proximate to large forests • Tends to be present in large accumulations or hotspots (i.e., "patchy") • Proportion from natural and anthropogenic origins varies by region	• Limited knowledge or quantitative estimates of driftwood supply rates and changes over time • Patchy distributions make it challenging to extrapolate from site-specific field data • Numerous factors contribute to changes in abundance over time, such that there is no clear consensus on the dominant driver(s)

Topic	Key Findings in Literature	Knowledge Gaps, Challenges and Limitations
Transport Drivers and Processes	• Coastal driftwood transport driven by currents, wind, waves, buoyancy (including settling) effects, and sea ice • Time-limited buoyancy a key factor influencing mobility • Beached driftwood can trap sediment (and other debris) • Presence/absence of root wads, bark and other irregularities influences buoyancy and mobility	• Majority of studies focused on riverine environments, tsunami-driven transport of debris, or oceanic scale transport of anthropogenic litter • Numerous factors governing the time-dependent buoyancy of driftwood makes it difficult to predict • Maximum travel distances for driftwood in ice-free seas and mechanisms leading to far-travelled driftwood not well understood • Driftwood beaching and washoff/mobilization processes not well understood • Effects of coastal landform and geomorphology on trapping of driftwood not well understood • Processes leading to wood entanglement and rafting in coastal waters not well understood • Proportion of wood entering rivers and coastal waters with root systems intact not well understood

Topic	Key Findings in Literature	Knowledge Gaps, Challenges and Limitations
Weathering and Degradation	• Weathering and degradation of wood occurs due to biological and physico-chemical processes, and human activities • Degradation influences mass and buoyancy over time, and therefore, mobility • Variety of factors related to wood characteristics and ambient environment affect degradation rates • Where active, marine boring organisms are the primary degrading agent • Travel distance/time from sources inversely proportional to presence of root systems and bark	• Cause-effect relationships between travel distance, degradation processes and wood roughness not well understood • Degradation rates difficult to predict, owing to variety of influencing factors and processes • Role of marine bacteria in degrading wood not well understood
Physical Modelling	• Laboratory experiments have provided important insights to the dynamics and impacts of driftwood in rivers and debris mobilized by tsunami • Physical modelling a useful alternative or complement to field studies, owing to challenges in observing/detecting driftwood or debris in the field	• Few laboratory studies investigating driftwood transport and fate in coastal waters • Constraints on spatial scales that can be investigated using physical modelling approaches, determined by flume/basin sizes and laboratory capabilities • Model scale effects introduce uncertainty in reduced-scale experiments

Topic	Key Findings in Literature	Knowledge Gaps, Challenges and Limitations
Numerical Modelling	• Majority of numerical studies focus on transport of wood in rivers, or anthropogenic marine litter at large regional oceanic scales • Most studies utilize Eulerian-Lagrangian (flow-transport) models, with stochastic (random walk) approach to diffusion • Lagrangian transport models well suited to patchy distributions associated with driftwood • Kinematic transport models generally preferred, owing to complexity and uncertainty in dynamic models	• Few numerical studies investigating driftwood transport and fate in coastal waters • Few studies incorporating driving nearshore transport processes (waves, littoral processes) • Few studies with sufficient spatial resolution to capture influence of complex coastal topographies and bathymetries • Beaching and washoff algorithms not physics-based or validated • Diverse temporal and spatial scales relevant to driftwood transport and fate a challenge for numerical models

2.3 Critical Review and Future Research Directions

The literature review presented in Section 2.2 summarizes the current state of knowledge surrounding the processes driving driftwood fate and transport in aquatic environments, and progress in developing predictive numerical models. Much of it derives from field and experimental studies focussed on river environments. While insights gained from studies of driftwood in rivers are useful in characterizing the fundamentals of transport by slow-varying currents, the spatio-temporal scales and processes in coastal, estuarine and oceanic environments are distinctly different to their riverine counterparts.

The role of driftwood in interacting with coastal hydrodynamics and geomorphology has been largely understudied (Kennedy & Woods, 2012). Limited field evidence indicates that driftwood can exert significant control on beach profiles (Kennedy & Woods, 2012; Kaminsky et

al., 2020), dune formation (Grilliot, 2019) and dune scarping (Davidson et al., 2020), but with distinct differences in behaviour depending on factors such as the beach sediment type (i.e., gravelly versus sandy). Indeed, experimental studies investigating the influence of anchored wood installations on beach profile evolution and wave run-up support the idea that wood can strongly influence beach morphodynamics (Wilson et al., 2020). However, the precise mechanisms and wave-driven processes leading to deposition, mobilization, and retention of driftwood on beaches are poorly understood. For example, Kennedy & Woods (2012) point out that the same wave events that lead to beach erosion can also deposit driftwood. Although experimental observations suggest that the morphology of driftwood pieces (e.g., length, presence of rootwads, roughness elements) plays an important role in determining the potential for beaching and mobilization by waves (Murphy et al., 2020), there are no known predictive models that describe the influence of these parameters on beaching or washoff of coastal driftwood. Pattiaratchi & Wijeratne's (2019) approach to numerical simulation of beaching and washoff of sea wrack provides some insight as to how the time history of waterlogging and desiccation, and other processes such as loss of buoyancy due to degradation, could conceivably be implemented in a model for driftwood. Improved deterministic and probabilistic models of driftwood-shore interactions, supported by field and experimental evidence, are needed to better describe and support predictive modelling of driftwood transport processes in coastal environments. Time-lapse photography has been successfully applied to field monitoring of driftwood transport in rivers (Kramer, 2016; MacVicar & Piégay, 2012) and at coastal sites (Kako et al., 2018), and could provide insight to driftwood-shore interactions over spatial scales of relevance, particularly with the advent of image processing and machine learning techniques that enable automated identification. Physical modelling can also provide a useful means to characterize these processes and support development and validation of predictive models. However, care is needed when designing experimental studies to ensure scale effects are adequately mitigated, particularly given the diversity of spatial and temporal scales of relevance to coastal driftwood fate and transport (Murphy et al., 2020).

Coastal driftwood tends to be heterogeneously distributed, meaning that it is present in substantial accumulations or hotspots, analogous to "jams" in riverine environments (Thiel & Gutow, 2005; Kramer, 2016; Steelandt et al., 2013). Although this may be an important factor defining the role of driftwood in promoting habitat diversity (Kramer, 2016), large concentrations also exacerbate the hazards posed by debris during extreme events (Nistor et al., 2017). The mechanisms and conditions leading to driftwood entanglement, rafting and accumulation under typical climatic or storm conditions in coastal waters are poorly understood. In particular, an improved understanding of the potential role of different types of coastal structures in trapping driftwood or initiating raft formation would support coastal engineering design guidance to better manage debris hazards and/or incorporate wood in nature-based systems. For example, Kaminsky et al.'s (2020) observations of naturally depositing driftwood at specific locations on beaches in the State of Washington, United States, provided the basis for siting a log groyne structure, which trapped driftwood as part of a nature-based shore protection system.

From the literature review, it is evident that the diverse temporal and spatial scales applicable to the transport and fate (including accumulation) of driftwood in coastal regions represent challenges for developing efficient and accurate predictive numerical models. The availability and supply of wood for recruitment to coastal zones may depend on forest dynamics over time scales of centuries, and/or episodic extreme (storm or flood) events lasting less than a day (Wohl et al., 2019). Individual pieces of driftwood in a patch within a coastal embayment may have been recruited in high mountain watersheds years, or even decades, prior to their delivery to the coast; or they may have been delivered directly to the coast by a single erosion event. Driftwood exposed to sea ice may even have experienced trans-oceanic transport (Dyke et al., 1997). The stability of beached driftwood may depend on time histories and clustering of storm events over timescales of days to years (Heathfield & Walker, 2011), or the occurrence of an extreme high water level lasting only a few hours. Spatial scales relevant to driftwood transport range from less than a metre (e.g., roughness elements on driftwood surfaces) to hundreds of kilometres or more (e.g., oceanic circulation patterns). These wide-ranging disparities in temporal and spatial scales create challenges for numerical models, which are typically good at capturing processes over large spatial scales and long timeframes, or small spatial scales and short timeframes, but not both. Opportunities to address these challenges may lie in developing analogues of the integrated, multi-scale numerical models that have recently been championed for assessing other types of coastal hazards (Roshanka, 2020; Vitousek et al., 2017).

Resolving tide- and wave-driven transport at coastal cell scales is expected to be crucial for accurate modelling of debris beaching and washoff processes, and therefore, the overall mobility of driftwood (Critchell et al., 2015; Mansui et al., 2015; Doong et al., 2011; Jalón-Rojas et al., 2019; Murphy et al., 2020). Although there have been some recent advances in numerical modelling of floating anthropogenic litter (e.g., plastics) transport at oceanic scales, most studies give only cursory attention to nearshore hydrodynamic processes and debris-shore interactions, or ignore them completely. Studies relying solely on global ocean circulation models (Lebreton et al., 2012) typically do not include tidal hydrodynamic forcing. If included at all, wave-driven transport of floating debris is most frequently treated in a simplistic manner by modifying the advection terms to account for Stokes drift (Mansui et al., 2015; Pattiaratchi & Wijeratne, 2019), or by lumping wave-driven transport together with wind effects (Zhang, 2017). However, the latter approach is only appropriate if local waves are strongly correlated with local winds, and does not account for swell-driven transport (Sobey & Barker, 1997), littoral processes, or wave-driven circulation in nearshore areas (e.g., rip currents) (Murphy et al., 2020). In fact, the authors are not aware of any numerical studies that incorporate the physics of littoral and swash zone processes in simulating driftwood transport. Most studies that investigate debris transport in regional seas either tend to ignore beaching altogether (Mansui et al., 2015), or make very simplistic assumptions with respect to debris-shore interactions, such as fully reflective boundaries (Neumann et al., 2014) or permanent beaching following contact with the shoreline (Critchell et al., 2015). In the examples cited above, these assumptions are identified as limitations of the models, and areas where research is needed.

The majority of numerical models developed for simulating fate and transport of driftwood in riverine environments and anthropogenic debris in ocean environments adopt Lagrangian or Lagrangian-Eulerian particle-tracking methods. Such approaches offer the most promise for predictive modelling of driftwood transport in coastal environments, for a number of reasons. Lagrangian methods are efficient and accurate when the transported quantity (in this case, driftwood) occupies a relatively small portion of the model domain (Hunter, 1987; Dimou & Adams, 1993), and are therefore ideally suited to heterogeneously-distributed (patchy) coastal driftwood. Furthermore, Lagrangian or Lagrangian-Eulerian techniques tend to:

- Have more relaxed time-step constraints compared to Eulerian models (Neuman, 1981);
- Allow for stable, accurate, non-diffusive advection, particularly in cases of high Péclet numbers (i.e., convection-dominated systems) where steep concentration gradients persist (Szymczak & Ladd, 2003; Neuman, 1981; Hunter, 1987); and
- Permit full decoupling of driftwood transport from hydrodynamics.

These properties make Lagrangian models attractive options for conducting long-term (i.e., multi-decadal) simulations at oceanic scales (Lebreton et al., 2012), or large ensembles of simulations (e.g., Monte Carlo) to assess probabilistic distributions. Another inherent advantage of these Lagrangian methods (over, say, Eulerian methods) is that they are conveniently suited to evaluating integral parameters such as residence time, variance, and age (Dimou & Adams, 1993); which are of relevance to an improved understanding of driftwood transport and fate, and amenable to integration of models describing driftwood weathering and degradation over time. Particle-tracking models are well suited to parallel computing (Dimou & Adams, 1993; Dalrymple et al., 2010) and therefore, present an attractive option to leverage the paradigm shift in high performance computing brought about by developments in graphics processing units (GPU) technology.

Another potential advantage of Lagrangian and Lagrangian-Eulerian models for simulating driftwood transport relates to the apparent randomness or element of chance that affects the potential for driftwood jams or accumulations to initiate in rivers (Bocchiola et al., 2008; Schmocker & Hager, 2011), and presumably, too, in coastal settings. This inherent randomness in jam and raft initiation processes, as well as in wood characteristics and processes such as wood recruitment, wood characteristics and breakage (Eaton et al., 2013), lends itself well to stochastic modelling approaches. Lagrangian, random walk particle-tracking models offer possibilities to integrate deterministic (e.g., advection) and stochastic (e.g., turbulence, jam/raft initiation) processes and have been successfully applied to simulate the fate and transport of various agents in coastal waters and other environmental settings (Grech et al., 2016; Aylor & Flesch, 2001).

Due to the long spatial scales over which marine driftwood is transported, and challenges in obtaining representative field data on spatial distributions using conventional survey techniques (owing to heterogeneity), remote sensing techniques present promising opportunities to advance the body of knowledge surrounding marine driftwood fate and transport. The buoyancy (though

time-limited) of wood makes aerial or satellite imagery ideally suited to detecting driftwood (Kramer, 2016). Some advances have been made in remotely sensing driftwood. Doong et al. (2011) used backscatter data from high-resolution (8 m), multispectral satellite images to detect the quantity and distribution of driftwood in coastal waters of Taiwan, after Typhoon Morakot in 2009. Eamer & Walker (2010) used 20-cm resolution digital aerial ortho-photographs and 2-m resolution digital elevation data derived from co-located light detection and ranging (LiDAR) surveys to develop sand and drift log elevation surfaces in coastal regions of British Columbia. Heathfield & Walker (2011) analysed ortho-rectified aerial photography dating back to the 1970s to support an examination of trends in coastal driftwood abundance and distribution, and geomorphic responses. Kramer (2016) geo-rectified oblique aerial imagery to record the distribution and type of large driftwood accumulations in Great Slave Lake, Canada. Such data can be valuable in identifying hotspots for driftwood accumulation, and supporting the development and validation of predictive models.

2.4 Conclusions

The present state of knowledge surrounding the fate and transport of driftwood in coastal zones is substantially founded on research focussed on riverine environments, anthropogenic litter and debris transport at oceanic scales, and/or tsunami-driven processes. The limited attention given to driftwood transport in coastal environments has led to several knowledge gaps that constrain predictive capabilities, and therefore, humankind's capacity to sustainably balance the risks posed by coastal driftwood (including the contribution of manufactured/processed wood to the marine litter problem) with its many ecosystem services. Key knowledge gaps pertain to:

1. Driftwood supply to coastal regions, including quantities/rates of supply, wood characteristics and condition, and the dominant drivers of changes in supply;
2. The fundamental physics underlying driftwood interactions with coastal hydrodynamics and geomorphology (e.g., littoral transport processes, beaching and washoff, effects of driftwood on coastal morphodynamics, time-dependency of driftwood buoyancy);
3. Interactions between driftwood and coastal structures (e.g., retention of driftwood by different structures, storm- or wave-driven impacts, effects of driftwood on stability of structures, interactions with wave run-up and overtopping, integration of wood in nature-based shore protection systems);
4. Processes and conditions leading to driftwood rafting and accumulation in hotspots; and
5. The influence of weathering and degradation on driftwood transport processes, including degradation rates based on wood characteristics and ambient environmental conditions.

The diverse temporal and spatial scales affecting the mobility of coastal driftwood necessitate multi-disciplinary research that leverages field, experimental, and remote-sensing data to develop multi-scale, predictive models for driftwood fate and transport in coastal environments leading to sustainable, evidence-based management practices.

Chapter 3. Physical Modelling Experiments

This chapter is a preprint of a modified version of the following published article:

Murphy, E., Cornett, A., Nistor, I., & Baker, S. (2020). Modeling Transport and Fate of Woody Debris in Coastal Waters. In *Proceedings of the virtual Conference on Coastal Engineering*, 36v, https://doi.org/10.9753/icce.v36v.papers.1

Abstract:

Driftwood or woody debris is ubiquitous in coastal waters, and on shorelines proximate to forested regions. Logs and driftwood play a vital role in coastal and global ecosystems, and can provide valuable data to support studies of oceanography, geomorphology, ecology, history and archaeology. There is growing interest in the role that wood can play in nature-based coastal engineering solutions. However, large quantities of woody debris in coastal waters can pose significant hazards to communities, infrastructure, navigation and ecosystems. Thus, the changing abundance and distribution of coastal driftwood, driven by factors including human activities and climate change, has potential for both positive and negative consequences. A better understanding of coastal driftwood fate and transport processes is needed to inform management practices, uses, and sustainable ecosystem management. To date, research on physical transport of driftwood, has been concentrated on tsunami and inland (riverine) environments, where spatiotemporal scales and driving processes are significantly different from typical climatic or even extreme (storm) conditions in coastal waters. In this paper, we describe a series of scale physical model experiments, conducted to provide insight to driftwood transport processes in coastal waters under a range of controlled wave and water level conditions. The experiments were conducted in a 50.4-metre by 29.4-metre wave basin, in which a 1/30 scale model of a natural shoreline comprised of a shallow fringing reef, a sandy shoreline, and several small coastal structures (groynes and breakwaters) was constructed. Wooden dowels and tree branches, scaled to replicate the size distribution of driftwood observed on Pacific Northwest shorelines, were released in the model. Despite some limitations (e.g., model scale effects), the experimental test results provided several valuable insights to factors affecting driftwood mobility in coastal areas. The results will inform the parameterization of important physical processes in a numerical model being developed to predict the fate and transport of driftwood in coastal waters.

Keywords: Woody debris; driftwood; physical modelling; littoral drift; wave drift forces.

3.1 Introduction

Driftwood is abundant in coastal waters and on shorelines around the world (Thiel & Gutow, 2005). Logs and driftwood play a vital role in coastal and global ecosystems, providing habitat, structure, nutrients, and carbon storage (Gonor et al., 1988; Kennedy & Woods 2012;

Grilliot, 2019). Driftwood is of interest to researchers in a variety of fields, providing data to support studies of oceanography, geomorphology, ecology and human occupation (Steelandt et al., 2015). The distribution of driftwood on shorelines can provide insight to historical water levels at sites where gauged records do not exist, or are discontinuous (Harper at al., 1988; Kim et al., 2020). Driftwood has traditionally been used for firewood, tools and construction (Lepofsky et al., 2003; Alix, 2005). Recently, there has been renewed interest in driftwood and logs for use in sustainable energy supply (Bartocci et al., 2017) and as components of nature-based shore protection schemes (Wilson et al., 2020).

Driftwood can have also negative impacts on ecosystems and human activities in coastal zones, particularly when present in excessive quantities. Debris accumulations near log booming grounds have been known to smother benthic ecosystems, reduce biodiversity, reduce photosynthesis in submerged aquatic vegetation, leach toxic compounds, and de-oxygenate coastal waters (Edgell & Ross, 1983). As agents of dispersion, floating wood pieces can contribute to the spread of invasive species (Convey et al., 2002). Driftwood often poses a significant hazard in coastal waters, impacting navigation (Doong et al., 2011), causing damage to boats and structures during storm or tsunami events (Nistor et al., 2017; Edgell & Ross, 1983). The societal cost of managing these risks is significant (Edgell & Ross, 1983; Bartocci et al., 2017; Doong et al. 2011).

The abundance and distribution of coastal driftwood is dynamic in response to a variety of drivers including climate change, and human activity (Kramer, 2016). An improved understanding of driftwood behaviour in coastal areas is needed to inform management practices and achieve a sustainable balance in terms of maximizing the environmental benefits of driftwood, while appropriately managing risk.

3.2 Overview of Driftwood Transport Processes in Coastal Waters

Most published literature concerning driftwood and woody debris transport is focused on tsunami events or riverine environments. In coastal environments, waves can play an important role in driving transport processes and interactions with the shore. Coastal driftwood can become “beached” or stranded on the shore, as a result of wave action and water level fluctuations. Driftwood deposited at higher elevations has a lower probability of being remobilized by subsequent high water level or wave events, or associated erosion (Thiel & Gutow, 2005). Wood pieces or matrices can progressively trap sediment and become partially or completely buried (Heathfield & Walker ,2011; Eamer & Walker, 2010;, Kennedy & Woods, 2012; Grilliot, 2019), unless remobilized or washed off by extreme events.

In addition to ambient drivers (waves, currents, wind, ice), the physical characteristics of driftwood influence transport rates and processes. Time-dependent buoyancy is a major factor determining the capacity for driftwood transport (Häggblom, 1982; Alix, 2005; Kramer, 2016), and is largely controlled by wood taxa (which determines volume and specific gravity),

wetting/drying history, and degradation. Field and laboratory studies of driftwood transport in rivers identify piece length as a key predictor of mobility (Wohl & Goode, 2008; Bocchiola et al., 2008; Davidson et al., 2015). However, field studies are biased towards small river channels, where longer pieces exceed the channel width (Braudrick & Grant, 2000). Driftwood morphology, i.e., the presence or absence of root systems (or bark and other irregularities), can affect fate and transport by influencing buoyancy/draft (Braudrick & Grant, 2000) and interactions with shorelines or other debris. Morphology varies substantially by region. Driftwood on Arctic coastlines is smoother (more degraded) than on Pacific coasts of North America, owing to the relatively large distances travelled from the boreal forest treeline via rivers and ice to the Arctic Ocean (Alix, 2005; Steelandt et al., 2015).

3.3 Experimental Methods

3.3.1 1/30 scale coastal model

Experiments were conducted in a 50.4 m by 29.4 m indoor basin at the National Research Council Canada's Ocean, Coastal and River Engineering Research Centre in Ottawa, Canada (Figure 3-1 and Figure 3-2). The study made use of an existing, geometrically undistorted, Froude-scaled, mobile-bed coastal shoreline and nearshore bathymetry built to a geometric scale of 1/30. The model represented an approximately 1.5 km-long prototype coastal reach, comprising narrow, sandy beaches with rubble mound structures (groynes), and subtidal, fringing coral reefs. Cross-shore profiles consisted of relatively steep (approximately 1:7.5 vertical:horizontal) intertidal and supratidal beach slopes, transitioning to flatter subtidal terraces with slopes in the range 1:30 to 1:100. These profiles are typical of high-energy, reflective, coarse-sediment beaches (Scott et al., 2011). Two banks of portable wave machines were used to generate irregular, long-crested sea states with significant heights, H_s, in the range 0.015 m to 0.100 m at model scale (0.45 m to 3.7 m at prototype scale), and peak wave periods, T_p, in the range 1.1 s to 2.6 s (6 s to 14 s prototype scale). The wave machines were oriented to generate waves from 300° (clockwise relative to true north) (Figure 3-2). The mobile bed portion of the model extended approximately between the +2.0 m and -2.0 m Mean Sea Level (MSL) contours (hatched area in Figure 3-2). The mobile-bed material consisted of silica sand with a median diameter of 0.166 mm (model scale), scaled to achieve similar fall velocities to the prototype beach sand (median diameter of approximately 0.39 mm). The fixed-bed portion of the model, extending seaward of the -2.0 m MSL contour, consisted of a 5 cm thick skin of concrete grout on top of a bed of compacted fine gravel. In some areas, the concrete surface was roughened using a coarse broom to simulate the texture of the coral reef. Stones and gravel were also embedded in the wet concrete surface to simulate coral outcrops. Rubble-mound structures (groynes and breakwaters) were constructed using limestone with a unit weight of approximately 2,650 kg m^{-3}, scaled to faithfully represent the stability of the prototype 2- to 4-tonne rock under wave action. A correction to Froude scaling principles, based on the Hudson formula, was used to adjust the size of the rock used in the model to account for the use of freshwater in the model.

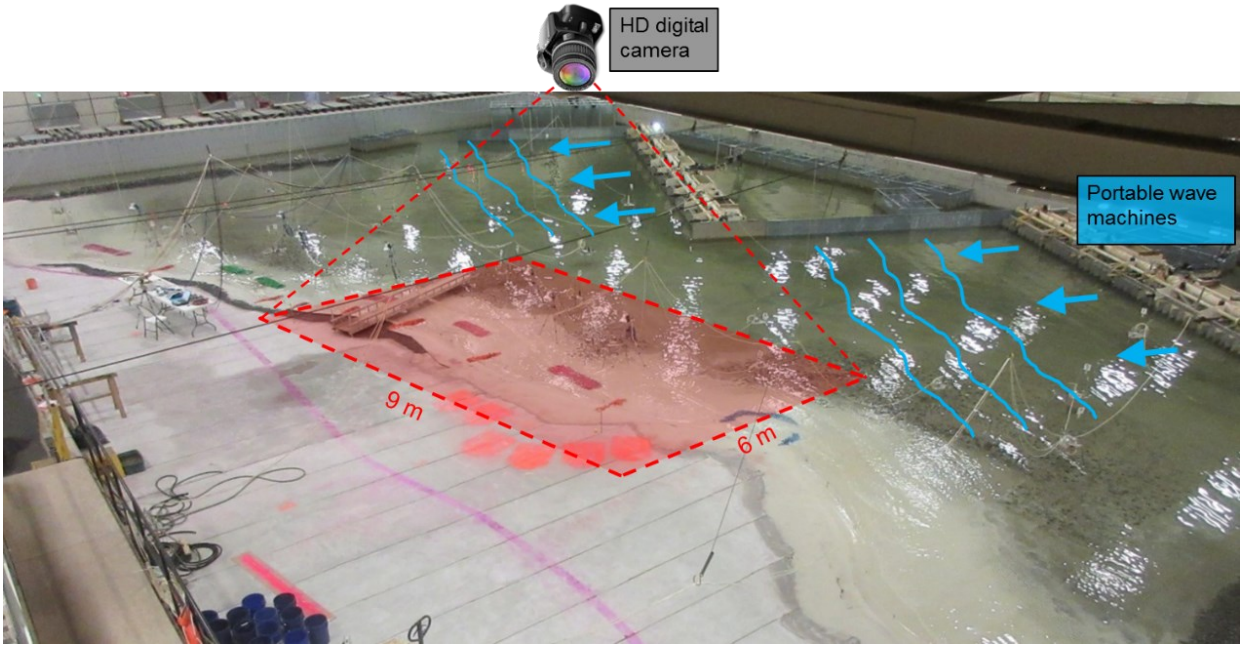

Figure 3-1. Overview of the 1/30 scale coastal model and experimental setup.

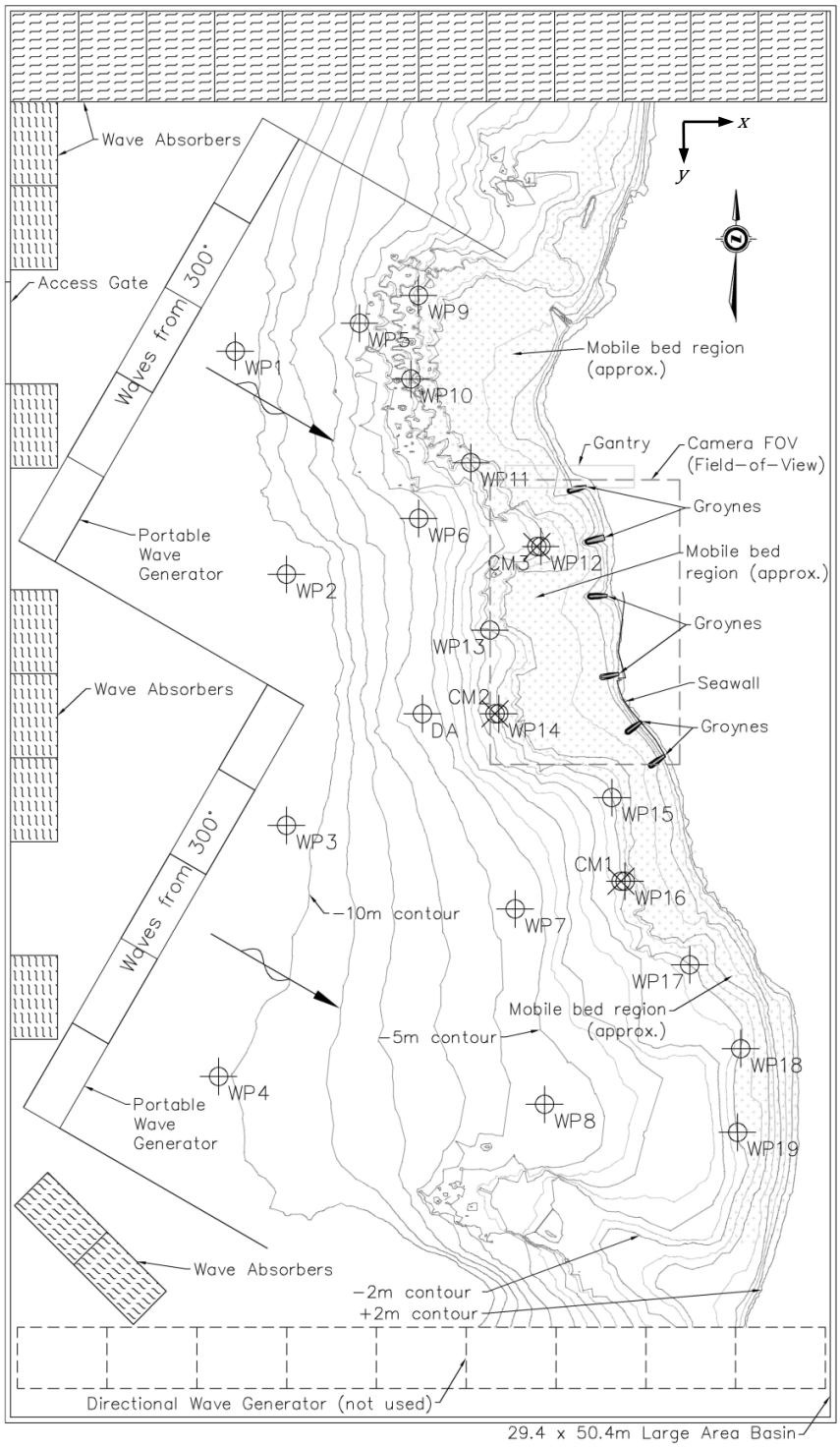

Figure 3-2. Layout of the 1/30 scale coastal model in the National Research Council of Canada's Large Area Basin. Capacitance probes are labelled WP1 to WP19. Electromagnetic current meters are labelled CM1 to CM3.

3.3.1.1 Instrumentation

A Nikon D5300 high-definition (HD) digital camera with a 35 mm lens was mounted on a gantry approximately 9 m above the basin, in a downward-looking position (Figure 3-1). The camera was configured to automatically record HD images (6000 x 4000 pixels) at capture frequencies between 0.3 and 1.0 Hz (determined by trial and error depending on the observed mobility of the driftwood within the camera field-of-view), when triggered remotely. The camera field-of-view (FOV) covered a central portion of the model coast and nearshore area approximately 9 m in the alongshore (y-) direction by 6 m in the cross-shore (x-) direction ($Y_B = 270$ m by $X_B = 180$ m at prototype scale) (shaded red area in Figure 3-1 and dashed rectangle in Figure 3-2). The x- and y- directions were respectively aligned with true east and true south as indicated in Figure 3-2. The central location of the FOV was chosen to focus on a nearshore portion of the physical model where wave-driven circulation was expected to be most realistic (i.e., minimizing lateral boundary effects).

Waves were measured in the model using an array of capacitance probes (WP1 to WP19 in Figure 3-2), sampling at 50 Hz (model scale). Four of the probes were located within the FOV of the downward-looking HD camera (Figure 3-2). Orbital velocities and wave-induced currents in two dimensions (u and v) were measured using electromagnetic current meters, two of which were located within the camera FOV (CM2 and CM3 in Figure 3-2) near the -2.0 m depth contour, and also sampling at 50 Hz (model scale). The wave and current data were post-processed and analyzed using the GEDAP™ software package (Miles 1990). The current meter records were post-processed to isolate low-frequency (wave-induced current) and high-frequency (orbital velocities) components. The low-frequency component was determined using a low pass filter with a cut-off frequency of 1/30 Hz (prototype scale). Nearshore wave-induced circulation patterns were qualitatively assessed by observing plumes of colored dye injected onto the water surface from the model shore.

Water depth limitations prevented deployment of wave and current probes very close to the shore. The shallowest water depths in which probes could practically be installed were in the range 7.1 cm to 8.6 cm (depending on still water level), corresponding to prototype depths in the range 2.13 m to 2.58 m. Consequently, all probes were situated outside or at the outer edge of the surf zone.

3.3.1.2 Shoreline and structure configurations

Experiments were conducted for four different shore configurations (Figure 3-3), in order to investigate the influence of different coastal features and structures on driftwood transport and dispersion. The four shore configurations (layouts) are described as follows:

- L1 – the baseline shore configuration incorporating a series of shore-perpendicular rock groynes;

- L2 – a configuration incorporating a series of low-crested barrier beaches with shorelines oriented approximately parallel to incident wave crests, and with stabilizing terminal groynes;
- L3 – a shore configuration incorporating a series of detached (offshore), 1.2 m long (model scale), shore-parallel breakwaters; and
- L4 – a shore configuration incorporating a series of detached (offshore), 0.6 m long (model scale), shore-parallel breakwaters.

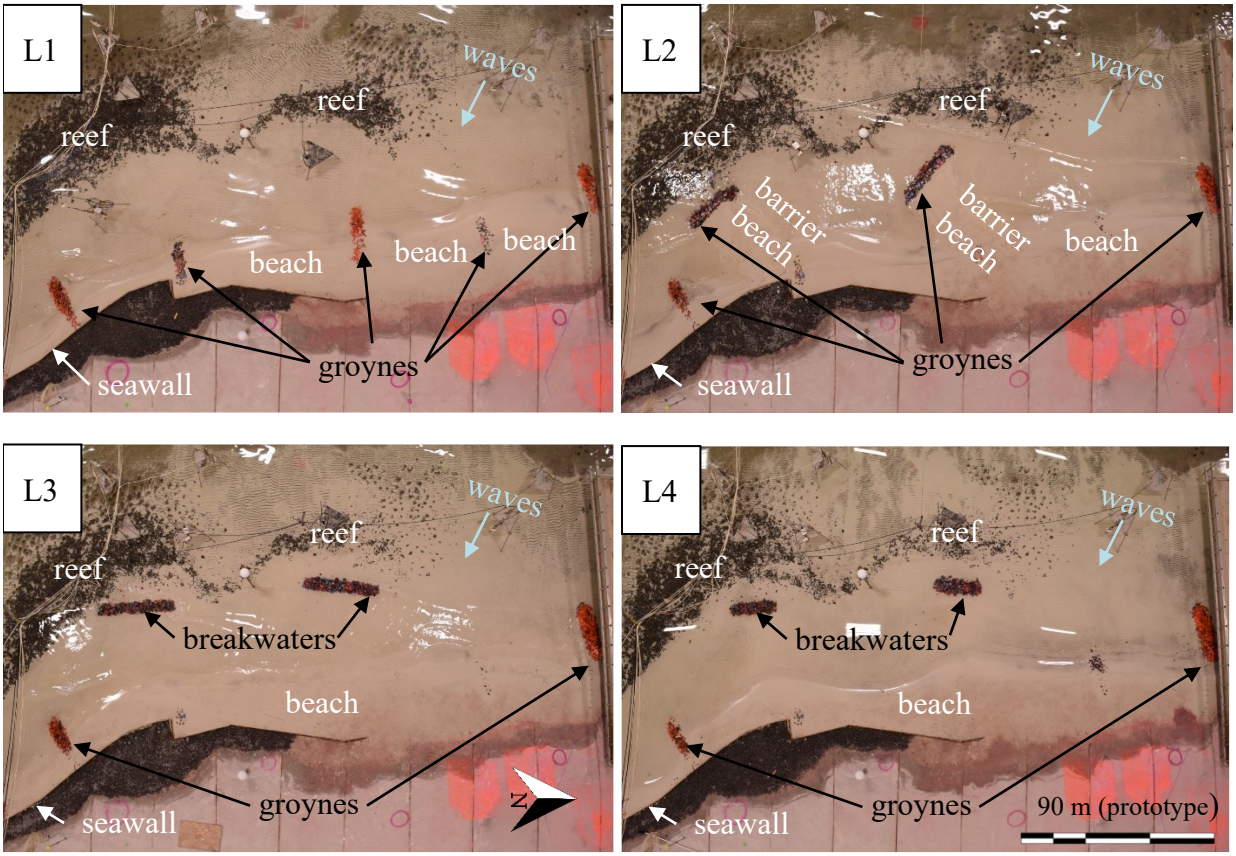

Figure 3-3. Shoreline and structure layouts within the camera FOV.

3.3.2 Model driftwood

Model driftwood was scaled to approximately match the size distributions (length and diameter) of pieces observed on sandy beaches at Ediz Hook, Washington, United States (Ian Miller, personal communication). Two types of model driftwood were used: (i) smooth, cylindrical wooden dowels (Figure 3-4a), and (ii) approximately cylindrical but irregularly-shaped deciduous tree branches (which were devoid of bark) (Figure 3-4b). The average density of the model driftwood pieces, measured soon after completion of all testing, was 686 kg m^{-3} (± 153 kg m^{-3}) and 774 kg m^{-3} (± 128 kg m^{-3}) for the dowels and branches, respectively. Four discrete size classes of driftwood were defined based on their length, L_P. The model driftwood was spray-painted distinctive colours by size class (Figure 3-4), to facilitate optical tracking (Chapter 4) and to observe differences in behavior. The four size classes (and associated paint colours) were L_P =

100 mm (yellow), 200 mm (maroon), 300 mm (blue) and 400 mm (green); corresponding to L_P = 3 m, 6 m, 9 m, and 12 m at prototype scale. Length, diameter, and density distributions for the model driftwood inventory are shown in Figure 3-5 compared to characteristics of large wood observed at Ediz Hook, and on marshes and mudflats adjacent to armored dykes at two sites (Delta and Surrey) in Boundary Bay, British Columbia (BC), Canada (M. Côté, personal communication). Model driftwood length and diameter distributions closely matched the larger driftwood observed at the more exposed Ediz Hook site. Wood density data was only available for the Delta and Surrey sites, which were surveyed by the Geological Survey of Canada (Figure 3-6) to inform the design of nature-based infrastructure pilot installations (Provan et al., 2023). Densities were obtained by extracting 51 mm diameter core samples from the surface of the wood using a hand drill, and weighing the samples (M. Côté, personal communication). The average density of wood sampled at the Delta and Surrey sites was 579 kg m^{-3} with a standard deviation of 163 kg m^{-3}. The model driftwood densities were deemed reasonably representative of field conditions, allowing for decreases in density that would presumably have occurred during desiccation of the stranded field specimens at the Delta and Surrey sites, and the wide variability in specific gravities reported in the literature (Chapter 2).

Figure 3-4. Model driftwood: a) dowels, and b) tree branches.

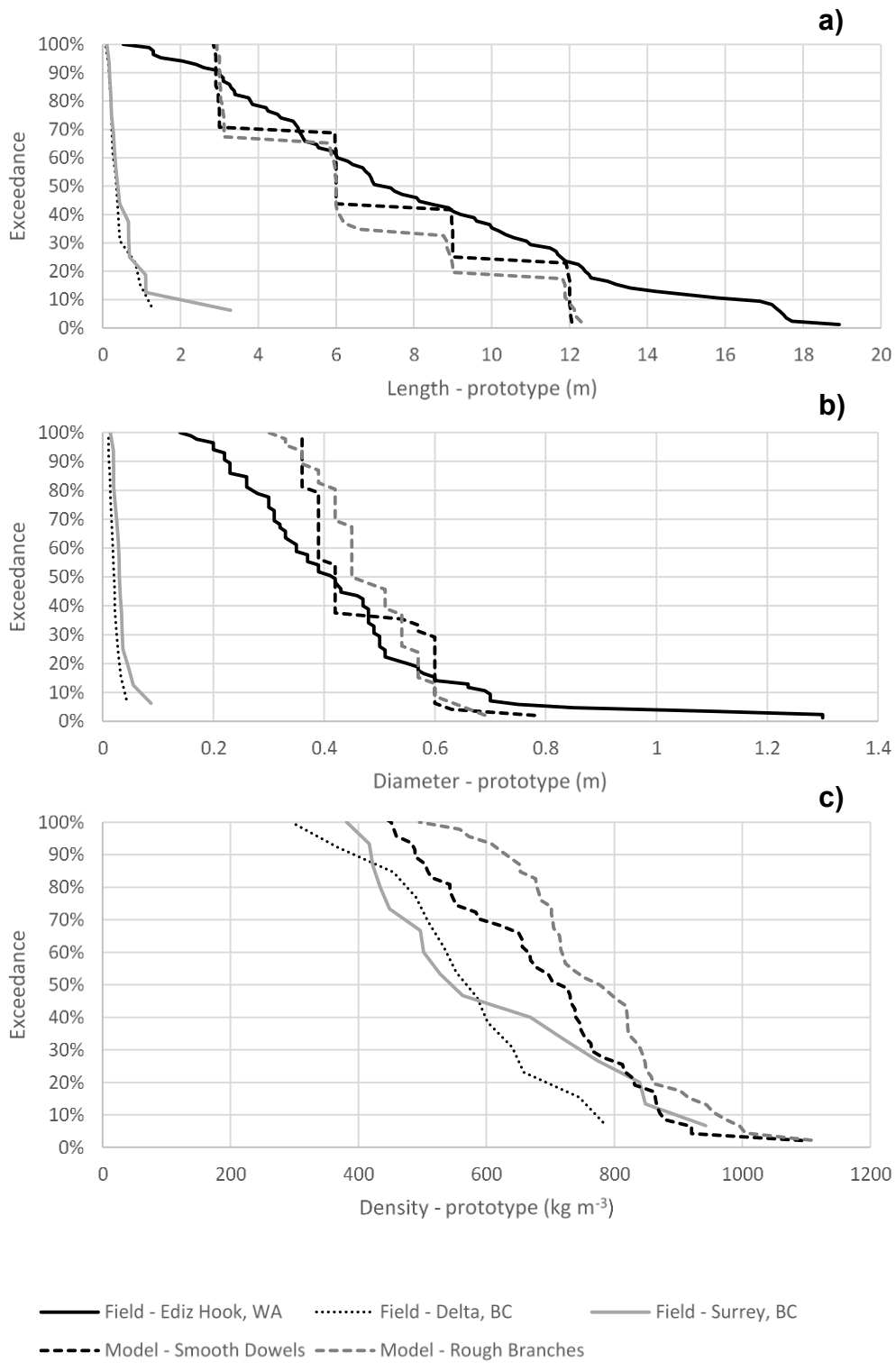

Figure 3-5. Observed (field) and model wood a) length, b) diameter, and c) density distributions.

Figure 3-6. Examples of driftwood specimens at the Surrey, BC, site surveyed by the Geological Survey of Canada. Photo credit: Gwyn Lintern.

3.3.3 Test program and procedures

The experimental test procedure involved manually releasing the model driftwood on the water surface from a gantry at the updrift (northern) end of the HD camera FOV (i.e., on the right-hand side of the panels in Figure 3-3), to approximate instantaneous point releases. The movement of the driftwood in response to waves and wave-driven circulation, and interactions with the shore and structures, was observed. Driftwood was released only after at least 10 waves had reached the beaches, to allow time for wave-driven circulation to develop. Tests were conducted for nine unique sea state and water level combinations, and four shoreline and structure configurations (layouts L1 to L4 in Figure 3-3) as shown in Table 3-1.

As explained in Section 3.3.1, the experiments were opportunistic, making use of an existing physical model. The test program was also constrained by the limited timeframe for accessing the experimental facility. All waves approached the shoreline obliquely, at angles of approximately 30° to the shore normal. For each sea state and water level combination, an ensemble of 5 to 8 driftwood release experiments (realizations) was conducted. The duration of each experiment was at least 2 hours (prototype time scale), or until all driftwood had passed through the camera field of view, whichever the shorter. Between each realization in an ensemble, any driftwood retained on the beaches or structures was removed using a long-armed grabber tool to avoid disturbing the silica sand or stones. After the last realization of each test ensemble, any driftwood remaining trapped on the beaches or rubble mound structures was left in place, and

subsequently exposed to a different set of wave and water level conditions to investigate the potential for remobilization.

The severity of the sea state conditions was progressively increased to minimize changes in the beach morphology between tests. However, higher waves and longer wave periods resulted in transport of the silica sand, requiring re-profiling of the mobile-bed portion of the model at intervals between some tests. The mobile-bed portion of the model was also periodically surveyed using a FARO Focus^{3D}-Multi Sensor laser scanner, providing a high-resolution digital elevation model of the nearshore area, which could potentially allow for an analysis of the influence of changes in beach and nearshore morphology on driftwood transport in the future, if desired. However, an evaluation of driftwood interaction with morphodynamics beyond the scope of this thesis.

Table 3-1. Summary of experimental conditions (all prototype scale).

Test Series	Number of realizations	η (m)	H_s (m)	T_p (s)	U_{CM2} (m s^{-1})	U_{CM3} (m s^{-1})	Model driftwood type	Shore layout	L_P = 3 m (yellow)	$\sum N_P$ L_P = 9 m (blue)	L_P = 12 m (green)	f_s (Hz)
1	8	0.35	0.45	8	0.03	0.05	Smooth dowels	L1	112	49	54	0.06
2	8	0.35	0.65	8	0.06	0.09	Smooth dowels	L1	127	56	64	0.06
3	7	0.35	0.80	11	0.21	0.17	Smooth dowels	L1	110	49	63	0.06
4	8	0.70	0.80	11	0.14	0.13	Smooth dowels	L1	127	71	56	0.06-0.09*
5	8	0.70	0.80	14	0.18	0.16	Smooth dowels	L1	111	56	70	0.09
6	8	0.70	1.20	6	0.27	0.21	Smooth dowels	L1	127	56	88	0.09
7	8	0.35	0.65	11	0.13	0.10	Smooth dowels	L1	125	56	88	0.09
8	8	0.70	3.70	10	0.99	0.74	Smooth dowels	L1	70	40	64	0.18
9	8	0.70	0.80	11	0.14	0.12	Rough branches	L1	111	52	68	0.09
10	8	0.70	1.20	6	0.28	0.20	Rough branches	L1	123	56	72	0.09
11	8	0.35	0.65	8	0.10	0.09	Rough branches	L1	128	56	72	0.09
12	5	0.35	0.65	11	0.17	0.10	Rough branches	L2	80	35	40	0.09
14	8	0.70	1.20	6	0.22	0.13	Rough branches	L2	125	56	64	0.09
15	8	0.70	1.30	10	0.40	0.19	Rough branches	L2	128	56	64	0.09
16	8	0.35	0.65	11	0.16	0.07	Rough branches	L3	133	56	70	0.09
17	8	0.70	1.20	6	0.24	0.12	Rough branches	L3	128	56	64	0.09
18	8	0.35	0.65	11	0.18	0.07	Rough branches	L4	134	56	64	0.09
19	8	0.70	1.20	6	0.23	0.11	Rough branches	L4	130	56	64	0.09

*Note: f_s increased from 0.06 Hz to 0.09 Hz after first three realizations of test series.

3.4 Results and Discussion – Wave-Driven Currents and Circulation

Mean (low-pass filtered) current speed magnitudes measured by the two current meters within the camera FOV are shown in Table 3-1 for all test series, and were in the ranges $U_{\mathrm{CM2}} =$ 0.03 to 0.99 m s^{-1} and $U_{\mathrm{CM3}} = 0.05$ to 0.74 m s^{-1} (prototype scale). For all but the most energetic sea states investigated (e.g., Test Series 8), the current meters were generally located just on or outside the edge of the surf zone.

Observations of dye injected onto the water surface in the model nearshore revealed that, for layouts L1, L3, and L4, a classical longshore current profile developed with peak current speeds inside the surf zone near the shore (Figure 3-7). The effects of groynes and breakwaters on circulation were confined to the immediate vicinity of the structures. By contrast, the barrier-beaches in layout L4 created rotational gyres and offshore-directed rip currents on the updrift side of the features (Figure 3-8).

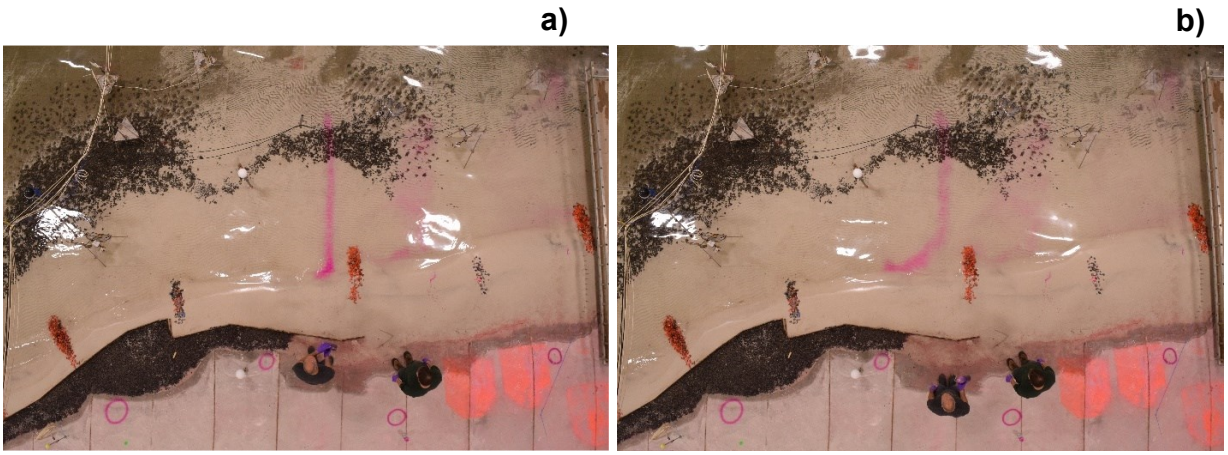

Figure 3-7. Snapshots of dye distributions at a) $t = 0$ and b) $t = 82$ s ($10\,T_p$) during Test Series 1 (layout L1).

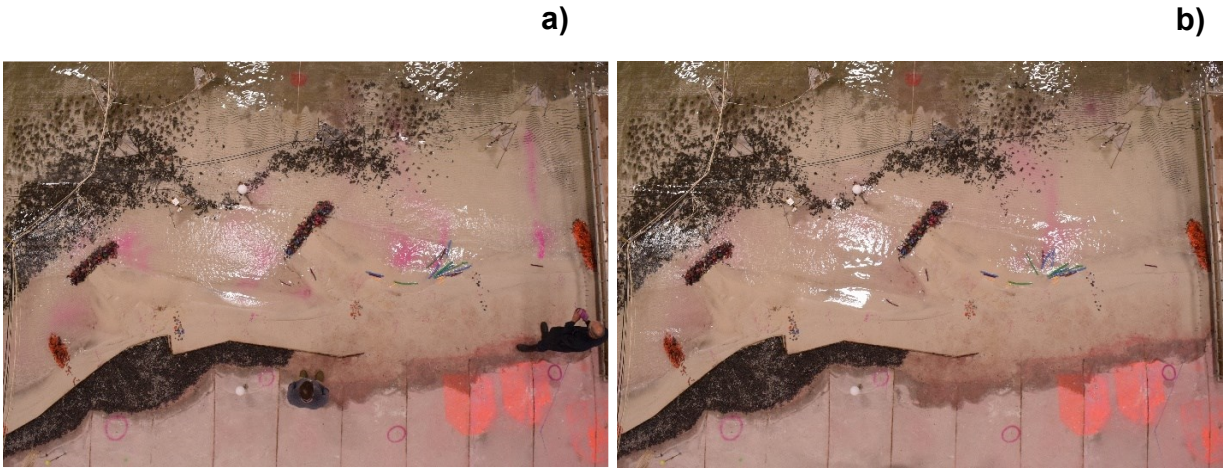

Figure 3-8. Snapshots of dye distributions at a) $t = 0$ and b) $t = 110$ s ($10\,T_p$) during Test Series 12 (layout L2).

3.5 Results and Discussion – Driftwood Mobility

Direct visual observations of the driftwood release experiments revealed four key factors affecting driftwood mobility: (i) sea state and wave-induced circulation; (ii) driftwood length; (iii) driftwood morphology; and (iv) beaching/washoff processes. Details of how these parameters were found to affect driftwood mobility are described in the following paragraphs, with illustrative images from the experiments.

3.5.1 Sea state and wave-induced circulation

In general, more energetic sea states resulted in more rapid transport and dispersion of driftwood in the alongshore direction by littoral processes. The rate of transport increased with significant wave height and peak wave period. The differential transport rates are evident from the photographs shown in Figure 3-9, which show model driftwood (tree branch) positions during two experiments approximately 10 minutes (model time, corresponding to approximately 1 hour at full scale) after release from the updrift position ($t = 0$). These two example experiments were selected as being representative of typical driftwood behaviour observed across the 8-member ensembles. In the experiment with more energetic sea state conditions (TS4), most driftwood has travelled further downdrift (to the bottom of the image).

Figure 3-9. Snapshots (at t = 3286 s) of experiments a) TS2 and b) TS4, illustrating the effects of sea state on driftwood mobility.

Wave-driven circulation was strongly determined by the shoreline configuration relative to the incident waves. Recirculating eddies and rip currents were observed updrift of the groynes and other structures. The movement of driftwood appeared to be governed by a balance between the offshore eddy/rip current forcing and the onshore wave-induced drift. Three distinct cases illustrating this balance were observed: (i) the rip currents ejected driftwood offshore (Figure 3-10a), (ii) direct wave forcing transported driftwood through the rip current and alongshore, and (iii) driftwood became trapped in a shore-perpendicular alignment at the shore, reflecting a balance between forcing by onshore waves and eddy currents (Figure 3-10b).

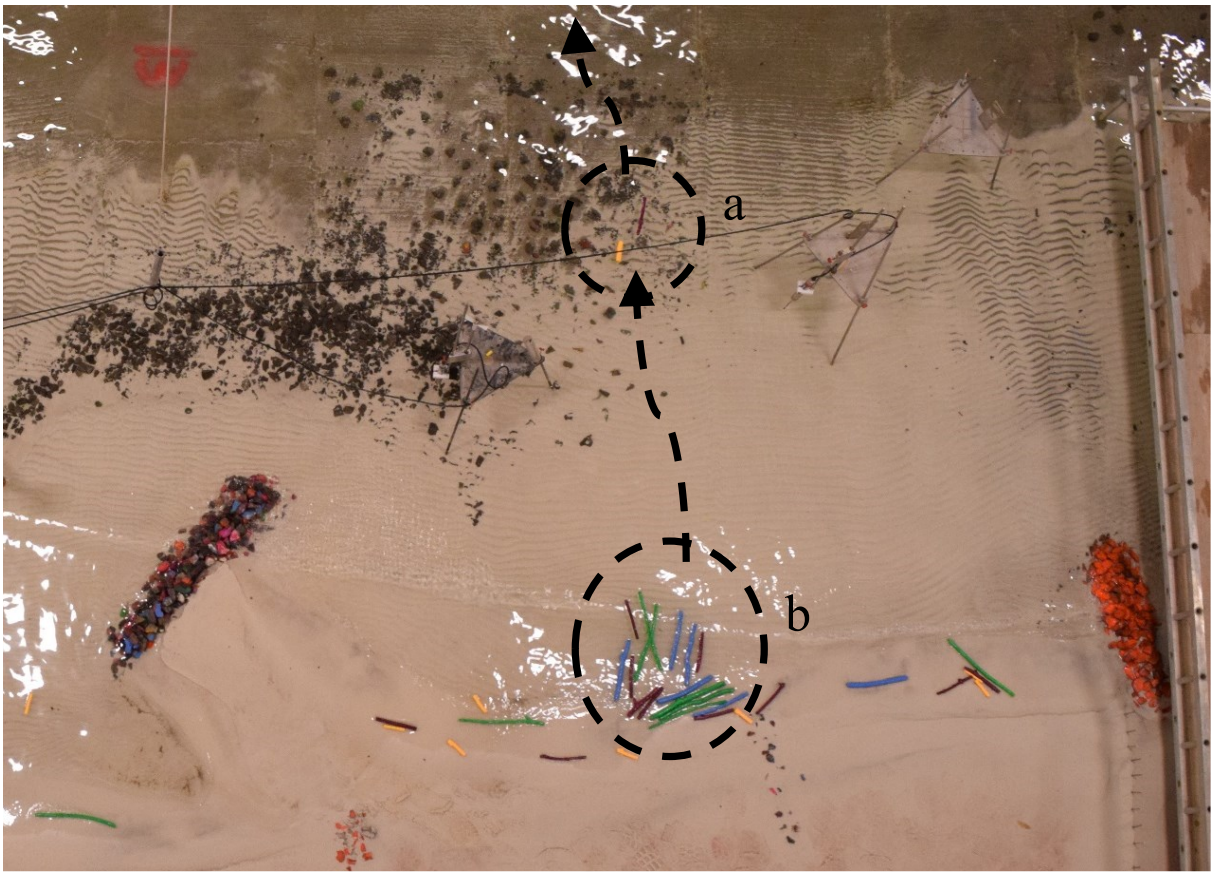

Figure 3-10. Snapshot showing effects of wave-driven circulation on driftwood transport

3.5.2 Driftwood length

Shorter driftwood pieces (particularly the 100 mm length class) were transported more rapidly alongshore by littoral processes (e.g., Figure 3-9).

By contrast to observations of the driftwood response to waves inside the littoral zone, shorter (yellow) driftwood pieces ejected offshore by rip/eddy currents were less likely to be transported back onshore by waves (Figure 3-10a). This is consistent with Newman's (1965) analytical study of wave drift forces on unrestrained, slender floating objects in open water, which showed that wave-induced drift forces decrease with increasing ratios of wavelength to object length (λ/L_P), for $\lambda/L_P > 0.75$. In this range, shorter driftwood pieces are therefore less susceptible to transport by wave drift forces in open water. In cases where driftwood was trapped perpendicular to the shore (Figure 3-10b), the pieces tended to be longer (i.e., 300 mm and 400 mm length classes).

These observations contradict Braudrick & Grant's (2000) hypothesis that driftwood mobility is only strongly influenced by length in small river channels where the driftwood length exceeds the channel dimensions.

3.5.3 Driftwood morphology

The smooth, cylindrical dowels were more mobile than the tree branches (Figure 3-11 and Figure 3-12). Dowels pushed up or deposited on the upper beach by a wave run-up event were more likely to roll back down the beach when impacted by a subsequent run-up event. The tree branch irregularities tended to inhibit rolling on the beach face, requiring higher wave run-up events and floatation of the pieces to cause full remobilization. The reduced mobility of the tree branches compared to the dowels may also be explained by the tilting of driftwood out of the water that occurs when irregularities contact the bed (Braudrick & Grant 2000), and/or embedment of irregularities in the sand. Although these observations indicate driftwood morphology plays an important role in determining mobility, the average density of the tree branches was approximately 13% higher than the dowels, which may have exaggerated the observed differences in model driftwood behaviour.

Figure 3-11. Instantaneous snapshots of driftwood in TS2 ($\eta = 0.35$ m, $H_{m0} = 0.65$ s, and $T_p = 8.0$ s) at $t = 400$ s ($12T_p$) after release, for a) smooth dowels, and b) rough tree branches.

Figure 3-12. Instantaneous snapshots of driftwood in TS6 ($\eta = 0.70$ m, $H_{m0} = 1.20$ s, and $T_p = 6.0$ s) at $t = 1643$ s ($274T_p$) after release, for a) smooth dowels, and b) rough tree branches.

3.5.4 Beaching and washoff processes

Silica sand accumulated around driftwood deposited on the upper beach, or around pieces of driftwood trapped on groyne structures, sometimes resulting in partial burial of the driftwood (Figure 3-13). Driftwood pieces impacted by wave run-up events in quick succession after becoming deposited on the beach were frequently washed off. The longer a piece of driftwood remained beached in areas where sand was mobile and accreting without being remobilized by subsequent wave run-up events, the more sediment tended to accumulate in its vicinity, leading to more stable driftwood deposits. Although the time scales for burial processes were likely distorted by model scale effects, the results suggest that the recurrence, time history and clustering of wave run-up events are important factors controlling the stability of driftwood accumulations on sandy shores, consistent with field observations (Heathfield & Walker, 2011; Eamer & Walker, 2010; Kennedy & Woods, 2012; Grilliot, 2019). Field evidence that partially buried driftwood may be completely exhumed by erosional events (Heathfield & Walker 2011; Grilliot, 2019) were not supported by the experimental data, even for sea states corresponding to extreme storm conditions (TS8).

Figure 3-13. Driftwood partially buried by silica sand.

3.6 Scale Effects and Limitations

The driftwood experiments described above were opportunistic, taking advantage of an existing model, with a short lead time for experimental design. There were a number of limitations and sources of uncertainty, including model scale effects. For example, scaling laws indicate that viscous and surface tension forces were exaggerated in the 1/30 scale model by $O(100)$. Consequently, the kinematics of nearshore wave-driven currents (e.g., the locations of rips and eddies) may not have been representative of prototype conditions, owing to smaller Reynolds numbers in the model compared to the prototype. Inline forces (drag and inertia) on the driftwood, and interstitial flows within matrices of driftwood (rafts or accumulations on beaches), may also have been inaccurately modelled due to viscous scale effects. Reynolds numbers based on the driftwood diameters, and Keulegan-Carpenter numbers, were in ranges where inline forces are strongly dependent on Reynolds number (Sumer & Fredsoe, 2002), so deviations from prototype conditions could have resulted in a poor characterization of driftwood dynamics. Wave motions in shallow waters and wave runup on the shoreline would have been excessively damped by viscous and surface tension effects in the model, potentially under-estimating driftwood mobility and beaching elevations.

The model driftwood material (wood) was essentially the same as the prototype, and thus would have exhibited similar elasticity. However, at model scale, the stiffness characteristics of the driftwood would have been overestimated, incorrectly representing driftwood interactions with other driftwood or structures, breakage/fracturing potential, and wave slamming forces on the driftwood.

For driftwood material densities similar to prototype values, the use of freshwater in the model as a proxy for seawater would underestimate the net buoyancy and thus, the mobility, of the driftwood. However, there is broad variability and time dependency of driftwood buoyancy in the field; owing to factors like water density, wood species/taxa, driftwood volume, proportion of heartwood to sapwood, initial moisture content, degradation and desiccation (Häggblom, 1982; D'Aoust & Millar, 2000; Ruiz-Villanueva et al., 2015; Kramer, 2016). Relative densities for the model driftwood were within ranges corresponding to field conditions, as reported in literature.

The silica sand in the mobile-bed portion of the model was scaled to achieve similar fall velocities to the prototype material, as recommended by Dean (1985) for small-scale modelling of surf-zone sediment transport processes. This resulted in sediment grain diameters that were oversized compared to the prototype, meaning that Shields parameters were distorted. Time scales associated with scour and driftwood self-burial processes, which influenced driftwood mobility, were therefore likely more consistent with larger sediment grain sizes, though, as pointed out by Sumer & Fredsøe (2002), the effect of Shields parameter on scour and self-burial is expected to be weak under the live-bed conditions that are typically prevalent in surf zones. Furthermore, armouring effects have an important influence on scour and self-burial in the vicinity of cylinders (Sumer & Fredsoe, 2002), such that larger sediment grain sizes may underestimate the potential for scour, and self-burial (and therefore likely overestimate the mobility) of driftwood. Using coarser model sediment would also result in steeper beaches (reducing the potential for beaching of driftwood), and exaggerated bedforms. Larger scale physical models, or field experiments, would be required to quantify uncertainty associated with these effects.

3.7 Conclusion

Scale physical model tests were conducted to provide insight to driftwood transport processes in coastal waters under a range of controlled wave and water level conditions. Four key factors affecting driftwood mobility were identified: (i) sea state and wave-induced circulation; (ii) driftwood length; (iii) driftwood morphology; and (iv) beaching/washoff processes. An optical tracking analysis of the experimental data was conducted to provide additional insight to these variables and processes, and to quantify the driftwood mean transport and dispersion characteristics (Chapter 4). The results of the physical model tests were also used to inform the parameterization of important physical processes (e.g., beaching and washoff) in a Lagrangian (numerical) model to predict the fate and transport of driftwood in wave-dominated coastal environments (Chapter 5).

Chapter 4. Optical Tracking Analysis

This chapter is a preprint of a modified version of the following published article:

Murphy, E., Nistor, I., Cornett, A., Rayner, A., Baker, S., & Stolle, J. (2024). Application of an optical tracking technique to characterize nearshore wave-driven transport and dispersion of model driftwood. *Coastal Engineering*, 104481. ttps://doi.org/10.1016/j.coastaleng.2024.104481

Abstract:

Driftwood is abundant in coastal zones, and is increasingly being incorporated in nature-based shore protection and restoration projects. However, accumulations of driftwood, and their mobilization by storms or other disturbances, can pose hazards to coastal communities, infrastructure, and ecosystems. An improved understanding of driftwood dynamics in nearshore, wave-dominated environments is needed to inform sustainable use and management of wood in coastal zones. An optical tracking technique was applied to quantify mean transport and dispersion of driftwood in a 1/30 Froude-scaled coastal model exposed to oblique waves. The results provided new insight to factors controlling driftwood mobility and dispersion on beaches exposed to oblique waves, including the effects of sea state, wave-induced currents and circulation, water levels, driftwood length, driftwood roughness, driftwood buoyancy, and coastal structures.

Keywords: Driftwood; woody debris; physical modelling; optical tracking; dispersion; surf zone.

4.1 Introduction

Driftwood, which consists of logs, tree fragments, and woody debris transported in or over water (Murphy et al., 2021), is abundant in the world's oceans and coastal zones, particularly in northern oceans where boreal forests are a major source (Thiel & Gutow, 2005). Wohl & Iskin's (2021) first order estimate is that 4.7 million m^3 of large wood is delivered to the world's oceans on an annual basis, despite a reduction in supply over the past few centuries resulting from human activities associated with deforestation, damming of rivers, and driftwood removal from rivers and coasts.

Wood in coastal and estuarine systems is widely considered to provide a variety of ecosystem services, including carbon and water storage, habitat, structure, nutrients, fuel, and materials for construction or industry (Rangel-Buitrago et al., 2021; Wohl & Iskin, 2021; Hood, 2023). Despite broad acceptance of the positive role driftwood can play in coastal and estuarine environments, evidence of the ecological benefits of wood for certain fauna, such as threatened or endangered fish species, is limited, inconclusive, and sometimes conflicting (Hood, 2023). Nevertheless, the perceived positive ecological role and benefits of driftwood in coastal systems has led to the increasing utilization of trees, logs, and wood in so-called nature-based shore

protection systems and coastal restoration projects. The application of wood for such purposes can range from coastal forest plantations (Chang & Mori, 2021), loose placement or embedment of logs or root wads on the shore (Bayle et al., 2021; Gates et al., 2018), brushwood dams (Vuik et al., 2019; Provan et al., 2023), and anchored log or large wood installations (Falkenrich et al., 2021; Wilson, 2020). The evidence base surrounding the efficacy of such solutions from a coastal engineering standpoint is also limited, predominantly anecdotal, and sometimes conflicting (Wilson, 2020; Falkenrich et al., 2021; Braun et al., 2022; Elliott et al., 2016). The limited understanding of how driftwood interacts with shorelines is a barrier to incorporating its effects in coastal morphological models (Sherwood et al., 2022), which are often the basis for coastal engineering design. Even if outstanding questions on the ecological and engineering benefits of wood in the coastal zone were settled, there is no evidence-based guidance on effective sizes, types, or quantities of wood for use in coastal restorations (Hood, 2023) or nature-based shore protection systems (Braun et al., 2022).

Large accumulations of driftwood are known to pose hazards to navigation, coastal infrastructure, and communities, particularly when mobilized by storms or other disturbances (Doong et al., 2011; Bula, 2022; Ballard, 2022; Swenson, 2022; Miller et al., 2015; Miller & Rella, 2015; Nistor et al., 2017). In a forensic analysis of engineered shorelines in New York state impacted by three storms, Miller et al. (2015) determined that erosion and scour induced by floating large woody debris was the primary cause of damage at several of the surveyed sites. The costs of managing excessive quantities of driftwood in coastal zones, which typically involves trapping and removal, can be substantial (Doong et al., 2011; Cotana et al., 2016; Miller et al., 2015; Thonon, 2006; Rangel-Buitrago et al., 2021). Large accumulations of driftwood can also damage the natural environment, through physical disruption to benthic ecosystems, compaction of sediments, smothering of vegetation, de-oxygenation of coastal waters, leaching of toxic compounds, and dispersion of invasive species (Edgell & Ross, 1983; Rangel-Buitrago et al., 2021). For these reasons, log removal is often a precursor for tidal marsh restoration (Ducks Unlimited Canada, 2023).

The desire to harness the ecosystem services provided by coastal driftwood, while at the same time managing the risks posed by large accumulations, points to the need for an improved understanding of driftwood dynamics in the nearshore (Murphy et al., 2021). Coastal managers need to understand where and how wood can be beneficially incorporated in nature-based solutions or coastal restoration projects, and in what quantities, without creating or exacerbating physical or ecological risks. In areas where there are known or recurring risks arising from mobile driftwood, knowledge of the processes underlying transport and fate can guide management solutions (such as strategic deployment of booms, fences, or cleanup activities), and coastal engineering design. While driftwood dynamics associated with riverine and tsunami hydrodynamic forcing have been studied extensively, there is scarce information on the mechanisms of driftwood mobilization and transport in nearshore, wave-dominated environments (Murphy et al., 2021; Braun et al., 2022).

As explained in a review by Murphy et al. (2021), physical hydraulic models have provided valuable insight to processes driving fate and transport of driftwood mobilized by rivers (Braudrick & Grant, 2000; Davidson et al., 2015; Schmocker & Hager, 2011; Schmocker & Hager, 2013) and tsunami (Ikeno et al., 2016; Nouri et al., 2010). However, to the authors' knowledge, the first physical modelling investigation of driftwood transport in a coastal, wave-dominated setting is that described by Murphy et al. (2020). Murphy et al. (2020) conducted scale physical model experiments involving point releases of model driftwood in the nearshore of a 1/30 scale coastal model constructed in a wave basin at the National Research Council of Canada's Ocean, Coastal and River Engineering laboratory in Ottawa, Canada, for a range of wave and water level conditions. A qualitative interpretation of the observed driftwood transport patterns revealed four key factors affecting driftwood mobility: (i) sea states and wave-induced circulation; (ii) driftwood length; (iii) driftwood morphology/roughness; and (iv) beaching/washoff processes (Murphy et al., 2020). Here, an image processing technique, adapted from Stolle et al. (2016), is applied to the experimental data to track the model driftwood movement and interactions with the shore, quantifying Lagrangian transport and dispersion characteristics of driftwood in a wave-dominated nearshore setting. To the authors' knowledge, no previous studies have quantified mean transport and dispersion of driftwood in response to nearshore waves. The analysis therefore provides new insight to key factors affecting transport and dispersion rates for driftwood in nearshore, wave-dominated environments.

4.2 Mass Transport and Dispersion in Nearshore, Wave-Dominated Environments

4.2.1 Surf-zone and swash-zone dynamics

A prerequisite for describing driftwood transport in nearshore environments is an understanding of surf zone and swash zone dynamics, and the resulting mass transport. The importance of these topics to coastal engineering practice has driven extensive research since early work on littoral processes and nearshore sediment transport by, for example, Longuet-Higgins & Stewart (1960), Inman & Bagnold (1962), and Longuet-Higgins (1970). Comprehensive reviews and descriptions of surf zone dynamics are provided by Battjes (1988), and Elfring & Baldock (2002). Simply put, wind waves approaching a coast at oblique angles transform (by processes such as shoaling and refraction) and eventually break in response to the bathymetry, and induce currents, wave setup, long waves, and turbulence (Svendsen, 1992). On a long, straight coast exposed to oblique, breaking waves, the induced longshore current represents the balance between radiation stress gradients (Longuet-Higgins & Stewart, 1960), bottom friction, and lateral dispersion (Svendsen, 1992). Currents and circulation in the surf zone are strongly three-dimensional (Putrevu & Svendsen, 1999) with the onshore-directed mass transport by breaking waves being balanced by an offshore-directed undertow (Svendsen, 1992). Under certain circumstances, gradients in breaking wave heights, bathymetric variations, shear instabilities, groynes and coastal structures, or other mechanisms can generate offshore-directed rip currents,

which may extend well beyond the edge of the surf zone (Dalrymple et al., 2011; Castelle et al., 2016; Pattiaratchi et al., 2009; Kennedy & Thomas, 2004; Shepard et al., 1941). Superimposed on Eulerian mean currents is Stokes drift, which contributes to mass transport within and outside the surf zone (Winckler et al., 2013; Pearson et al., 2009; Monismith & Fong, 2004).

Mixing in nearshore, wave-dominated environments is understood to be driven predominantly by shear dispersion associated with the combined effects of: gradients in longshore currents and turbulence, with velocities and diffusivities tending to zero at the shoreline (Longuet-Higgins, 1970; Thornton, 1970); cross-shore circulation caused by breaking waves (Svendsen & Putrevu, 1994) and the vertical non-uniformity of wave-averaged horizontal velocities (Putrevu & Svendsen, 1999); eddies and transient or stationary rip currents driven by a variety of mechanisms (Dalrymple et al., 2011; Feddersen, 2007; Peregrine, 1998; Clarke et al., 2007); variations in forcing that result from random waves breaking at different times and locations (Svendsen & Putrevu, 1994; Thornton & Guza, 1986); turbulent diffusion driven by breaking waves and bores (Feddersen, 2007); and spatio-temporal variations in Stokes drift (Herterich & Hasselmann, 1982). The terms “diffusion” and “dispersion” are used inconsistently in the literature and sometimes conflated. In this paper, turbulent diffusion is reserved for describing mixing by random, turbulent motions, whereas dispersive mixing is understood to include the combined effects of current shear and turbulence.

4.2.2 Lagrangian experiments and techniques in nearshore, wave-dominated environments

Lagrangian dye (tracer) and drifter (drogue) release studies have long been applied to characterize ocean circulation and mixing in open-water settings (Swallow & Worthington, 1957; Okubo, 1971; Davis, 1991; LaCasce, 2008; Lumpkin et al., 2017; van Sebille et al., 2018). Despite logistical challenges in conducting such studies in nearshore environments (Pawlowicz et al., 2019), numerous dye and drifter release studies have been conducted in field and laboratory settings to evaluate circulation, mass transport, and dispersion on wave-dominated coasts. Some of the earliest drifter studies by Shepard et al. (1941) and Shepard & Inman (1950) focused on characterizing nearshore circulation and rip currents in the field, which has remained a topic of active research. Tanaka et al. (1980) reproduced thermal effluent transport and dispersion by irregular waves using a 1/150 scale model in a wave basin, and observed that breaking waves confined the effluent near the shoreline, except where rip currents transported warm water offshore. Schmidt et al. (2003) found that drifters deployed near rip currents were often ejected from the surf zone and transported offshore. Clarke et al. (2007) observed similar transport of dye by offshore-directed rip currents during discrete release experiments conducted on three beaches in California. Pattiaratchi et al. (2009) conducted drifter experiments in the lee of a shore-perpendicular groyne exposed to oblique waves in Western Australia, and characterized the rip currents and recirculating eddies that formed on both the updrift and downdrift sides of the groyne. Higher waves were observed to generate stronger, larger eddies adjacent to the groyne, higher offshore-directed current speeds, and shifted the divergence point on the shoreline away from the

groyne (Pattiaratchi et al., 2009). Kennedy & Thomas (2004) conducted drifter experiments in a laboratory wave basin to investigate rip current dynamics and showed that, for energetic wave conditions inside the surf zone, Stokes drift must be taken into account when comparing velocities inferred from drifters to Eulerian velocity measurements. Castelle et al. (2010) conducted drifter (balloon) releases in a laboratory wave basin, and corroborated observations from the field by MacMahan et al. (2010), finding that approximately 10-20% of drifters caught in rip circulations were ejected from the surf zone.

Methods for characterizing diffusion and dispersion using Lagrangian tracers or drifters have generally relied on evaluating the rate of change of variance (of the tracer concentrations or drifter positions). Dispersion coefficients in the cross-shore and along-shore directions are by definition (List et al., 1990):

$$K_x = \frac{1}{2}\frac{\partial \sigma_x^2}{\partial t} \approx \frac{1}{2}\frac{\Delta \sigma_x^2}{\Delta t}, K_y = \frac{1}{2}\frac{d\sigma_y^2}{dt} \approx \frac{1}{2}\frac{\Delta \sigma_y^2}{\Delta t} \quad (4\text{-}1)$$

where σ_x^2 and σ_y^2 are spatial variances of tracer concentrations or drifter positions in the cross-shore and along-shore directions, respectively, and t is time.

List et al. (1990) used these relationships to evaluate diffusion and dispersion from multiple deployments of six drogues in open coastal waters of southern California, but pointed out that the relationships are only valid for a large number of drogues and under the assumption that any single drogue experiment (realization) is representative of a larger ensemble. The importance of using multiple realizations (i.e., ensemble-based approaches) in Lagrangian studies designed to characterize dispersion coefficients was emphasized (List et al., 1990). Strictly speaking, Equation 4-1 only applies after sufficient time has elapsed such that the variance of a tracer or drifter cloud grows linearly with time and the dispersion coefficient becomes constant (asymptotic), often referred to as the Lagrangian or Fickian time scale (Fischer et al., 1979). This time scale is also representative of the time for a tracer particle or drifter to lose correlation with, or "memory" of, its initial condition (Fischer et al., 1979; LaCasce, 2008; van Sebille et al., 2018).

Takekawa et al. (2003) conducted an instantaneous dye release experiment in a longshore current on the edge of a breaking wave field in Japan, and found that, after a brief initial period, the standard deviation of the dye patch concentration in the alongshore direction, σ_y, grew at a faster rate than the standard deviation in the cross-shore direction, σ_x. Spydell et al. (2007) and Spydell & Feddersen (2009) found similar time-dependent patterns of dispersion from drifter releases in and adjacent to the surf zone on relatively uniform (plane) beaches, with dispersion coefficients in the cross-shore and alongshore directions (referred to as diffusion coefficients by the authors) asymptoting to $K_x = 0.7\text{-}1.5$ m^2 s^{-1} and $K_y = 2\text{-}4.5$ m^2 s^{-1}, respectively. Brown et al. (2009) deployed clusters of drifters near beaches with rip currents in California, and determined asymptotic (long-time) values of $K_x = 0.9\text{-}2.2$ m^2 s^{-1} and $K_y = 2.8\text{-}3.8$ m^2 s^{-1}. By tracking floats exposed to irregular waves ($H_b = 2.2\text{-}5.7$ m, $T = 7.2\text{-}30.6$ s) in a 1/150 scale physical model

within a wave basin, Tanaka et al. (1980) found steady values of K_x = 0.8-20.2 m^2 s^{-1} and K_y = 15.4-73.8 m^2 s^{-1} (prototype) were reached in the surf zone after about 1-2 minutes and 10 minutes, respectively. Jones & Pattiaratchi (2005) deployed five drifters in fifteen clusters outside the surf zone near a river mouth in South Australia and observed enhanced onshore transport when drifters entered the surf zone. Dispersion coefficients were evaluated based on least squares linear regressions of the measured drifter variances plotted against time, yielding $K_x = 0.13 \pm 0.08$ m^2 s^{-1} and $K_y = 0.28 \pm 0.19$ m^2 s^{-1} (Jones & Pattiaratchi, 2005). Mariani & Pattiaratchi (2007) conducted multiple releases of five drifter units at or just outside the breaker line on a beach in Western Australia and found $K_x = 0.935 \pm 0.599$ m^2 s^{-1} and $K_y = 0.965 \pm 0.495$ m^2 s^{-1}. The greater uncertainty in K_x was attributed to variability resulting from a "surfing effect" experienced by buoyant drifters in breaking waves.

Indeed, mass transport characteristics inferred from drifter studies require careful interpretation, and dispersion coefficients inferred from drifters and tracers may differ (Clark et al., 2010). Johnson & Pattiaratchi (2004b) summarized previous studies utilizing drifters to investigate nearshore and surf zone hydrodynamics, and described the surfing effect, whereby surface rollers transport buoyant drifters shoreward faster than the orbital velocities beneath the wave. In their laboratory experiments, Castelle et al. (2010) used balloons to resist this effect. Conversely, Clark et al. (2010) explain that some drifters can "duck" under breaking waves, avoiding entrainment in the bores. Johnson & Pattiaratchi (2004b) also pointed out biases in vertical sampling of velocities by drifters, which, as explained by Feddersen (2007), is one of several reasons why tracers and drifters exhibit different dispersion characteristics in surf zones. These observations are highly relevant to transport of driftwood in breaking environments, given the known influence of driftwood buoyancy on mobility and, most likely, beaching and washoff processes (Murphy et al., 2021). Few drifter studies have given consideration to beaching or grounding processes at the coast (Lumpkin et al., 2012; Pawlowicz, 2021).

A variety of scaling relationships have been proposed for dispersion coefficients associated with wave-driven mixing in nearshore environments. Citing research by Harleman & Ippen (1960), Harris et al. (1963) suggest that surf zone dispersion coefficients may be related to a representative eddy length scale characterized by H_b, the breaking wave height, and the rate of energy dissipation by breaking waves, proportional to $H_b T^{-1}$, yielding $K_x, K_y \sim H_b^2 T^{-1}$. Harris et al. (1963) plotted this relationship using dispersion coefficients evaluated from dye releases in waves on a steep (1:7.5 slope) beach in an outdoor basin, and there appeared to be some correlation. Clark et al. (2010) cited Harris et al.'s (1963) work, and used scaling arguments for bore-induced mixing to propose $K_x \sim H_b^2 T^{-1}$, similar to a relationship proposed later by Chin (2022), which was tested against observations from six continuous tracer release experiments in the surf zone at Huntington Beach, California. The correlation between observed K_x values (in the range 0.5-2.5 m^2 s^{-1}) and $H_s^2 T_m^{-1}$, where H_s is the significant wave height and T_m is the mean wave period, was weak (Clark et al., 2010). Pearson et al. (2009) used theoretical arguments and the results of dye experiments

in a wave basin to support a hypothesis that cross-shore mixing in the surf zone is proportional to $H_b^{2/3}$, although there was some scatter in the experimental data.

All of the tracer and drifter studies described above were designed to investigate nearshore hydrodynamics, or transport of contaminants, solutes, or suspended sediments. For studies involving buoyant drifters, care was often taken to minimize interactions with bores inside the surf zone, or remove surfing effects through post-processing (Jones & Pattiaratchi, 2005). However, these effects may actually be important in the context of driftwood fate and transport in nearshore, wave-dominated environments, considering the known influence of time-dependent buoyancy on long-term driftwood transport (Murphy et al., 2021) (Chapter 2). Driftwood-shore interactions are also likely to be distinctly different from tracer or drogue interactions with the shore, owing to the effects of mass, buoyancy, and geometry (length, width or diameter, roughness). Aside from the qualitative observations by Murphy et al. (2020) (Chapter 3), there are no known previous field or laboratory studies attempting to realistically track transport and dispersion of driftwood in nearshore settings.

4.3 Image Processing

An optical technique, adapted from Stolle et al. (2016) and automated using the MATLAB Image Processing Toolbox, was applied to the images captured by the downward-looking HD camera discussed in Chapter 3, to track the movement and orientation of model driftwood within the basin during experiments conducted by Murphy et al. (2020). The technique involved six steps, summarized as follows:

1. *Image Georectification.* Each image was georectified using a minimum of four surveyed control points located within the basin.
2. *Masking.* Areas within each image where driftwood was unlikely to be detected (e.g., upland areas of the model) were masked and removed to reduce computational effort.
3. *Colour Space Conversion*. The image was transformed to a colour space suited to efficiently differentiating between colours associated with the driftwood and other features or reflections within the basin. The YCbCr colour space described in Stolle et al. (2016) was selected to enable colour thresholding for the blue, green and yellow-coloured driftwood. The Hue-Saturation-Value (HSV) colour space was found to be marginally more suitable and efficient for detecting the maroon-coloured driftwood, due to excessive noise when the YCbCr colour space was applied.
4. *Colour Thresholding.* Image pixels with colour band values lying within pre-defined ranges, selected in advance to match the driftwood paint colours using the Image Tool within the MATLAB Image Processing Toolbox, were flagged as driftwood candidates.
5. *Blob Analysis.* Noise filtering procedures were performed on clusters of pixels flagged during the colour thresholding step, and the properties of pixel clusters (area, aspect ratio)

were analysed to confirm or reject driftwood candidates, to distinguish between touching pieces of driftwood, and to identify relevant driftwood characteristics (centroid, orientation).

6. *Prediction-Correction.* This step was required to preserve the identity of individual driftwood pieces across multiple image frames (i.e., tracking). It involved predicting the centroid location of driftwood pieces using a Kalman filter and then making a correction based on actual detections in the subsequent image capture, using the so-called Hungarian (Munkres) algorithm (Stolle et al., 2016).

4.4 Driftwood Track Analysis

Following application of the optical tracking algorithm, the driftwood centroid tracks were analysed to identify mean transport and dispersion indicators in both the cross-shore (x) and alongshore (y) directions. Mean centroid travel distances, $X(t)$ and $Y(t)$, and variances, $\sigma_x^2(t)$ and $\sigma_y^2(t)$, were computed for each image following a driftwood release using the method described by List et al. (1990) for drifters deployed in coastal waters, i.e.:

$$X(t) = \frac{\sum_{j=1}^{N_d} x_j(t)}{N_d(t)} \tag{4-2}$$

$$Y(t) = \frac{\sum_{j=1}^{N_d} y_j(t)}{N_d(t)} \tag{4-3}$$

$$\sigma_x^2(t) = \frac{\sum_{j=1}^{N_d} \left(x_j(t) - X(t)\right)^2}{N_d(t) - 1} \tag{4-4}$$

$$\sigma_y^2(t) = \frac{\sum_{j=1}^{N_d} \left(y_j(t) - Y(t)\right)^2}{N_d(t) - 1} \tag{4-5}$$

where $N_d(t)$ is the number of driftwood centroids detected using the optical tracking technique, and $x_j(t)$ and $y_j(t)$ are the cross-shore and alongshore co-ordinates of the centroid of driftwood piece j. The time between image captures was used to identify rates of change in both sets of parameters. Ensemble averages of each parameter were computed and are denoted by angle brackets, < >.

Ensemble mean transport velocities in the cross-shore and alongshore directions were evaluated as $\langle X(t = T_d)\rangle/T_d$ and $\langle Y(t = T_d)\rangle/T_d$, respectively. T_d is the time at which the ensemble-average number of driftwood centroids detected, $\langle N_d \rangle$, fell to less than two-thirds of the number of driftwood pieces initially released, N_P, for at least 50 consecutive image captures. This was to exclude data corresponding to later times when a substantial proportion of the driftwood

pieces (nominally one-third, on an ensemble-average basis) were transported outside the camera FOV, resulting in underestimates of the true mean driftwood velocities and variances.

Dispersion coefficients in the cross-shore and along-shore directions were evaluated based on Equation 4-1. For each series of tests, $\langle K_x \rangle$ and $\langle K_y \rangle$ were estimated from least squares linear fits to the ensemble-averaged variances $\langle \sigma_x^2(t) \rangle$ and $\langle \sigma_y^2(t) \rangle$ plotted versus time following the methods described by Jones & Pattiaratchi (2005) and Clark et al. (2010), with forced zero intercepts (i.e., representing a true point release with zero variance). The linear fits were applied to data in the range $t = 0$ to $t = T_d$ only. For some experiments, particularly those involving rough branches (i.e., Test Series 9 to 19) where extensive, prolonged beaching of the model driftwood occurred, T_d was never reached and $\langle K_x \rangle$ and $\langle K_y \rangle$ were determined from linear regressions to the entire variance datasets.

4.5 Results and Discussion

4.5.1 Optical tracking technique

The optical tracking algorithm provided a relatively quick and accurate means to automatically determine driftwood tracks and orientations by length class from the high-resolution digital photographs; both for the smooth, regularly-shaped dowels and the irregularly-shaped tree branches. For reference, generation of driftwood centroid tracks and orientations for the three driftwood length classes over 300-700 frames took approximately 2-5 hours on a Dell® laptop with 16 GB RAM using one core of an Intel® Core™ i9-9880H 2.30 GHz processor. Computation times were highly variable depending on lighting conditions and reflections in the laboratory (which depended on sea state conditions), the number of driftwood pieces in each length (colour) class, and the condition of paint on the driftwood (which degraded during the experiments). It is anticipated that computation times could be further reduced by refining noise filtering parameters, paint colour selections for the driftwood, leveraging parallel processing, or by terminating the process when certain criteria are reached (e.g., driftwood remains beached for a certain length of time, or when a predefined fraction of the driftwood exits the camera FOV).

As explained in Stolle et al. (2016), the error in the centroid position of an individual piece of model driftwood is dependent on the surface area detected using the optical tracking technique. Based on visual inspections of multiple images when selecting thresholds for the present driftwood analysis, errors in thresholding generally resulted when: (i) pixels at the edges of the long axes of the driftwood were in shadow; (ii) pixels in the interior of the blob when obscured by other pieces of driftwood, equipment or turbulent water (e.g., temporary or partial submergence during the passage of breaking wave bores), or when light was reflected on the wet surface of the driftwood; or (iii) in situations where paint had degraded or washed off the model driftwood. Noise filtering procedures generally eliminated potential errors in centroid position for the latter two thresholding error types described above. Only the errors associated with item (i) above had potential to skew the detected centroid position for true positive detections; for example, if one side of the driftwood

was in partial shadow (falling outside the prescribed threshold) and the other was not. However, systematic checks on pixel cluster properties imposed during the blob analysis step of the optical tracking methodology, specifically requiring that at least 80% of the known surface area of a piece of driftwood be detected to constitute a positive detection, limited this error to at most 20% of the longest dimension of the driftwood for true positive detections. This is a conservatively high estimate of the error because visual inspections revealed that thresholding errors were less common at the sharp cut ends of the model driftwood, meaning that 20% of the shortest dimension (diameter) of the driftwood is expected to be a more representative maximum error estimate for true positive detections. For the largest diameter driftwood (~0.8 m prototype), this amounts to an absolute positional error of approximately ±5 mm at model scale (±0.16 m prototype). This is in the same order of magnitude as the positional errors (in two dimensions) in centroid estimates determined for a single, stationary piece of driftwood (shortest length class), evaluated by computing the standard deviation in centroid position over 500 images: ±2.2-2.9 mm (±0.07-0.09 m prototype). Driftwood mean travel distances and standard deviations were typically orders of magnitude greater than these values after exposure to several wave periods, quickly rendering the positional error negligible when assessing mean transport velocities and dispersion coefficients. Failed or false detections likely represent a much greater source of error in computed transport velocities and dispersion coefficients, since they result in centroid positional errors of the same order of magnitude as the camera field-of-view dimensions.

Some challenges with detection of the $L_P = 6$ m driftwood length class resulted from a poor choice of paint colour. The maroon colour selected for this length class was similar to other features within the wave basin, such as reefs and rocks. Consequently, large numbers of pixels were falsely flagged as potential driftwood candidates at the colour thresholding step, resulting in long processing times, high sensitivity of colour thresholds to changes in lighting conditions within the basin, and false or failed driftwood detections. For these reasons, optical tracking of the maroon-coloured driftwood was abandoned, and the analysis hereafter concentrates on the yellow ($L_P = 3$ m), blue ($L_P = 9$ m), and green ($L_P = 12$ m) driftwood pieces, which were not as prone to these effects.

Driftwood centroid detection percentages, $N_d/N_P \times 100$, versus time are shown in panel e) of Figure 4-1**,** Figure 4-2**,** and Figure 4-3 for Test Series 1 and the three driftwood length classes tracked. Similar plots for all 18 test series are provided in Figures A-1 to A-54 in Appendix A. For tests involving smooth dowels (i.e., Test Series 1 to 8), detections were generally highest at the beginning of the experiments, falling over time as driftwood pieces exited the camera FOV. Detections during tests involving rough branches (Test Series 9 to 19) tended to be more stable over time, as the model driftwood was trapped on beaches and structures and retained within the camera FOV. Failed detections sometimes occurred in instances where driftwood was obscured by overlapping pieces, instruments, or reflected light within the wave basin. False positive detections (e.g., as indicated by $N_d/N_P \times 100 > 100$ % in Figure 4-1e were more prevalent for the $L_P = 3$ m driftwood length class, as intense light reflections on the water surface were more easily

confused with the short, yellow-coloured model driftwood pieces by the optical tracking algorithm. However, true positive detection rates for the shorter, yellow-coloured driftwood were also highest because of the stronger colour contrast with other features in the basin, and because the shorter pieces were less prone to being obscured by reflections, driftwood, or instruments. Detection rates were generally lower for the longer (green) driftwood pieces because the colour was not as easy to differentiate from other features in the basin, there were fewer pieces, and they were more likely to be at least partially obscured by reflections, or other pieces of driftwood, or equipment in the basin. The green paint was also more susceptible to removal by abrasion during testing, requiring frequent repainting between tests. Following initial work to identify appropriate colour spaces, select colour band thresholds, and tune image noise filtering parameters, the optical tracking process was heavily automated and detection rates in the initial period following release and disentanglement were mostly greater than 90% for the yellow and blue driftwood, and 60% for the green driftwood (Figures A-1 to A-54 in Appendix A).

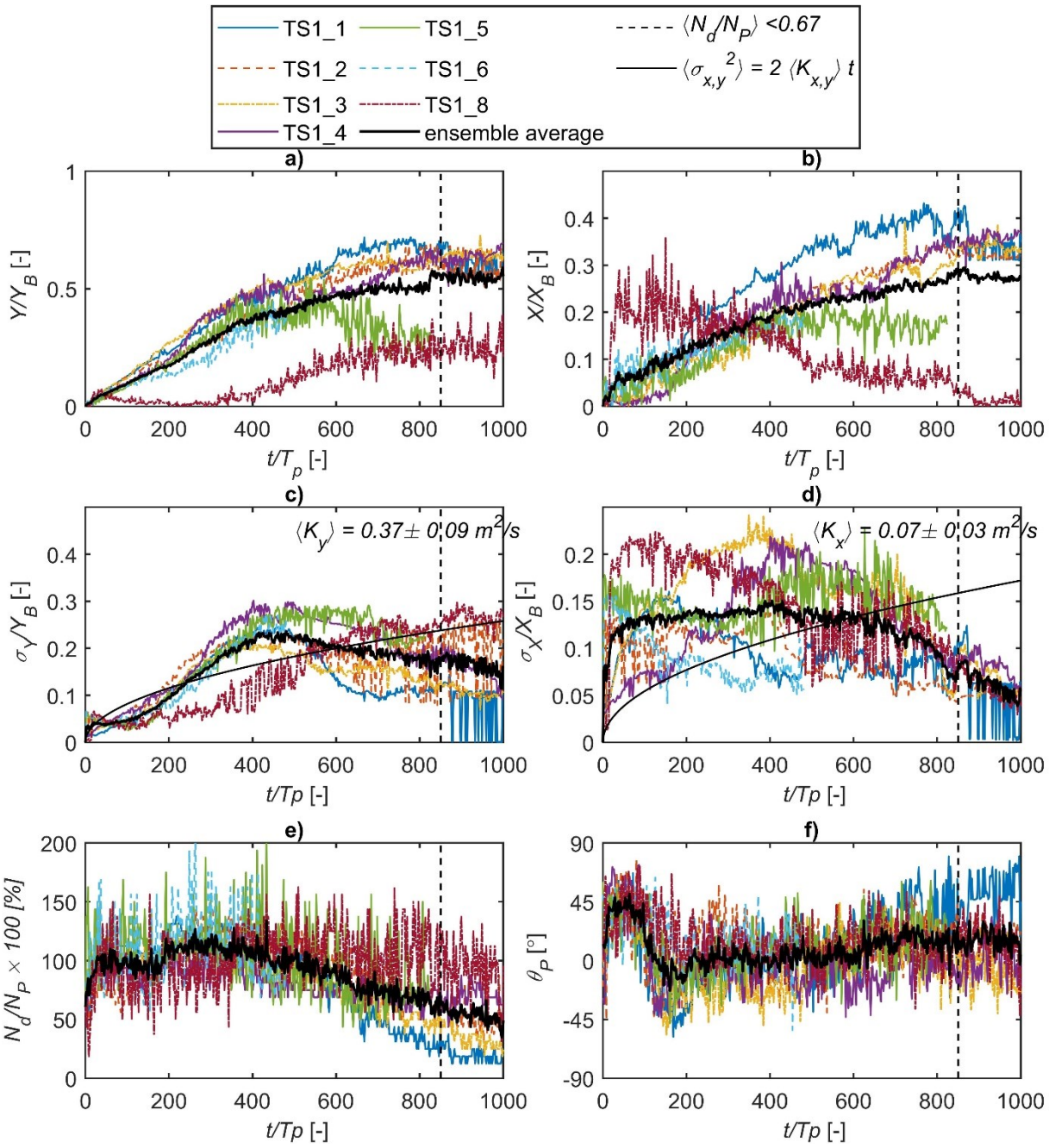

Figure 4-1. a) Mean alongshore relative travel distance, b) mean cross-shore relative travel distance, c) alongshore standard deviation, d) cross-shore standard deviation, e) detection rate, and f) mean orientation versus time for smooth driftwood length class L_P = 3 m (yellow) during test series TS1 (η = 0.35 m, H_s = 0.45 m, T_p = 8 s).

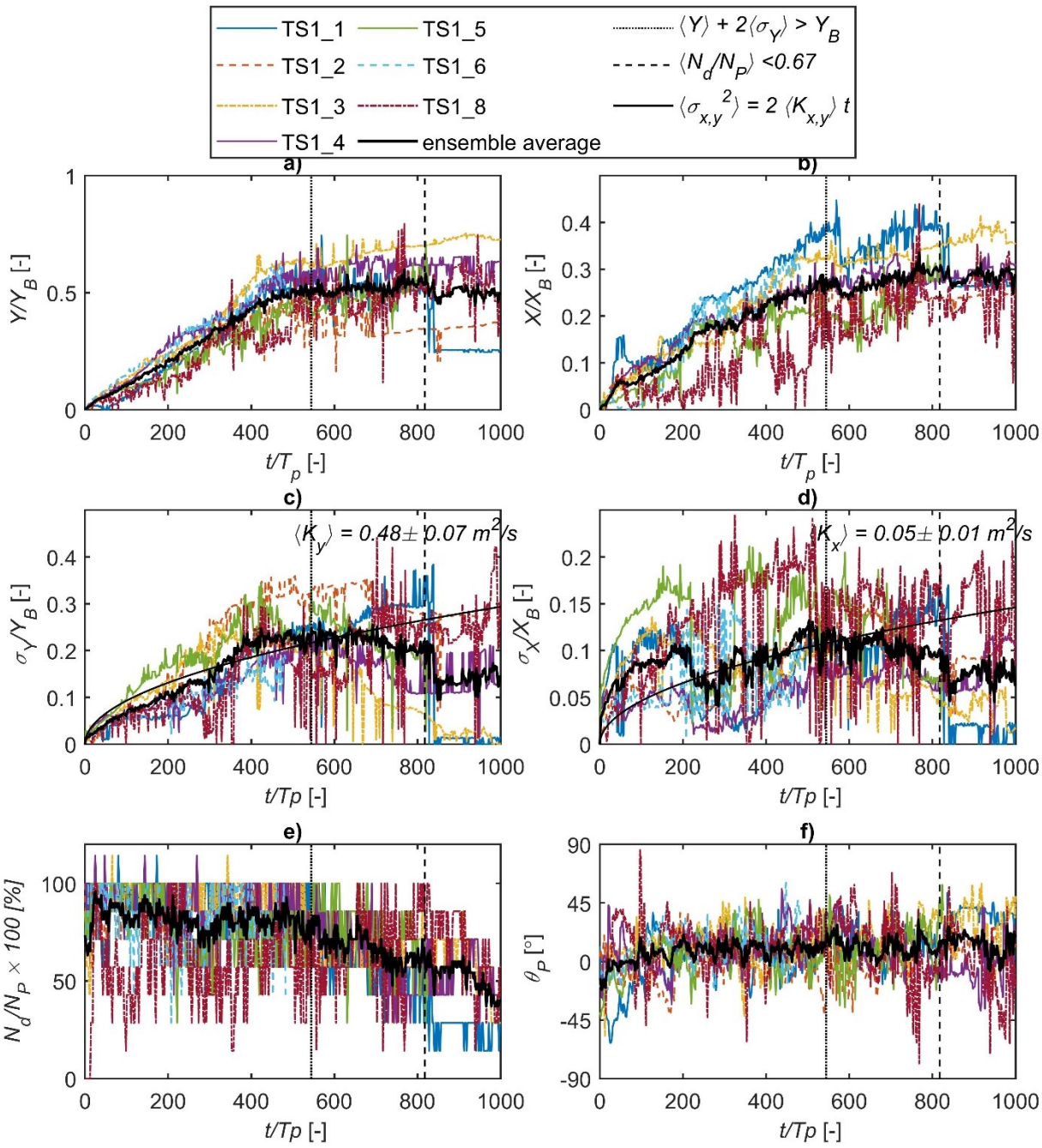

Figure 4-2. a) Mean alongshore relative travel distance, b) mean cross-shore relative travel distance, c) alongshore standard deviation, d) cross-shore standard deviation, e) detection rate, and f) mean orientation versus time for smooth driftwood length class L_P = 9 m (blue) during test series TS1 (η = 0.35 m, H_s = 0.45 m, T_p = 8 s).

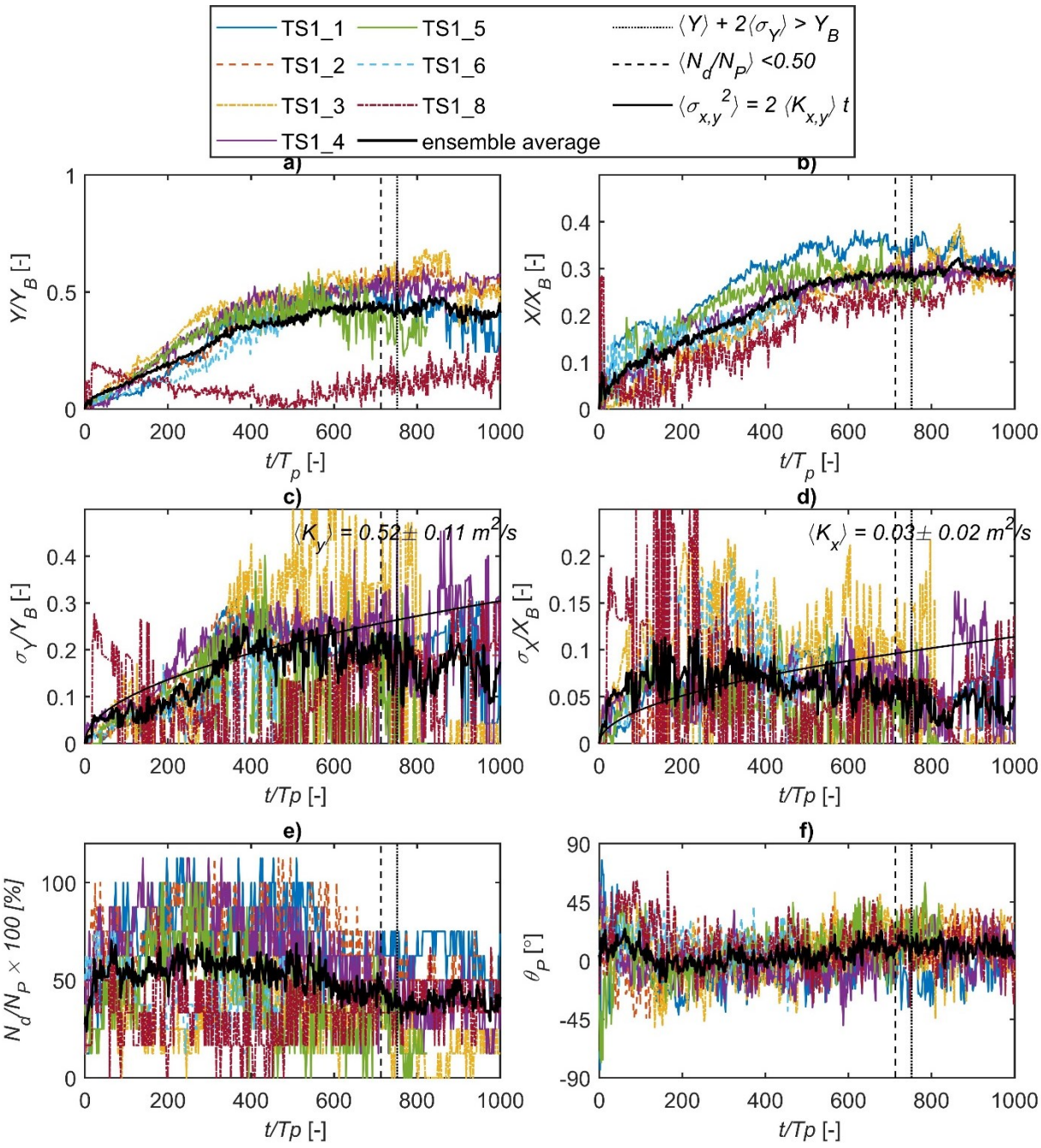

Figure 4-3. a) Mean alongshore relative travel distance, b) mean cross-shore relative travel distance, c) alongshore standard deviation, d) cross-shore standard deviation, e) detection rate, and f) mean orientation versus time for smooth driftwood length class L_P = 12 m (green) during test series TS1 (η = 0.35 m, H_s= 0.45 m, T_p = 8 s).

Benefits of the optical tracking technique were that it allowed for aggregation and statistical analysis of tracks from multiple realizations, and analysis of the behavior of different driftwood size classes for experiments involving the simultaneous release of multiple size classes. For example, the combined centroid tracks from all eight members of the Test Series 3 ensemble are

shown in Figure 4-4, isolated by length class. In this instance, all driftwood length classes followed similar paths, except that shorter pieces were more likely to be transported offshore. Discontinuities in the tracks are evident in areas containing instrumentation and light reflections from the surface of the water, for reasons described above.

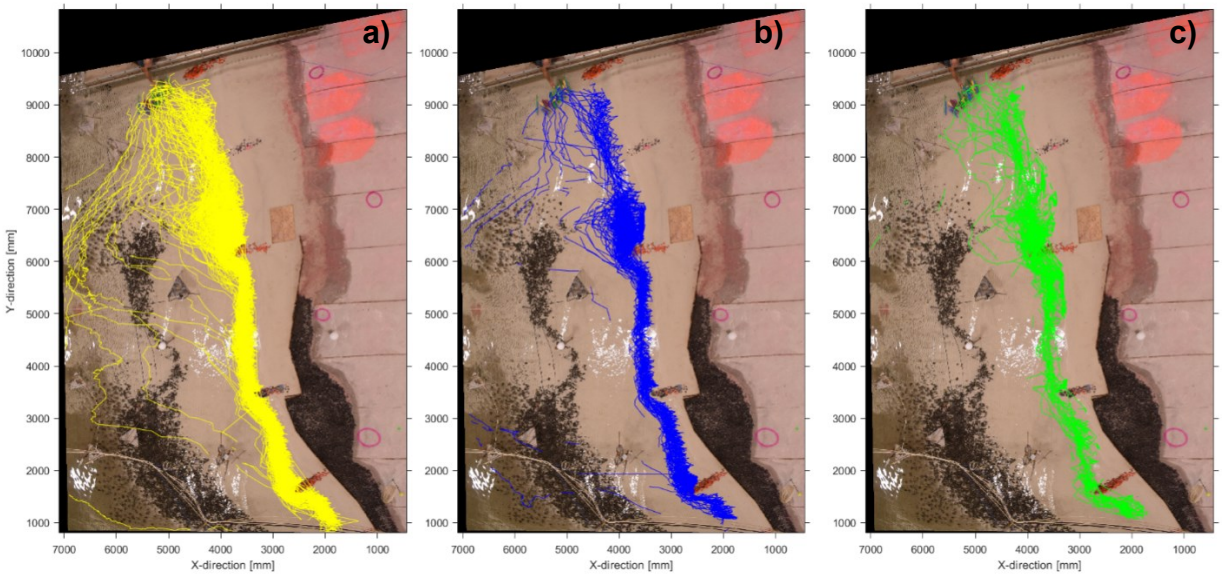

Figure 4-4. Test Series 3 ensemble-aggregated driftwood centroid tracks for a) L_P = 3 m (N_P = 110), b) L_P = 9 m (N_P = 49), and c) L_P = 12 m (N_P = 63) length classes.

4.5.2 Mean driftwood travel distance and speed

Mean alongshore and cross-shore driftwood travel distances versus time are shown in panels a) and b), respectively, of Figure 4-1, Figure 4-2, and Figure 4-3 for Test Series 1 (and in Figures A-1 to A-54 of Appendix A for all 18 test series), and for each of the three driftwood size classes tracked. Travel distances are shown normalized by the camera FOV dimensions in the alongshore and cross-shore directions, Y_B and X_B, respectively. Individual realizations are shown as coloured lines, and ensemble averages are shown as solid black lines. Although the number of realizations in each ensemble (between 5 and 8, as discussed in Section 3.3.3) was limited by the time available to access the experimental facility, an analysis of the Test Series 1 results showed that key driftwood transport statistics (mean alongshore travel distances and variances at $t = T_d$) converged to within 22 % of final values for 5 realizations, and to within 13 % for 6 realizations.

Ensemble-averaged mean driftwood transport velocity components in the cross-shore and alongshore directions, $\langle U_P \rangle$ and $\langle V_P \rangle$, respectively, evaluated at $t = T_d$ (or at the end of the ensemble when criteria for T_d were not met), are listed in Table 4-1. Measured mean current speeds at the two current meter probe locations within the camera FOV, U_{CM2} and U_{CM3}, are listed in Table 3-1 (Chapter 3) for comparison. Mean driftwood transport speeds ($\sqrt{\langle U_P \rangle^2 + \langle V_P \rangle^2}$) were most closely correlated with current speeds measured at current meter CM3, likely because CM3 was closer to the centre of the camera FOV than CM2 and, therefore, more representative of the

flow field experienced by the driftwood. However, the correlation between driftwood transport speeds and U_{CM3} for the two shorter driftwood length classes, $L_P = 3$ m and 9 m, was relatively weak (R^2 = 0.23 and 0.67, respectively, compared to R^2 = 0.86 for $L_P = 12$ m). This may indicate that mean wave-induced currents at the edge of the surf zone are not necessarily representative of mean driftwood transport inside the surf zone, and that other factors such as driftwood interactions with boundaries, Stokes drift, non-uniformities in surf zone circulation, and surfing effects exert control over driftwood mobility.

Table 4-1. Time scales and mean driftwood velocity components.

Test Series	T_d/T_p			$\langle V_P \rangle$ (m s^{-1})			$\langle U_P \rangle$ (m s^{-1})		
	L_P = 3 m (yellow)	L_P = 9 m (blue)	L_P = 12 m (green)	L_P = 3 m (yellow)	L_P = 9 m (blue)	L_P = 12 m (green)	L_P = 3 m (yellow)	L_P = 9 m (blue)	L_P = 12 m (green)
1	850	817	713*	0.026	0.025	0.024	0.009	0.009	0.010
2	1000	836	479*	0.020	0.028	0.035	0.008	0.010	0.014
3	326	432	290*	0.046	0.034	0.046	0.015	0.011	0.017
4	190	125	117	0.071	0.108	0.106	0.026	0.037	0.039
5	113	98	74	0.099	0.113	0.141	0.036	0.039	0.050
6	126	155	142	0.225	0.173	0.185	0.085	0.058	0.063
7	180	224	175	0.072	0.066	0.072	0.029	0.025	0.027
8	40	96	25*	0.283	0.106	0.490	0.130	0.057	0.202
9	259	n/a	n/a	0.043	0.009	0.008	0.019	0.004	0.004
10	n/a	n/a	n/a	0.016	0.018	0.015	0.007	0.007	0.006
11	n/a	n/a	n/a	0.010	0.006	0.005	0.005	0.005	0.005
12	150†	158	n/a	0.039	0.026	0.010	0.017	0.016	0.005
14	n/a	n/a	n/a	0.020	0.016	0.023	0.009	0.007	0.006
15	n/a	n/a	n/a	0.013	0.012	0.016	0.004	0.003	0.004
16	n/a	n/a	n/a	0.020	0.019	0.022	0.008	0.008	0.009
17	n/a	n/a	n/a	0.031	0.023	0.024	0.010	0.009	0.009
18	n/a	n/a	n/a	0.017	0.013	0.011	0.006	0.005	0.005
19	n/a	n/a	n/a	0.042	0.039	0.048	0.016	0.016	0.016

*Note: Criteria for evaluation of T_d was relaxed from $\langle N_d/N_p \rangle < 0.67$ to $\langle N_d/N_p \rangle < 0.5$ for 50 consecutive time steps for these ensembles, due to low average detection rates.

†Note: Criterion for evaluation of T_d was changed from 50 consecutive time steps to 10 consecutive time steps due to false positive detections and higher variability associated with the smaller ensemble size.

4.5.2.1 Layout L1 – shore-perpendicular groynes

Visual inspection of panels a) and b) in Figures A-1 to A-54 reveals that, for experiments involving the smooth dowels (Test Series 1 to 8, refer to Table 3-1 in Chapter 3) and layout L1 (Figure 3-3 in Chapter 3), mean driftwood centroid travel distances tended to increase approximately linearly with time for a short initial period after the release (in the range 50-300T_p depending on sea state conditions), before contact with the first shore-perpendicular groyne at $y \approx 0.4Y_B$ slowed advancement in the alongshore direction, and contact with the shoreline at $y \approx 0.2Y_B$ inhibited cross-shore movement of driftwood. The smooth, cylindrical dowels were observed to roll freely up and down the sandy slope in response to wave run-up and run-down events. Trapping on the groynes was therefore the main mechanism inhibiting alongshore transport of the smooth model driftwood.

The $L_P = 12$ m model driftwood length class (green colour) was slightly longer than the first shore-perpendicular groyne at the still water line (Figure 3-3 – L1), and was therefore not susceptible to prolonged trapping by the groyne. Upon contact with the groyne, one end of the model driftwood tended to remain exposed to waves and currents in deeper water (particularly for experiments at the lower water level, $\eta = 0.35$ m). By contrast, the $L_P = 3$ m and $L_P = 9$ m length classes were shorter than the groyne at the still water line, and were more susceptible to trapping and isolation from the alongshore wave-induced currents. This potentially explains a stronger linear correlation between mean driftwood transport speeds and measured mean current speeds at the two probes for the $L_P = 12$ m length class ($R^2 > 0.94$ for Test Series 1 to 8), compared to the $L_P = 3$ m and $L_P = 9$ m length classes (R^2 = 0.12-0.75).

The effect of peak wave period on mean driftwood transport is illustrated by a comparison of alongshore transport distances with time for two ensembles, Test Series' 2 and 7 (Figure 4-5). The longer periods (T_P = 11 s) result in higher alongshore transport speeds initially, as driftwood migrates onshore (i.e., for $t < 500$ s in Figure 4-5) but converge to similar speeds upon contact with the shoreline, where velocities and diffusivities tend to zero. A similar dependence on water level is illustrated by Figure 4-6, which compares alongshore displacements for Test Series' 3 and 4, presumably because the higher water level condition results in waves breaking closer to the shore, and therefore more energetic conditions at the point of driftwood release. No clear link between offshore significant wave heights (or even the offshore wave energy flux, characterized by $H_s^2 T_p$) and mean alongshore transport was observed, which either suggests that wave breaking is a limiter, or that other factors are more important in controlling mean driftwood transport (e.g., retention on beaches or structures).

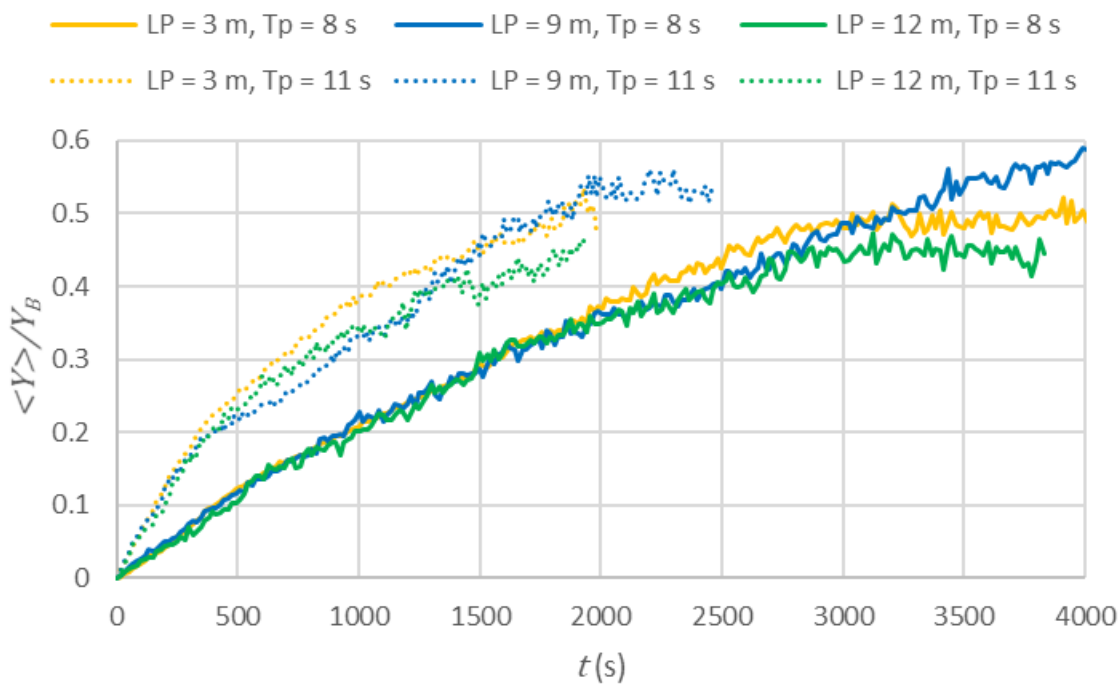

Figure 4-5. Ensemble average alongshore displacements versus time for Test Series' 2 (solid lines) and 7 (dotted lines) (smooth dowels, η = 0.35 m, H_s = 0.65 m).

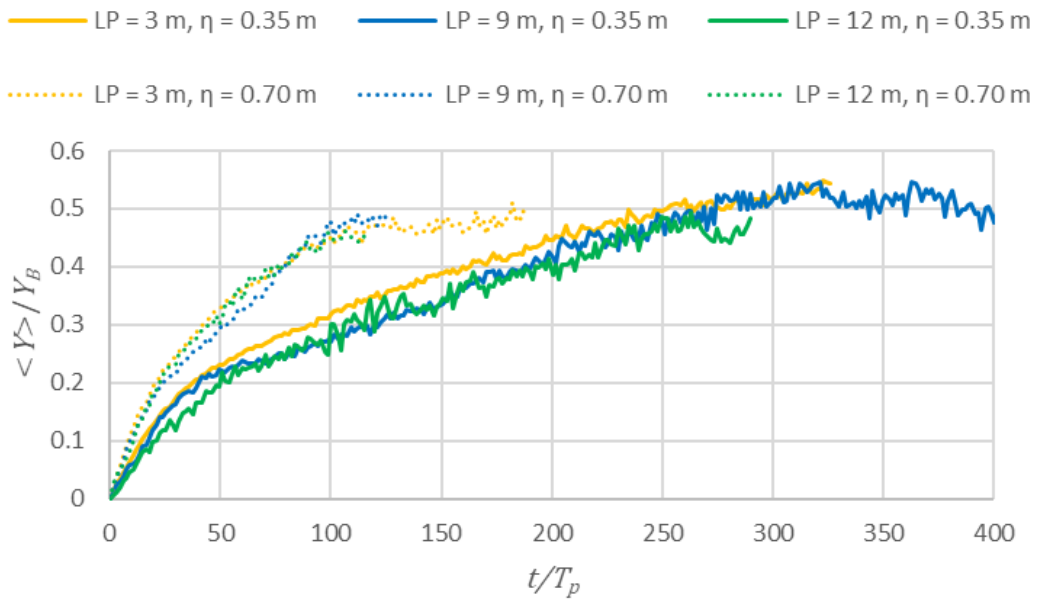

Figure 4-6. Ensemble average alongshore displacements versus time for Test Series' 3 (solid lines) and 4 (dotted lines) (smooth dowels, H_s = 0.65 m, T_p = 11 s).

For given hydrodynamic conditions defined by η, H_s and T_p, the rough model driftwood (tree branches) exhibited consistently lower mean alongshore transport speeds compared to the smooth dowels. Comparisons of $\langle U_P \rangle$ and $\langle V_P \rangle$ for ensemble pairs with identical hydrodynamic

conditions in Figure 4-7 show that driftwood roughness reduced transport velocity components by 40% to 93% (alongshore) and 28% to 92% (cross-shore). The reduction in mean alongshore transport speed associated with roughness was generally proportional to the driftwood length (or inversely proportional to relative roughness). These results indicate that both driftwood length and relative roughness exert control over mean transport by waves on reaches featuring shore-perpendicular groynes. It also suggests that the dominant mechanism of retention on the shoreline can switch between trapping by groynes and beaching, depending on both the roughness of driftwood and the driftwood length relative to the groyne length at the water line.

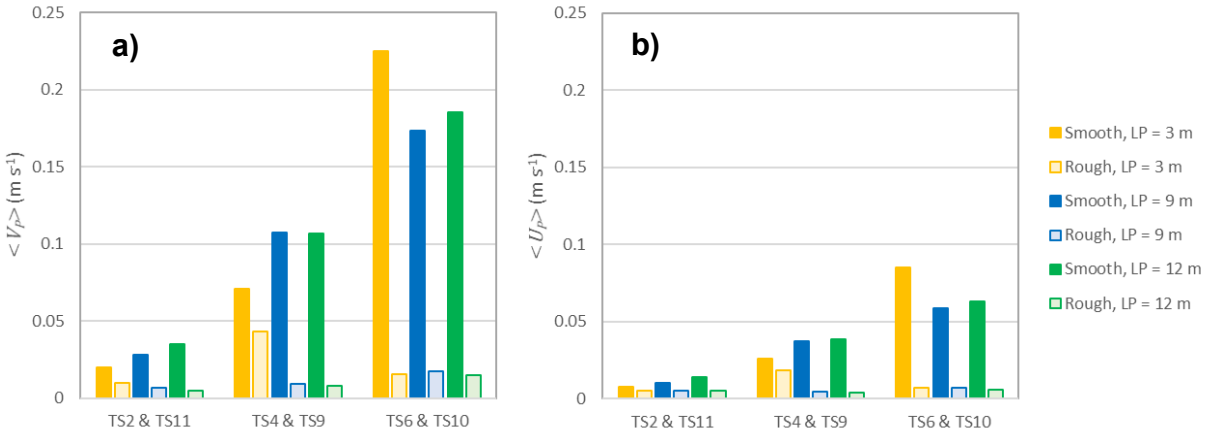

Figure 4-7. Influence of driftwood roughness on ensemble mean driftwood transport velocity components, a) alongshore and b) cross-shore, for ensemble pairs with identical hydrodynamic conditions.

4.5.2.2 Layouts L2, L3, and L4

Ensemble mean driftwood centroid velocity components in the alongshore direction (evaluated consistently at t/T_p = 550) are shown in Figure 4-8 for two sea state conditions and the four different layouts. For the more energetic sea state (η = 0.70 m, H_s = 1.20 m, T_p = 6 s, Figure 4-8b), mean alongshore driftwood transport rates were higher for layouts L3 and L4 (detached breakwaters) than for layouts L1 (shore-perpendicular groynes) and L2 (barrier beaches). This is attributed to the greater physical barrier to alongshore transport presented by the shore-perpendicular groynes and barrier beaches, compared to the detached breakwaters. Alongshore transport rates were higher for L4 (18 m long detached breakwaters) compared to L3 (36 m long detached breakwaters), owing to the greater efficacy of the longer breakwaters in trapping driftwood or slowing alongshore transport in the lee.

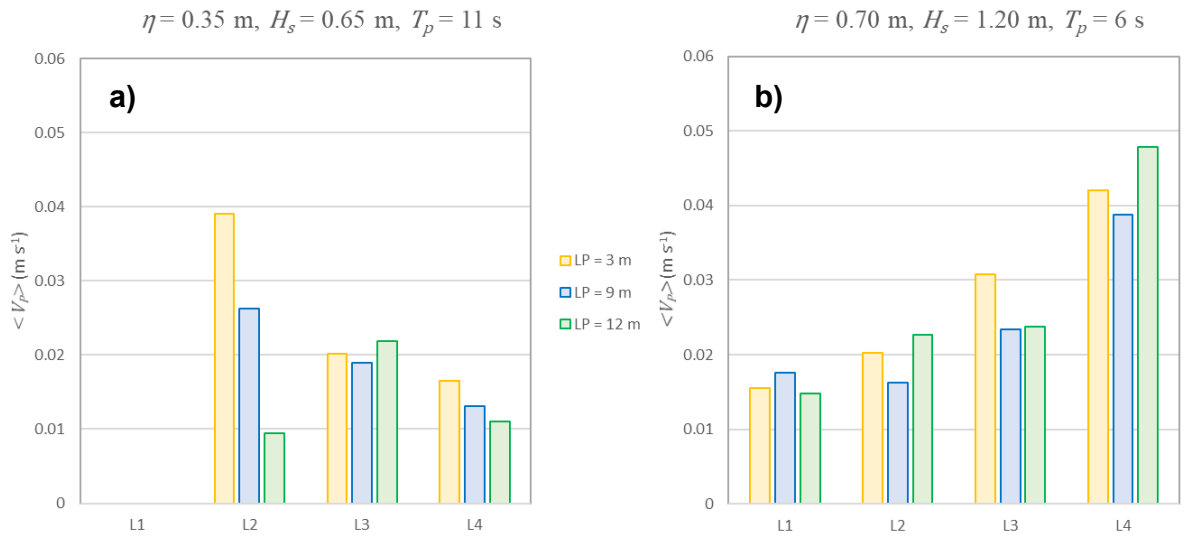

Figure 4-8. Influence of shoreline and structure configuration on ensemble mean alongshore (rough) driftwood transport velocity components, a) alongshore and b) cross-shore, evaluated at t/T_p = 550 for two hydrodynamic conditions.

For the less energetic sea state (η = 0.35 m, H_s = 0.65 m, T_p = 11 s, Figure 4-8a), mean alongshore driftwood transport rates were reduced for the layouts with detached breakwaters (L3 and L4). However, alongshore transport rates for the two shorter driftwood length classes, L_P = 3 m and L_P = 9 m, were higher for L2 (barrier beaches) compared to L3 and L4, and L2 for the more energetic (but shorter period) wave conditions. This is attributed to the strong offshore-directed rip currents that developed in Test Series 12 (η = 0.35 m, H_s = 0.65 m, T_p = 11 s), which transported shorter driftwood pieces around the barrier beach features, whereas longer pieces remained trapped at the point of divergence on the shore (Figure 3-8b in Chapter 3). As explained by Murphy et al. (2020), shorter pieces transported offshore were also less likely to be returned back onshore by waves, owing to the inverse relationship between wave-induced drift forces in open water and wavelength-to-driftwood length ratios (λ/L_P) (Newman 1965). Rip currents were also observed in Test Series 14 (η = 0.70 m, H_s = 1.20 m, T_p = 6 s) but driftwood was predominantly driven onshore by breaking waves, and the points of divergence of the rip currents were closer to the barrier beaches, resulting in tighter eddies that were less likely to transport driftwood offshore and around the features. This appears to contrast with Pattiaratchi et al.'s (2009) drifter-based field observations that higher waves resulted in larger, stronger eddies adjacent to groynes. However, it is noted that Pattiaratchi et al.'s (2009) drifters were specifically designed to resist surfing effects, whereas the model driftwood in this study was not. For buoyant driftwood in surf zones with rip currents, it appears that mobility may be governed by a balance between offshore-directed currents, onshore-directed transport by breaking waves and Stokes drift, and stabilizing interactions with the shore or structures.

4.5.3 Driftwood dispersion coefficients

Dispersion coefficients based on ensemble-averaged driftwood centroid variances in the alongshore and cross-shore directions for each test series are listed in Table 4-2. Error estimates shown are standard errors based on the linear fits to ensemble-averaged variances versus time.

Ensemble average alongshore dispersion coefficients were significantly correlated (two-tailed *t*-test with a significance level $\alpha = 0.05$) with cross-shore dispersion coefficients for all three driftwood size classes. However, the strength of the correlation varied with driftwood length, from weak for the $L_P = 3$ m size class ($R^2 = 0.37$) to strong for the $L_P = 12$ m size class ($R^2 = 0.83$). The correlation coefficient for the $L_P = 3$ m driftwood length class was negatively impacted by a single outlier ensemble (Test Series 12) which exhibited substantial variability in cross-shore variances between realizations (contributing to uncertainty in $\langle K_x \rangle$), depending on whether the driftwood was transported offshore by rip currents. When this data point was removed, the correlation coefficient increased from $R^2 = 0.37$ to $R^2 = 0.71$. Alongshore dispersion coefficients were typically an order of magnitude higher than cross-shore dispersion coefficients, which is consistent with many field observations of drifters in nearshore areas (Mariani & Pattiaratchi, 2007; Jones & Pattiaratchi, 2005; Spydell et al., 2007; Spydell & Feddersen, 2009; Brown et al., 2009).

4.5.3.1 Layout L1 – shore-perpendicular groynes

There was statistically significant ($\alpha = 0.05$) correlation between ensemble average alongshore dispersion coefficients and $H_s^2 T_p^{-1}$ (resembling the $K_y \sim H_b^2 T_b^{-1}$ scaling proposed by Harris et al. (1963) and the $K_y \sim H_s^2 T_m^{-1}$ relationship explored by Clark et al. (2010)) for the smooth dowel experiments, with $R^2 = 0.94$, 0.71, and 0.93 for the $L_P = 3$ m, 9 m, and 12 m driftwood length classes, respectively (Figure 4-9a). These correlations were sensitive to the Test Series 8 outlier data points (Figure 4-9b), which corresponded to the most energetic sea states investigated (Table 3-1). Correlation coefficients (R^2 values) decreased to 0.65, 0.57, and 0.58, respectively, when Test Series 8 data points were removed from the linear regressions. R^2 values also decreased when the three experiments with rough driftwood were included in the analysis, to 0.88, 0.59, and 0.83, respectively. This suggests that driftwood roughness and resulting interactions with the shore exert some influence on alongshore dispersion. The effect of driftwood roughness was to reduce ensemble average alongshore dispersion coefficients by 37-90% (Figure 4-10a). A similar effect of roughness on cross-shore dispersion was observed, with coefficients reduced by 22-96% compared to experiments with smooth dowels (Figure 4-10b).

Table 4-2. Dispersion coefficients.

Test Series	$\langle K_y \rangle$ ($m^2\ s^{-1}$)			$\langle K_x \rangle$ ($m^2\ s^{-1}$)		
	L_P = 3 m (yellow)	L_P = 9 m (blue)	L_P = 12 m (green)	L_P = 3 m (yellow)	L_P = 9 m (blue)	L_P = 12 m (green)
1	0.37 ± 0.09	0.48 ± 0.07	0.52 ± 0.11	0.07 ± 0.03	0.05 ± 0.01	0.03 ± 0.02
2	0.35 ± 0.08	0.23 ± 0.05	0.56 ± 0.05	0.02 ± 0.01	0.02 ± 0.01	0.04 ± 0.01
3	0.60 ± 0.07	0.61 ± 0.07	0.85 ± 0.07	0.08 ± 0.03	0.06 ± 0.02	0.05 ± 0.01
4	1.09 ± 0.07	1.19 ± 0.09	1.04 ± 0.09	0.09 ± 0.02	0.09 ± 0.03	0.08 ± 0.03
5	1.51 ± 0.10	1.33 ± 0.18	1.65 ± 0.19	0.15 ± 0.08	0.09 ± 0.02	0.10 ± 0.03
6	2.06 ± 0.10	1.93 ± 0.22	2.18 ± 0.17	0.15 ± 0.02	0.13 ± 0.04	0.14 ± 0.02
7	0.99 ± 0.11	0.77 ± 0.10	0.74 ± 0.07	0.18 ± 0.04	0.07 ± 0.02	0.10 ± 0.03
8	5.73 ± 0.62	2.83 ± 0.39	5.11 ± 0.78	0.26 ± 0.05	0.10 ± 0.02	0.20 ± 0.06
9	0.53 ± 0.14	0.14 ± 0.03	0.10 ± 0.04	0.07 ± 0.06	0.00 ± 0.00	0.00 ± 0.00
10	0.36 ± 0.10	0.21 ± 0.07	0.40 ± 0.08	0.02 ± 0.01	0.01 ± 0.00	0.01 ± 0.00
11	0.19 ± 0.06	0.07 ± 0.03	0.09 ± 0.03	0.01 ± 0.00	0.00 ± 0.00	0.00 ± 0.00
12	0.53 ± 0.06	0.25 ± 0.05	0.03 ± 0.02	0.30 ± 0.13	0.06 ± 0.04	0.01 ± 0.01
14	0.35 ± 0.05	0.15 ± 0.04	0.18 ± 0.06	0.01 ± 0.01	0.01 ± 0.00	0.01 ± 0.00
15	0.25 ± 0.03	0.09 ± 0.02	0.09 ± 0.03	0.01 ± 0.00	0.01 ± 0.00	0.01 ± 0.00
16	0.49 ± 0.11	0.28 ± 0.05	0.20 ± 0.05	0.02 ± 0.01	0.01 ± 0.01	0.00 ± 0.00
17	0.61 ± 0.19	0.44 ± 0.10	0.37 ± 0.08	0.03 ± 0.01	0.01 ± 0.00	0.01 ± 0.00
18	0.43 ± 0.07	0.10 ± 0.03	0.24 ± 0.03	0.02 ± 0.01	0.00 ± 0.00	0.01 ± 0.00
19	1.20 ± 0.30	0.68 ± 0.08	0.96 ± 0.07	0.05 ± 0.01	0.02 ± 0.01	0.02 ± 0.00

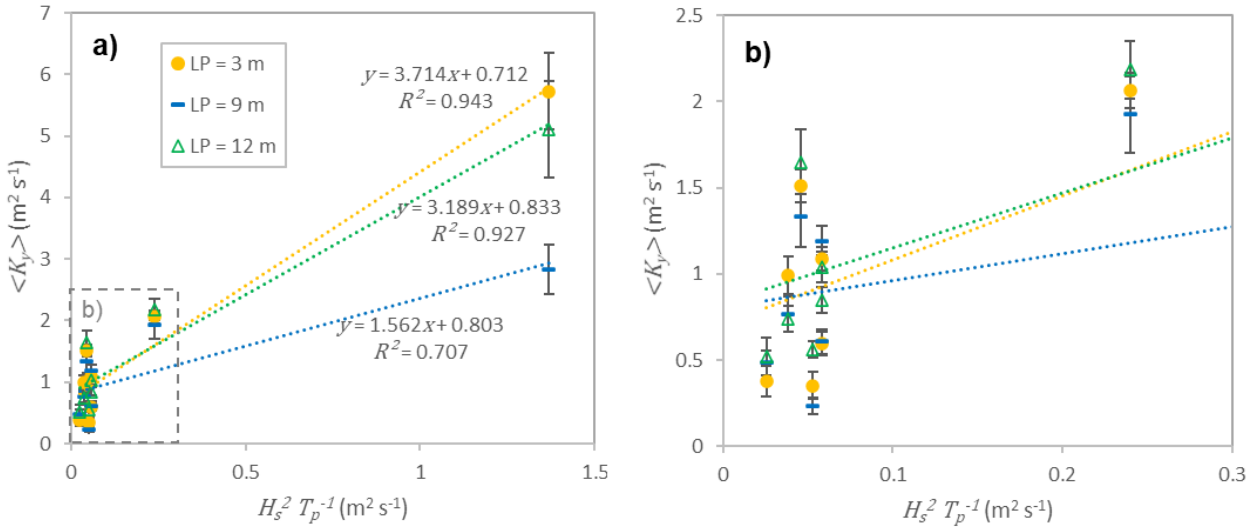

Figure 4-9. Ensemble average alongshore dispersion coefficients versus $H_s^2 T_p^{-1}$ for a) all smooth-dowel experiments, and b) smooth-dowel experiments with $H_s^2 T_p^{-1} < 0.3$. Error bars represent standard errors in dispersion coefficients based on linear fits to ensemble-averaged variances versus time.

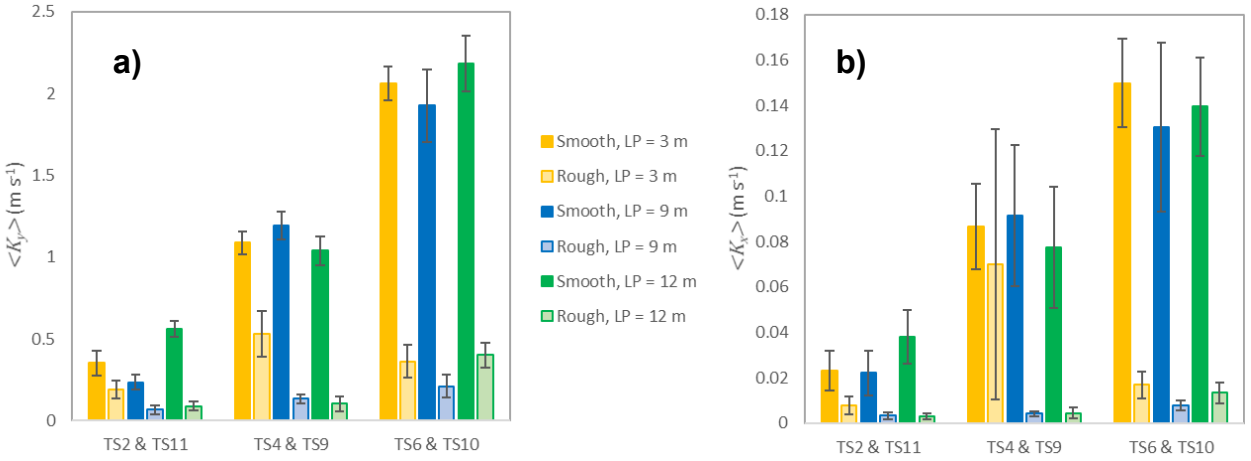

Figure 4-10. Influence of model driftwood roughness on a) alongshore dispersion coefficients, and b) cross-shore dispersion coefficients. Error bars represent standard errors in dispersion coefficients based on linear fits to ensemble-averaged variances versus time.

Driftwood roughness had a lesser influence on dispersion coefficients for the short driftwood length class ($L_P = 3$ m) than for the $L_P = 9$ and 12 m classes. This aligns with observations that rough branches in the $L_P = 3$ m class were less prone to becoming stranded on the sand beaches. The dependence of driftwood beaching and remobilization on both driftwood length and roughness is supported by force balance considerations (Braudrick & Grant, 2000), where the stabilizing friction force at the driftwood-beach interface is proportional to both a coefficient of friction (which depends on roughness of the driftwood and beach material) and L_P.

The general effect of roughness was to cause driftwood to become deposited and trapped in "dead zones" on the shoreline. The observed decreases in dispersion coefficients with roughness were therefore somewhat counterintuitive, since the effect of dead zones is generally to enhance dispersion (Valentine & Wood, 1977; Nepf et al., 1997). The opposite effect (i.e., reduced driftwood dispersion with roughness) observed here may be associated with the prolonged beaching and overall decrease in mobility that was observed (Figure 4-7). In other words, for the experiments with rough branches, beaching of driftwood dominated (and restricted) alongshore transport and dispersion. This is in contrast to the smooth dowel experiments, where beaching was minimal, trapping of shorter pieces by shore-perpendicular groynes weakly constrained alongshore transport or was limited to shorter pieces (see Section 6.3.1), and dispersion was correlated with nearshore hydrodynamic conditions. Considering the observed dependence of dispersion coefficients on both length and roughness, it is possible that experiments with a wider range of driftwood roughnesses and length class gradations could have yielded more variable interactions with the shoreline, and potentially enhanced dispersion for some conditions.

4.5.3.2 Layouts L2, L3, and L4

Alongshore dispersion coefficients for two hydrodynamic conditions are shown in Figure 4-11 to illustrate the effect of the different shoreline configurations (layouts) on dispersion. For the more energetic sea state (η = 0.70 m, H_s = 1.20 m, T_p = 6 s), alongshore dispersion coefficients were higher for layouts L3 and L4 (detached breakwaters) than for layouts L1 (shore-perpendicular groynes) and L2 (barrier beaches) (Figure 4-11b). This is interpreted as a consequence of driftwood trapping by the shore-perpendicular groynes and barrier beaches.

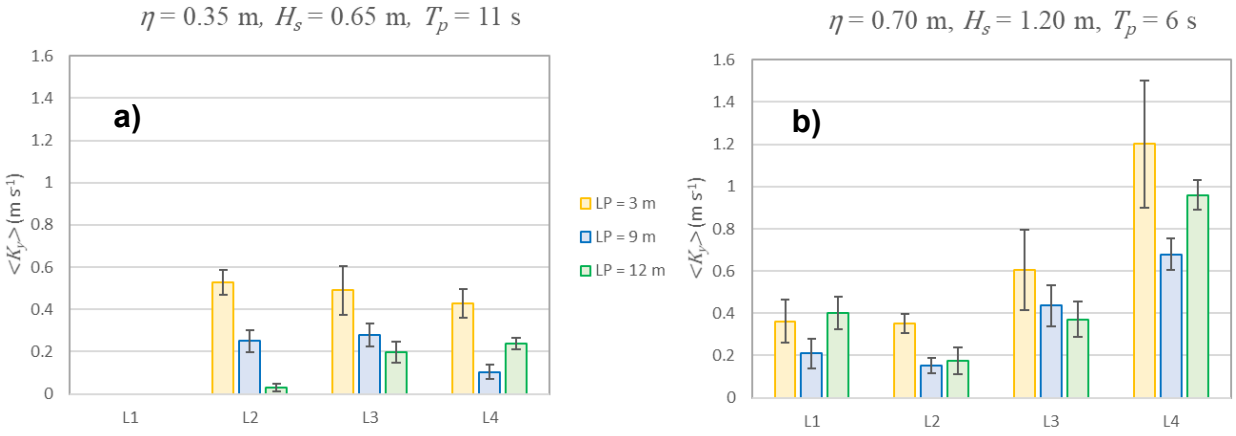

Figure 4-11. Influence of shoreline and structure configuration on ensemble mean alongshore driftwood dispersion coefficients (rough driftwood) for two hydrodynamic conditions. Error bars represent standard errors in dispersion coefficients based on linear fits to ensemble-averaged variances versus time.

For the less energetic sea state (η = 0.35 m, H_s = 0.65 m, T_p = 11 s), alongshore dispersion coefficients for layout L2 were comparable to those for layouts L3 and L4 (Figure 4-11a) because offshore-directed rip currents transported driftwood (particularly the shortest length class) around

the barrier beaches (see discussion in Section 6.3.2). This effect is also reflected in the cross-shore dispersion coefficients for the $L_P = 3$ m class, which were an order of magnitude higher for layout L2 than L3 and L4 under these hydrodynamic conditions (Figure 4-12a).

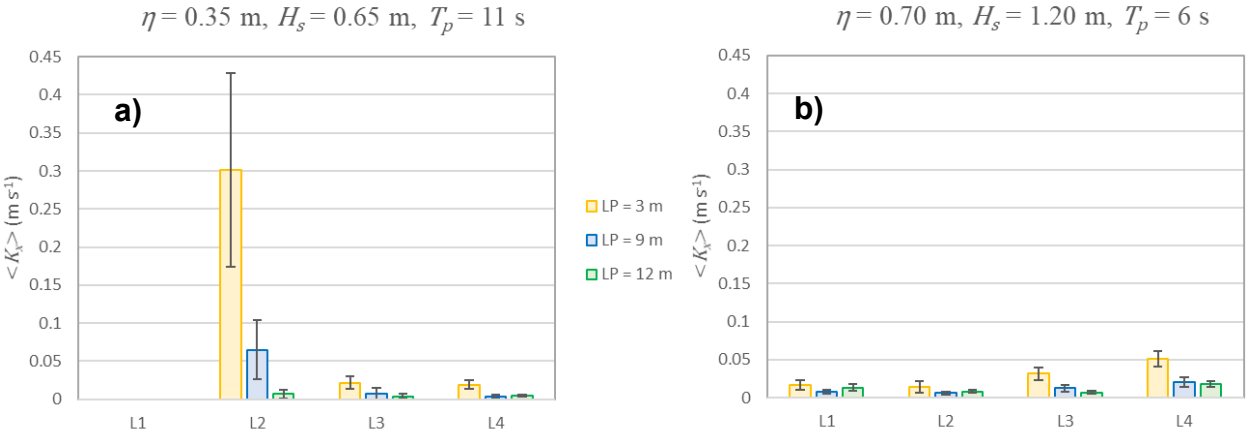

Figure 4-12. Influence of shoreline and structure configuration on ensemble mean cross-shore driftwood dispersion coefficients (rough driftwood) for two hydrodynamic conditions. Error bars represent standard errors in dispersion coefficients based on linear fits to ensemble-averaged variances versus time.

4.5.4 Driftwood orientations

After a period in each experiment when driftwood orientations were controlled by the initial conditions of the release (typically, $t/T_p \lesssim 50$ to 100), orientations tended towards $-45° < \theta_P < 45°$ (i.e., approximately shore parallel), as pieces made contact with the shore (Figures A-1f to A-54f). Variability in θ_P was reduced for experiments involving rough branches compared to those with smooth dowels (e.g., compare Figures A-4f and A-31f), due to the greater tendency for the rough driftwood to become beached and stranded in a shore-parallel orientation. Variability in θ_P was generally increased for layout L2 (Figures A-34f to A-42f), as rotational eddies and rip currents induced by the barrier beach features caused driftwood pieces to be trapped in shore-perpendicular orientations and transported offshore (Figure 3-8 and Figure 3-10 in Chapter 3).

4.6 Conclusion

An optical image processing technique was used to generate and analyze driftwood tracks from experiments by Murphy et al. (2020) in a 1/30 scale physical model of a coastal reach containing sandy beaches and various structures exposed to oblique waves. The results of the quantitative analysis verified Murphy et al.'s (2020) observations (Chapter 3), and further elucidated key factors affecting driftwood mobility, namely:

1) *Sea state and wave-induced circulation.* Sea state conditions only govern driftwood transport to the extent that mobility is not constrained by interactions with beaches or structures. Under conditions where driftwood-shore interactions do not severely restrict transport (i.e., smooth

driftwood), alongshore dispersion coefficients are strongly correlated with $H_s^2 T_p^{-1}$, consistent with scalings derived from previous field and laboratory studies with drifters. The vertical profile of wave-induced horizontal velocities in the surf zone is an important factor controlling driftwood interactions with the shore, as predominantly onshore-directed surface currents push buoyant driftwood towards land (see discussion of buoyancy below). Where wave-structure interactions induce offshore-directed rip currents, mean transport and dispersion of buoyant driftwood is governed by balances between the strength of the rip current, onshore-directed transport by breaking wave bores and Stokes drift, and stabilizing friction at the driftwood-beach interface.

2) *Water levels.* Water levels exert control on driftwood transport through their influence on depth-induced wave breaking and wave-induced circulation, as well as by controlling the length of shore-perpendicular structures at the water line, which affects their capacity to trap driftwood transported alongshore.
3) *Driftwood length.* Driftwood length exerts control over mean transport and dispersion through its influence on:
    a) Beaching – longer driftwood has greater capacity to mobilize stabilizing friction forces during contact with beach faces;
    b) Trapping by shore-perpendicular structures – driftwood pieces that are longer than groynes or other physical barriers to littoral transport at the water line are less likely to be trapped by those structures; and
    c) Wave-induced drift forces in open water – longer driftwood pieces are more susceptible to onshore transport by wave-induced drift.
4) *Driftwood roughness.* For the two driftwood types studied (smooth dowels and rough tree branches), roughness was found to inhibit mean transport and dispersion of driftwood through its influence on beaching, particularly for longer driftwood pieces that had larger contact interfaces with beaches. It is hypothesized that intermediate driftwood roughnesses (i.e., between the limits investigated) and/or a wider range of driftwood length distributions could lead to more variability in driftwood-beach interactions and enhanced dispersion.
5) *Driftwood buoyancy.* The time-dependent buoyancy of driftwood is known to be a key factor influencing mobility over multi-year timeframes and oceanic spatial scales (Murphy et al., 2021). However, buoyancy also influences driftwood transport in the surf zone at smaller spatio-temporal scales, by exposing driftwood to breaking wave bores at the water surface, and controlling contact with the beach. For these reasons, care should be taken when attempting to infer mean driftwood transport and dispersion characteristics in the surf zone from drogue and tracer studies, particularly since drogues are often designed to resist the surfing effects that may dominate driftwood transport in the nearshore.

These new insights to factors affecting driftwood mobility in nearshore areas exposed to oblique waves may help to guide wood use and management in coastal zones, e.g., by informing the identification of potential hot spots, coastal engineering and nature-based infrastructure design to prevent excessive accumulation of driftwood, and design of traps for efficient wood removal or

storage (Chapter 6). The experimental data was also used to support the development and validation of numerical models to predict driftwood fate and transport in coastal environments (Chapter 5).

Chapter 5. Numerical Driftwood Model

This chapter is a preprint of a modified version of the following article under review by the Journal of Waterway, Port, Coastal, and Ocean Engineering (American Society of Civil Engineers):

Murphy, E., Cornett, A., Nistor, I., & Pilechi, A. (2024). Development and experimental validation of a Lagrangian particle-tracking model to simulate wave-driven transport of coastal driftwood.

Abstract:

Wood is a natural feature on beaches, and can contribute to healthy coastal ecosystem function. However, large quantities of driftwood and woody debris mobilized by storm waves pose hazards to coastal communities, infrastructure and valued assets, including sensitive ecosystems. Predictive numerical tools are needed to guide assessment and management of the associated risks, and to identify opportunities to leverage the benefits of driftwood on the coast. Models developed to predict driftwood fate and transport in rivers or by tsunami do not incorporate the effects of wind waves, surf-zone processes, or the wave-driftwood-shore interactions that exert important controls on coastal driftwood dynamics. Lagrangian transport models, developed to simulate oil spill trajectories and marine debris transport at oceanic scales, typically do not resolve beaching and washoff processes, despite sensitivity to these mechanisms. Here, a novel Lagrangian model for simulating coastal driftwood transport by waves, which includes a computationally-efficient, dynamics-based beaching and washoff algorithm, was developed and compared to observations from a previous experimental study by the authors. Hydrodynamic forcing by two "state-of-the-art" phase-resolving, non-linear shallow water equations solvers (XBeach and SWASH) reveals that driftwood dynamics are sensitive to the vertical resolution of wave-induced velocities in the surf zone, and the ability to accurately reproduce swash zone velocity residuals. The driftwood model provides insight to factors affecting beaching, and parameterization of probabilistic washoff algorithms for simulating buoyant debris transport on wave-dominated coasts.

Keywords: Driftwood; woody debris; numerical modelling; waves; Lagrangian particle-tracking.

5.1 Introduction

Driftwood and woody debris are abundant in the world's coastal zones, and originate from both natural and anthropogenic sources (Murphy et al., 2021; Thiel & Gutow, 2005). Wood is believed to provide many ecosystem services in coastal and estuarine systems (Rangel-Buitrago et al., 2021; Hood, 2023; Wohl & Iskin, 2021), which has spurred increasing interest in its use as a material for nature-based coastal protection or restoration schemes (Dickson et al., 2023; Falkenrich et al., 2021; Elliott et al., 2016; Bayle et al., 2021; Provan et al., 2023). However, large

driftwood accumulations can pose hazards to people, infrastructure and valued assets (including sensitive ecosystems), particularly when mobilized by storms or other forcing factors (e.g., tsunami) (Doong et al., 2011; Nistor et al., 2017; Edgell & Ross, 1983; Miller & Rella, 2015; Cinar et al., 2023). Large quantities of coastal driftwood mobilized by storm waves can clog harbors, damage coastal structures, and smother salt marshes. The ability to predict the fate and transport of buoyant driftwood by storm wave action is a prerequisite for effectively managing and balancing the benefits and risks of wood in coastal zones.

As identified in a review by Murphy et al. (2021), numerical modeling studies of driftwood transport in the literature are largely confined to river systems. These studies (Stockstill et al., 2009; Ruiz-Villanueva et al., 2014b; Kang & Kimura, 2018; Persi et al., 2019; Bladé et al., 2016; Kimura & Kitazono, 2018; Akahori et al., 2023) typically couple two-dimensional, Eulerian, shallow-water Navier-Stokes solvers with Lagrangian driftwood transport models. However, these models are not designed to simulate nearshore hydrodynamics, wave-driven and surf-zone transport processes, or the wave-driftwood-shore interactions that can exert important controls on coastal driftwood dynamics (Li et al., 2023; Murphy et al., 2024).

Driftwood in river basins and coastal zones is sometimes referred to as woody debris, generally when emphasizing negative aspects or associated risks, and shares some characteristics with other types of marine debris (e.g., buoyancy). To provide insight to possibilities for numerical modelling of driftwood in coastal areas, Murphy et al. (2021) reviewed numerical modelling studies of marine debris transport, which predominantly relied on kinematics-based Lagrangian transport models coupled with Eulerian ocean models to simulate transport of anthropogenic litter (e.g., plastics) at global oceanic scales. Lagrangian methods are particularly efficient and accurate when the transported quantity (e.g., oil, debris, or driftwood) occupies a relatively small portion of the model domain (Hunter, 1987; Dimou & Adams, 1993), which is often applicable to coastal driftwood since it has a tendency to accumulate in “patches”, “hotspots”, or “driftcretions” (Murphy et al., 2021; Kramer, 2016; Thiel & Gutow, 2005). Lagrangian models allow for stable, accurate, non-diffusive advection, particularly in cases of high Péclet numbers (i.e., convection-dominated systems) where steep concentration gradients persist (Szymczak & Ladd, 2003; Neuman, 1981; Hunter, 1987). These properties make Lagrangian models attractive options for conducting long-term (e.g., multi-decadal) simulations at oceanic scales (Lebreton et al., 2012), or large ensembles of simulations (e.g., Monte Carlo) to assess probabilistic distributions. Another inherent advantage of Lagrangian methods (over, say, Eulerian methods) is that they are conveniently suited to evaluating integral parameters such as residence time, variance, and age (Dimou & Adams, 1993); which are of relevance to an improved understanding of driftwood transport and fate, and amenable to integration of models describing driftwood weathering and degradation over time. Particle-tracking models are well suited to parallel computing (Dalrymple et al., 2010; Pilechi et al., 2022; Dimou & Adams, 1993) and therefore, present an attractive option to leverage the paradigm shift in high performance computing brought about by developments in graphics processing units (GPU) technology. Many Lagrangian models for marine debris were

originally developed to simulate oil spills and adapted to include processes relevant to plastics and other types of debris (Critchell & Lambrechts, 2016). A few of these studies used relatively high-resolution nearshore models to capture the effects of complex bathymetries and shoreline configurations on debris transport (Critchell et al., 2015).

Despite evidence that beaching (grounding) and washoff (mobilization) processes exert significant control on fate and transport of marine debris in the nearshore (Lebreton et al., 2012; Critchell & Lambrechts, 2016; Murphy et al., 2024), few numerical studies adopt process-based approaches to simulating beaching or washoff, if they even consider those processes at all. The few numerical modelling studies that consider debris beaching and mobilization processes tend to use relatively simple parametric or stochastic approaches, often requiring user-specified inputs (e.g., characteristic time scales for beaching and remobilization, or diffusivities) with no clear relations to driving physical processes or shoreline/debris characteristics. Model results are often highly sensitive to these user-specified parameters (Critchell & Lambrechts, 2016), and there is little guidance available for selecting inputs. Consequently, there is a need for improved methods for simulating floating debris (including driftwood) beaching and washoff processes, which are grounded in physics but computationally efficient enough for integration in marine debris models covering large regions.

In addition to hydrodynamic drivers, debris and driftwood physical characteristics (buoyancy, roughness, and geometry) have been found to play important roles in controlling beaching and remobilization in wave-dominated settings (Li et al., 2023; Murphy et al., 2020; Murphy et al., 2024). The buoyancy of marine debris, which for driftwood is time-dependent (Murphy et al., 2021), is known to influence the potential for beaching and washoff (Li et al., 2023) due, in part, to the three-dimensionality of surf zone hydrodynamics (Murphy et al., 2024). Strongly buoyant driftwood and debris is more easily transported up the beach face, and tends to be deposited higher on the beach (Li et al., 2023), which can isolate it from hydrodynamic forcing; however, it is also more easily floated and remobilized during extreme high water-level or wave events. Relatively dense driftwood and debris sits lower in the water, is therefore less susceptible to onshore transport by breaking wave bores or “surfing” effects (Li et al., 2023), and is deposited lower on the beach, where it may either be remobilized by subsequent large waves, or experience self-burial by sediments if wave forcing does not exceed thresholds for remobilization. Driftwood or debris roughness influences frictional resistance at the beach interface during contact, and can exert considerable control on driftwood mobility (Murphy et al., 2024; Stolle et al., 2018). Driftwood or debris dimensions (i.e., characteristic lengths) are expected to affect beaching and washoff likelihoods because longer pieces mobilize greater stabilizing frictional forces when in contact with beaches, are less susceptible to trapping by shore-perpendicular structures, and are potentially more susceptible to onshore transport by wave-induced drift (Murphy et al., 2024). Given the important influence these physical characteristics have on debris-shore interactions, they must surely be considered in any parameterization of beaching and washoff processes in marine debris or driftwood transport models.

Here, a Lagrangian-based driftwood transport model called WOODRIFTSIM was developed in MATLAB (The MathWorks Inc., 2022), coupled (off-line) with two phase-resolving wave models, the reduced 2-layer version of XBeach Non-hydrostatic (XB-NH+) and SWASH, and validated using experimental data from a scale physical model of a sandy coastal reach described by Murphy et al. (2020; 2024) (Chapter 3 and Chapter 4). The model was used to simulate driftwood transport along the coast by oblique, breaking waves, and to test a new, computationally efficient, dynamics-based beaching and washoff algorithm that would enable regional-scale modelling of coastal driftwood (or other buoyant debris) transport with improved realism compared to existing models.

5.2 Beaching and Washoff in Marine Debris Models

As discussed in Section 5.1, the few marine debris transport models that incorporate beaching and washoff processes do so using relatively simple, stochastic approaches. For example, Critchell and Lambrechts (2016) describe a typical method whereby particles (representing macro- or micro-plastics) are assumed to become immediately beached whenever wind pushes them onto the shoreline, i.e., when a particle displacement causes it to cross a boundary segment of the model grid. Beached particles have a chance to be re-mobilized at each timestep, based on a constant, first-order resuspension rate prescribed by the modeler; to which model results were found to be highly sensitive (Critchell & Lambrechts, 2016). As discussed by Critchell & Lambrechts, "…there are no data on this process; presumably this resuspension may be better parameterised in the future by including a model of the wave field along a rugged coastline and the effect of the waves on the resuspension. This is another suggested priority research area." Jalón-Rojas et al. (2019) present a similar approach, whereby beached particles have a probability of being remobilized,

$$P = 0.5^{-t_B/T_{50}} \tag{5-1}$$

where t_B is the time since the last beaching and T_{50} is a prescribed "half-life" for beached debris to remain stranded before becoming remobilized. This method can be traced back to Lagrangian oil spill trajectory models, where the half-life parameter is used to describe the "absorbancy" of a shoreline, or the potential for re-entrainment of material after coming into contact with the shoreline (Shen et al., 1987; Zelenke et al., 2012). T_{50} may be specified or estimated based on some knowledge of the physical characteristics of the shoreline, or its exposure to wind and waves (Shen et al., 1987; Al-Rabeh et al., 2000; Zelenke et al., 2012). Liubartseva et al. (2018) used a similar stochastic approach, whereby the probability of mobilization of beached particles decays exponentially with time, i.e.:

$$P = \begin{cases} a_{\text{mob}} e^{-t_B/T_R}, & \text{if } t_B < T_{stg} \\ 0, & \text{otherwise,} \end{cases} \tag{5-2}$$

where a_{mob} is the specific rate of mobilization (units s^{-1}), T_R is the mean retention (or residence) time on the beach, and T_{stg} is a time limit beyond which beached particles are assumed to be permanently immobilized; all of these are user-specified inputs. Half-life (Equation 5-1) and mean retention time (Equation 5-2) are related by $T_{50} = T_R \ln 2$.

Kataoka et al. (2013) demonstrated, by marking and recapturing fishing floats on a beach in Japan, that the population of floats decayed according to this exponential relationship, which implies that the offshore-directed flux of debris from a beach can be expressed as a one-dimensional diffusive process, i.e.,

$$D \sim \frac{B^2}{T_R} \tag{5-3}$$

where D is a diffusion coefficient, and B is a cross-shore length scale (e.g., the width of beach occupied by the debris). Kataoka et al. (2013) hypothesized that this diffusive process encompasses a sequence of onshore transport, washoff, transport in the nearshore, and onshore or offshore transport; and that the residence time depends on the statistics of waves, wind, and wind-/wave-driven currents in the nearshore, beach sediment characteristics (e.g., grain size), the concentration of debris on the beach, and the geometry (e.g., representative length) of debris pieces. Pawlowicz (2021) also found, based on observations of drifters in the Salish Sea, that grounding was statistically well-modelled by a classical diffusivity formulation.

The simplistic treatment of beaching and washoff processes in most marine debris models may be a consequence of: (i) the complexities and small spatio-temporal scales associated with beaching dynamics, which are incompatible with long-term simulations of debris transport at oceanic scales (Van Der Mheen et al., 2020; Jalón-Rojas et al., 2019); and the limited studies or evidence on which to base parameterizations. Despite a plethora of field surveys of debris on beaches (Eriksson et al., 2013), the actual drivers and processes governing debris beaching and mobilization are, remarkably, poorly understood (Kataoka et al., 2015; Forsberg et al., 2020; Critchell et al., 2015; Pawlowicz, 2021). This is perhaps because different sampling methods and timescales make survey data difficult to interpret (Van Der Mheen et al., 2020), and because of local variability in drivers of beaching and washoff. The following examples illustrate some of the inter-site and inter-study variability and discrepancies in research attempting to characterize debris beaching and washoff processes and drivers. Johnson (1989) and Johnson & Eiler (1999) conducted surveys of trawl web on beaches in Alaska, and concluded that the deposition and washoff is largely controlled by storms, with significantly more trawl web being washed onshore and offshore during the storm season. From surveys of five isolated beaches in New South Wales, Australia, Taffs & Cullen (2005) determined that marine debris was predominantly deposited between the high tide and the storm surge marks on beaches exposed to ocean swells, and accumulated at the terminus of littoral (alongshore) drift cells. Kennedy & Woods (2012) observed that coarse woody debris tended to be deposited at the limit of wave swash on gravel beaches. Eriksson et al. (2013) observed that debris accumulation rates on some sub-Antarctic island

beaches were correlated with high tides and strong onshore winds. MacLeod & Dallimore (2021) applied Structure from Motion techniques to images captured by Unoccupied Aerial Vehicles and air photos to confirm that the highest driftwood accumulations at multiple, relatively sheltered sites near Tuktoyaktuk on the Beaufort Sea coast were mobilized and deposited by a historical storm surge event in 1970, which was corroborated by a numerical hindcast by Kim et al. (2021). MacLeod & Dallimore (2021) attributed variability in driftwood elevations at some of the sites to differing degrees of wave exposure. Braun et al. (2022) analysed multi-year aerial and drone imagery datasets covering a 750-m long sandy reach of the Lake Michigan shore, and concluded that large wood (pieces greater than 0.1 m diameter and 1 m length) was mobilized when the sum of wave heights and lake levels reached a threshold elevation 0.5 m above the average beach elevation. Ferguson et al. (2022) found that the elevations of debris and wrack lines on shores in the Gulf of Saint Lawrence were generally well represented by historical high-water levels estimated using a numerical hydrodynamic model that considered the combined effects of tides and storm surges (i.e., excluding waves); though slightly underestimated in areas of relatively high wave exposure. By contrast, Pawlowicz (2021) observed only a marginal tendency for drifters to run aground at high (or falling) water levels from his statistical analysis of drifter tracks in the Salish Sea. Pawlowicz (2021) ignored wave effects on the basis that Stokes drift velocities in the region are small, and because the drifters were drogued, i.e., they sampled water velocities at depths below the surface where Stokes drift is influential.

One of the only known exceptions to the simplistic or probabilistic treatment of beaching in most marine debris transport models is a recent study by Li et al. (2023), which used a high-resolution, Smoothed Particle Hydrodynamics (SPH) numerical flume to simulate wave-driven transport of debris by low-energy ($H = 4$ to 20 cm, $T = 0.6$ to 1.4 s), regular waves normally incident on a smooth, 1:10 (vertical:horizontal) beach slope. The SPH model was validated using laboratory flume experiments by the same authors. Floating debris (rigid bodies) with varying shapes, sizes and relative densities (buoyancies) were released outside the surf zone. Upon entering the surf zone, Li et al. (2023) found that onshore transport of debris was driven by "surfing" effects associated with breaking (plunging) wave bores, followed by translation up the beach slope and deposition by the swash tongue (wave runup). These observations are consistent with experimental results of Murphy et al. (2024), which showed that buoyant driftwood transport by oblique waves in a 1:30 scale physical model was strongly influenced by surfing effects. The theory underlying these surfing effects is described by Deike et al. (2017), which are the result of water particle accelerations in a localized region on the face of a breaking wave, near the crest. The resulting mean particle velocities may be an order of magnitude higher than Stokes drift velocities in non-breaking waves (Deike et al., 2017). Through a parametric study using the SPH model, Li et al. (2023) found that steeper waves (i.e., higher ak, where a is wave amplitude and k is wave number) resulted in more rapid onshore transport of floating debris, and required fewer waves to cause beaching. Higher relative depths (h/λ where h is water depth and λ is wavelength at the toe of the beach) also resulted in more rapid onshore transport. Debris with lower relative density (greater buoyancy), ρ_D/ρ, was more likely to be transported onshore by these processes and was

deposited higher on the beach. The characteristic size (length) of debris also influenced where the debris was deposited, with shorter pieces being deposited higher on the beach. However, the debris cross-sectional shape (circular, rectangular, triangular, square) had relatively little influence on beaching (Li et al., 2023). Based on the simulation results, Li et al. (2023) identified durations (time for beaching to occur) and thresholds for beaching of floating marine debris in waves outside the surf zone that depend on wave steepness and relative density. For a given relative density, the time for beaching to occur depends on wave steepness above a certain threshold. Below this wave steepness threshold, which increases with ρ_D/ρ, beaching will rarely occur. Although limited to relatively low-energy wave conditions, these findings align with some field studies that have observed higher rates of debris beaching during stormy conditions that tend to be associated with higher wave steepnesses (Johnson, 1989; Eriksson et al., 2013). Acknowledging that high-resolution SPH models are impractical for applications at most scales of interest outside the laboratory due to the high computational demand, Li et al. (2023) showed that water particle velocities linked to surface displacements by a second-order Lagrangian wave theory, solved using a Runge-Kutte method, could be used with the Morison equation to adequately and more efficiently predict the onshore drift of debris outside the surf zone. However, this method broke down when the floating debris encountered wave breaking. It is therefore predominantly useful, if coupled with regional ocean models, for determining if floating debris exposed to waves will enter the surf zone, which in itself does not guarantee that beaching will occur (Murphy et al., 2024); especially in cases where oblique waves may drive littoral transport. Moreover, Li et al.'s (2023) study considered an idealized, smooth beach slope with "small" bottom friction. Consequently, debris with circular cross-sectional areas (e.g., spheres) had no rolling resistance and did not actually beach in the model; beaching positions for these debris types were taken as the highest point reached on the slope. These are significant limitations, considering that Murphy et al.'s (2024) experiments demonstrated that driftwood roughness can exert significant control on beaching and washoff potential, and restrict alongshore transport and dispersion by obliquely-incident, breaking waves. Moreover, rolling or sliding is a potentially important mechanism of driftwood transport in shallow water (Kang & Kimura, 2018), or on sloping beaches (Section 3.5.3). Thus, there remains a need to develop new methods for simulating floating debris and driftwood beaching and washoff processes that are grounded in physics but computationally efficient enough for integration in relatively coarse-resolution regional marine debris models (Davidson et al., 2023).

5.3 Physical Model Experiments

The physical model and driftwood release experiments described in Chapter 3, and driftwood tracks determined from the optical tracking analysis described in Chapter 4, provided a basis for validating numerical models of nearshore hydrodynamics (Section 5.4.1), and driftwood transport (Section 5.4.2), respectively.

5.4 Numerical Models

5.4.1 Hydrodynamics – XBeach and SWASH

Two "state-of-the-art" phase-resolving wave models were applied to numerically simulate nearshore waves and wave-induced circulation in the laboratory wave basin at prototype scale: the reduced two-layer version of XBeach Non-hydrostatic (XB-NH+) version 1.22.4867 (Smit et al., 2010; de Ridder et al., 2021), and SWASH version 10.01 (Zijlema et al., 2011; The SWASH Team, 2023).

XB-NH+ computes wave-induced free-surface elevations, horizontal velocities at the centers of two layers with thicknesses proportional to the local water depth, and vertical velocities and non-hydrostatic pressure at the layer interfaces, by solving the layer-integrated non-linear shallow water equations with a non-hydrostatic pressure correction (de Ridder et al., 2021). The equations are solved using second-order accurate (in time and space) finite difference techniques on staggered, horizontal Cartesian grids (uniform or non-uniform), whereby free surface, pressure and vertical velocity variables are computed at grid cell centers, and horizontal velocities are computed at cell faces (Smit et al., 2010). The reduced two-layer model offers improved dispersive behaviour compared to the default, single-layer XBeach Non-hydrostatic model but uses the simplifying assumption that the pressure is hydrostatic in the lower layer to reduce the computational burden (de Ridder et al., 2021). Wave breaking is parameterized in XB-NH+ using a hydrostatic front approximation (HFA) (Smit et al., 2013; Smit et al., 2014), which effectively reduces the model to a single-layer model locally (i.e., in the front of a breaking wave), setting the non-hydrostatic pressure and the velocity difference between the upper and lower layers to zero (de Ridder et al., 2021). The HFA is applied in grid cells where the rate of change of the free-surface elevation, $\partial\eta/\partial t$, exceeds a user-prescribed threshold, and then removed whenever $\partial\eta/\partial t$ falls below a second (lower) threshold that indicates the breaking wave front has passed (Smit et al., 2010; de Ridder et al., 2021). This approach is used to trigger wave breaking and accurately parameterize the associated energy dissipation, which would otherwise be delayed in non-hydrostatic models when the vertical (layer) resolutions are not sufficient to capture breaker dynamics, particularly the high near-surface horizontal velocities at the onset of wave breaking (Smit et al., 2014). However, this parameterization of wave breaking neglects vertical accelerations and reduces wave-induced velocities to depth averages, locally; which is a gross oversimplification of the kinematics at the point of breaking, where velocities near the surface of the steepening wave approach the wave celerity, c, and velocities in the lower portion of the water column are ~0.1-0.4 c (Smit et al., 2010; Smit et al., 2013). Indeed, Elsayed et al. (2022) demonstrated that, despite tuning to accurately predict wave heights, XB-NH+ could not accurately reproduce the observed onshore-directed surface velocities and near-bed undertow observed in the nearshore of barred beach systems. Elsayed et al. (2022) concluded that two layers were insufficient to accurately characterize vertical variations in horizontal wave-induced velocities within the surf zone for such systems.

Like XB-NH+, SWASH (The SWASH Team, 2023; Zijlema et al., 2011) uses second-order finite-difference techniques and explicit (or optionally, semi-implicit) time discretization to solve the nonlinear shallow water (NLSW) equations on staggered computational grids. For the default explicit time integration, a dynamic time step adjustment is performed based on a Courant–Friedrichs–Lewy (CFL) stability condition, with upper and lower bounds for the Courant number prescribed by the user. In contrast to XB-NH+, SWASH allows users to prescribe more than two terrain-following (sigma) layers. When the vertical (layer) resolution is relatively coarse, the HFA can be applied in SWASH to prevent the delayed onset of breaking and achieve the correct dissipation. However, when the number of sigma layers is sufficient, the model can accurately simulate some details of wave breaking processes without the need for parameterization, including the onset of breaking, amplitude dispersion, and breaking-induced energy dissipation (The SWASH Team, 2023; St.-Germain et al., 2014; Zijlema, 2014), and to some degree of accuracy, near-surface horizontal velocities (Zijlema, 2014).

5.4.2 Driftwood transport model – WOODRIFTSIM

A Lagrangian particle-tracking model was developed in MATLAB (The MathWorks Inc., 2022) to simulate driftwood transport in a nearshore environment by waves and wave-driven circulation, and is hereafter referred to as WOODRIFTSIM. The MATLAB code for the model is provided in Appendix B. The Lagrangian driftwood transport model was driven by spatiotemporally varying, gridded (Eulerian) hydrodynamic output (depth, h, velocities, u and v, and horizontal eddy viscosity, ν_h, from the XB-NH+ and SWASH models described in Section 5.4.1, which were set up to replicate the physical modelling experiments (Chapter 3 and Chapter 4) at full (prototype) scale.

In WOODRIFTSIM, each piece of driftwood is assumed cylindrical, and is represented by three particles (Figure 5-1); one located at the centroid, and one at each end. This is a simplified version of the method of Kang & Kimura (2018), which allows for an arbitrary number of particles and complex geometries. Each centroidal particle is initially assigned a set of state variables defining the length (L_p) and diameter (D_p) of the piece of driftwood they represent. Though not used in this study, WOODRIFTSIM provides an option for driftwood lengths and diameters to vary with time (e.g., in response to degradation) by prescribing a first-order decay constant.

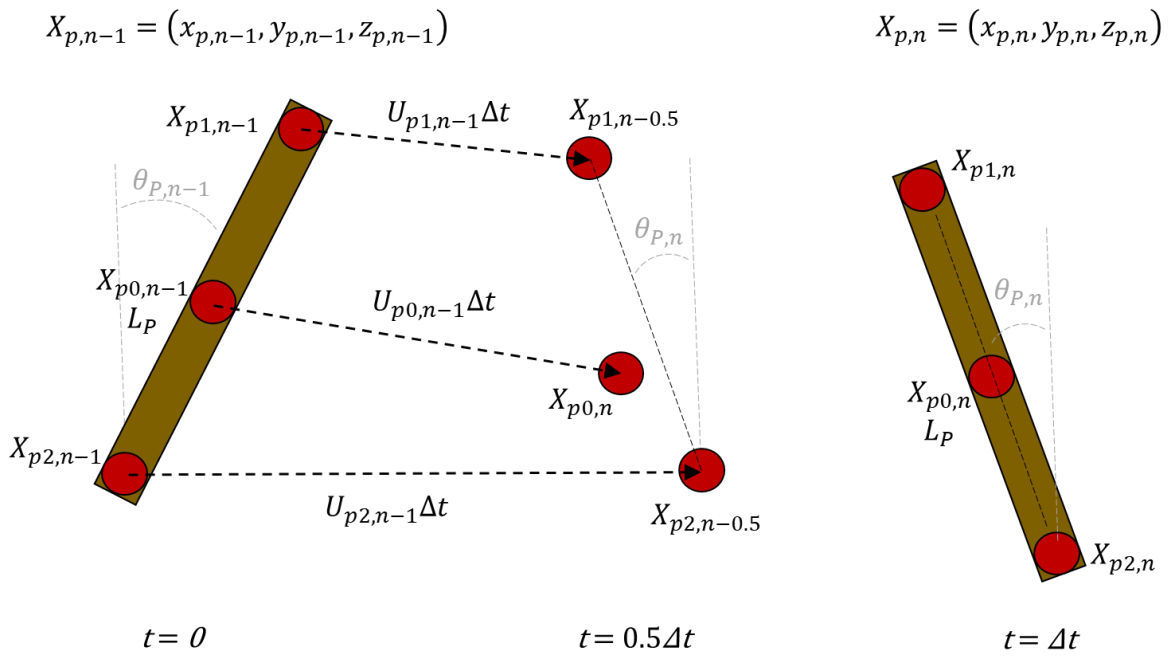

Figure 5-1. First-order particle advection in WOODRIFTSIM.

Following the random-walk approach (Dimou & Adams, 1993), the displacement of each particle associated with a piece of driftwood is initially calculated as the sum of a deterministic, advective component and a stochastic component, based on the Langevin equation:

$$\frac{dX_p}{dt} = Adv + Disp \tag{5-4}$$

where $X_p(t)$ is the position of a particle at time t, and Adv is a vector representing the effect of the deterministic advection process on particle displacement. $Disp$ is a stochastic term characterizing dispersion, which is the combined effects of velocity shear and turbulence at scales smaller than those resolved by the Eulerian velocity fields on particle transport.

5.4.2.1 Advection

A first-order (Euler) approximation of the advection term in Equation 5-4 is $Adv = U_p$ (e.g., Black & Gay, 1990; Pilechi et al., 2022), where $U_p(x, y, z, t) = u_p, v_p, w_p$ is the deterministic (advective) component of the particle velocity. The subscript p is used to differentiate parameters associated with (Lagrangian) particles from Eulerian parameters. Discretizing Equation 5-1, the advective contribution to the displacement of a particle after a time step, Δt, is $U_p\Delta t$. In a three-dimensional, Cartesian co-ordinate system, particle displacements due to advection in each component direction, $\Delta X_p = (u_{p,n-1}, v_{p,n-1}, w_{p,n-1})\Delta t$, are added to the original position co-ordinates, $X_{p,n-1} = (x_{p,n-1}, y_{p,n-1}, z_{p,n-1})$, to determine the new particle position, $X_{p,n} = (x_{p,n}, y_{p,n}, z_{p,n})$, i.e.:

$$x_{p,n} = x_{p,n-1} + u_{p,n-1}\Delta t$$
$$y_{p,n} = y_{p,n-1} + v_{p,n-1}\Delta t \quad (5\text{-}5)$$
$$z_{p,n} = z_{p,n-1} + w_{p,n-1}\Delta t.$$

$u_{p,n-1}$, $v_{p,n-1}$, and $w_{p,n-1}$ may be determined based on kinematics of the Eulerian flow field (i.e., assuming particle velocities are identical to fluid velocities), or by taking into account forces acting on the driftwood (and also potentially on the fluid). Although the latter, dynamical approach is more consistent with the physics of driftwood transport, Bladé et al. (2016) identified advantages and disadvantages of both kinematic and dynamic approaches, and concluded that simpler, kinematic approaches can accurately capture log transport in rivers. A challenge with dynamics-based models is the selection of appropriate force coefficients (e.g., drag coefficients), which introduce uncertainty. In WOODRIFTSIM, the horizontal components of the particle velocity were based on linearly-interpolated wave-induced velocities output from the XB-NH+ (depth average) and SWASH (surface layer) models, except where driftwood was determined to come in contact with the bed (Section 5.4.2.4). For positively buoyant driftwood, i.e., $\rho_D < \rho$, where $\rho_D(t)$ is the time-dependent density of driftwood and ρ is the density of water, the driftwood remains at the surface and vertical displacements are assumed negligible, i.e., $w_{p,n-1} = 0$. While this condition was met for the simulations explored here, WOODRIFTSIM includes the option to compute a settling velocity for driftwood in situations where $\rho_D > \rho$ (e.g., waterlogged conditions). An option also exists to activate windage and prescribe surface wind forcing, in which case the draft (submerged portion) of the driftwood determines the relative contribution of wind and water velocities to the overall advection, following the method of Jalón-Rojas et al. (2019).

Higher-order advection methods account for the existence of gradients in velocity fields along the particle trajectory. A second-order accurate advection scheme (Black & Gay, 1990) was also implemented in WOODRIFTSIM, giving horizontal particle positions:

$$x_{p,n} = x_{p,n-1} + \left[\frac{u'_p + \frac{1}{2}\left(u_{py,n-1}v'_p - v_{py,n-1}u'_p\right)\Delta t}{\left(1 - \frac{1}{2}u_{px,n-1}\Delta t\right)\left(1 - \frac{1}{2}v_{py,n-1}\Delta t\right) - \frac{1}{4}u_{py,n-1}v_{px,n-1}\Delta t^2}\right]\Delta t$$
$$y_{p,n} = y_{p,n-1} + \left[\frac{v'_p + \frac{1}{2}\left(v_{px,n-1}u'_p - u_{px,n-1}v'_p\right)\Delta t}{\left(1 - \frac{1}{2}u_{py,n-1}\Delta t\right)\left(1 - \frac{1}{2}v_{px,n-1}\Delta t\right) - \frac{1}{4}u_{px,n-1}v_{py,n-1}\Delta t^2}\right]\Delta t \quad (5\text{-}6)$$

where

$$u'_p = u_{p,n-1} + 0.5u_{pt}\Delta t \text{ and } v'_p = v_{p,n-1} + 0.5v_{pt}\Delta t, \quad (5\text{-}7)$$

$u_{px,n-1}$, $v_{px,n-1}$, $u_{py,n-1}$, $v_{py,n-1}$ are spatial gradients in velocity fields at the particle location at time $n-1$, and u_{pt} and v_{pt} are temporal velocity gradients.

5.4.2.2 Dispersion

From the central limit theorem, particle dispersion may be approximated as a random walk process (e.g., p.35 Fischer et al. (1979)), i.e.:

$$Disp = \frac{R}{\Delta t}\sqrt{2K\Delta t} \tag{5-8}$$

where R is a rational number selected randomly from a standard normal distribution (zero mean and unit standard deviation), and K is the dispersion coefficient (e.g., Pilechi et al., 2022). K may be isotropic or anisotropic, homogeneous or inhomogeneous, temporally varying or constant, and prescribed or determined based on Eulerian model output (e.g., Smagorinsky eddy viscosities exported from XB-NH+ or SWASH). It is noted that, in the case of spatio-temporally varying diffusivity fields, the so-called "naïve" random walk model represented by Equation 5-8 can lead to artificial accumulation of particles in low-diffusivity regions (Hunter et al., 1993; Visser, 1997). Future improvements of WOODRIFTSIM may employ corrections to the dispersion term to allow for spatio-temporal variations in diffusivity or dispersion coefficients (Pilechi et al., 2022).

5.4.2.3 Driftwood rotation

The orientation of each driftwood piece in the horizontal plane is updated at each time step to reflect the angle between the x-axis of the Eulerian grid, and a straight line between the two end-particles after advection. After advection and dispersion of the centroid, the positions of end-particles are adjusted by translation to align with the centroid, and along the driftwood major axis to preserve length according to the state variable tracked at the centroid (Figure 5-1).

5.4.2.4 Beaching and mobilization

If they include beaching and mobilization processes at all, marine debris transport models tend to utilize simplistic algorithms to simulate these processes, which often require user-specified parameters that have limited or no physical meaning (Critchell & Lambrechts, 2016; Jalón-Rojas et al., 2019; Davidson et al., 2023). However, the recent experimental study by Murphy et al. (2024) found that beaching and mobilization processes, which depend on driftwood geometry, buoyancy and roughness, exert significant control on driftwood transport and dispersion in wave-dominated, nearshore environments. In WOODRIFTSIM, a beaching and mobilization scheme was developed based on Kang & Kimura's (2018) numerical implementation of Braudrick & Grant's (2000) force-balance framework for log entrainment in rivers, adapted to consider wave forces (inertia, drag, and lift) (Figure 5-2). The scheme also simulates sliding or rolling of beached driftwood on sloping beaches, the latter having been observed to be an important mechanism involved in transport of smooth, cylindrical driftwood in the physical model experiments (Section 3.5.3 of this thesis).

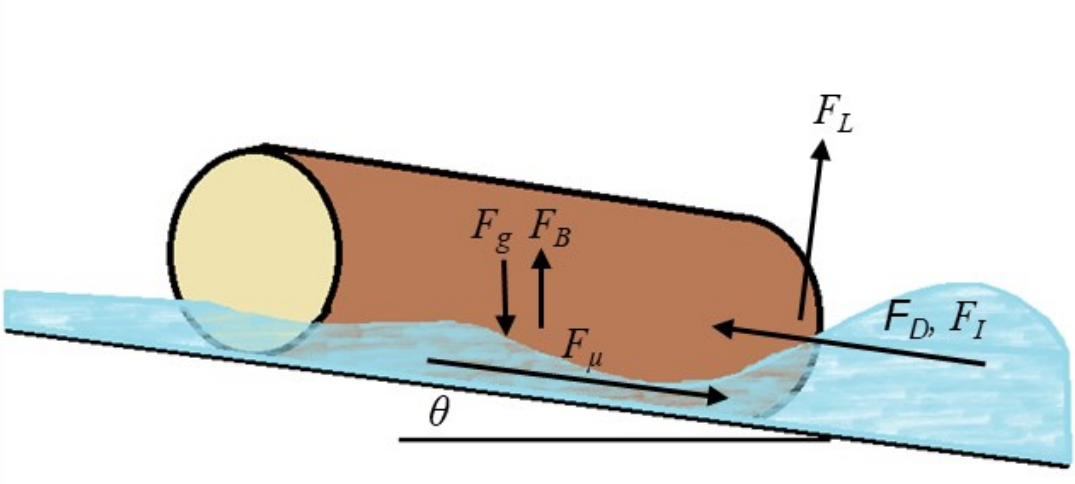

Figure 5-2. Forces acting on a piece of driftwood in contact with a sloping beach and exposed to waves.

The steps in the beaching and mobilization algorithm are:

1. The theoretical (open water) draft, d_p, of each driftwood piece (i.e., the maximum dimension of the driftwood below the water surface) is computed at the centroid by first balancing gravitational (self-weight) and buoyancy forces, which trivially shows that the submerged volume fraction is equal to ρ_D/ρ. Setting the submerged cross-sectional area, A_s, equal to the area of a circular segment then yields:

$$\frac{\rho_D}{\rho}\frac{\pi D_p^2}{4} = \frac{D_p^2}{4}\cos^{-1}\left(1-\frac{2d_p}{D_p}\right) - \left(\frac{D_p}{2}-d_p\right)\sqrt{\frac{D_p^2}{4}-\left(\frac{D_p}{2}-d_p\right)^2} \qquad (5\text{-}9)$$

   which may be solved iteratively for d_p since all other variables are known.
2. If the water depth at the centroid is less than or equal to the open water draft, $h_p \leq d_p$, the driftwood is considered to be in contact with the bed, triggering an evaluation of the balance between stabilizing and destabilizing forces acting on the driftwood. Since the draft cannot exceed the local water depth, the former is also updated, i.e., d_p is set equal to h_p.

Destabilizing forces acting on a piece of driftwood in contact with a sloping bed within the surf zone may include (Figure 5-2): (i) buoyancy forces (F_B), (ii) gravity force (F_g) components acting in the downslope direction, and (iii) wave forces.

From Equation 5-9, the balance of vertical gravitational and buoyancy (Archimedean) forces are evaluated as:

$$F_g - F_B = \rho_D g \frac{\pi D_p^2}{4} L_p - \rho g A_s L_p \qquad (5\text{-}10)$$

Ignoring impulsive forces due to wave breaking, the in-line wave-induced forces on a stationary, cylindrical piece of driftwood, F_H, may be evaluated based on the Morison equation (Morison et al., 1950; Endresen & Tørum, 1992; Sumer & Fredsøe, 2006):

$$F_H = F_D + F_I = \frac{1}{2}\rho C_D D_P L_P U|U| \cos\alpha_P + \frac{\pi}{4}\rho C_M D_p^2 L_p \frac{\partial U}{\partial t}\cos\alpha_P \quad (5\text{-}11)$$

where F_D is the drag force, C_D is the drag coefficient, F_I is the inertia force, C_M is the inertia coefficient, U is the wave-induced orbital velocity, and α_P is the angle between the orbital velocity vector and the long axis of the driftwood.

The wave-induced vertical (lift) force, F_L, is given by:

$$F_L = \frac{1}{2}\rho C_L D_p L_p U|U| \cos\alpha_P \quad (5\text{-}12)$$

where C_L is the lift coefficient. For a wide range of Keulegan-Carpenter numbers, $4 \leq (KC = UT/D_P) \leq 65$, the drag, inertia, and lift coefficients for a cylinder near a wall (or bed) are practically independent of α_P (Sumer & Fredsøe, 2006, p. 163). Force coefficients of $C_D = 1$, $C_M = 4$, and $C_L = 3.29$ were selected based on typical values for cylinders near walls given in Sumer & Fredsøe (2006, p. 129 and p. 181).

The stabilizing frictional force mobilized at the sloping bed is the product of the normal force at the wood-bed interface, F_N, and a coefficient of (static or dynamic) friction, μ, i.e. (after Braudrick & Grant, 2000):

$$F_\mu = \max(\mu F_N, 0) = \max\left(\mu\left[\left(F_g - F_B\right)\cos\theta - F_L\right], 0\right) \quad (5\text{-}13)$$

where θ is the bed slope in the direction of in-line forces acting on the driftwood. F_μ acts in the opposing direction to the resultant destabilizing force parallel to the bed, which is the sum of the inline (drag and inertia) forces and the net buoyancy/gravitational component parallel to the bed, $F_D + F_I + \left(F_g - F_B\right)\sin\theta$. The inline wave forces may act in the same direction as the net buoyancy/gravity force component, or against it (e.g., in the case of an opposing bed slope). If $\left|F_\mu\right| \geq \left|F_D + F_I + \left(F_g - F_B\right)\sin\theta\right|$, the driftwood is beached and stationary; all associated particles retain their positions at the next time step. If $\left|F_\mu\right| < \left|F_D + F_I + \left(F_g - F_B\right)\sin\theta\right|$ and $|F_D + F_I| > \left|\left(F_g - F_B\right)\sin\theta\right|$, contact with the bed does not result in beaching, wave-driven hydrodynamics control driftwood motion, and particles are advected and dispersed as described in Sections 5.4.2.1 to 5.4.2.3. If $\left|F_\mu\right| < \left|F_D + F_I + \left(F_g - F_B\right)\sin\theta\right|$ and $|F_D + F_I| \leq \left|\left(F_g - F_B\right)\sin\theta\right|$, the beached driftwood motion is controlled by gravity (i.e., sliding or rolling), and particles are translated at a velocity determined by the resultant net force and Newton's second law, i.e.:

$$U_p = \frac{\left|\left(F_g - F_B\right)\sin\theta\right| \pm \left|F_D + F_I\right| - \left|F_\mu\right|}{\rho_D \frac{\pi D^2}{4} L}\Delta t \qquad (5\text{-}14)$$

Inspection of Equations 5-13 and 5-14 reveals that the beaching and mobilization processes described above are influenced by the choice of μ in WOODRIFTSIM. Kang & Kimura (2018) tuned anisotropic friction coefficients in a numerical model to simulate transport of cylindrical driftwood with and without rootwads in a river, by comparing the results to physical model experiments. They found that rolling resistance (μ = 0.001) controlled the motion of driftwood in shallow water, even for driftwood with rootwads, since friction coefficients related to sliding were orders of magnitude higher, μ = 0.4 (static) to 0.05 (dynamic). This is consistent with the experimental observations that smooth, cylindrical dowels exposed to oblique waves were prone to persistent rolling on the beach face (Section 3.5.3). Friction coefficients can also depend on beach sediment characteristics and saturation, and friction coefficients exceeding 0.6 have been measured for sand (Fall et al., 2014).

5.5 Hydrodynamic Model Setup, Calibration, Validation, and Simulations

The XB-NH+ and SWASH numerical models were set up to attempt to replicate, at prototype scale, the wave-driven hydrodynamics within a 270 m by 180 m area of interest (Area 'B' in Figure 5-3a and b) within the 1/30 scale physical model (Chapter 3). This area corresponded to the field of view of the camera used to track driftwood transport during the physical modelling experiments. Regular, rectangular computational grids with uniform horizontal spatial resolutions of 3 m were adopted for both numerical models, nominally based on the resolution of available bathymetry data (0.1 m at 1/30 model scale), which amounted to approximately 17-50 grid points per wavelength (based on peak periods in the range 6-14 s) at the offshore boundaries of the models. Bathymetry for the numerical models was obtained by surveying the physical model using a FARO Focus^{3D}-Multi Sensor laser scanner (Section 3.3.3). The resulting point cloud data was processed (georectified and interpolated to a 0.1-m regular grid) using CloudCompare software (CloudCompare, 2015), which involved manual removal of point cloud data representing instruments or cables in the wave basin, georectification, and resampling to a 0.1-m resolution, regular grid. The gridded bathymetry data was scaled up and interpolated to the XB-NH+ and SWASH computational grids using Blue Kenue software (Barton, 2019; Serrer, 2011).

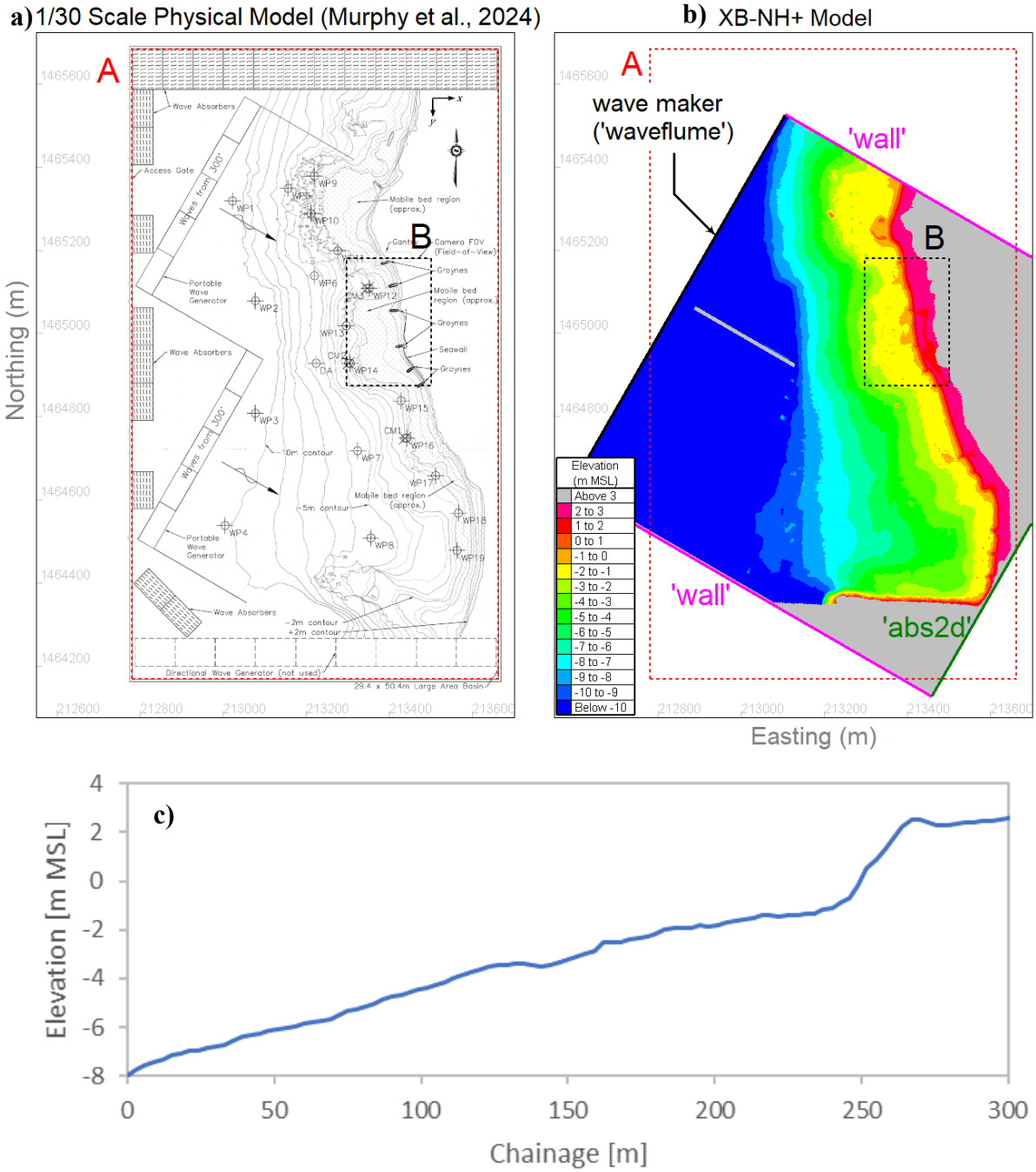

Figure 5-3. a) 1/30 scale physical model and instrumentation from Murphy et al. (2024), b) XB-NH+ model domain, bathymetry, and boundary conditions, and c) typical cross-shore profile. The red dashed rectangle 'A' indicates the laboratory wave basin walls. The black dashed rectangle 'B' indicates the area where model driftwood release experiments and tracking were conducted by Murphy et al. (2020, 2024) (Chapter 3 and Chapter 4). Solid, coloured lines indicate different boundary conditions, as labelled.

5.5.1 XB-NH+ model

The XB-NH+ model domain, bathymetry, and prescribed boundary condition types are shown in Figure 5-3. A 'waveflume' boundary type (Roelvink et al., 2015) was assigned to the northwestern side of the numerical domain, which was perpendicular to the direction of wave propagation, and spatio-temporally constant JONSWAP spectral parameters were prescribed to generate irregular, long-crested waves; replicating the sea states generated in the physical model. The central guide wall between the two banks of portable wave generators in the physical model was represented by two rows of grid cells elevated well above the water level. 'Wall'-type boundary conditions were specified along the lateral boundaries, and an absorbing ('abs2d') boundary condition was prescribed on the southeastern boundary, although it is noted that waves never reached this boundary.

The XB-NH+ model wave boundary conditions were first tuned by adjusting the prescribed offshore significant wave heights until simulated significant wave heights at the wave probe closest to the wave-maker (WP1) were within 10 % of measured values. Spectral significant wave heights, H_{m0}, were evaluated over a duration of 3600 s (approximately 250-600 waves, based on peak wave periods in the range 6-14 s) from root-mean-square wave heights (H_{rms}) output from XB-NH+, assuming a Rayleigh distribution, i.e., $H_{rms} = 0.707 H_{m0}$ (Goda, 2010). Model input parameters including bed friction coefficients (Chézy), horizontal viscosity formulations, and number of layers (i.e., single-layer or reduced two-layer mode) were adjusted until the RMSE in simulated significant wave heights at wave probes converged to a stable minimum. The Smagorinsky turbulence formulation was adopted and a spatially-varying Chézy coefficient was applied (Figure 5-1), with higher roughnesses (lower Chézy coefficients) prescribed between elevations of -3 m MSL and -1 m MSL where the bed of the physical model was deliberately roughened (and stones embedded in the concrete surface) to simulate fringing coral reefs (Section 3.3.1). The final, calibrated XB-NH+ model input parameters are listed in Table 5-1 (only non-default parameters are shown), and a comparison of measured and modelled spectral significant wave heights at the probe locations is shown in Figure 5-4a. The mean bias (-0.02 m) and Pearson correlation coefficient, r = 0.97, met performance guidelines suggested in Williams and Esteves (2017) for wave heights. The root-mean-square error, *RMSE* = 0.18 m (15 % of mean observed values) and scatter index, *SI* = 15.7 % both exceeded the guideline values of 10 %. However, Williams & Esteves (2017) note that *SI* has a tendency to understate the skill of wave models. Moreover, the model skill metrics are comparable to, and in many cases better than, those deemed acceptable in comparisons of XB-NH+ modelled wave heights to field measurements by others (De Beer et al., 2021; McCall et al., 2014; Roelvink et al., 2009; Elsayed et al., 2022).

Table 5-1. Summary of calibrated model input parameters.

Model process or parameter description	XB-NH+			SWASH		
	Selection	Keyword	Value	Selection	Keyword	Value
Pressure correction	Non-hydrostatic (reduced 2-layer)	wavemodel	nonh	Non-hydrostatic (standard central-differencing scheme)	NONHYD	STA
Number of layers	Reduced 2-layer	nonhq3d	1	4 layers	VERT	4
Layer distribution	Sigma, lower layer = $0.33h$	nhlay	0.33	Sigma, equidistant	thickness	no value specified
Bed friction formulation	Chézy formulation	bedfriction	chezy	Chézy formulation	FRIC	CHEZ
Bed friction	Spatially varying, read from file	bedfricfile	chezy.dep	Spatially varying, read from file	READINP FRIC	chezy.dep
Chézy coefficient	30 $m^{1/2}$ s^{-1} in reef areas (-3 m MSL < z_b < -1 m MSL), 35 $m^{1/2}$ s^{-1} elsewhere	bedefriccoef	[30, 35] read from file	30 $m^{1/2}$ s^{-1} in reef areas (-3 m MSL < z_b < -1 m MSL), 35 $m^{1/2}$ s^{-1} elsewhere	[cf]	[30, 35] read from file
Horizontal turbulence scheme	Smagorinsky	smag	1	Smagorinsky	VISC HOR	SMAG
Depth-induced wave breaking	Hydrostatic front approximation	nhbreaker	2	No parameterization	BRE	not used

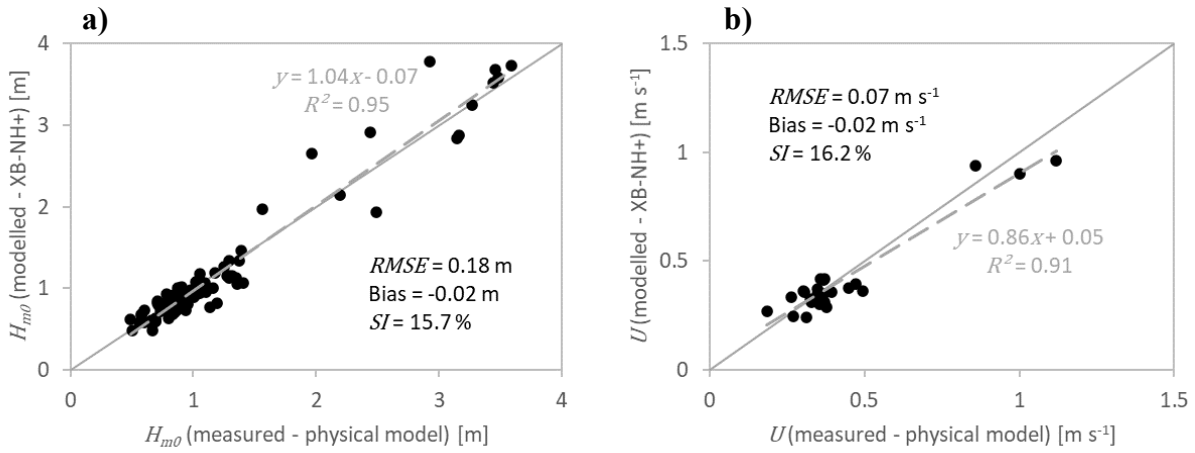

Figure 5-4. Measured (experimental) and modelled (XB-NH+) a) significant wave heights; and b) mean current speeds.

Following the general framework for model calibration and validation recommended by Williams & Esteves (2017), the XB-NH+ model was then validated by evaluating simulated mean (temporally and depth averaged) current speeds at the location of the three current meters and comparing the results to measured values (Figure 5-4b). The *RMSE* (0.07 m s^{-1}, which corresponds to 16 % of mean observed values), mean bias (-0.02 m s^{-1}), and Pearson correlation coefficient (r = 0.95) all met performance guidelines suggested in Williams and Esteves (2017) for average current speeds. Again, the scatter index metric (*SI* =16.2 %) exceeds the guideline value of 10 %.

Surface-layer horizontal velocities, $U_{surf} = (u_{surf}, v_{surf})$, were computed from the XB-NH+ depth-averaged velocity output, U, as recommended by the XBeach user manual, i.e.:

$$U_{surf} = U - 0.33\Delta U \qquad (5\text{-}15)$$

where ΔU is the velocity difference between the upper and lower layers.

5.5.2 SWASH model

The SWASH model setup (Figure 5-5) was slightly modified from that of the XB-NH+ model, to eliminate instabilities that arose when waves were reflected back towards the wave generation boundary. The model domain was extended to the northeast, bathymetry in the southwest of the domain was smoothed (downdrift of the area of interest 'B' in Figure 5-5), the central guide wall between the two banks of portable wave generators in the physical model was removed (since the two banks of wave generators were synchronized in the physical model anyway), and Sommerfeld radiation-type boundary conditions (The SWASH Team, 2023) were prescribed on the lateral (non-wave-generating) boundaries. Four equidistant sigma layers were prescribed (higher resolutions tended to result in instability, even with substantially reduced initial time steps from the prescribed value of 0.0001 s and prescribed upper limits for the Courant number as low as 0.2), and parameterization of wave breaking was not activated. All other model

input parameters (JONSWAP spectral parameters, Chézy coefficients, and Smagorinsky turbulence formulation) were identical to those determined from the XB-NH+ model calibration. Spatio-temporally constant JONSWAP spectral wave parameters were prescribed at the northwestern boundary of the model to generate irregular, long-crested waves.

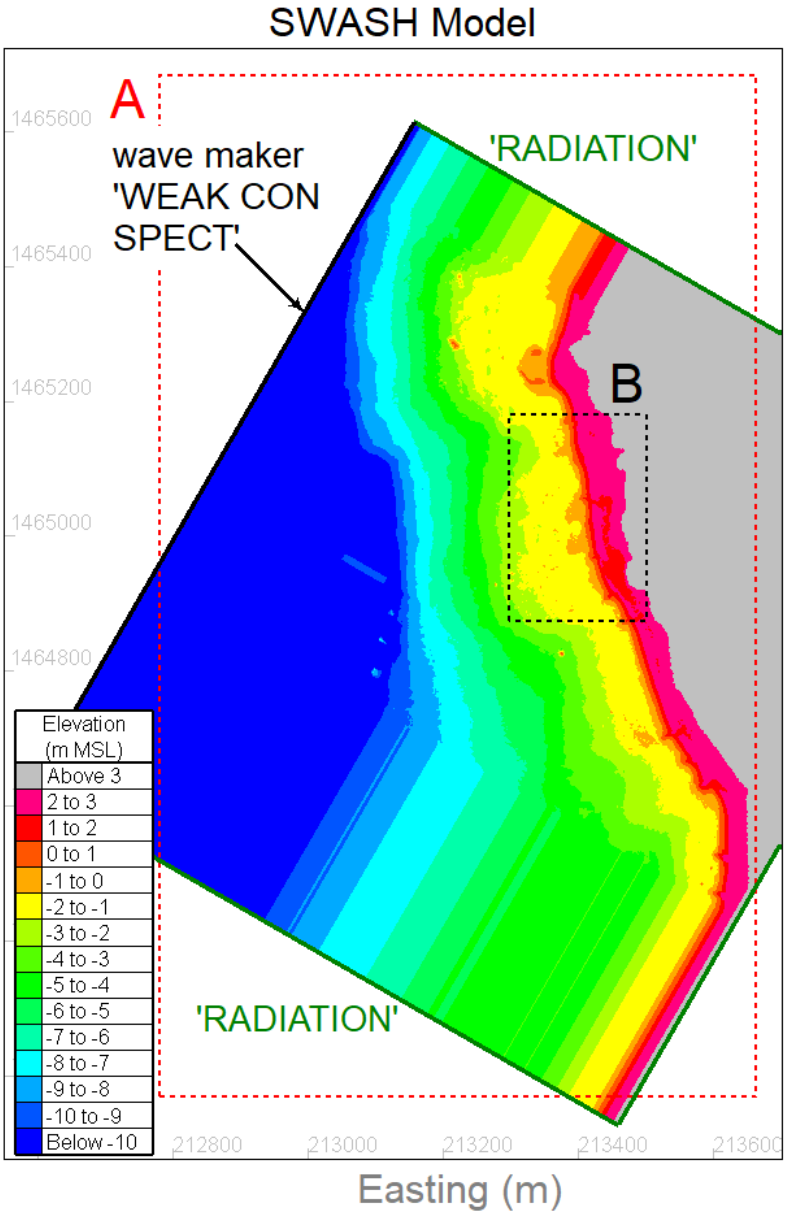

Figure 5-5. SWASH model domain, bathymetry, and boundary conditions. The red dashed rectangle 'A' indicates the laboratory wave basin walls. The black dashed rectangle 'B' indicates the area where model driftwood release experiments and tracking were conducted (Chapter 3 and Chapter 4). Solid, coloured lines indicate different boundary conditions, as labelled.

Measured (experimental) and modelled (SWASH) significant wave heights and mean (temporally and depth averaged) current speeds are shown in Figure 5-6. Model skill metrics for

wave heights and mean current speeds both worsened by comparison to XB-NH+. However, the SWASH model significant wave height skill metrics are based on fewer measurements due to the domain modifications described above (measurements in areas south of Area B in Figure 5-5 were not used, since the bathymetry was smoothed). Interestingly, the SWASH model showed a tendency to slightly underpredict H_{m0} for the more energetic sea state conditions simulated ($H_{m0} > 3.0$ m), while simultaneously overpredicting U. This may be a consequence of the staggered grid approach in SWASH, which computes velocities at cell faces and elevations at cell centers, and by default smooths the input bathymetry grid when interpolating to cell centers. Despite the slight deterioration in model skill metrics compared to the XB-NH+ results, the *RMSE* and bias metrics for significant wave heights were within ranges deemed "moderate" to "good" by others (Risandi et al., 2020).

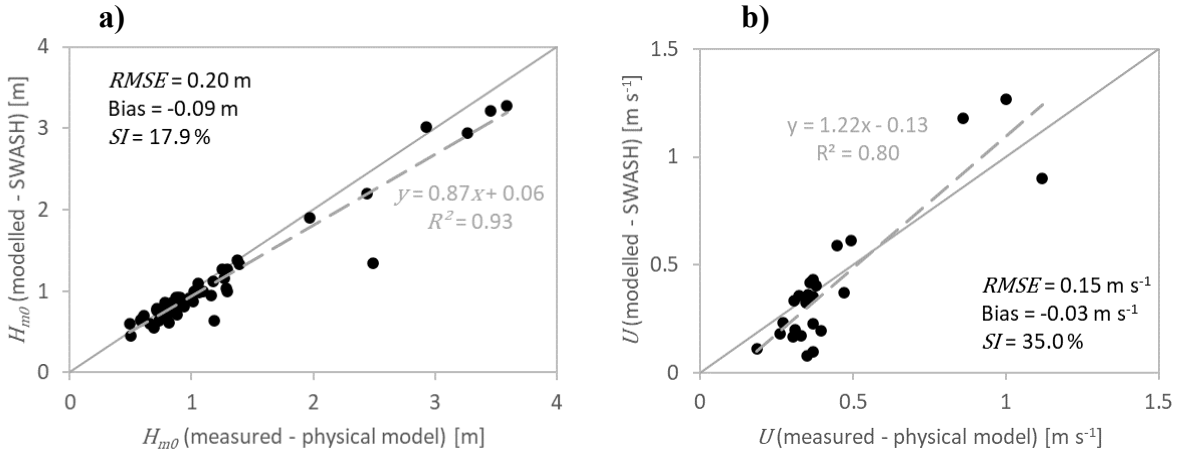

Figure 5-6. Measured (experimental) and modelled (SWASH) a) significant wave heights; and b) mean current speeds.

5.5.3 Production Simulations

Eight XB-NH+ and SWASH simulations were implemented to replicate, at prototype scale, the hydrodynamic conditions in Test Series (TS) 1-11 of the experiments described in Chapter 3, as indicated in Table 5-2. TS1-8 represented experiments with smooth cylindrical dowels in Chapter 3. TS11, TS9, and TS10 consisted of experiments with rough branches but with hydrodynamic conditions identical to TS2, TS4, and TS6, respectively.

Table 5-2. Summary of experimental conditions replicated using XB-NH+ and SWASH.

Test Series ID (Murphy et al., 2024)	η (m)	H_s (m)	T_p (s)	Number of driftwood pieces $\sum N_P$		
				L_P = 3 m (yellow)	L_P = 9 m (blue)	L_P = 12 m (green)
1	0.35	0.45	8	112	49	54
2 (11*)	0.35	0.65	8	127 (128)	56 (56)	64 (72)
3	0.35	0.80	11	110	49	63
4 (9*)	0.70	0.80	11	127 (111)	71 (62)	56 (68)
5	0.70	0.80	14	111	56	70
6 (10*)	0.70	1.20	6	127 (123)	56 (56)	88 (72)
7	0.35	0.65	11	125	56	88
8	0.70	3.70	10	70	40	64

*Note: Test Series in parentheses represent experiments in Chapter 3 with rough model driftwood at prototype scale. All other Test Series used smooth cylindrical dowels.

5.6 Driftwood Transport Simulations

Using spatiotemporally varying water depth, velocity, and diffusivity fields from the XB-NH+ and SWASH model simulations (Section 5.5) as input, Lagrangian driftwood simulations were implemented to replicate the experimental ensembles (TS1-11) in Chapter 3 and Chapter 4, which were comprised of multiple releases of driftwood (approximating point releases) at the updrift end of Area B in Figure 5-3 and Figure 5-5. The number of driftwood pieces in each length class (L_P = 3, 9, and 12 m) was prescribed as input to the Lagrangian model based on the total number released over multiple realizations for each experimental ensemble, $\sum N_P$ (Table 5-2). Initial driftwood positions and orientations were randomly distributed over a 20-m diameter release zone. Spatiotemporally varying, isotropic dispersion coefficients were prescribed based on the XB-NH+ and SWASH model horizontal eddy diffusivity (ν_h) output, assuming a turbulent Schmidt number, $Sc_t = \nu_h/K = 1$.

The time step for the Lagrangian model was set equal to the time step of the output from the XB-NH+ and SWASH models, i.e., $\Delta t = 1$ s. For wave-induced velocities $\sim O(1)$ m s^{-1} (e.g., Figure 5-4), and the Eulerian grid resolution of $\Delta x = \Delta y = 3$ m, this time step was sufficient to ensure particles were generally not advected through multiple grid cells in a single time step, which is a criterion often adopted for Lagrangian marine debris modelling studies (Lebreton et al., 2012; Jalón-Rojas et al., 2019). Since $\min(\partial^2\nu_h/\partial x^2, \partial^2\nu_h/\partial y^2) \sim O(1)$ m^2 s^{-1}, the selected time step did not meet more stringent criteria for time step selection in Lagrangian models with spatially varying diffusivity fields recommended by Ross & Sharples (2004), which would have required $\Delta t \sim O(0.001)$ s. However, considering that the naïve form of the random walk equation for dispersion currently incorporated in WOODRIFTSIM does not account for gradients in spatially varying diffusivity fields, this is considered an area for future improvement and investigation. It is not a major limitation for this study, since the experiments in Chapter 3 and Chapter 4 corresponded to advection-dominated conditions with driftwood Péclet numbers, $Pe = \langle V_P \rangle Y_B / \langle K_y \rangle > 1$.

Model skill was assessed qualitatively by visual comparison of simulated and observed driftwood centroid tracks, and quantitatively by comparison of simulated and observed driftwood mean transport velocities and variances.

5.7 Results and Discussion

5.7.1 Hydrodynamics

The spatial distribution of mean wave-induced velocity fields was sensitive to model selection (and associated vertical resolution), particularly within the surf zone and swash zone. As an illustrative example, temporal mean (i.e., residual) velocities from the two NLSW equation models for TS6 are shown in Figure 5-7. Depth average and surface layer velocity residuals are shown. XB-NH+ residual velocities (both depth average and surface layer) were predominantly

directed alongshore or slightly offshore, except within the swash zone where residual velocities were directed offshore (i.e., downrush-dominated). The differences between depth average and surface layer velocities from the XB-NH+ model were minimal, consistent with previous studies by others (Elsayed et al., 2022).

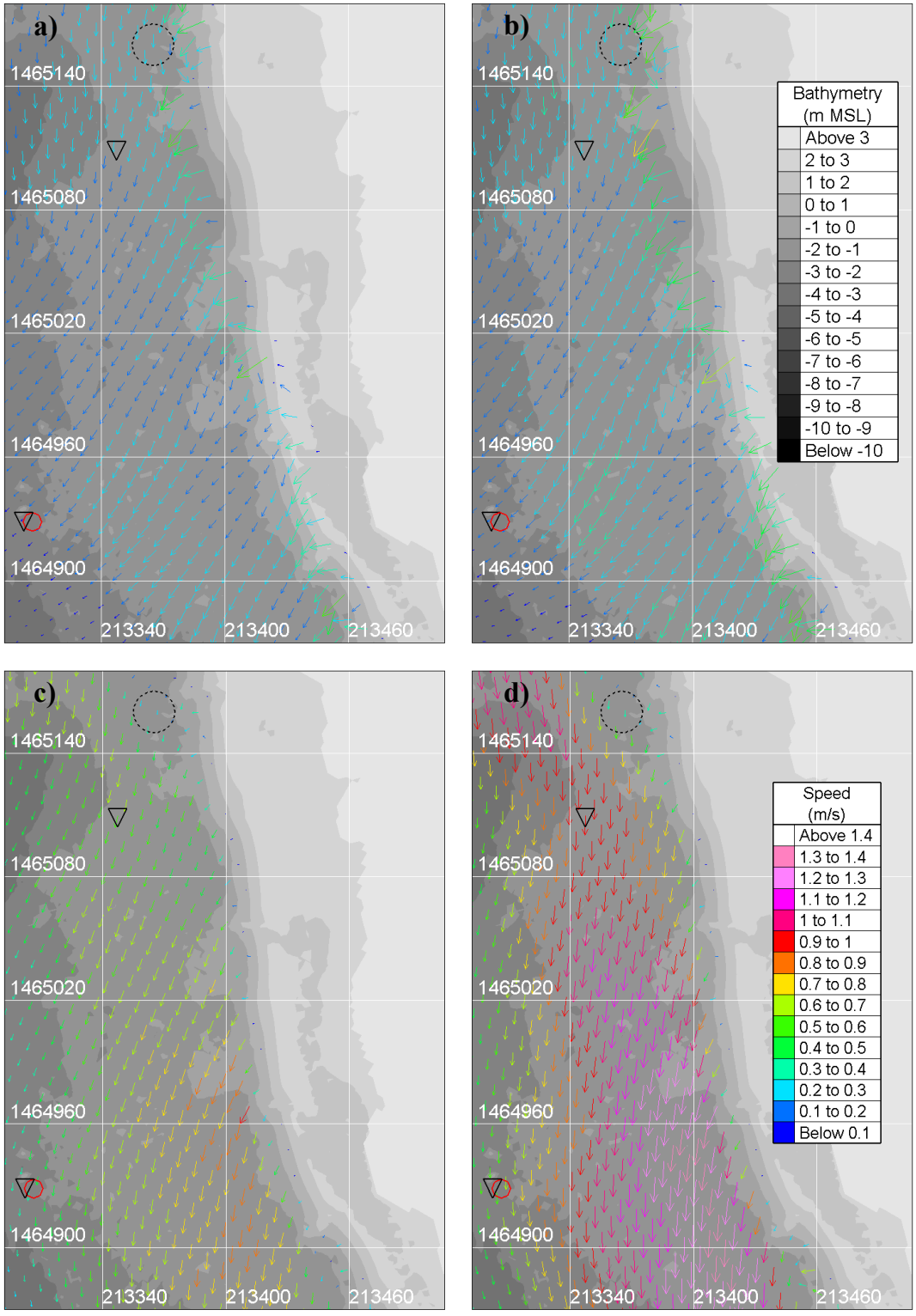

Figure 5-7. Residual velocity vectors for TS6 from a) XB-NH+ (depth average), b) XB-NH+ (surface layer), c) SWASH (depth average), and d) SWASH (surface layer). The driftwood release location is indicated by a dashed circle. Current meter locations are indicated by triangles and wave probe WP14 is indicated by an open (red) circle.

By contrast to XB-NH+, the residual velocity fields from the SWASH model generally exhibited stronger onshore-directed components (especially residual velocities in the surface layer), and more significant differences between surface layer and depth-averaged output, as might be expected given the higher layer resolution compared to XB-NH+, and the absence of the HFA breaking parametrization. This strong vertical variability in horizontal wave-induced velocities from the SWASH model may partly explain the weaker correlation between depth average mean current speeds from SWASH and the point measurements from current meters in the physical model. Although residual velocities in the surf zone were generally higher in SWASH than in XB-NH+, the SWASH residuals generally decayed much more sharply to zero within the swash zone than in XB-NH+, which exhibited relatively strong offshore-directed mean velocities in this region. In other words, temporal mean downrush velocities associated with swash events exceeded uprush velocities in XB-NH+. This was also observed in SWASH velocity residuals for three of the Test Series (TS3, TS4, and TS7). Temporal mean velocities have potentially important implications for driftwood transport within the swash zone, since, as pointed out by Masselink et al. (2009), net mass transport in the swash zone is characterized by a "small net difference between two large numbers", and "resolving this small net difference is considered one of the key challenges in swash zone research". The ability to accurately predict swash zone velocities may ultimately determine whether driftwood beaching can occur, and therefore, control the overall mobility and dispersion of driftwood on wave-dominated coasts.

The sensitivity of wave-driven driftwood transport in WOODRIFTSIM to hydrodynamic model selection and vertical resolution is illustrated in Figure 5-8 and Figure 5-9, which show snapshots of simulated driftwood positions during TS2 ($\eta = 0.35$ m, $H_{m0} = 0.65$ s, and $T_p = 8.0$ s) at $t = 100$ s and 400 s after a release, respectively. To isolate the influence of hydrodynamics, the results in Figure 5-8 and Figure 5-9 are for simulations with a constant driftwood friction coefficient, $\mu = 0.001$, prescribed based on the rolling resistance of cylinders determined by Kang & Kimura (2018). The driftwood in Figure 5-8 and Figure 5-9 is shown colored by length class, consistent with the paint colors adopted in the physical model experiments in Murphy et al. (2024), i.e., $L_P = 3$ m (yellow), 9 m (blue), and 12 m (green). Beached, stationary driftwood is shown colored red (regardless of length class), and driftwood that is beached but rolling or sliding on the beach surface is shown colored orange. There was little difference between driftwood distributions from the simulations driven by depth average (Figure 5-8a) and surface (Figure 5-8b) velocities from XB-NH+, reflecting the weak vertical variation in horizontal wave-induced velocities in the reduced 2-layer model. Mean driftwood transport by XB-NH+ in the alongshore direction was relatively slow due to the weak residual currents in the surf zone (Figure 5-7), and spreading of the patch of driftwood was predominantly in the cross-shore direction (Figure 5-9a and b) despite dispersion coefficients being isotropic, owing to stronger gradients in velocities in the direction of wave propagation (Figure 5-7). By contrast, WOODRIFTSIM simulations driven by SWASH hydrodynamic output showed a greater tendency for onshore-directed transport, particularly when driven by surface velocities, which was more consistent with the experimental observations (e.g., Figure 3-11 and Figure 3-12 in Chapter 3). Mean alongshore transport velocities for the

simulations driven by SWASH were higher than both the simulations driven by XB-NH+ and the physical model experiments, with the centroid of the driftwood patch located approximately 200 m downdrift of the release location after 400 s (Figure 5-9c and d). Of these four examples, only the WOODRIFTSIM simulation driven by SWASH surface velocities resulted in driftwood being transported onshore, as seen in experiments (Chapter 3 and Chapter 4), triggering beaching and rolling (Figure 5-8d).

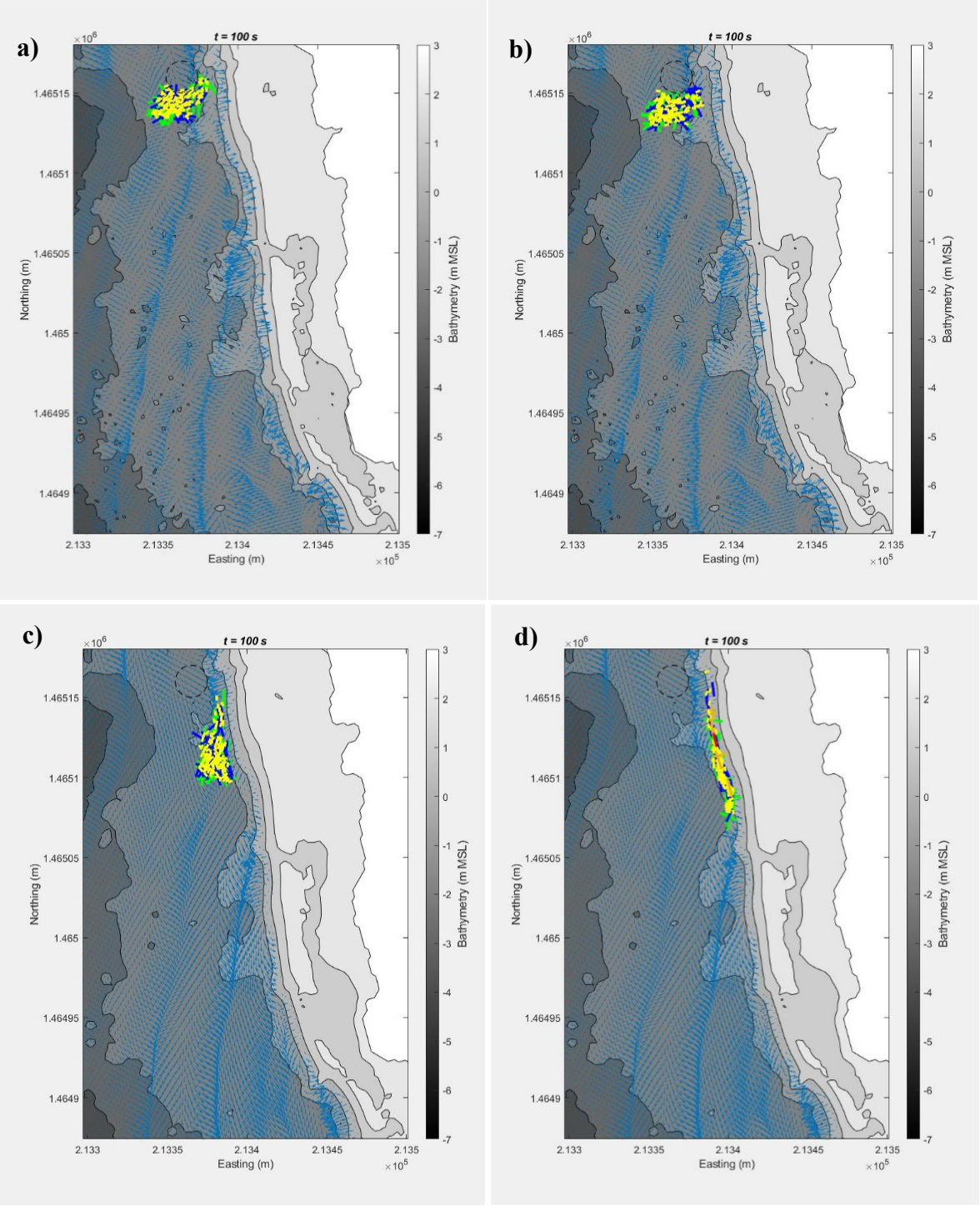

Figure 5-8. Instantaneous snapshots of simulated driftwood positions and orientations for TS2 ($\eta = 0.35$ m, $H_{m0} = 0.65$ s, and $T_p = 8.0$ s) at t = 100 s ($12T_p$) after release, from simulations driven by a) depth average velocities from XB-NH+, b) surface velocities from XB-NH+, c) depth average velocities from SWASH, and d) surface velocities from SWASH. The release area is indicated by a dashed circle. Instantaneous velocity fields are indicated by blue arrows.

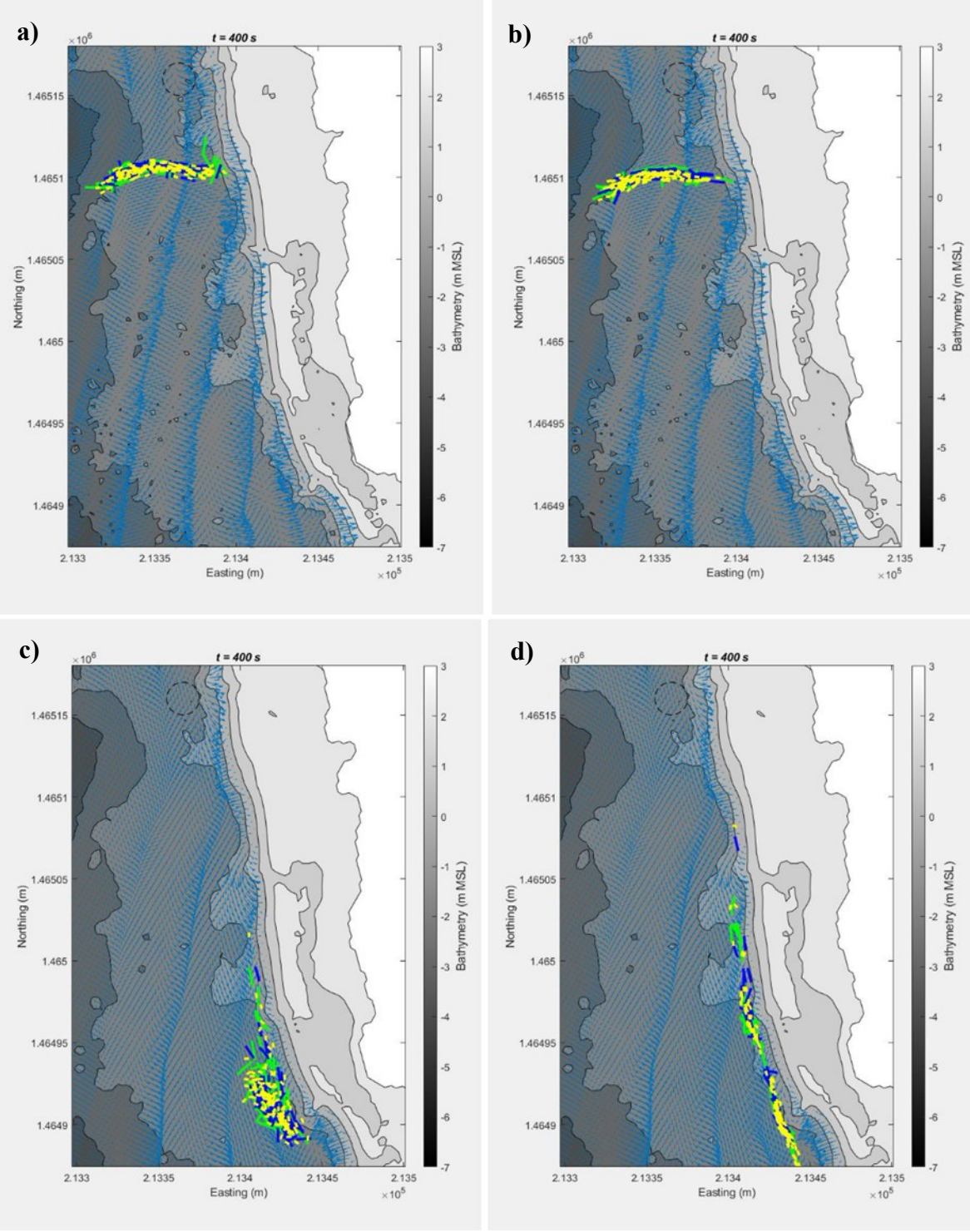

Figure 5-9. Instantaneous snapshots of simulated driftwood positions and orientations for TS2 ($\eta = 0.35$ m, $H_{m0} = 0.65$ s, and $T_p = 8.0$ s) at t = 400 s ($50T_p$) after release, from simulations driven by a) depth average velocities from XB-NH+, b) surface velocities from XB-NH+, c) depth average velocities from SWASH, and d) surface velocities from SWASH. The release area is indicated by a dashed circle. Instantaneous velocity fields are indicated by blue arrows.

Although all simulations driven by SWASH surface velocity fields resulted in driftwood being transported closer to shore than the corresponding XB-NH+ simulations, not all resulted in driftwood reaching the shore. Beaching did not occur in simulations of TS4, and was relatively infrequent in simulations of TS3, and TS7, whereas some beaching was observed in all three experimental test series ensembles.

5.7.2 Mean transport rates and dispersion

Simulated mean driftwood transport rates and dispersion were strongly influenced by the choice of hydrodynamic model, depth-averaged or surface velocities, and vertical resolution. The temporal evolution of mean driftwood transport distances and dispersion (represented by the standard deviation of the driftwood centroids with respect to their mean position) in the alongshore and cross-shore directions based on simulations using the XB-NH+ and SWASH model hydrodynamics (depth average and surface layer) as driving input is shown in Figure 5-10 for TS2, compared to experimental measurements derived from the optical tracking analysis in Chapter 4. In Figure 5-10, mean transport distances (Y and X) and standard deviations (σ_y and σ_x) are shown normalized by the dimensions of Area B (Figure 5-3 and Figure 5-5) in the alongshore and cross-shore directions, $Y_B = 270$ m and $X_B = 180$ m, respectively. Time is normalized by the peak wave period, T_p. The termini of curves in Figure 5-10 corresponds to the time $t = T_d$ when more than one-third of the driftwood pieces exited Area B in Figure 5-3, consistent with the methodology for evaluating mean transport distances and standard deviations in Chapter 4.

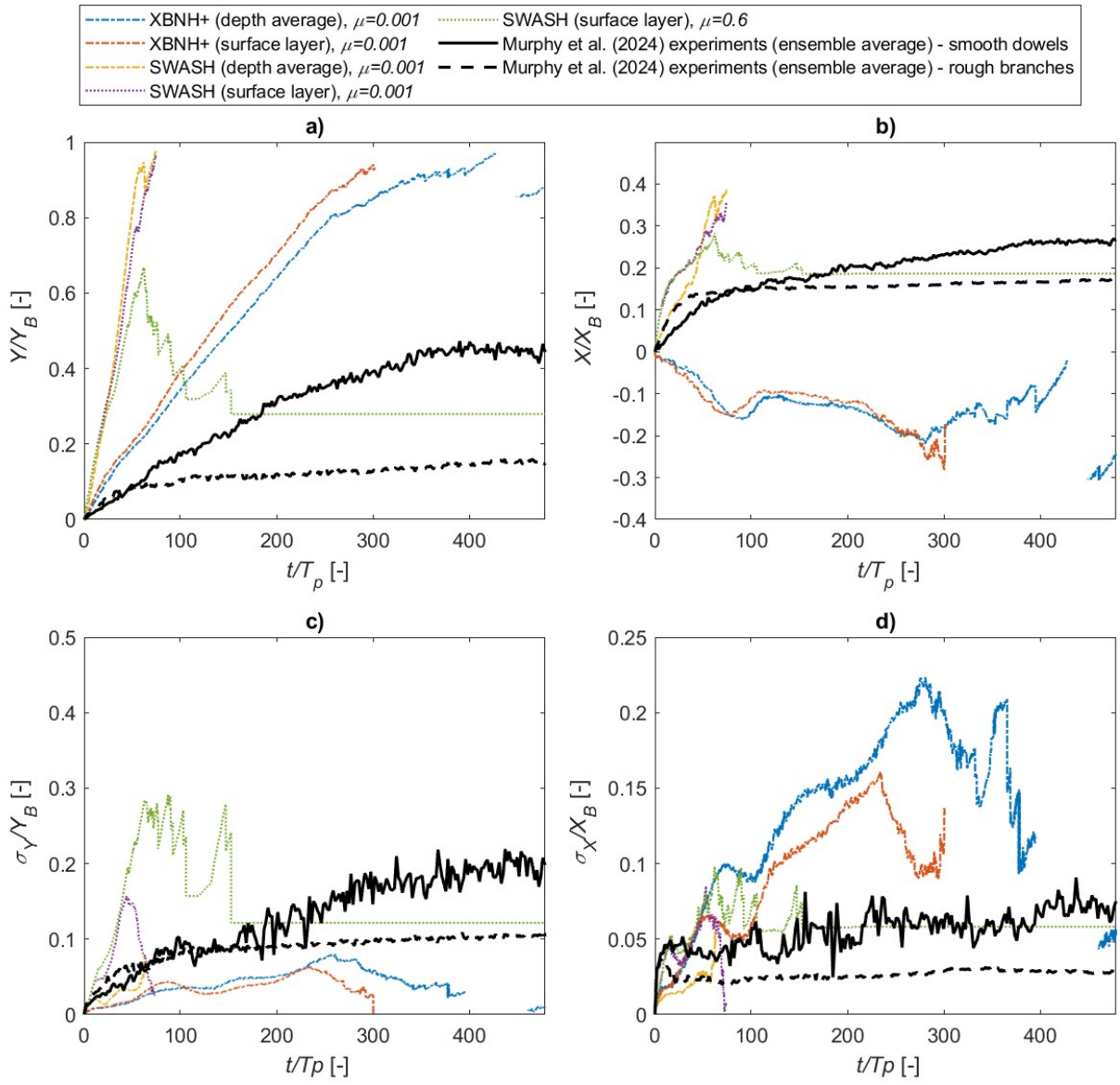

Figure 5-10. a) Mean alongshore relative travel distance, b) mean cross-shore relative travel distance, c) alongshore standard deviation, and d) cross-shore standard deviation for driftwood length class L_P = 12 m (green) during TS2 ($\eta = 0.35$ m, $H_{m0} = 0.65$ s, and $T_p = 8.0$ s).

The results for this Test Series (which are typical) show that simulations driven by XB-NH+ failed to replicate the onshore-directed transport of driftwood and subsequent beaching that was observed to inhibit driftwood mean transport and dispersion in the physical model experiments (Chapter 4). Instead, simulations using XB-NH+ generally resulted in driftwood being transported offshore, as indicated by negative values of X/X_B in Figure 5-10b. Simulations driven by XB-NH+ tended to over-estimate cross-shore dispersion and under-estimate alongshore dispersion of driftwood, respectively.

WOODRIFTSIM simulations driven by SWASH surface-layer velocities resulted in onshore-directed transport (and repeated beaching) of driftwood for TS1, TS2, TS5, TS6, and TS8; which was qualitatively more consistent with the experimental observations (Chapter 3). For TS4, the SWASH model surface layer velocities exhibited a dominant downrush phase of the swash zone velocity cycle (similar to XB-NH+), which prevented driftwood moving onshore (there were no beaching events for this scenario) and resulted in rapid alongshore transport (i.e., exceeding alongshore transport rates observed in the experiments, where beaching inhibited transport) close to the seaward limit of the swash zone. Following an initial small number of beaching and washoff events shortly after the driftwood releases, SWASH-WOODRIFTSIM simulation results for TS3 and TS7 exhibited similar driftwood transport behaviours (rapid alongshore transport at the seaward edge of the swash zone, and no further beaching). For simulations where SWASH surface layer velocities drove driftwood onshore (TS1, TS2, TS5, TS6, and TS8), mean driftwood transport and dispersion rates were reasonably consistent with the experimental observations (Figure 5-11), though sensitive to driftwood friction coefficients (Section 5.7.3).

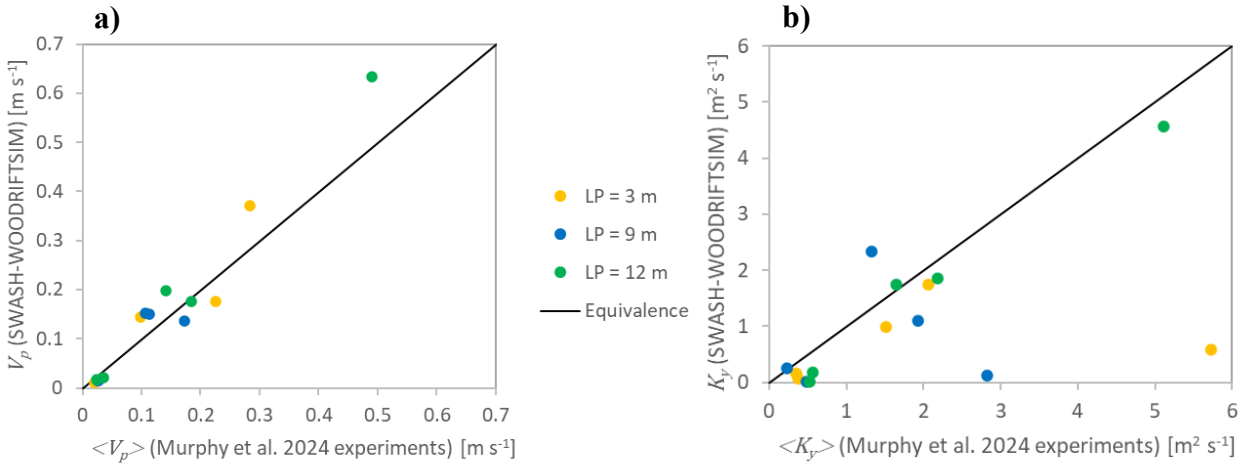

Figure 5-11. Measured (Chapter 4) and modelled (WOODRIFTSIM driven by SWASH surface layer velocities and μ = 0.6) a) mean alongshore driftwood transport rates, and b) alongshore dispersion coefficients, for Test Series involving frequent beaching events (TS1, TS2, TS5, TS6, and TS8).

5.7.3 Sensitivity to friction coefficient and driftwood length

For WOODRIFTSIM simulations where driftwood came in contact with the shoreline (i.e., primarily those driven by SWASH surface-layer velocities), increased driftwood-beach friction coefficients within the range $0.001 \leq \mu \leq 0.6$ (consistent with the range of values in the literature) generally resulted in more frequent and sustained beaching, which inhibited alongshore mean transport and dispersion (Figure 5-12 and Figure 5-13). This is exemplified by the sharp decrease and then stabilization of Y in the range $t/T_p \gtrsim 50$ in Figure 5-12 and Figure 5-13 for TS2 simulations with $\mu \geq O(0.1)$, when a fraction of the driftwood exits Area B and the rest is retained (beached). Higher μ values resulted in more persistent beaching, as indicated by red-colored driftwood in Figure 5-14c and d ($\mu = 0.6$), whereas intermediate values of μ caused

driftwood that was deposited on the beach by waves to roll back down the beach face into the surf zone (orange-colored driftwood in Figure 5-14a and b), where it was transported alongshore by wave-driven currents. This variability in mobility and transport behavior in response to changes in driftwood roughness was qualitatively consistent with the experimental observations for smooth and rough model driftwood (Chapter 3). Figure 5-14a and b show that trapping by shore-perpendicular groynes was the main mechanism inhibiting alongshore transport of smoother driftwood (i.e., $\mu = 0.1$), also in agreement with the experiments (Section 4.6).

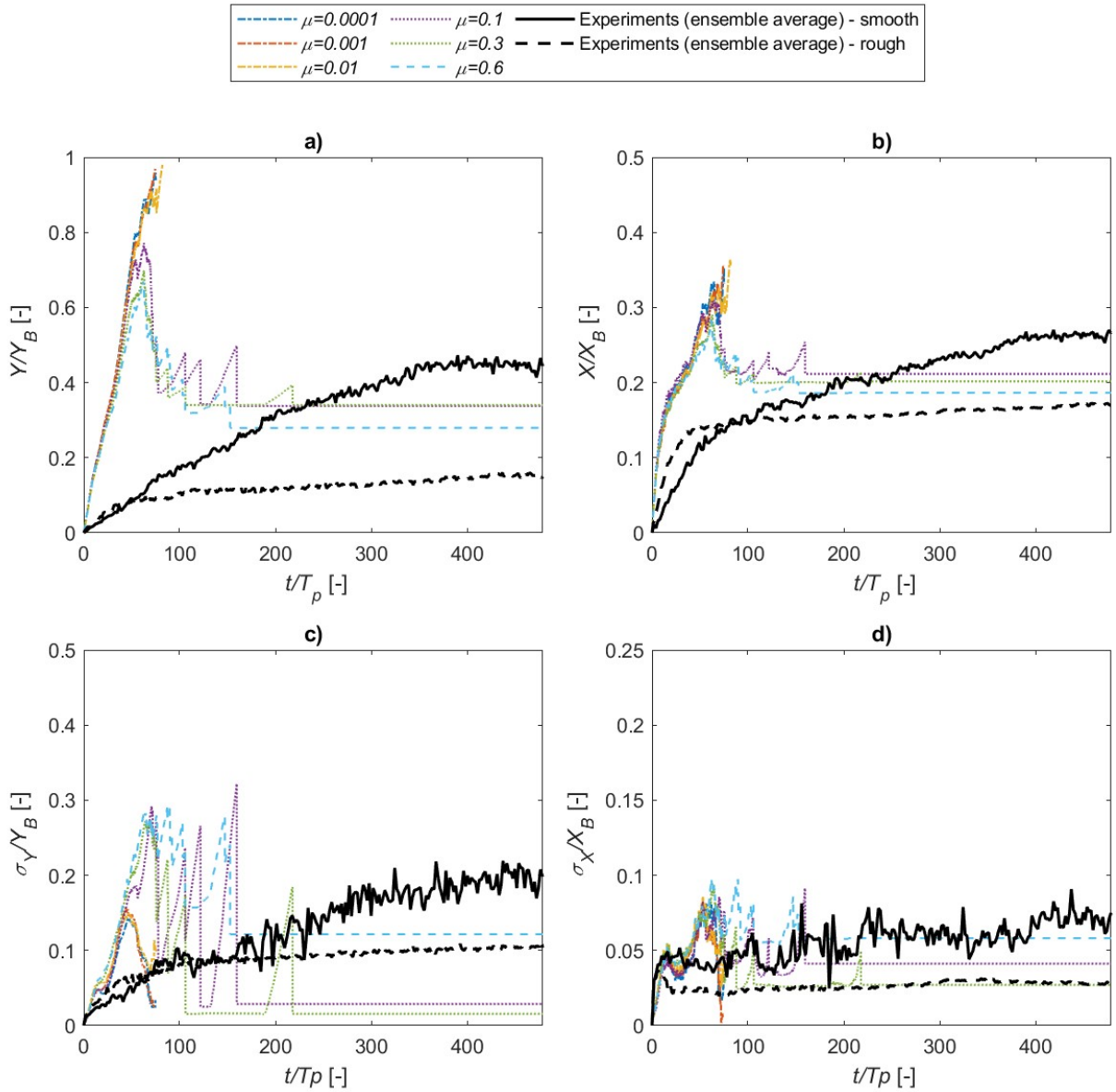

Figure 5-12. Variation in a) mean alongshore relative travel distance, b) mean cross-shore relative travel distance, c) alongshore standard deviation, and d) cross-shore standard deviation with friction coefficients in the range μ = 0.001 to 0.6 for driftwood length class L_P = 12 m (green) during TS2 ($\eta = 0.35$ m, $H_{m0} = 0.65$ s, and $T_p = 8.0$ s).

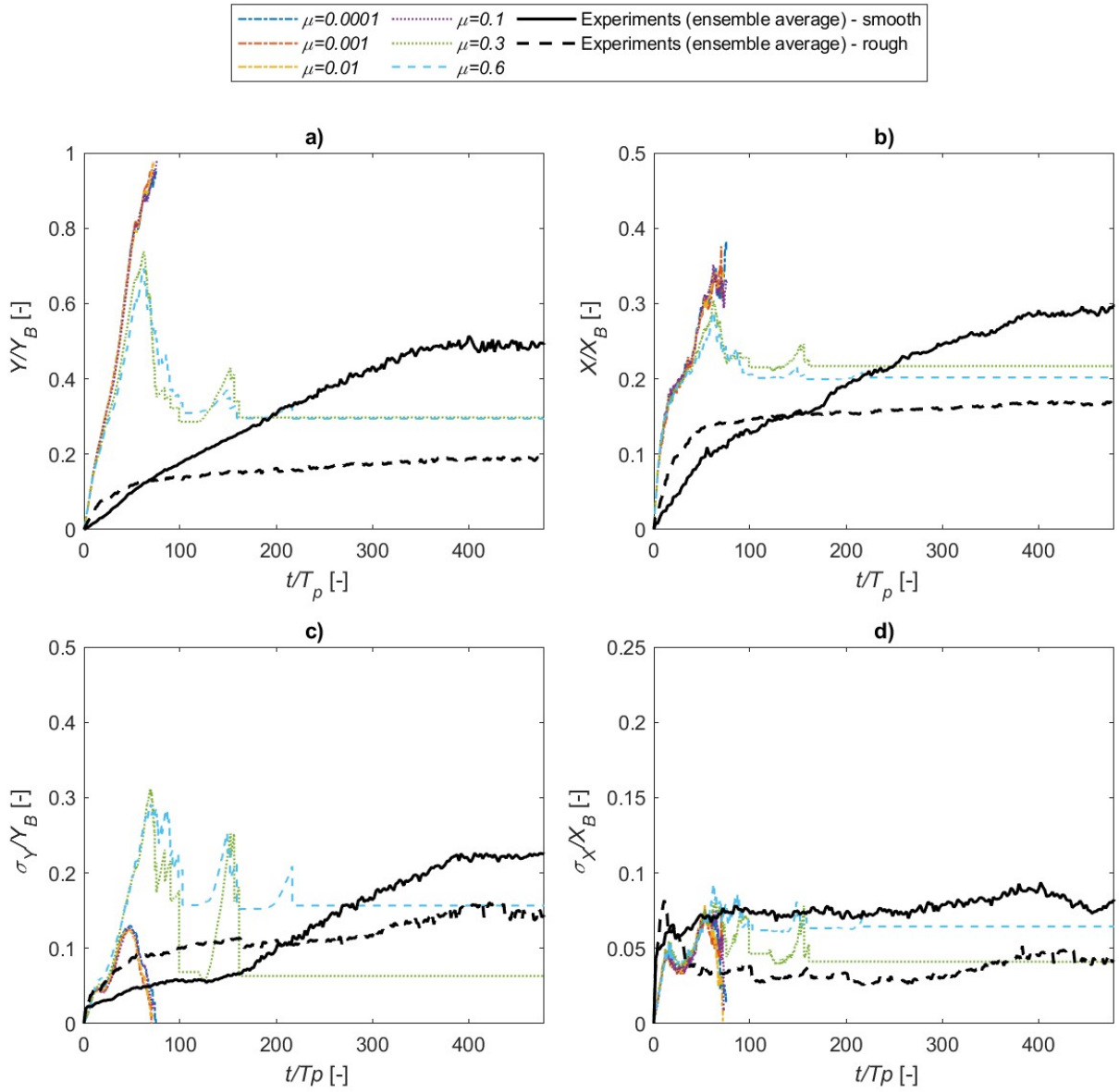

Figure 5-13. Variation in a) mean alongshore relative travel distance, b) mean cross-shore relative travel distance, c) alongshore standard deviation, and d) cross-shore standard deviation with friction coefficients in the range μ = 0.001 to 0.6 for driftwood length class L_P = 3 m (yellow) during TS2 ($\eta = 0.35$ m, $H_{m0} = 0.65$ s, and $T_p = 8.0$ s).

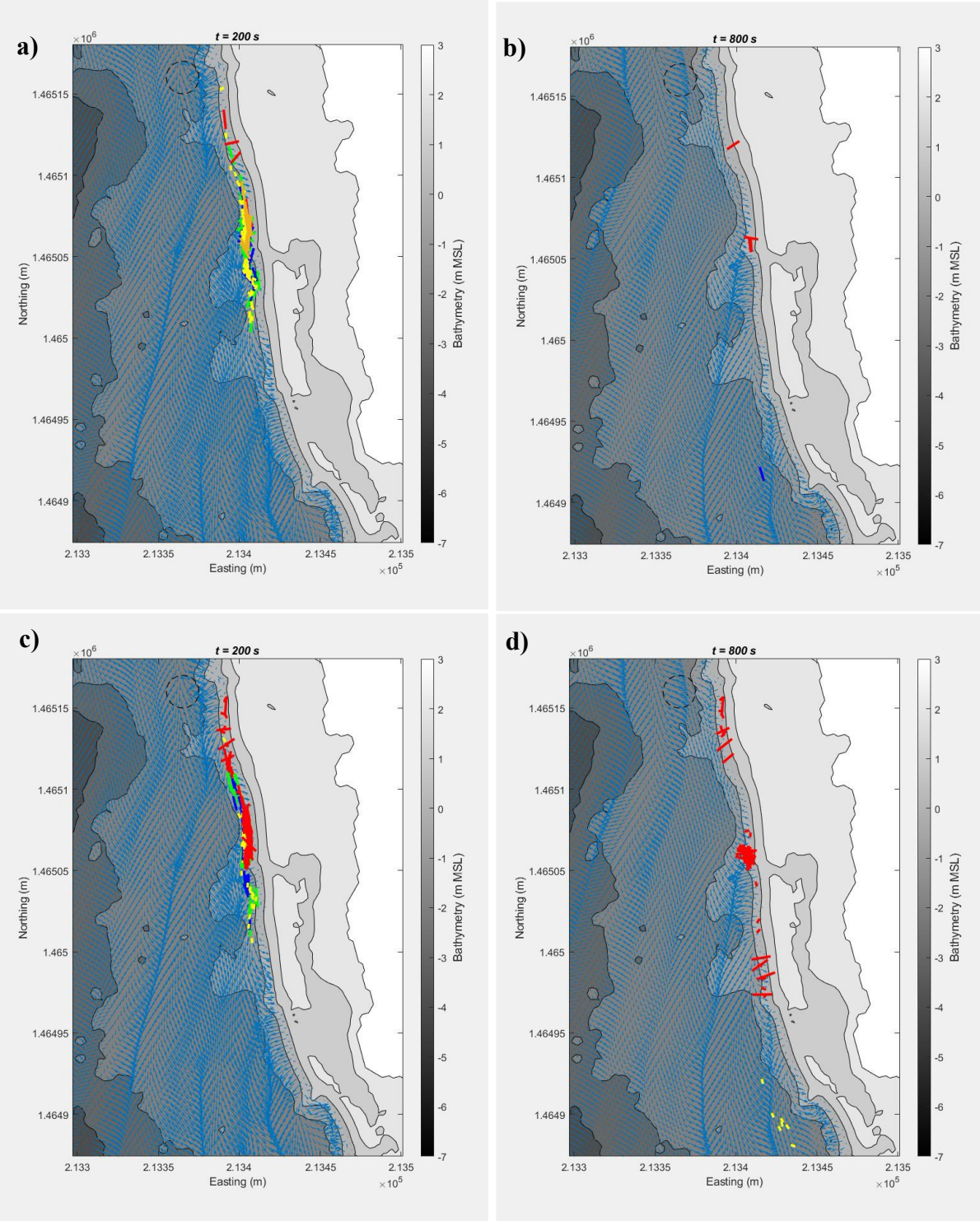

Figure 5-14. Instantaneous snapshots of simulated driftwood positions and orientations for TS2 ($\eta = 0.35$ m, $H_{m0} = 0.65$ s, and $T_p = 8.0$ s) at t = 200 s ($25T_p$) and 800 s ($100T_p$) after release, from simulations driven by surface velocities from SWASH with μ = 0.1 (panels a and b) and μ = 0.6 (panels c and d). The release area is indicated by a dashed circle. Instantaneous velocity fields are indicated by blue arrows.

The decreasing mobility and dispersion of driftwood with increasing roughness is consistent with the experimental observations (Sections 3.5.3 and 4.6). The influence of friction (or driftwood roughness) was more pronounced for longer driftwood pieces. For example, more than two-thirds of driftwood pieces in the L_P = 12 m (green) length class were retained on the beaches within Area B for simulations of TS2 with $\mu \geq 0.1$ (Figure 5-12) but this threshold increased to $\mu \geq 0.3$ for the L_P = 3 m (yellow) length class (Figure 5-13). This dependence corroborates the hypothesis (Section 4.6) that both driftwood length and relative roughness are factors controlling driftwood transport and dispersion on wave-dominated coasts. However, it is interesting to note that the force balance for beaching calculations in WOODRIFTSIM are presently performed only at the driftwood centroid, and are therefore independent of driftwood length. Moreover, inertial effects, which are expected to increase beaching likelihoods for larger (longer) pieces (Davidson et al., 2023), are not presently considered in WOODRIFTSIM. Driftwood length controls on beaching may therefore be, at least in part, intrinsically related to how the longer pieces interact with swash-zone kinematics, as opposed to a consequence of longer pieces mobilizing more bed friction or inertia. The relative importance of these phenomena could be further elucidated by computing force balances at driftwood end particles and incorporating inertial effects in future versions of WOODRIFTSIM.

5.7.4 Washoff probabilities

For all driftwood beaching events in each simulation (N_{events}), the time elapsed before a piece of beached driftwood was remobilized (i.e., washed off), t_B, was tracked. Example histograms showing the relative frequency (or probability, as $N_{events} \rightarrow \infty$) of remobilization versus t_B for driftwood length class L_P = 12 m (green) during TS2 ($\eta = 0.35$ m, $H_{m0} = 0.65$ s, and $T_p = 8.0$ s) and two values of the friction coefficient are shown in Figure 5-15. For most simulations where driftwood beaching events occurred, the data conforms to Equations 5-1 and 5-2, i.e., the washoff probability decays exponentially with t_B.

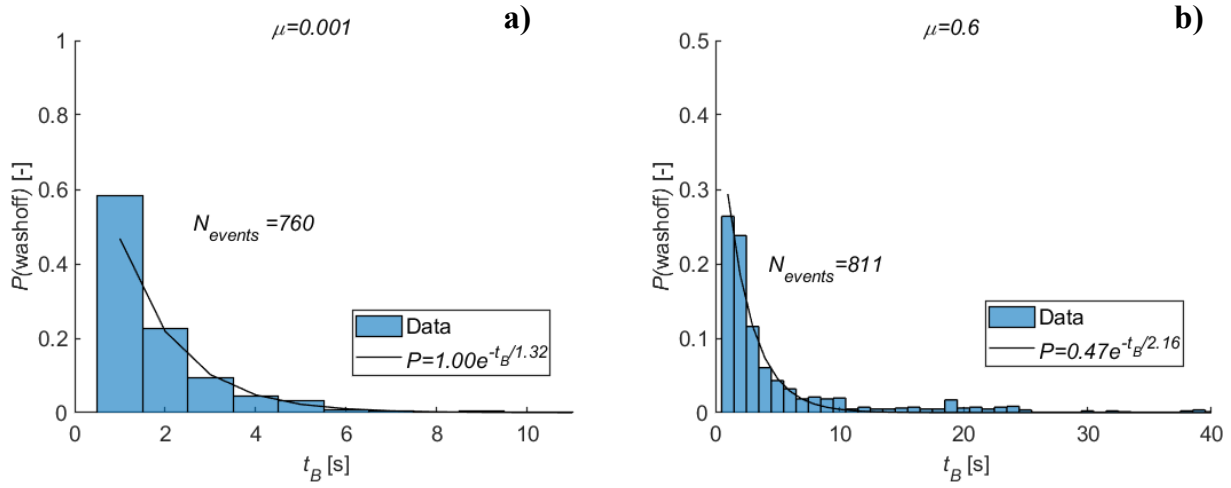

Figure 5-15. Washoff event probability versus time during for driftwood length class L_P = 12 m (green) during TS2 ($\eta = 0.35$ m, $H_{m0} = 0.65$ s, and $T_p = 8.0$ s) for a) μ = 0.001, and b) μ = 0.6.

Equation 5-2 is shown in Figure 5-15a and b based on linear, least-squares fits to the natural logarithm of the relative frequencies of washoff events in each t_B bin, with the constraint $a_{\text{mob}} \leq 1$ (since the probability of a beached driftwood piece washing off cannot exceed unity). The fit was limited to data in the region close to $t_B = 0$ exhibiting truly exponential behavior by performing multiple linear regressions to the natural logarithm of the relative frequencies for a progressively increasing number of data points, and then selecting the fit with the highest correlation coefficient. The upper bound of t_B used in this regression may be interpreted as T_{stg} in Equation 5-2. The specific rate of mobilization, a_{mob}, the mean retention time on beaches, T_R, and the half-life for washing off, T_{50}, were all determined directly from the exponential fits (Table 5-3). Figure 5-15a shows that, for TS2 simulations, the majority of beached driftwood pieces with $\mu = 0.001$ were washed off after a single Lagrangian (1 s) time step. However, only 26% of pieces with $\mu = 0.6$ were washed off after one time step (Figure 5-15b). T_R and T_{50} were less than T_p for all simulations (Table 5-3), meaning that most driftwood touching the beach was washed off by the same wave runup event that deposited it, or the next event. For any driftwood remaining on the beach for more than a few wave periods, the probability of remobilization rapidly declined (Figure 5-15).

For a given set of hydrodynamic conditions, a_{mob} tended to decrease and T_R and T_{50} increased with increasing μ, confirming experimental observations (Chapter 3 and Chapter 4) that driftwood roughness inhibits mobility (Table 5-3). However, there was no clear correlation between nearshore wave conditions and fit parameters. Counter-intuitively, a_{mob} values were often lower, and T_R and T_{50} longer, for more energetic wave conditions (e.g., TS6 and TS8, compared to TS2) (Table 5-3). In some cases (e.g., TS6), this was because higher water levels and wave runup resulted in driftwood being deposited higher on the beach profile where gradients were not as steep (Figure 5-3c), such that subsequent wave runup events did not re-mobilize the driftwood. Thus, in addition to hydrodynamics and driftwood length and roughness characteristics, coastal morphology is expected to play an important role in controlling a_{mob}, T_R and T_{50}. Moreover, for the most energetic wave conditions (TS8), episodic extreme wave run-up events sometimes led to deposition and stranding of substantial quantities of driftwood landward of the beach berm (a phenomenon also observed in experiments by Murphy et al., 2024), which remained beached for a relatively long time before remobilization by a subsequent extreme run-up event. This resulted in a "fat tail" in the washoff probability distribution, violating the basic assumptions underlying the exponential form of Equations 5-1 and 5-2. Thus, Equations 5-1 and 5-2 may be adequate to describe washoff processes on wave-dominated coasts under typical or normal climatic wave exposure conditions but are likely inadequate for describing the potential for stranding or mobilization of driftwood during extreme storm events.

.

Table 5-3. Number of washoff events, specific rates of washing off, mean residence times, and half-lives of beached driftwood.

Test Series ID	$\boldsymbol{\mu}$ [-]	$\boldsymbol{N}_{\text{events}}$ [-]			$\boldsymbol{a}_{\text{mob}}$ [s^{-1}]			$\boldsymbol{T_R}$ [s]			$\boldsymbol{T_{50}}$ [s]		
		L_P = 3 m	L_P = 9 m	L_P = 12 m	L_P = 3 m	L_P = 9 m	L_P = 12 m	L_P = 3 m	L_P = 9 m	L_P = 12 m	L_P = 3 m	L_P = 9 m	L_P = 12 m
1	0.0001	392	301	354	1.00	1.00	1.00	0.90	1.08	1.33	0.62	0.75	0.92
	0.001	281	273	233	1.00	1.00	1.00	0.87	1.13	1.29	0.60	0.79	0.89
	0.01	285	133	222	1.00	1.00	1.00	0.83	1.13	1.24	0.57	0.78	0.86
	0.1	526	277	351	1.00	0.97	0.62	1.03	1.27	1.87	0.71	0.88	1.26
	0.3	502	297	318	0.94	0.97	0.83	1.30	1.22	1.33	0.90	0.84	0.92
	0.6	454	332	317	0.36	0.54	0.42	2.85	1.91	2.29	1.97	1.32	1.59
2	0.0001	1032	788	813	1.00	1.00	1.00	0.87	1.14	1.18	0.60	0.79	0.82
	0.001	1143	822	760	1.00	1.00	1.00	0.85	1.15	1.32	0.59	0.80	0.91
	0.01	1163	865	877	1.00	1.00	1.00	0.81	1.20	1.24	0.56	0.83	0.86
	0.1	1222	762	876	1.00	1.00	1.00	1.13	1.21	1.22	0.78	0.84	0.85
	0.3	1447	964	840	0.98	0.85	0.69	1.24	1.39	1.66	0.86	0.97	1.15
	0.6	1585	830	811	0.39	0.63	0.47	2.56	1.76	2.16	1.78	1.22	1.50
3	0.0001	36	32	9	1.00	1.00	1.00	0.92	1.02	1.11	0.63	0.71	0.77
	0.001	23	31	25	1.00	1.00	1.00	1.06	1.26	1.06	0.74	0.87	0.73
	0.01	26	11	32	1.00	1.00	1.00	1.08	1.28	1.05	0.75	0.89	0.73
	0.1	47	4	32	1.00	1.00	1.00	1.00	1.63	1.09	0.69	1.13	0.75
	0.3	24	13	27	1.00	1.00	1.00	1.01	1.15	1.23	0.70	0.79	0.86
	0.6	52	55	15	0.68	0.82	0.40	1.57	1.82	2.14	1.09	1.26	1.48
5	0.0001	800	650	616	1.00	1.00	1.00	0.87	1.03	1.11	0.60	0.71	0.77
	0.001	949	682	713	1.00	1.00	1.00	0.87	1.03	1.20	0.60	0.72	0.83
	0.01	826	658	647	1.00	1.00	1.00	0.92	1.14	1.16	0.64	0.79	0.80
	0.1	1099	871	621	1.00	1.00	1.00	1.10	1.09	1.09	0.77	0.76	0.75
	0.3	1155	806	611	1.00	1.00	1.00	1.15	1.13	1.13	0.80	0.79	0.78
	0.6	1173	871	711	0.52	0.72	0.65	1.77	1.49	1.70	1.23	1.03	1.18
6	0.0001	1156	811	1127	1.00	1.00	1.00	0.91	1.24	1.26	0.63	0.86	0.87
	0.001	1197	1037	1493	1.00	1.00	1.00	0.93	1.23	1.31	0.65	0.85	0.91
	0.01	835	740	336	1.00	1.00	1.00	0.96	1.23	1.29	0.67	0.85	0.89
	0.1	1260	705	690	1.00	1.00	0.99	1.20	1.26	1.26	0.83	0.87	0.87
	0.3	700	388	522	0.53	0.77	0.71	1.83	1.39	1.52	1.27	0.96	1.05
	0.6	811	241	549	0.38	0.44	0.43	2.43	2.16	2.15	1.68	1.50	1.49
7	0.0001	24	31	13	1.00	1.00	1.00	1.01	1.10	1.19	0.70	0.76	0.82
	0.001	24	18	25	n/a*	1.00	1.00	n/a*	1.12	0.99	n/a*	0.78	0.68
	0.01	34	8	32	1.00	n/a*	1.00	1.08	n/a*	1.20	0.75	n/a*	0.83
	0.1	17	23	17	1.00	1.00	1.00	1.23	1.10	1.18	0.85	0.76	0.82
	0.3	44	17	36	1.00	0.65	1.00	1.16	1.89	1.16	0.80	1.31	0.80
	0.6	32	44	42	0.41	1.00	0.55	2.97	1.24	2.21	2.06	0.86	1.53
8	0.0001	1887	1147	1951	0.90	0.22	1.00	0.9	2.2	0.8	0.6	1.5	0.6
	0.001	3299	2087	2620	0.57	1.00	1.00	1.1	0.9	0.8	0.8	0.6	0.6
	0.01	2078	1707	2887	1.00	0.46	1.00	0.9	1.5	0.8	0.6	1.0	0.6
	0.1	1108	331	1044	1.00	0.22	1.00	0.8	2.5	0.8	0.6	1.8	0.5
	0.3	567	397	422	0.07	0.25	0.22	5.4	2.4	2.6	3.7	1.6	1.8
	0.6	267	148	252	1.00	1.00	1.00	0.8	0.9	0.8	0.6	0.6	0.5

*Note: No beaching events exceeded 2 s duration for these simulations, which prevented a regression.

The failure to identify any clear correlation between sea state parameters and beaching likelihood may be a consequence of the under-estimation of onshore-directed transport by the hydrodynamic models (both XB-NH+ and SWASH) for some conditions (TS3, TS4, and TS7). Further field, experimental, or numerical investigations would be required to further elucidate and isolate the relative importance of driftwood characteristics, coastal morphology, and hydrodynamic forcing on beaching and washoff of buoyant driftwood on wave-dominated coasts, and to develop more generally applicable probabilistic washoff algorithms

5.8 Limitations and Future Research Needs

A limitation of this study was the lack of experimental observations of hydrodynamics inside the surf zone (where the majority of driftwood transport occurred) for numerical model validation, which was imposed by scale constraints in the physical model. Larger scale physical modelling or field experiments are needed to support further validation of the efficacy of NLSW equations solvers at simulating surf zone kinematics, and WOODRIFTSIM.

The NLSW models (XB-NH+ and SWASH) used in this study were applied with a limited number of sigma layers (2 and 4, respectively). Larger numbers of sigma layers may be prescribed in SWASH. However, sensitivity tests indicated that increasing the number of sigma layers in SWASH resulted in limited improvement, instability, and/or impractically long computation times. Given that the vision for WOODRIFTSIM is to support efficient simulation of driftwood transport at regional scales of relevance to coastal zone management, the emphasis was on attempting to reproduce mean transport and dispersion of driftwood using the lowest possible resolution.

The numerical driftwood simulations described herein, and the experiments they attempted to replicate (Chapter 3), were focused on driftwood with relatively simple geometries and limited roughness. However, larger scale driftwood roughness elements, such as root wads, are known to exert influence on driftwood mobility in riverine settings, mainly through their influence on draft (Braudrick & Grant, 2000; Kang & Kimura, 2018) and damming potential (Perry et al., 2018). Driftwood with intact root systems is observed on some exposed coasts proximate to expansive forests (Chapter 2). Further research is warranted to determine the influence of root wads on coastal driftwood transport (including windage) and interactions with the shore, and to assess needs for incorporating these effects in WOODRIFTSIM.

Driftwood-driftwood interactions were not included in WOODRIFTSIM. Although the model reproduced trapping of driftwood by shore-perpendicular groyne structures, modelling of driftwood interactions with hydraulic structures and constrictions in rivers suggests that driftwood collisions, rafting or entanglement may need to be incorporated to accurately simulate transport and trapping on structures under congested conditions (Kang et al., 2021). The extent to which interactions between individual pieces of driftwood influence mean transport and dispersion in coastal settings is less certain, and warrants further investigation, particularly since adding such

complexity to numerical models would increase computational burden, and potentially limit applications at regional or oceanic scales.

Sediment transport, morphodynamics, and driftwood interactions with sediment were not considered in the numerical simulations. Driftwood interactions with sediments (e.g., self-burial) may be important factors controlling driftwood residence times and mobility on wave-exposed beaches. Self-burial of beached driftwood by sediment was observed in the physical model experiments (Section 3.5.4), and may explain why friction coefficients on the order of $O(0.1)$, i.e., higher than the rolling resistance of smooth cylinders, were required in the numerical model to reproduce the mean transport characteristics of smooth dowels. Although the experiments were likely influenced by scale effects (Section 3.6), self-burial of beached driftwood by wave-transported sediment has been observed in natural settings. For example, the deposition and subsequent burial of a piece of driftwood by wave action on a sandy beach on the shore of Lake Ontario over a period of about 48 hours is shown in Figure 5-16a and b. This phenomenon undoubtedly reduces the probability of driftwood remobilization by waves; substantial force was required to exhume the partially buried piece of driftwood (Figure 5-16c). There is a need for further research on driftwood-geomorphology interactions to better understand the implications for driftwood mobility (Braun et al., 2023), and to guide the use of driftwood in nature-based coastal solutions.

Figure 5-16. a) Driftwood deposited on the beach surface at Sand Banks Provincial Park, Lake Ontario on 28 October 2023, b) the same piece of driftwood, partially buried by sediment on 30 October 2023, and c) depression in the beach surface after removal of the driftwood, indicating the depth of burial.

5.9 Conclusion

A Lagrangian model for simulating coastal driftwood transport by waves was developed and driven by output from two NLSW equations solvers, and the results were compared to scale physical model experiments. While both NLSW equations models (XBeach reduced 2-layer model, and SWASH with 4 layers) were capable of reasonably reproducing sea state parameters and mean wave-induced current speeds at the edge of the surf zone, there were distinct differences and variability in the hydrodynamic predictions inside the surf zone, which has profound implications for modelling coastal driftwood transport. Only Lagrangian driftwood simulations driven by SWASH surface layer velocities were capable of reproducing the onshore-directed wave-driven transport and beaching of driftwood observed in the experiments, though not for all sea state conditions. For simulations where driftwood was transported onshore, a simple dynamics-based beaching and washoff algorithm in the Lagrangian model was found to reasonably reproduce

mean driftwood transport and dispersion rates, with tuning of driftwood-beach friction coefficients. The sensitivity to friction coefficients confirms that driftwood roughness exerts substantial control on its mobility in wave-dominated settings. A statistical analysis of the simulated residence times of beached driftwood indicated some general conformity with probabilistic washoff models often used in marine debris simulations, which assume an exponential decay in the likelihood of remobilization with time following a beaching event. However, discrete wave runup event interactions with beach morphologies, and extreme (storm) wave events can result in washoff probability distributions with "fat tails" that deviate from this exponential form. Consequently, more sophisticated statistics-based (or machine learning-based) "metamodels" or computationally efficient physics-based models (e.g., Gaido-Lasserre et al., 2024) may be needed to develop suitable approximations of buoyant driftwood interactions with shorelines at wave- or swash-resolving spatiotemporal scales, for application in Lagrangian models spanning much larger scales.

Chapter 6. Synthesis and Discussion

6.1 Summary of Key Findings

Key findings pertaining to coastal driftwood fate and transport based on the literature review (Chapter 2), scale physical modelling experiments (Chapter 3 and Chapter 4), and numerical modelling (Chapter 5) are summarized as follows:

- Driftwood from natural and anthropogenic sources is abundant in coastal regions;
- Coastal driftwood supply and distribution varies in time and space in response to multiple natural and anthropogenic drivers;
- Wood weathers and degrades over time in response to biological and physico-chemical processes, and human activities;
- Driftwood tends to accumulate in "hotspots" (i.e., exhibits a "patchy" distribution);
- Key transport drivers in oceanic and coastal waters include currents, wind, waves, and sea ice dynamics;
- In physical modelling experiments, erosion of beach sediments was not observed to be a major driver of driftwood mobility even under fairly extreme (if depth-limited) wave forcing (nearshore $H_s = 3.70$ m and $T_p = 10$ s), with the caveat that driftwood-sediment interactions were prone to uncertainty associated with model scale effects. On the contrary, partial self-burial of driftwood was observed in the model and the field, which inhibits transport.
- Wave-induced transport and dispersion of driftwood in nearshore areas are controlled or constrained by:
    - Driftwood characteristics, including buoyancy (which is time-dependent in response to saturation and dessication), length, roughness (including presence of bark, root wads)
    - Nearshore hydrodynamic conditions, characterized in particular by:
        - Sea state forcing $\sim H_s^2 T_p^{-1}$;
        - Balances between: offshore-directed transport by rip currents, undertow, downrush in the swash zone, and rolling/sliding on the beach interface; onshore-directed transport by breaking wave bores (surfing), Stokes drift, uprush in the swash zone; and stabilizing friction at the driftwood-beach interface;
        - Vertical variations in horizontal wave-induced velocities within the surf zone. Driftwood transport is sensitive to mean surface velocities, which in the nearshore can differ significantly from depth-averaged velocities or Stokes drift; and
        - Water levels, which influence depth-induced wave breaking and wave-induced circulation, and determine the length of coastal structures at the water line.

    - Shoreline characteristics, including foreshore slope, backshore profile, sediments, roughness (e.g., vegetation), and planform geometry; and
    - Coastal structures (or nature-based features), including shore-perpendicular (e.g., groynes, barrier beaches) or nearshore (e.g., detached breakwaters) structures, and the length of structures at the water line.
- The probability of beached driftwood being remobilized by waves (for a given water level and sea state condition) generally decays exponentially with time after beaching. However, back beach morphologies, extreme wave events, and the tendency for driftwood to accumulate in hotspots can result in "fat tails" in the probability distribution.

6.2 Implications for Coastal Engineering Design and Coastal Zone Management

6.2.1 Predicting Wave-Driven Transport and Accumulation

Coastal engineers and coastal zone managers need to be able to accurately predict transport and fate of coastal driftwood for a variety of reasons, including:

- Identification of accumulation hot-spots (e.g., to guide efficient removal);
- Assessment of impacts and risk (e.g., damage to infrastructure, boats, sensitive ecosystems, or nature-based features);
- Management of wood supply (e.g., from forestry or industry) and distribution within the coastal zone;
- Control of the spread of invasive plant and animal species transported by driftwood;
- Design of coastal structures exposed to wood impacts;
- Design of nature-based solutions incorporating wood.

WOODRIFTSIM (Chapter 5) offers a potentially useful tool to support many of these applications, and has a number of additional features (e.g., windage, first order degradation and associated influence on wood volume) that were not explored in this thesis, which could be useful for predicting driftwood transport and fate in the field.

A major challenge in simulating coastal driftwood fate and transport is the diversity of spatiotemporal scales of relevance (Chapter 2). Driftwood can be transported thousands of kilometres by ice and ocean currents but its fate may also be determined by variability in wave-induced velocities in the surf zone with spatial scales on the order of tens of centimeters, and time scales on the order of wave periods. These scale disparities are inherently challenging and computationally burdensome for numerical models, requiring a range of resolutions and approaches. WOODRIFTSIM represents a pragmatic attempt to address these scale disparities, by making use of: (i) Lagrangian, kinematics-based techniques that are readily scalable and concentrate computational effort in parts of the domain where driftwood resides; and (ii) physics-based but computationally-efficient algorithms for key processes controlling driftwood mobility (beaching and washoff). However, the model is critically dependent on accurate hydrodynamic

input, and specifically, surf zone and swash zone velocities. Despite reproducing sea state parameters at the edge of the surf zone reasonably well, the (relatively) computationally intensive phase-resolving nonlinear shallow water equations solvers investigated in Chapter 5 (XBeach and SWASH) had some difficulty in accurately predicting aspects of surf zone and swash zone dynamics. Only SWASH, with 4 sigma layers, could predict surface layer velocities that were consistent with the observed onshore-directed transport of driftwood. Advancements in surf zone and swash zone dynamics models, and their integration in computationally-efficient, multi-scale modelling systems (Barnard et al., 2014; Crosby et al., 2023), are therefore needed to enable the application of debris transport models and predictive tools like WOODRIFTSIM.

The limited availability of driftwood data, particularly driftwood supply to the coastal zone, is also a barrier to more widespread field application of predictive models like WOODRIFTSIM. Remote sensing and machine learning-based computer vision techniques are emerging as promising methods for observing patchy distributions of driftwood over large spatial scales and multi-year temporal scales (Eamer & Walker, 2010; Heathfield & Walker, 2011; Doong et al., 2011; Kramer, 2016; Braun et al., 2022; Hood, 2023), and may be used in the future to support, validate, and augment driftwood models and budgets.

Beaching and remobilization were found to be critical processes affecting driftwood mobility. However, it is remarkable that these processes remain poorly understood, and crudely represented in most marine debris models using probabilistic algorithms. WOODRIFTSIM attempts to improve on the latter, and may provide a useful tool for developing more robust stochastic beaching-washoff models. However, the episodic nature of driftwood remobilization following a beaching event poses a challenge for probabilistic approaches.

6.2.2 Use of Wood in Nature-Based Shore Protection

Processed wood (or timber) has been used as a material in coastal engineering structures for centuries, owing to attractive properties including a high strength to weight ratio, natural durability, low environmental impacts and embodied carbon (if recycled or derived from a sustainably managed source), and aesthetics (Crossman & Simm, 2004). Typically, this has involved the construction of timber groynes to trap sediment transported alongshore (Perdok et al., 2003), or shore-parallel timber fences to trap windblown sediment in dunes (Crossman & Simm, 2004). However, the use of wood has declined as rock, concrete and steel have been more widely adopted (Perdok et al., 2003).

There has been renewed interest in the use of wood in shore protection schemes in recent years, partly in response to its promotion as a so-called “nature-based solution” in grey literature and guidance (Stewardship Centre for British Columbia, 2023; Johannessen et al., 2014). Unlike previous uses of wood that involved processed timber, recent iterations have typically involved

placement (and in some cases, anchoring) of logs, driftwood or large woody debris in various configurations on the shore[1]. Examples include:

- Anchored woody debris installations (Wilson, 2020)
- Log groynes (Kaminsky et al., 2020);
- Backshore barriers (Bayle et al., 2021);
- Tree reefs (Dickson et al., 2023);
- Brushwood dams or fences (Provan et al., 2023).

However, there is limited evidence on the role and efficacy of wood used in shore protection in these ways, particularly for high wave energy coastal settings (Wilson, 2020; Wilson et al., 2020; Falkenrich et al., 2021). The following sections provide insights based on the findings in Chapter 2 through Chapter 5, which may address some knowledge gaps and guide the use of wood in nature-based coastal solutions.

6.2.2.1 Service life

As discussed in Chapter 2, wood is subject to weathering and degradation by a variety of biological and physico-chemical processes, and human activities. Considering the implications for the service life of wood installations, this partly explains why more durable materials such as rock and concrete have been preferentially adopted in the past. However, the weathering and degradation processes themselves are likely an important aspect of how wood contributes positively to ecosystem function, nourishing biota and releasing nutrients. Degradation rates are highly site-specific, depending on wood characteristics (e.g., species) and environmental conditions (e.g., water chemistry, climate, presence and species of biota) (Section 2.2). Larger pieces of wood may be adopted by design to compensate for material degradation over time, and to extend service life.

6.2.2.2 Quantity

The use of wood in shore protection should only be considered a nature-based solution if it contributes to natural ecosystem function. Human interference in the supply and distribution of wood in coastal ecosystems through activities such as logging, damming and channelization of rivers, and wood removal, as well as the effects of climate change, has made it difficult to determine the "natural" or "reference" wood abundance by region (Hood, 2023). Considering the potential negative impacts of large quantities of driftwood on sensitive coastal ecosystems (such as marshes) and infrastructure, and the limited understanding of the ecological role of wood in coastal systems (Hood, 2023), it should probably only be introduced to coastal environments where wood is naturally present but where supply has been constrained (e.g., by historical removal, or deforestation).

[1] "Live" wood installations such as tree- or forest-planting, or mangroves, are beyond the scope of this thesis.

6.2.2.3 Stability

Wood in undisturbed coastal ecosystems is dynamic, a characteristic that is integral to some of the ecosystem services it purportedly provides (e.g., rafting and dispersal of seeds). By contrast, anchored woody debris installations (Wilson, 2020) are intended to be statically stable (though this is not always achieved), and/or to trap mobile driftwood (Johannessen et al., 2014). The extent to which anchored wood installations contribute to ecosystem function is uncertain, and the evidence for their engineering performance (in terms of durability, and controlling wave runup and erosion) in exposed coastal settings is underwhelming (Wilson, 2020). For unanchored wood installations where some mobility is inevitable or desirable, suggestions to maximize stability (if desired) are as follows:

- Simulations (using tools like WOODRIFTSIM) or observations of where wood naturally tends to accumulate and stabilize may inform placement (Kaminsky et al., 2020);
- Wood placed higher on the backshore is less likely to be mobilized by waves, and can contribute to shoreline stabilization by trapping windblown sediment (Grilliot, 2019). Interestingly, Johannessen et al. (2014) and Wilson (2020) recommend placing large wood above the highest tide but within the limit of wave runup.
- In wave-dominated environments, driftwood mobility correlates with $H_s^2 T_p^{-1}$ when unconstrained by shore interactions (Chapter 4). Wood that becomes mobilized in regions with wave climates exhibiting low $H_s^2 T_p^{-1}$ is therefore less likely to be transported over large distances from the site. This roughly aligns with existing guidance that suggests wood installations are not suitable for high wave energy environments (Johannessen et al., 2014);
- In the scale physical model experiments (Chapter 3) and numerical simulations (Chapter 5), there was a general tendency for beached driftwood to orient itself parallel to the shoreline (Figure 6-1), which is consistent with field observations by others (Braun et al., 2022). Observed shoreline morphologies, or dynamic equilibrium shoreline models (González & Medina, 2001; Hsu et al., 1989), may therefore be used to guide placement for maximum stability;
- Longer wood pieces are more stable;
- Rougher wood pieces (e.g., with branches or root wads) are expected to be more stable but these effects may diminish with time due to weathering and degradation;
- Partial burial of wood by sediment increases stability, and may occur naturally over time where exposed to swash;
- Although mobilization of partially buried wood by erosional events was not observed in the physical modelling experiments in which nearshore wave heights were depth-limited (Chapter 3), field evidence indicates that this is a possibility (Grilliot, 2019; Braun et al., 2022). Shoreline morphodynamics should therefore be considered when assessing the stability of placed wood;
- The temporal evolution of wood buoyancy should be considered in the context of exposure to water (e.g., through precipitation, inundation, wave action) and dessication. For wood placed above the elevation of tides, it may be prudent to assess buoyancy based on a fully dried scenario, representing the least stable (most mobile) condition.

- On shorelines with strong rip currents, mobilized wood may be transported offshore, and lost from the littoral system. The potential for rip currents to develop may therefore be a consideration for wood retention.

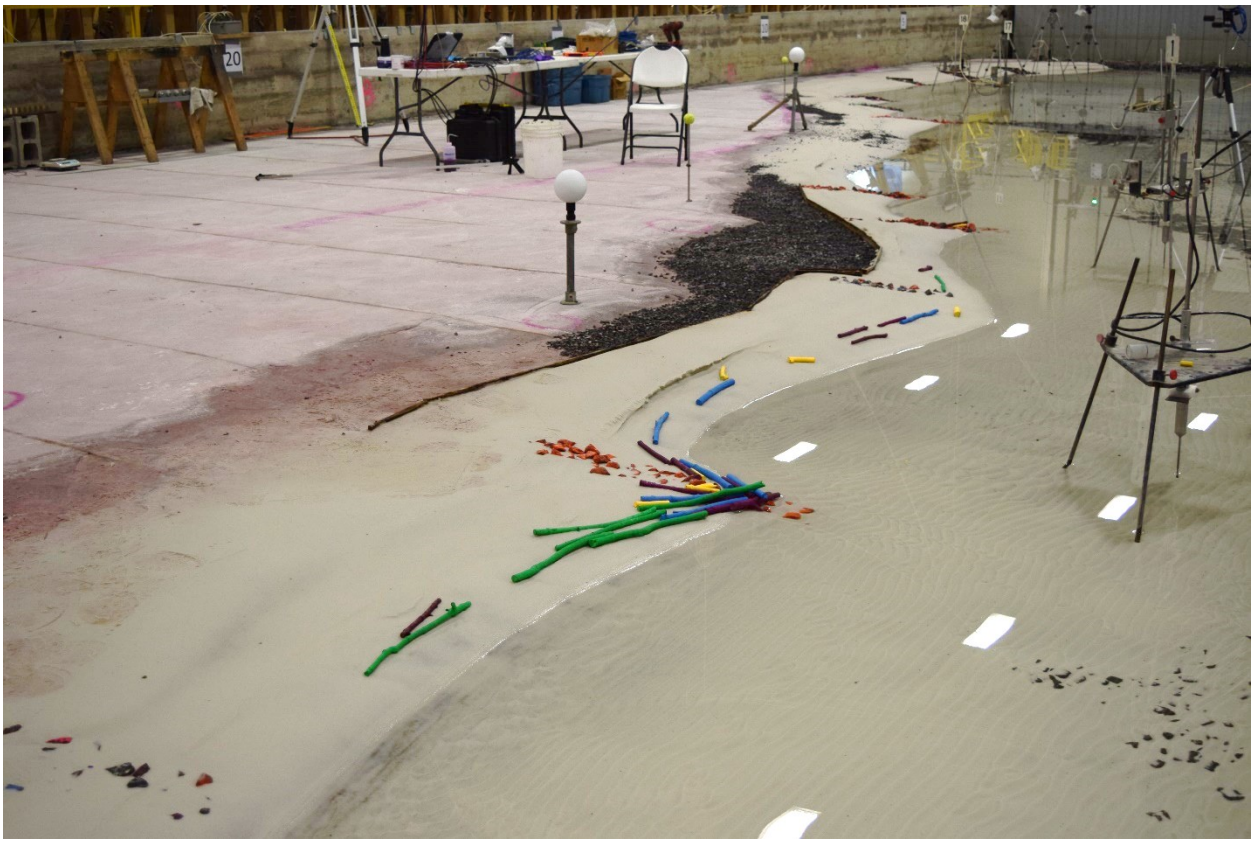

Figure 6-1. Model driftwood deposits on the beach following a scale physical model experiment.

For wood installations designed to be somewhat dynamic, the potential negative consequences of driftwood mobilization by various forcing factors (e.g., storms, tsunami) should be considered. These may include impacts and damage to infrastructure, and sensitive natural features (e.g., salt marshes). Potential pathways and fate may be explored using predictive tools, such as WOODRIFTSIM. The potential for wood to act as agent of dispersion should be considered both in the context of invasive species (negative) and natural ecosystem function, e.g., native seed dispersal (positive). Locally sourced and supplied native wood might be expected to minimize the risk of spreading invasives, and maximize compatibility with natural system processes.

6.2.2.4 Wave run-up

Based on a limited set of physical modelling experiments, Wilson (2020) determined that anchored large woody debris should not be relied upon to reduce wave run-up, and under certain circumstances can even amplify run-up. It is not clear how unanchored (potentially mobile) wood might influence wave run-up but it could constitute an additional hazard, and therefore should probably not be used for the purpose of suppressing wave run-up.

6.2.2.5 Geomorphic control

Matrices of wood on sandy backshores and dunes are proven to trap and stabilize windblown sediments (Grilliot, 2019; Walker & Barrie, 2006; Eamer & Walker, 2010; Heathfield & Walker, 2011; Braun et al., 2022). However, the geomorphic control exerted by wood in the foreshore is less clearly understood, and is likely dependent on sediment characteristics as well as wave exposure, which varies in time for a given site. By surveying paired (wooded and unwooded) beaches in New Zealand, Kennedy & Woods (2012) found that large wood on gravel beaches caused berm crests to be 0.5–1.0 m higher and beachface profiles to be steeper following storms than on beaches without wood. On sandy beaches, Kennedy & Woods (2012) determined that the main geomorphic influence of large wood in the foreshore was to trap sediments during calm wave conditions, which is consistent with observations in Chapter 5. However, Braun et al. (2022) determined from decadal observations on Lake Michigan that the influence of large wood on geomorphology was limited to short temporal and small spatial scales, and had no effect on the overall trajectory of erosion driven by rising water levels. Falkenrich et al. (2021) also determined from physical modelling experiments that, under different conditions of placement and wave exposure, anchored large wood can either contribute to, exacerbate or prevent erosion. These ambiguities and uncertainties suggest that placement of large wood in the foreshore is not a proven technique for erosion prevention on exposed coasts, particularly in the context of rising sea levels, and further research is needed to elucidate wood-geomorphology interactions in the foreshore. However, placement on sandy backshores and dunes can be effective in supporting dune stabilization and growth.

6.2.3 Coastal Structures

The physical model experiments and numerical simulations provided insight to how shore-perpendicular (groynes, barrier beaches) and shore-parallel (detached breakwater) structures influence driftwood mobility (Chapter 3 to Chapter 5). Depending on the context for application and the driftwood regime at a particular site, coastal structures may either be designed to trap, or avoid trapping driftwood. Trapping driftwood may be desirable to prevent impacts on nearby sensitive receptors, or to enable efficient removal. Structures designed to trap driftwood should be more robust and stable than those designed to avoid trapping.

For shore-perpendicular structures, the length of the structure at the waterline relative to the target driftwood length is a key determinant of trapping potential. Structures that are shorter than a target driftwood length are less likely to result in accumulation (Chapter 4). Keeping in mind that the length of the structure at the waterline may change in response to water level fluctuations, and the geometry and footprint of the structure, this information may be used to design structures to target or avoid trapping) driftwood within certain length class categories. In circumstances where trapping of driftwood is anticipated, the ability of the structure to withstand loads from driftwood accumulations should be considered. The length of a structure alone is not always a reliable predictor of driftwood trapping potential. Some shore-perpendicular structures and features – especially larger ones, such as the barrier beach features in Chapter 3 – may

contribute to the generation of rip currents that can actually enhance alongshore or offshore transport of driftwood. A strong understanding of nearshore dynamics and circulation, e.g., developed through a combination of field measurements and modelling, is needed to identify the potential for rip current development, which can inform design of structures to maximize (or minimize) driftwood trapping potential.

The physical modelling experiments described in Chapter 3 and Chapter 4 showed that detached (offshore) breakwaters or features are generally less inhibitive of driftwood transport and dispersion in the nearshore than shore-perpendicular structures. However, the duration of the experiments was not long enough to facilitate the formation of salient or tombolos in the lee of the breakwaters, which would likely contribute to trapping of driftwood. In general, longer detached breakwaters were more effective at delaying or preventing alongshore transport of driftwood in their lee, as might be expected based on conditions for sediment accumulation in existing design guidance for detached breakwaters (Rogers et al., 2010; Suh & Dalrymple, 1987).

Given the buoyant nature of driftwood, low-crested or submerged coastal structures may be considered where there is a desire to avoid trapping and accumulation of driftwood. The crest of the structure should be at or below the expected draft of target driftwood classes, based on the size and relative density of driftwood, and accounting for potential waterlogging and changes in seawater temperature and salinity. Assuming the goal is to avoid trapping of driftwood, it may be prudent to design crest levels based on the higher ranges of relative densities in local driftwood distributions, since a single trapped log may act as, in the terminology of wood jams in rivers (Eaton et al., 2013), a “key piece” that initiates trapping of others. However, this may result in crest levels that are too low for the structure to fulfill other design objectives (e.g., wave attenuation). Trade-offs and compromises may therefore be required.

Although not investigated in detail in this thesis, the slope, orientation, and roughness of structures may also determine the potential for trapping of driftwood. In the physical model experiments (Chapter 3), shorter driftwood pieces were generally more likely to be trapped on the rock groynes, settling into the interstices between rocks. Longer pieces were less prone to these effects, since they did not fit as easily into interstices, and because one end typically remained free of the structure, directly exposed to hydrodynamic forcing. It is possible that smoother or steeper-sloped structures (e.g., timber groynes, or rubble-mound groynes comprised of smaller rock size classes with smaller interstices) would not have been as effective at trapping the smaller pieces. Structures angled updrift seem by intuition more likely to trap driftwood, although further investigation is required to confirm this hypothesis.

6.3 Limitations and Recommendations for Further Research

The limitations of the physical modelling and numerical modelling studies presented in this thesis are discussed at length in Chapter 3, Chapter 4, and Chapter 5. Key limitations are summarized as follows:

- Scale effects in the physical model (Section 3.6);
- Limited hydrodynamic observations within the surf and swash zones in the physical model (Section 5.8);
- The effects of time-varying water levels (e.g., tides) and associated circulation on driftwood transport, beaching and mobilization were not considered (i.e., only wave effects at various still water levels);
- Practical challenges with the optical tracking technique (Section 4.5.1);
- Limitations in the capabilities of numerical wave models to accurately reproduce surf- and swash-zone hydrodynamics (Section 5.8);
- Simplifications within WOODRIFTSIM, and processes not considered, e.g. (Chapter 5):
    - Driftwood moves with the flow (i.e., kinematics-based approach) and inertial effects are neglected;
    - Driftwood-driftwood interactions, which may be important under congested conditions (e.g., rafting);
    - Evaluation of force balance for beaching and mobilization at driftwood centroids only;
    - The influence of spatially varying diffusivities on driftwood dispersion (i.e., naïve random walk);
    - Assumption that driftwood is well represented by cylinders (e.g., may not be valid for irregularly shaped driftwood, such as rootwads), and associated influences on driftwood interactions with the shore, structures, and wind;
    - Interactions with sediment transport and morphodynamics (e.g., self-burial, mobilization due to erosion, influence on beach morphology);
    - Inertia of driftwood, which may influence the beaching process.

Opportunities for further research on coastal driftwood fate and transport are also identified within Chapter 3, Chapter 4, and Chapter 5; which are summarized as follows:

- Identification and quantification of coastal driftwood supply from different sources, and changes resulting from climate change (e.g., impacts on the frequency and intensity of disturbances driving coastal driftwood supply), land use, and other human activities;
- Quantification of driftwood transformation (weathering, degradation, buoyancy) under different conditions;
- Coastal driftwood entanglement and rafting – mechanisms and drivers;

- Improved, computationally-efficient surf zone and swash zone hydrodynamic models;
- The ecological role of coastal driftwood;
- Driftwood-geomorphology interactions (e.g., scour and self-burial, influence on beach morphology, trapping of sediment);
- Transport and dispersion of irregularly-shaped driftwood;
- The influence of roughness elements and root wads on coastal driftwood transport (including windage) and interactions with the shore;
- Identification of threshold wave exposures for use of driftwood in nature-based coastal solutions;
- Testing and validation of recommendations for use of driftwood in nature-based coastal solutions;
- Further investigation of the relative importance of driftwood characteristics, coastal morphology, and hydrodynamic forcing on beaching and washoff of buoyant driftwood;
- Development of probabilistic beaching and washoff models grounded in physics;
- Integration of driftwood models with computationally-efficient, multi-scale flood and erosion hazard modelling systems;
- Field observations of driftwood transport, dispersion, and accumulation (including via remote sensing); and
- Field validation of numerical driftwood models.

Chapter 7. Conclusion

A comprehensive literature review, and scale physical modelling involving model driftwood release experiments was used to identify key factors and processes governing the fate and transport of coastal driftwood. A Lagrangian driftwood transport model, incorporating a novel, physics-based beaching and remobilization algorithm, was developed to replicate the physical model experiments, and to provide a tool for predicting driftwood transport, dispersion, and accumulation in wave-dominated nearshore environments. Together, the physical and numerical models elucidated key drivers and processes influencing driftwood mobility on wave-exposed sandy shores including various coastal structures, and pinpointed advantages and limitations of two existing, "state-of-the-art" coastal wave models in supporting driftwood transport and dispersion modelling. The literature review and modelling provided insight to the use of unanchored wood in design of nature-based shore protection, and implications for coastal structure design in regions with an abundance of driftwood. Needs for further research to better inform use and management of coastal driftwood were also identified.

References

Abbe, T., & Montgomery, D. (2003). Patterns and processes of wood debris accumulation in the Queets river basin, Washington. *Geomorphology, 51*(1-3), 81-107.

Akahori, R., Yamaguchi, S., Yabe, H., & Shimizu, Y. (2023). Transport Dynamics of Large Wood in a Stream Channel Affected by Spur Dikes. *Water Resources Research, 59*(2), e2021WR030740.

Alix, C. (2005). Deciphering the impact of change on the driftwood cycle: contribution to the study of human use of wood in the Arctic. *Global and Planetary Change, 47*(2-4), 83-98.

Al-Rabeh, A., Lardner, R., & Gunay, N. (2000). Gulfspill Version 2.0: a software package for oil spills in the Arabian Gulf. *Environmental Modelling & Software, 15*(4), 425-442.

Aylor, D., & Flesch, T. (2001). Estimating spore release rates using a Lagrangian stochastic simulation model. *Journal of Applied Meteorology and Climatology, 40*(7), 1196-1208.

Ballard, J. (2022). B.C. coastal communities assess damage, look to future after king tides, extreme weather wreak havoc. *CBC.* January 8. Accessed December 30, 2022. https://www.cbc.ca/news/canada/british-columbia/b-c-coastal-communities-assess-damage-look-to-future-after-king-tides-extreme-weather-wreak-havoc-1.6308798.

Barber, H., Dadswell, H., & Ingle, H. (1959). Transport of driftwood from south America to Tasmania and Macquarie Island. *Nature, 184*(4681), 203-204.

Barbier, E., Hacker, S., Kennedy, C., Koch, E., Stier, A., & Silliman, B. (2011). The value of estuarine and coastal ecosystem services. *Ecological Monographs, 81*(2), 168-193.

Barnard, P., van Ormondt, M., Erikson, L., Eshleman, J., Hapke, C., Ruggiero, P., Adams, P.N., & Foxgrover, A. (2014). Development of the Coastal Storm Modeling System (CoSMoS) for predicting the impact of storms on high-energy, active-margin coasts. *Natural Hazards, 74*, 1095-1125.

Bartocci, P., Barbanera, M., D'Amico, M., Laranci, P., Cavalaglio, G., Gelosia, M., Ingles, D., Bidini, G., Buratti, C., Cotana, F., & Fantozzi, F. (2017). Thermal degradation of driftwood: Determination of the concentration of sodium, calcium, magnesium, chlorine and sulfur containing compounds. *Waste Management*, 151-157.

Barton, A. (2019). Blue Kenue enhancements from 2014 to 2019. *XXVIth TELEMAC-MASCARET User Conference* (pp. 1-8). Toulouse: TELEMAC-MASCARET Consortium. doi:https://doi.org/10.5281/zenodo.3611511

Battjes, J.A. (1988). Surf-zone dynamics. *Annual Review of Fluid Mechanics, 20* (1), 257-291.

Bayle, P., Kaminsky, G., Blenkinsopp, C., Weiner, H., & Cottrell, D. (2021). Behaviour and performance of a dynamic cobble berm revetment during a spring tidal cycle in North Cove, Washington State, USA. *Coastal Engineering, 167*, 103898.

Bernardino, A., Smith, C., Baco, A., Altamira, I., & Sumida, P. (2010). Macrofaunal succession in sediments around kelp and wood falls in the deep NE Pacific and community overlap with other reducing habitats. *Deep Sea Research Part I: Oceanographic Research Papers, 57*(5), 708-723.

Bertoldi, W., Welber, M., Mao, L., Zanella, S., & Comiti, F. (2014). A flume experiment on wood storage and remobilization in braided river systems. *Earth Surface Processes and Landforms, 39*(6), 804-813.

Björdal, C., & Dayton, P. (2020). First evidence of microbial wood degradation in the coastal waters of the Antarctic. *Nature Scientific Reports, 10*(1), 1-8.

Black, K., & Gay, S. (1990). A numerical scheme for determining trajectories in particle models. *Acanthaster and the Coral Reef: A Theoretical Perspective. Lecture Notes in Biomathematics* (pp. 151-156). Berlin: Springer. doi:10.1007/978-3-642-46726-4_9

Bladé, E., Sánchez-Juny, M., & Ruiz-Villanueva, V. (2016). Strategies in the 2D numerical modelling of wood transport in rivers. *River Flow 2016 - 8th International Conference on Fluvial Hydraulics* (pp. 12-15). St. Louis: Taylor & Francis.

Bocchiola, D., Rulli, M., & Rosso, R. (2008). A flume experiment on the formation of wood jams in rivers. *Water Resources Research, 44*(2).

Borges, L., Cragg, S., Bergot, J., Williams, J., Shayler, B., & Sawyer, G. (2008). Laboratory screening of tropical hardwoods for natural resistance to the marine borer Limnoria quadripunctata: The role of leachable and non-leachable factors. *Holzforschung, 62*(1), 99-111.

Braudrick, C., & Grant, G. (2000). When do logs move in rivers? *Water Resources Research, 36*(2), 571-583.

Braudrick, C., & Grant, G. (2001). Transport and deposition of large woody debris in streams: a flume experiment. *Geomorphology, 41*(4), 263-283.

Braun, K., Mattheus, C., & Theuerkauf, E. (2022). The geomorphic role of large wood in the coastal zone: Mobilization threshold and beach morphology impacts in the North American Great Lakes. *Geomorphology, 411*, 108292.

Bridges, T., King, J., Simm, J., Beck, M., Collins, G., Lodder, Q., & Mohan, R. (eds.). (2021). *International Guidelines on Natural and Nature-Based Features for Flood Risk Management.* Vicksburg, MS: U.S. Army Engineer Research and Development Center.

Brown, A., & Niedzwecki, J. (2018). Review of Modeling Techniques for Marine Debris Flows. *OCEANS 2018 MTS/IEEE* (pp. 1-7). Charleston: Institute of Electrical and Electronics Engineers. doi:10.1109/OCEANS.2018.8604605

Brown, J., MacMahan, J., Reniers, A., & Thornton, E. (2009). Surf zone diffusivity on a rip-channeled beach. *Journal of Geophysical Research: Oceans, 114*(C11015), 1-20.

Bula, F. (2022). Vancouver waterfront in need of repairs after severe winter storm. *The Globe and Mail.* January 11. Accessed December 30, 2022. https://www.theglobeandmail.com/canada/british-columbia/article-vancouver-assesses-waterfront-repairs-after-storms/.

Castelle, B., Michallet, H., Marieu, V., Leckler, F., Dubardier, B., Lambert, A., Berni, C., Bonneton, P., Barthelemy, E., & Bouchette, F. (2010). Laboratory experiment on rip current circulations over a moveable bed: Drifter measurements. *Journal of Geophysical Research: Oceans, 115*(C12008), 1-17.

Castelle, B., Scott, T., Brander, R., & McCarroll, R. (2016). Rip current types, circulation and hazard. *Earth-Science Reviews, 163*, 1-21.

Chang, C.W., & Mori, N. (2021). Green infrastructure for the reduction of coastal disasters: A review of the protective role of coastal forests against tsunami, storm surge, and wind waves." *Coastal Engineering Journal, 63*(3), 370-385.

Chin, D. (2022). Contaminant transport in the surf zone. *Oceanologia, 64*(4), 651-664.

Cinar, G., Keen, A., & Lynett, P. (2023). Motion of a Debris Line Source Under Currents and Waves: Experimental Study. *Journal of Waterway, Port, Coastal, and Ocean Engineering, 149*(2), 04022033.

Clark, D.B., Feddersen, F., & Guza, R.T. (2010). Cross-shore surfzone tracer dispersion in an alongshore current. *Journal of Geophysical Research, 115*(C10035). doi:10.1029/2009JC005683.

Clarke, L.B., Ackerman, D., & Largier, J. (2007). Dye dispersion in the surf zone: Measurements and simple models. *Continental Shelf Research, 27*, 650-669.

CloudCompare. (2015). *CloudCompare Version 2.6.1.* GPL software. Retrieved 16 February, 2024, from http://www.cloudcompare.org/

Convey, P., Barnes, D., & Morton, A. (2002). Debris accumulation on oceanic island shores of the Scotia Arc, Antarctica. *Polar Biology, 25*(8), 612-617.

Cornett, A., Knox, P., Menninger, J., Lux, R., & Provan, M. (2017). Assessment of debris issues impacting design of a flood diversion project in a large scale physical model. *37th IAHR*

World Congress (pp. 1-9). Kuala Lumpur: International Association for Hydro-Environment Engineering and Research.

Cornett, A., Provan, M., & Bear, M. (2018). Assessment of Debris Mitigation Systems for Tidal and River Turbines. *7th International Conference on Ocean Energy* (pp. 1-6). Cherbourg: ICOE.

Cotana, F., Buratti, C., Barbanera, M., Cavalaglio, G., Foschini, D., Nicolini, A., & Pisello, A. (2016). Driftwood biomass in Italy: estimation and characterization. *Sustainability, 8*(8), 725.

Critchell, K., & Lambrechts, J. (2016). Modelling accumulation of marine plastics in the coastal zone; what are the dominant physical processes? *Estuarine, Coastal and Shelf Science, 171*, 111-122.

Critchell, K., Grech, A., Schlaefer, J., Andutta, F., Lambrechts, J., Wolanski, E., & Hamann, M. (2015). Modelling the fate of marine debris along a complex shoreline: lessons from the Great Barrier Reef. *Estuarine, Coastal and Shelf Science, 167*(B), 414-426.

Crosby, S., Nederhoff, C., VanArendonk, N., & Grossman, E. (2023). Efficient modeling of wave generation and propagation in a semi-enclosed estuary. *Ocean Modelling, 184*, 102231.

Crossman, M., & Simm, J. (2004). *Manual on the use of timber in coastal and river engineering.* London: Thomas Telford.

Dalaiden, Q., Goosse, H., Lecomte, O., & Docquier, D. (2018). A model to interpret driftwood transport in the Arctic. *Quaternary Science Reviews, 191*, 89-100.

Dalrymple, R., Hérault, A., Bilotta, G., & Farahani, R. (2010). GPU-accelerated SPH model for water waves and other free surface flows. *Proc. 32nd International Conference on Coastal Engineering* (pp. 1-5). Shanghai: ICCE.

Dalrymple, R., MacMahan, J.H., Reniers, A.J., & Nelko, V. (2011). Rip currents. *Annual Review of Fluid Mechanics, 43*, 551-581.

D'Aoust, S., & Millar, R. (2000). Stability of ballasted woody debris habitat structures. *Journal of Hydraulic Engineering, 126*(11), 810-817.

Davidson, B., Brenner, J., & Pujara, N. (2023). Beaching model for buoyant marine debris in bore-driven swash. *Flow*, 3, E35.

Davidson, S., Hesp, P., & Silva, G. (2020). Controls on dune scarping. *Progress in Physical Geography: Earth and Environment, 44*(6), 923-947.

Davidson, S., MacKenzie, L., & Eaton, B. (2015). Large wood transport and jam formation in a series of flume experiments. *Water Resources Research, 51*(12), 10065-10077.

Davis, R.E. (1991). Lagrangian ocean studies. *Annual Review of Fluid Mechanics*, *23*(1), 43-64.

Dayton, P. (1971). Competition, disturbance, and community organization: the provision and subsequent utilization of space in a rocky intertidal community. *Ecological Monographs*, 351-389.

Dean, R. (1985). Physical modelling of littoral processes. In R.A. Dalrymple, *Physical Modelling in Coastal Engineering* (288 pp.). Boca Raton: CRC Press.

De Beer, A., McCall, R., Long, J., Tissier, M., & Reniers, A. (2021). Simulating wave runup on an intermediate–reflective beach using a wave-resolving and a wave-averaged version of XBeach. *Coastal Engineering, 163*, 103788.

de Ridder, M., Smit, P., van Dongeren, A., McCall, R., Nederhoff, K., & Reniers, A. (2021). Efficient two-layer non-hydrostatic wave model with accurate dispersive behaviour. *Coastal Engineering, 164*, 103808.

Deike, L., Pizzo, N., & Melville, W. (2017). Lagrangian transport by breaking surface waves. *Journal of Fluid Mechanics, 829*, 364-391.

Dickson, J., Franken, O., Watson, M., Monnich, B., Holthuijsen, S., Eriksson, B., . . . Bouma, T. (2023). Who lives in a pear tree under the sea? A first look at tree reefs as a complex natural biodegradable structure to enhance biodiversity in marine systems. *Frontiers in Marine Science, 10*, 1213790. doi:10.3389/fmars.2023.1213790

Dimou, K., & Adams, E. (1993). A random-walk, particle tracking model for well-mixed estuaries and coastal waters. *Estuarine, Coastal and Shelf Science, 37*(1), 99-110.

Doong, D., Chuang, H., Shieh, C., & Hu, J. (2011). Quantity, distribution, and impacts of coastal driftwood triggered by a typhoon. *Marine Pollution Bulletin, 62*(7), 1446-1454.

Ducks Unlimited Canada. (2023). *Boundary Bay Tidal Marsh Restoration Project.* Accessed October 10, 2023. https://www.ducks.ca/places/british-columbia/boundary-bay-tidal-marsh-restoration/.

Dyke, A., England, J., Reimnitz, E., & Jetté, H. (1997). Changes in driftwood delivery to the Canadian Arctic Archipelago: The hypothesis of postglacial oscillations of the Transpolar Drift. *Arctic*, 1-16.

Eamer, J., & Walker, I. (2010). Quantifying sand storage capacity of large woody debris on beaches using LiDAR. *Geomorphology, 118*(1-2), 33-47.

Eaton, B., Hassan, M., & Davidson, S. (2013). Scale-dependent interactions between wood and channel dynamics: Modeling jam formation and sediment storage in gravel-bed streams. *Journal of Geophysical Research: Earth Surface, 118*(4), 2500-2508.

Edgell, M., & Ross, W. (1983). Marine log transportation and handling systems in British Columbia: impacts on coastal management. *Coastal Management, 11*(1-2), 41-69.

Elfring, B., & Baldock, T. (2002). Hydrodynamics and sediment transport in the swash zone: a review and perspectives. *Coastal Engineering, 45*, 149-167.

Elliott, M., Mander, L., Mazik, K., Simenstad, C., Valesini, F., Whitfield, A., & Wolanski, E. (2016). Ecoengineering with ecohydrology: successes and failures in estuarine restoration. *Estuarine, Coastal and Shelf Science, 176*, 12-35.

Elsayed, S., Gijsman, R., Schlurmann, T., & Goseberg, N. (2022). Nonhydrostatic numerical modeling of fixed and mobile barred beaches: Limitations of depth-averaged wave resolving models around sandbars. *Journal of Waterway, Port, Coastal, and Ocean Engineering, 148*(1), 04021045.

Endresen, H., & Tørum, A. (1992). Wave forces on a pipeline through the surf zone. *Coastal Engineering, 18*(3-4), 267-281.

Eriksson, C., Burton, H., Fitch, S., Schulz, M., & van den Hoff, J. (2013). Daily accumulation rates of marine debris on sub-Antarctic island beaches. *Marine Pollution Bulletin, 66*(1-2), 199-208.

Everett, R., & Ruiz, G. (1993). Coarse woody debris as a refuge from predation in aquatic communities. *Oecologia, 93*(4), 475-486.

Falkenrich, P., Wilson, J., Nistor, I., Goseberg, N., Cornett, A., & Mohammadian, A. (2021). Nature-Based Coastal Protection by Large Woody Debris as Compared to Seawalls: A Physical Model Study of Beach Morphology and Wave Reflection. *Water, 13*(15), 20.

Fall, A., Weber, B., Pakpour, M., Lenoir, N., Shahidzadeh, N., Fiscina, J., Wagner, C., & Bonn, D. (2014). Sliding friction on wet and dry sand. *Physical Review Letters*, 175502.

Feddersen, F. (2007). Breaking wave induced cross-shore tracer dispersion in the surf zone: Model results and scalings. *Journal of Geophysical Research: Oceans, 112*(C09012), 1-12.

Ferguson, S., Provan, M., Murphy, E., Bérubé, D., Desrosiers, M., Robichaud, A., & Kim, J. (2022). Assessing Numerical Model Skill at Simulating Coastal Flooding Using Field Observations of Deposited Debris and Photographic Evidence. *Water, 14*(4), 589.

Fischer, H., List, E., Koh, R., Imberger, J., & Brooks, N. (1979). *Mixing in Inland and Coastal Waters.* London: Academic Press.

Forsberg, P., Sous, D., Stocchino, A., & Chemin, R. (2020). Behaviour of plastic litter in nearshore waters: first insights from wind and wave laboratory experiments. *Marine Pollution Bulletin, 153*, 111023.

Gaido-Lasserre, C., Nederhoff, K., Storlazzi, C., Reguero, B., & Beck, M. (2024). Improved efficient physics-based computational modeling of regional wave-driven coastal flooding for reef-lined coastlines. *Ocean Modelling, 189*, 102358.

Gall, S., & Thompson, R. (2015). The impact of debris on marine life. *Marine Pollution Bulletin, 92*(1-2), 170-179.

Gates, J., Mallette, T., Merrill, S.B., & Ballestero, T. (2018). *Two Northeastern DOTs Consider Green Infrastructure Techniques for Coastal Highway Resilience: A Joint Study with Divergent Outcomes.* Technical Report, Washington: US Federal Highway Administration. https://rosap.ntl.bts.gov/view/dot/58162.

Giddings, J. (1952). Driftwood and problems of Arctic sea currents. *Proceedings of the American Philosophical Society, 96*(2), 129-142.

Glover, A. W., & Dahlgren, T. (2013). Bone-eating worms from the Antarctic: the contrasting fate of whale and wood remains on the Southern Ocean seafloor. *Proceedings of the Royal Society B: Biological Sciences, 280*(1768), 20131390.

Goda, Y. (2010). Reanalysis of regular and random breaking wave statistics. *Coastal Engineering Journal, 52*(1), 71-106.

Golik, A., & Gertner, Y. (1992). Litter on the Israeli coastline. *Marine Environmental Research, 33*(1), 1-15.

Gonor, J., Sedell, J., & Benner, P. (1988). What we know about large trees in estuaries, in the sea, and on coastal beaches. In C. Maser, R. Tarrant, J. Trappe, & J. Franklin, *From the forest to the sea, a story of fallen trees* (p. 153). Portland: U.S. Department of Agriculture, Forest Service, Pacific Northwest Research Station.

González, M., & Medina, R. (2001). On the application of static equilibrium bay formulations to natural and man-made beaches. *Coastal Engineering, 43*(3-4), 209-225.

Gracia, A., Rangel-Buitrago, N., & Flórez, P. (2018). Beach litter and woody-debris colonizers on the Atlantico department Caribbean coastline, Colombia. *Marine Pollution Bulletin, 128*, 185-196.

Gräwe, U., Deleersnijder, E., Shah, S., & Heemink, A. (2012). Why the Euler scheme in particle tracking is not enough: the shallow-sea pycnocline test case. *Ocean Dynamics, 62*(4), 501-514.

Grech, A., Wolter, J., Coles, R., McKenzie, L., Rasheed, M., Thomas, C., Waycott, M., & Hanert, E. (2016). Spatial patterns of seagrass dispersal and settlement. *Diversity and Distributions, 22*(11), 1150-1162.

Grilliot, M. (2019). *The Role of Large Woody Debris on Sandy Beach-Dune Morphodynamics.* Victoria: University of Victoria.

Grilliot, M., Walker, I., & Bauer, B. (2019). Aeolian sand transport and deposition patterns within a large woody debris matrix fronting a foredune. *Geomorphology, 338*, 1-15.

Haehnel, R., & Daly, S. (2004). Maximum impact force of woody debris on floodplain structures. *Journal of Hydraulic Engineering, 130*(2), 112-120.

Häggblom, A. (1982). Driftwood in Svalbard as an indicator of sea ice conditions: a preliminary report. *Geografiska Annaler: Series A, Physical Geography, 64*(1-2), 81-94.

Harmon, M., & Hua, C. (1991). Coarse woody debris dynamics in two old-growth ecosystems. *BioScience, 41*(9), 604-610.

Harper, J., Henry, R., & Stewart, G. (1988). Maximum storm surge elevations in the Tuktoyaktuk region of the Canadian Beaufort Sea. *Arctic*, 48-52.

Harris, J.F.W., Jordaan, J.M., McMurray, W.R., Verwey, C.J., & Anderson, F.P. (1963). Mixing in the surf zone. *International Journal of Air and Water Pollution, 7*, 649-667.

Heathfield, D., & Walker, I. (2011). Analysis of coastal dune dynamics, shoreline position, and large woody debris at Wickaninnish Bay, Pacific Rim National Park, British Columbia. *Canadian Journal of Earth Sciences, 48*(7), 1185-1198.

Herterich, K., & Hasselmann, K. (1982). The horizontal diffusion of tracers by surface waves. *Journal of Physical Oceanography, 12*, 704-711.

Hood, W. (2007). Large woody debris influences vegetation zonation in an oligohaline tidal marsh. *Estuaries and Coasts, 30*(3), 441-450.

Hood, W. (2023). Distribution of Large Wood in River Delta Tidal Marshes: Implications for Habitat Restoration. *Estuaries and Coasts, 46*, 1-19. doi:ttps://doi.org/10.1007/s12237-022-01122-5

Hsu, J., Silvester, R., & Xia, Y. (1989). Generalities on static equilibrium bays. *Coastal Engineering, 12*(4), 353-369.

Hunter, J. (1987). The application of Lagrangian particle-tracking techniques to modelling of dispersion in the sea. *North-Holland Mathematics Studies, 147*, 257-269.

Hunter, J., Craig, P., & Phillips, H. (1993). On the use of random walk models with spatially variable diffusivity. *Journal of Computational Physics, 106*(2), 366-376.

Ikeno, M., Takabatake, D., Kihara, N., Kaida, H., Miyagawa, Y., & Shibayama, A. (2016). Improvement of collision force formula for woody debris by airborne and hydraulic experiments. *Coastal Engineering Journal, 58*(04), 1640022.

Inman, D.L., & Bagnold, R.A. (1962). Beach and nearshore processes: littoral processes. *The Sea, 2,* 529-553.

Iwasaki, S., Isobe, A., Kako, S., Uchida, K., & Tokai, T. (2017). Fate of microplastics and mesoplastics carried by surface currents and wind waves: A numerical model approach in the Sea of Japan. *Marine Pollution Bulletin, 121*(1-2), 85-96.

Jalón-Rojas, I., Wang, X., & Fredj, E. (2019). A 3D numerical model to track marine plastic debris (TrackMPD): sensitivity of microplastic trajectories and fates to particle dynamical properties and physical processes. *Marine Pollution Bulletin, 141*, 256-272.

Johannessen, J., MacLennan, A., Blue, A., Waggoner, J., Williams, S., Gerstel, W., . . . Shipman, H. (2014). *Marine Shoreline Design Guidelines.* Olympia: Washington Department of Fish and Wildlife.

Johansen, S. (1999). Origin of driftwood in north Norway and its relevance for transport routes of drift ice and pollution to the Barents Sea. *Science of the Total Environment, 231*(2-3), 201-225.

Johnson, D., & Pattiaratchi, C. (2004a). Transient rip currents and nearshore circulation on a swell-dominated beach. *Journal of Geophysical Research: Oceans, 109*(C02026), 1-10.

Johnson, D., & Pattiaratchi, C. (2004b). Application, modelling and validation of surfzone drifters. *Coastal Engineering, 51*, 455-471.

Johnson, S. (1989). Deposition, fate, and characteristics of derelict trawl web on an Alaskan beach. *Marine Pollution Bulletin, 20*(4), 164-168.

Johnson, S., & Eiler, J. (1999). Fate of radio-tagged trawl web on an Alaskan beach. *Marine Pollution Bulletin, 38*(2), 136-141.

Jones, R.A., & Pattiaratchi, C. (2005). Nearshore Currents and Surf Zone Dispersion on Adelaide Metropolitan Beaches. *Proceedings Coasts and Ports 2005: Coastal Living - Living Coast.* Barton: Institution of Engineers, Australia. 625-630.

Kako, S., Isobe, A., Kataoka, T., Yufu, K., Sugizono, S., Plybon, C., & Murphy, T. (2018). Sequential webcam monitoring and modeling of marine debris abundance. *Marine Pollution Bulletin, 132*, 33-43.

Kako, S., Isobe, A., Magome, S., Hinata, H., Seino, S., & Kojima, A. (2011). Establishment of numerical beach-litter hindcast/forecast models: An application to Goto Islands, Japan. *Marine Pollution Bulletin, 62*(2), 293-302.

Kaminsky, G., Cottrell, D., & Glore, G. (2020). Nature-based dynamic revetment construction at North Cove, Washington, USA. *International Conference on Coastal Engineering* (p. 1). Virtual: American Society of Civil Engineers.

Kang, T., & Kimura, I. (2018). Computational modeling for large wood dynamics with root wad and anisotropic bed friction in shallow flows. *Advances in Water Resources, 121*, 419-431.

Kang, T., Kimura, I., & Onda, S. (2021). Application of computational modeling for large wood dynamics with collisions on moveable channel beds. *Advances in Water Resources, 152*, 103912.

Kasprak, A., Magilligan, F., Nislow, K., & Snyder, N. (2012). A Lidar-derived evaluation of watershed-scale large woody debris sources and recruitment mechanisms: Coastal Maine, USA. *River Research and Applications, 28*(9), 1462-1476.

Kataoka, T., Hinata, H., & Kato, S. (2013). Analysis of a beach as a time-invariant input/output system of marine litter. *Marine Pollution Bulletin, 77*(1-2), 266-273.

Kataoka, T., Hinata, H., & Kato, S. (2015). Backwash process of marine macroplastics from a beach by nearshore currents around a submerged breakwater. *Marine Pollution Bulletin, 101*(2), 539-548.

Kennedy, A.B., & Thomas, D. (2004). Drifter measurements in a laboratory rip current. *Journal of Geophysical Research: Oceans, 109*(C08005), 1-16.

Kennedy, D., & Woods, J. (2012). The influence of coarse woody debris on gravel beach geomorphology. *Geomorphology, 159*, 106-115.

Kim, J., Murphy, E., Nistor, I., Ferguson, S., & Provan, M. (2020). On the use of the ERA5 Reanalysis, Driftwood Lines, and Sea Ice Data for Numerical Investigation of Storm Surges in the Beaufort Sea. *Arctic Change 2020. 7*, p. 1. Virtual: ArcticNet. Retrieved from https://cdnsciencepub.com/doi/full/10.1139/as-2021-0001

Kim, J., Murphy, E., Nistor, I., Ferguson, S., & Provan, M. (2021). Numerical Analysis of Storm Surges on Canada's Western Arctic Coastline. *Journal of Marine Science and Engineering, 9*(3), 326.

Kimura, I., & Kitazono, K. (2018). Studies on driftwood motions around obstacles by laboratory and numerical experiments. *River Flow 2018 - 9th International Conference on Fluvial Hydraulics* (p. 02032). Lyon: EDP Sciences. doi:10.1051/e3sconf/20184002032

Kimura, I., & Kitazono, K. (2019). Effects of the driftwood Richardson number and applicability of a 3D–2D model to heavy wood jamming around obstacles. *Environmental Fluid Mechanics*, 1-23.

Knox, P., Cornett, A., Provan, M., Menninger, J., Lux, R., & Abbas, S. (2018). Assessment of Debris Issues Impacting Design of a Flood Diversion Project in a Large-Scale Physical Model. *Canadian Dam Association Bulletin* (pp. 10-19). Quebec: Canadian Dam Association.

Kramer, N. (2016). *Great river wood dynamics in Northern Canada.* Fort Collins: Colorado State University.

Krauss, K., Doyle, T., Twilley, R., Smith III, T., Whelan, K., & Sullivan, J. (2005). Woody Debris in the Mangrove Forests of South Florida. *Biotropica: The Journal of Biology and Conservation, 37*(1), 9-15.

Kubota, M. (1994). A mechanism for the accumulation of floating marine debris north of Hawaii. *Journal of Physical Oceanography, 24*(5), 1059-1064.

LaCasce, J.H. (2008). Statistics from Lagrangian observations. *Progress in Oceanography, 77*, 1-29.

Lebreton, L.-M., Greer, S., & Borrero, J. (2012). Numerical modelling of floating debris in the world's oceans. *Marine Pollution Bulletin, 64*(3), 653-661.

Lee, S., Lie, H., Song, K., & Lim, C. (2005). A second-order particle tracking method. *Ocean Science Journal, 40*(4), 201-208.

Lepofsky, D., Lyons, N., & Moss, M. (2003). The use of driftwood on the North Pacific Coast: an example from Southeast Alaska. *Journal of Ethnobiology, 23*(1), 125-142.

Li, H., Feng, X., Ni, X., & Feng, W. (2023). Beaching process of floating marine debris associated with the evolution of the nearshore wave. *Marine Pollution Bulletin, 197*, 115695.

List, E.J., Gartrell, G., & Winant, C.D. (1990). Diffusion and Dispersion in Coastal Waters. *Journal of Hydraulic Engineering, 116*(10), 1158-1179.

Liubartseva, S., Coppini, G., Lecci, R., & Clementi, E. (2018). Tracking plastics in the Mediterranean: 2D Lagrangian model. *Marine Pollution Bulletin, 129*(1), 151-162.

Longuet-Higgins, M.S. (1970). Longshore currents generated by obliquely incident sea waves, 1. *Journal of Geophysical Research, 75*(33), 6778-6789.

Longuet-Higgins, M.S., & Stewart, R.W. (1960). Changes in the form of short gravity waves on long waves and tidal currents. *Journal of Fluid Mechanics, 8*(4), 565-583.

Lumpkin, R., Maximenko, N., & Pazos, M. (2012). Evaluating where and why drifters die. *Journal of Atmospheric and Oceanic Technology, 29*(2), 300-308.

Lumpkin, R., Özgökmen, T., & Centurioni, L. (2017). Advances in the application of surface drifters. *Annual Review of Marine Science, 9*, 59-81.

MacLeod, R., & Dallimore, S. (2021). Assessment of storm surge history as recorded by driftwood in the MacKenzie Delta and Tuktoyaktuk Coastlands, Arctic Canada. *Frontiers in Earth Science, 9*, 698660.

MacMahan, J., Brown, J., Brown, J., Thornton, E., Reniers, A., Stanton, T., Henriquez, M., Gallagher, E., Morrison, J., Austin, M.J., Scott, T.M., & Senechal, N. (2010). Mean Lagrangian flow behavior on an open coast rip-channeled beach: A new perspective. *Marine Geology, 268*(1-4), 1-15.

MacVicar, B., & Piégay, H. (2012). Implementation and validation of video monitoring for wood budgeting in a wandering piedmont river, the Ain River (France). *Earth Surface Processes and Landforms, 37,* 1272-1289.

Mansui, J., Molcard, A., & Ourmieres, Y. (2015). Modelling the transport and accumulation of floating marine debris in the Mediterranean basin. *Marine Pollution Bulletin, 91*(1), 249-257.

Mariani, A., & Pattiaratchi, C.B. (2007). A field investigation of dispersion in a surfzone dominated by longshore currents. *Coasts and Ports 2007: 18th Australasian Coastal and Ocean Engineering Conference 2007 and the 11th Australasian Port and Harbour Conference 2007.* Melbourne: Engineers Australia. 586-591.

Masselink, G., Russell, P., Turner, I., & Blenkinsopp, C. (2009). Net sediment transport and morphological change in the swash zone of a high-energy sandy beach from swash event to tidal cycle time scales. *Marine Geology, 267*(1-2), 18-35.

Matsutomi, H. (2009). Method for estimating collision force of driftwood accompanying tsunami inundation flow. *Journal of Disaster Research, 4*(6), 435-440.

McCall, R., Masselink, G., Poate, T., Roelvink, J., Almeida, L., Davidson, M., & Russell, P. (2014). Modelling storm hydrodynamics on gravel beaches with XBeach-G. *Coastal Engineering, 91*, 231-250.

Miller, J., Rella, A., & Hopson, E. (2015). *Hudson River Sustainable Shorelines Forensic Analysis: Common Project Performance Factors.* Staatsburg: Hudson River National Estuarine Research Reserve in Association with Stevens Institute of Technology.

Miller, J., & Rella, A. (2015). The Performance of Ecologically-Enhanced Urban Shorelines in NYC duringSuperstorm Sandy. *Coastal Structures and Solutions to Coastal Disasters* (pp. 392-400). Boston: American Society of Civil Engineers.

Monismith, S.G., & Fong, D.A. (2004). A note on the potential transport of scalars and organisms by surface waves. *Limnology and Oceanography, 49*(4), 891-1224.

Mori, N., Yasuda, T., Arikawa, T., Kataoka, T., Nakajo, S., Suzuki, K., Yamanaka, Y., & Webb, A. (2019). 2018 Typhoon Jebi post-event survey of coastal damage in the Kansai region, Japan. *Coastal Engineering Journal, 61*(3), 278-294.

Morison, J., O'Brien, M., Johnson, J., & Schaaf, S. (1950). The force exerted by surface waves on piles. *Petroleum Transactions, 189*, 149-154.

Murphy, E., Cornett, A., Nistor, I., & Baker, S. (2020). Modelling Transport and Fate of Woody Debris in Coastal Waters. *Coastal Engineering Proceedings* (p. 11). virtual: American Society of Civil Engineers. doi:https://doi.org/10.9753/icce.v36v.papers.1

Murphy, E., Cornett, A., & Nistor, I. (2023). Numerical simulation of driftwood transport by waves in a laboratory basin. *Coastal Engineering Proceedings, 37.* Sydney: American Society of Civil Engineers. doi:https://doi.org/10.9753/icce.v37.management.7

Murphy, E., Cornett, A., van Proosdij, D., & Mulligan, R.P. (2024a). *Nature-Based Infrastructure for Coastal Flood and Erosion Risk Management – A Canadian Design Guide.* Ottawa: National Research Council of Canada.

Murphy, E., Nistor, I., Cornett, A., Rayner, A., Baker, S., & Stolle, J. (2024b). Application of an optical tracking technique to characterize nearshore wave-driven transport and dispersion of model driftwood. *Coastal Engineering*, 104481.

Murphy, E., Nistor, I., Cornett, A., Wilson, J., & Pilechi, A. (2021). Fate and transport of coastal driftwood: A critical review. *Marine Pollution Bulletin, 170*, 112649.

Nepf, H.M., Mugnier, C.G., & Zavistoski, R.A. (1997). The effects of vegetation on longitudinal dispersion. *Estuarine, Coastal and Shelf Science, 44*(6), 675-684.

Neuman, S. (1981). A Eulerian-Lagrangian numerical scheme for the dispersion-convection equation using conjugate space-time grids. *Journal of Computational Physics, 41*(2), 270-294.

Neumann, D., Callies, U., & Matthies, M. (2014). Marine litter ensemble transport simulations in the southern North Sea. *Marine Pollution Bulletin, 86*(1-2), 219-228.

Newman, J. (1965). *The drift forces and moment on ships in waves.* Washington: US Naval Surface Warfare Center.

Nistor, I., Goseberg, N., & Stolle, J. (2017). Tsunami-driven debris motion and loads: A critical review. *Frontiers in Built Environment, 3*, 1-11.

Nistor, I., Goseberg, N., Stolle, J., Mikami, T., Shibayama, T., Nakamura, R., & Matsuba, S. (2017). Experimental investigations of debris dynamics over a horizontal plane. *Journal of Waterway, Port, Coastal, and Ocean Engineering, 143*(3), 04016022.

Nordam, T., Nepstad, R., Litzler, E., & Röhrs, J. (2019). On the use of random walk schemes in oil spill modelling. *Marine Pollution Bulletin, 146*, 631-638.

Nouri, Y., Nistor, I., Palermo, D., & Cornett, A. (2010). Experimental investigation of tsunami impact on free standing structures. *Coastal Engineering Journal, 42*(01), 43-70.

Okubo, Y. (1971). Oceanic diffusion diagrams. *Deep-Sea Research, 18*, 789-802.

Pailleret, M., Haga, T., Petit, P., Privé-Gill, C., Saedlou, N., Gaill, F., & Zbinden, M. (2007). Sunken wood from the Vanuatu Islands: identification of wood substrates and preliminary description of associated fauna. *Marine Ecology, 28*(1), 233-241.

Pattiaratchi, C., Olsson, D., Hetzel, Y., & Lowe, R. (2009). Wave-driven circulation patterns in the lee of groynes. *Continental Shelf Research, 29*, 1961-1974.

Pattiaratchi, C., & Wijeratne, S. (2019). Seagrass Wrack and Coastal Structures: Lessons from South-Western Australia. *Coastal Structures 2019* (pp. 622-631). Karlsruhe: Bundesanstalt für Wasserbau.

Pawlowicz, R. (2021). The grounding of floating objects in a marginal sea. *Journal of Physical Oceanography, 51*(2), 537-551.

Pawlowicz, R., Hannah, C., & Rosenberger, A. (2019). Lagrangian observations of estuarine residence times, dispersion, and trapping in the Salish Sea. *Estuarine, Coastal and Shelf Science, 225*, 106246.

Pearson, J.M., Guymer, I., West, J.R., & Coates, L.E. (2009). Solute mixing in the surf zone. *Journal of Waterway, Port, Coastal, and Ocean engineering, 135*(4), 127-134.

Perdok, U., Crossman, M., Verhagen, H., Howard, S., & Simm, J. (2003). Design of timber groynes. *Coastal Structures 2003* (pp. 962-974). Portland: American Society of Civil Engineers.

Peregrine, D.H. (1998). Surf zone currents. *Theoretical and Computational Fluid Dynamics, 10*(1), 295-309.

Perry, B., Rennie, C., Cornett, A., & Knox, P. (2018). Comparison of Large Woody Debris Prototypes in a Large Scale Non-flume Physical Model. *River Flow 2018 - Ninth International Conference on Fluvial Hydraulics. 40*, p. 05010. Lyon-Villeurbanne: EDP Sciences, E3S Web of Conferences.

Persi, E., Petaccia, G., Sibilla, S., Brufau, P., & García-Navarro, P. (2019). Calibration of a dynamic Eulerian-lagrangian model for the computation of wood cylinders transport in shallow water flow. *Journal of Hydroinformatics, 21*(1), 164-179.

Pilechi, A., Mohammadian, A., & Murphy, E. (2022). A numerical framework for modeling fate and transport of microplastics in inland and coastal waters. *Marine Pollution Bulletin, 184*, 114119.

Provan, M., Murphy, E., Rahman, A., Morris, E., & Matfin, A. (2023). Experimental study of wave and sediment interactions with edge treatment features on a living dyke. *Coastal Sediments 2023* (pp. 2162-2175). New Orleans: World Scientific. doi:10.1142/9789811275135_0199

Putrevu, U., & Svendsen, I.A. (1999). Three-dimensional dispersion of momentum in wave-induced nearshore currents. *European Journal of Mechanics-B/Fluids, 18*(3), 409-427.

Rangel-Buitrago, N., Mendoza, A., Gracia, A., Neal, W., & Pilkey, O. (2021). Woody debris on beach environments: Magnitudes, collateral effects, and management. *Estuarine, Coastal and Shelf Science, 251*, 107195.

Rangel-Buitrago, N., Williams, A., Anfuso, G., Arias, M., & Gracia, A. (2017). Magnitudes, sources, and management of beach litter along the Atlantico department coastline, Caribbean coast of Colombia. *Ocean & Coastal Management, 138*, 142-157.

Rech, S., Macaya-Caquilpán, V., Pantoja, J., Rivadeneira, M., Madariaga, D., & Thiel, M. (2014). Rivers as a source of marine litter–a study from the SE Pacific. *Marine Pollution Bulletin, 82*(1-2), 66-75.

Rich, S., Shaffer, J., Fix, M., & Dawson, J. (2014). Restoration considerations of large woody debris in the Elwha River nearshore, Olympic Peninsula, Washington. *Ecological Restoration*, 306-313.

Risandi, J., Rijnsdorp, D., Hansen, J., & Lowe, R. (2020). Hydrodynamic modeling of a reef-fringed pocket beach using a phase-resolved non-hydrostatic model. *Journal of Marine Science and Engineering, 8*(11), 877.

Roelvink, D., Reniers, A., Van Dongeren, A., De Vries, J., McCall, R., & Lescinski, J. (2009). Modelling storm impacts on beaches, dunes and barrier islands. *Coastal Engineering, 56*(11-12), 1133-1152.

Roelvink, D., van Dongeren, A., McCall, R., Hoonhout, B., van Rooijen, A., van Geer, P., de Vet, L., Nederhoff, K., & Quataert, E. (2015). *XBeach Technical Reference: Kingsday Release.* Delft: Deltares.

Rogers, J., Hamer, B., Brampton, A., Challinor, S., Glennerster, S., Brenton, P., & Bradbury, A. (2010). *Beach Management Manual* (2nd ed.). London: CIRIA.

Rosevelt, C., Los Huertos, M., Garza, C., & Nevins, H. (2013). Marine debris in central California: Quantifying type and abundance of beach litter in Monterey Bay, CA. *Marine Pollution Bulletin, 71*(1-2), 299-306.

Roshanka, R. (2020). On the need for a new generation of coastal change models for the 21st century. *Nature Scientific Reports, 10*(1).

Ross, O., & Sharples, J. (2004). Recipe for 1-D Lagrangian particle tracking models in space-varying diffusivity. *Limnology and Oceanography: Methods, 2*(9), 289-302.

Rueben, M., Cox, D., Holman, R., Shin, S., & Stanley, J. (2015). Optical measurements of tsunami inundation and debris movement in a large-scale wave basin. *Journal of Waterway, Port, Coastal, and Ocean Engineering, 141*(1).

Ruiz-Villanueva, V., Bladé Castellet, E., Díez-Herrero, A., Bodoque, J., & Sánchez-Juny, M. (2014a). Two-dimensional modelling of large wood transport during flash floods. *Earth Surface Processes and Landforms, 39*(4), 438-449.

Ruiz-Villanueva, V., Bladé, E., Sánchez-Juny, M., Marti-Cardona, B., Díez-Herrero, A., & Bodoque, J. (2014b). Two-dimensional numerical modeling of wood transport. *Journal of Hydroinformatics, 16*(5), 1077-1096.

Ruiz-Villanueva, V., Piégay, H., Stoffel, M., Gaertner, V., & Perret, F. (2015). Analysis of Wood Density to Improve Understanding of Wood Buoyancy in Rivers. In G. Lollino, M. Arattano, M. Rinaldi, O. Giustolisi, J.C. Marechal, & G. Grant (eds.), *Engineering Geology for Society and Territory* (pp. 163-166). Geneva: Springer International Publishing. doi:10.1007/978-3-319-09054-2_33.

Ryan, P. (2013). A simple technique for counting marine debris at sea reveals steep litter gradients between the Straits of Malacca and the Bay of Bengal. *Marine Pollution Bulletin, 69*(1-2), 128-136.

Schalko, I., Schmocker, L., Weitbrecht, V., & Boes, R. (2018). Backwater rise due to large wood accumulations. *Journal of Hydraulic Engineering*, 04018056.

Schmidt, W.E., Woodward, B.T., Millikan, K.S., Guza, R.T., Raubenheimer, B., & Elgar, S. (2003). A GPS-tracked surf zone drifter. *Journal of Atmospheric and Oceanic Technology* 20 (7): 1069-1075.

Schmocker, L., & Hager, W. (2011). Probability of drift blockage at bridge decks. *Journal of Hydraulic Engineering, 137*(4), 470-479.

Schmocker, L., & Hager, W. (2013). Scale modeling of wooden debris accumulation at a debris rack. *Journal of Hydraulic Engineering, 139*(8), 827-836.

Schmocker, L., & Weitbrecht, V. (2013). Driftwood: Risk analysis and engineering measures. *Journal of Hydraulic Engineering, 139*(7), 683-695.

Scott, T., Masselink, G., & Russell, P. (2011). Morphodynamic characteristics and classification of beaches in England and Wales. *Marine Geology, 286*(1-4), 1-20.

Seo, J. I., Nakamura, F., Nakano, D., Ichiyanagi, H., & Chun, K. W. (2008). Factors controlling the fluvial export of large woody debris, and its contribution to organic carbon budgets at watershed scales. *Water Resources Research, 44*(4).

Serrer, M. (2011). *Blue Kenue Reference Manual.* Ottawa: National Research Council of Canada, Canadian Hydraulics Centre.

Shafiei, S., Melville, B., Shamseldin, A., Beskhyroun, S., & Adams, K. (2016). Measurements of tsunami-borne debris impact on structures using an embedded accelerometer. *Journal of Hydraulic Research*, 1-15.

Shaw, J. (2012). Economies of driftwood: Fuel harvesting strategies in the Kodiak Archipelago. *Études/Inuit/Studies, 36*(1), 63-88.

Shen, H., Yapa, P., & Petroski, M. (1987). A simulation model for oil slick transport in lakes. *Water Resources Research, 23*(10), 1949-1957.

Shepard, F.P., & Inman, D.L. (1950). Nearshore water circulation related to bottom topography and wave refraction. *Transactions American Geophysical Union, 31*(2), 196-212.

Shepard, F.P., Emery, K.O., & La Fond, E.C. (1941). Rip currents: a process of geological importance. *The Journal of Geology, 49*(4), 337-369.

Sherwood, C.R., Van Dongeren, A., Doyle, J., Hegermiller, C.A., Hsu, T.J., Kalra, T.S., Olabarrieta, M., Penko, A.M., Rafati, Y., Roelvink, D., van der Lugt, M., Veeramony, J., & Warner, J.C. (2022). Modeling the morphodynamics of coastal responses to extreme events: what shape are we in? *Annual Review of Marine Science, 14*, 457-492.

Simenstad, C., Wick, A., Van de Wetering, S., & Bottom, D. (2003). Dynamics and ecological functions of wood in estuarine and coastal marine ecosystems. *American Fisheries Society Symposium*, 265-277.

Smit, P., Janssen, T., Holthuijsen, L., & Smith, J. (2014). Non-hydrostatic modeling of surf zone wave dynamics. *Coastal Engineering, 83*, 36-48.

Smit, P., Stelling, G., Roelvink, D., van Thiel de Vries, J., McCall, R., van Dongeren, A., Zwinkels, C., & Jacobs, R. (2010). *XBeach: Non-hydrostatic model.* Delft: Delft University of Technology and Deltares.

Smit, P., Zijlema, M., & Stelling, G. (2013). Depth-induced wave breaking in a non-hydrostatic, near-shore wave model. *Coastal Engineering, 76*, 1-16.

Sobey, R., & Barker, C. (1997). Wave-driven transport of surface oil. *Journal of Coastal Research*, 490-496.

Spagnol, S., Wolanski, E., Deleersnijder, E., Brinkman, R., McAllister, F., Cushman-Roisin, B., & Hanert, E. (2002). An error frequently made in the evaluation of advective transport in two-dimensional Lagrangian models of advection-diffusion in coral reef waters. *Marine Ecology Progress Series, 235*, 299-302.

Spydell, M., & Feddersen, F. (2009). Lagrangian drifter dispersion in the surf zone: directionally spread, normally incident waves. *Journal of Physical Oceanography, 39*, 809-830.

Spydell, M., Feddersen, F., Guza, R.T., & Schmidt, W.E. (2007). Observing surf-zone dispersion with drifters. *Journal of Physical Oceanography, 37*, 2920-2939.

St.-Germain, P., Nistor, I., Readshaw, J., & Lamont, G. (2014). Numerical modeling of coastal dike overtopping using SPH and non-hydrostatic NLSW equations. *Coastal Engineering Proceedings. 34*, pp. 1-15. Seoul: Coastal Engineering Research Council. doi:10.9753/icce.v34.structures.10

Steelandt, S., Bhiry, N., Marguerie, D., Desbiens, C., Napartuk, M., & Desrosiers, P. (2013). Inuit knowledge and use of wood resources on the west coast of Nunavik, Canada. *Études/Inuit/Studies, 37*(1), 147-173.

Steelandt, S., Marguerie, D., Bhiry, N., & Delwaide, A. (2015). A study of the composition, characteristics, and origin of modern driftwood on the western coast of Nunavik (Quebec, Canada). *Journal of Geophysical Research: Biogeosciences, 120*(3).

Stewardship Centre for British Columbia. (2023). *Green Shores for Homes Credits and Ratings Guide.* Stewardship Centre for British Columbia. Retrieved from https://stewardshipcentrebc.ca/PDF_docs/greenshores/Resources/GSHCreditsandRatingsGuide.pdf

Stockstill, R., Daly, S., & Hopkins, M. (2009). Modeling floating objects at river structures. *Journal of Hydraulic Engineering, 135*(5), 403-414.

Stolle, J., Nistor, I., & Goseberg, N. (2016). Optical tracking of floating shipping containers in a high-velocity flow. *Coastal Engineering Journal, 58*(2), 1650005.

Stolle, J., Takabatake, T., Nistor, I., Mikami, T., Nishizaki, S., Hamano, G., & Petriu, E. (2018). Experimental investigation of debris damming loads under transient supercritical flow conditions. *Coastal Engineering, 139*, 16-31.

Storry, K., Weldrick, C., Mews, M., Zimmer, M., & Jelinski, D. (2006). Intertidal coarse woody debris: A spatial subsidy as shelter or feeding habitat for gastropods? *Estuarine, Coastal and Shelf Science, 66*(1-2), 197-203.

Suh, K., & Dalrymple, R. (1987). Offshore breakwaters in laboratory and field. *Journal of Waterway, Port, Coastal, and Ocean Engineering, 113*(2), 105-121.

Sumer, B., & Fredsøe, J. (2002). *The Mechanics of Scour in the Marine Environment* (Advanced Series on Ocean Engineering - Vol. 17). Singapore: World Scientific.

Sumer, B., & Fredsøe, J. (2006). *Hydrodynamics Around Cylindrical Structures* (Advanced Series on Ocean Engineering - Vol. 26). London: World Scientific.

Svendsen, I.A. (1992). Surf Zone Dynamics. In *Breaking Waves*, by M.L. Banner and R.H.J. Grimshaw, 55-68. Berlin: Springer-Verlag.

Svendsen, I.A., & Putrevu, U. (1994). Nearshore mixing and dispersion. *Proceedings of the Royal Society of London. Series A: Mathematical and Physical Sciences, 445*(1925), 561-576.

Swallow, J.C., & Worthington, L.V. (1957). Measurements of deep currents in the western North Atlantic. *Nature, 179*(4571), 1183-1184.

Swenson, C. (2022). Town starts cleaning up storm debris from beach. *Coastal Observer.* October 20. Accessed December 30, 2022. https://coastalobserver.com/town-starts-cleaning-up-storm-debris-from-beach/.

Szymczak, P., & Ladd, A. (2003). Boundary conditions for stochastic solutions of the convection-diffusion equation. *Physical Review E, 68*(3), 036704.

Taffs, K., & Cullen, M. (2005). The distribution and abundance of beach debris on isolated beaches of northern New South Wales, Australia. *Australasian Journal of Environmental Management, 12*(4), 244-250.

Takewaka, S., Misaki, S., & Nakamura, T. (2003). Dye diffusion experiment in a longshore current. *Coastal Engineering Journal, 45*(3), 471-487.

Tanaka, H., Wada, A., Komori, S., & Takeuchi, I. (1980). Effects of nearshore currents on diffusion in the surf zone. *Coastal Engineering in Japan,* 231-249.

The MathWorks Inc. (2022). MATLAB version: 9.13.0 (R2022b). Natick, Massachusetts: The MathWorks Inc. Retrieved from https://www.mathworks.com

The SWASH Team. (2023). *SWASH User Manual.* Delft: Delft University of Technology.

Thiel, M., & Gutow, L. (2005). The ecology of rafting in the marine environment. I. The floating substrata. *Oceanography and Marine Biology: An Annual Review, 42*, 181-264.

Thiel, M., Hinojosa, I., Joschko, T., & Gutow, L. (2011). Spatio-temporal distribution of floating objects in the German Bight (North Sea). *Journal of Sea Research, 65*(3), 368-379.

Thiel, M., Hinojosa, I., Miranda, L., Pantoja, J., Rivadeneira, M., & Vásquez, N. (2013). Anthropogenic marine debris in the coastal environment: a multi-year comparison between coastal waters and local shores. *Marine Pollution Bulletin, 71*(1-2), 307-316.

Thonon, I. (2006). *The Fraser River Debris Trap: A Cost Benefit Analysis.* Vancouver: Fraser Basin Council.

Thornton, E.B. (1970). Variation of longshore currents across the surf zone. *Proceedings of the 12th Conference on Coastal Engineering.* Washington, D.C.: American Society of Civil Engineers. 291-308.

Thornton, E.B., & Guza, R.T. (1986). Surf zone longshore currents and random waves: Field data and models. *Journal of Physical Oceanography, 16*(7), 1165-1178.

Tipa, G. (2009). Exploring indigenous understandings of river dynamics and river flows: a case from New Zealand. *Environmental Communication, 3*(1), 95-120.

Valentine, E.M., & Wood, I.R. (1977). Longitudinal dispersion with dead zones. *Journal of the Hydraulics Division, 103*(9), 975-990.

Van Der Mheen, M., Van Sebille, E., & Pattiaratchi, C. (2020). Beaching patterns of plastic debris along the Indian Ocean rim. *Ocean Science, 16*(5), 1317-1336.

van Sebille, E., Griffies, S., Abernathey, R., Adams, T., Berloff, P., Biastoch, A., Blanke, B., Chassignet, E.P., Cheng, Y., Cotter, C.J., Deleersnijder, E., Doos, K., Drake, H.F., Drijfhout, S., Gary, S.F., Heemink, A.W., Kjellsson, J., Koszalka, I.M., Lange, M., Lique, C., MacGilchrist, G.A., Marsh, R., Adame, C.G.M., McAdam, R., Nencioli, F., Paris, C.B., Piggott, M.D., Polton, J.A., Ruhs, S., Shah, S.H.A.M., Thomas, M.D., Wang, J., Wolfram, P.J., Zanna, L., & Zika, J.D. (2018). Lagrangian ocean analysis: Fundamentals and practices. *Ocean Modelling*, 49-75.

Viehman, S., Vander Pluym, J., & Schellinger, J. (2011). Characterization of marine debris in North Carolina salt marshes. *Marine Pollution Bulletin, 62*(12), 2771-2779.

Visser, A. (1997). Using random walk models to simulate the vertical distribution of particles in a turbulent water column. *Marine Ecology Progress Series, 158*, 275-281.

Vitousek, S., Barnard, P., Limber, P., Erikson, L., & Cole, B. (2017). A model integrating longshore and cross-shore processes for predicting long-term shoreline response to climate change. *Journal of Geophysical Research: Earth Surface*, 782-806.

Vuik, V., Borsje, B.W., Willemsen, P.W., & Jonkman, S.N. (2019). Salt marshes for flood risk reduction: Quantifying long-term effectiveness and life-cycle costs. *Ocean & Coastal Management, 171*, 96-110.

Walker, I., & Barrie, J. (2006). Geomorphology and sea-level rise on one of Canada's most sensitive coasts: Northeast Graham Island, British Columbia. *Journal of Coastal Research*, 220-226.

Williams, A., & Simmons, S. (1997). Estuarine litter at the river/beach interface in the Bristol Channel, United Kingdom. *Journal of Coastal Research*, 1159-1165.

Williams, J., & Esteves, L. (2017). Guidance on setup, calibration, and validation of hydrodynamic, wave, and sediment models for shelf seas and estuaries. *Advances in Civil Engineering, 2017*(5251902), 25.

Williams, R. (2005). *Weathering of Wood. Handbook of Wood Chemistry and Wood Composites.* Boca Raton: CRC Press.

Willis, K., Hardesty, B., Kriwoken, L., & Wilcox, C. (2017). Differentiating littering, urban runoff and marine transport as sources of marine debris in coastal and estuarine environments. *Nature Scientific Reports, 7*(1), 1-9.

Wilson, J. (2020). *The efficacy and design of coastal protection using large woody debris.* Ottawa: University of Ottawa.

Wilson, J., Nistor, I., Mohammadian, A., Cornett, A., Falkenrich, P., & Lamont, G. (2020). Nature-based coastal protection using large woody debris (LWD). *International Conference on Coastal Engineering, 36v,* https://doi.org/10.9753/icce.v36v.management.8.

Winckler, P., Liu, P.L.F., & Mei, C.C. (2013). Advective diffusion of contaminants in the surf zone. *Journal of Waterway, Port, Coastal, and Ocean engineering, 139*(6), 437-454.

Wohl, E. (2017). Bridging the gaps: An overview of wood across time and space in diverse rivers. *Geomorphology, 279*, 3-26.

Wohl, E., & Goode, J.R. (2008). Wood dynamics in headwater streams of the Colorado Rocky Mountains. *Water Resources Research*, *44*(9), W09429.

Wohl, E., & Iskin, E. (2021). Damming the wood falls. *Science Advances, 7*(50), eabj0988.

Wohl, E., Kramer, N., Ruiz-Villanueva, V., Scott, D., Comiti, F., Gurnell, A., Piegay, H., Lininger, K.B., Jaeger, K.L., Walters, D.M., & Fausch, K. (2019). The natural wood regime in rivers. *BioScience, 69*(4), 259-273.

Wolff, T. (1979). Magrofaunal utilization of plant remains in the deep sea. *Sarsia, 64*(1-2), 117-143.

Yoon, J., Kawano, S., & Igawa, S. (2010). Modeling of marine litter drift and beaching in the Japan Sea. *Marine Pollution Bulletin, 60*(3), 448-463.

Zelenke, B., O'Connor, C., Barker, C., Beegle-Krause, C., & Eclipse, L. (2012). *General NOAA Operational Modeling Environment (GNOME) Technical Documentation.* Seattle: Emergency Response Division, NOAA.

Zhang, H. (2017). Transport of microplastics in coastal seas. *Estuarine, Coastal and Shelf Science, 199*, 74-86.

Zijlema, M. (2014). Modelling vertical variation of turbulent flow across a surf zone using SWASH. *Coastal Engineering Proceedings. 34*, pp. 1-11. Seoul: Coastal Engineering Research Council. doi:10.9753/icce.v34.waves.3

Zijlema, M., Stelling, G., & Smit, P. (2011). SWASH: An operational public domain code for simulating wave fields and rapidly varied flows in coastal waters. *Coastal Engineering, 58*(10), 992-1012.

Appendix A. Optical Tracking Analysis Results

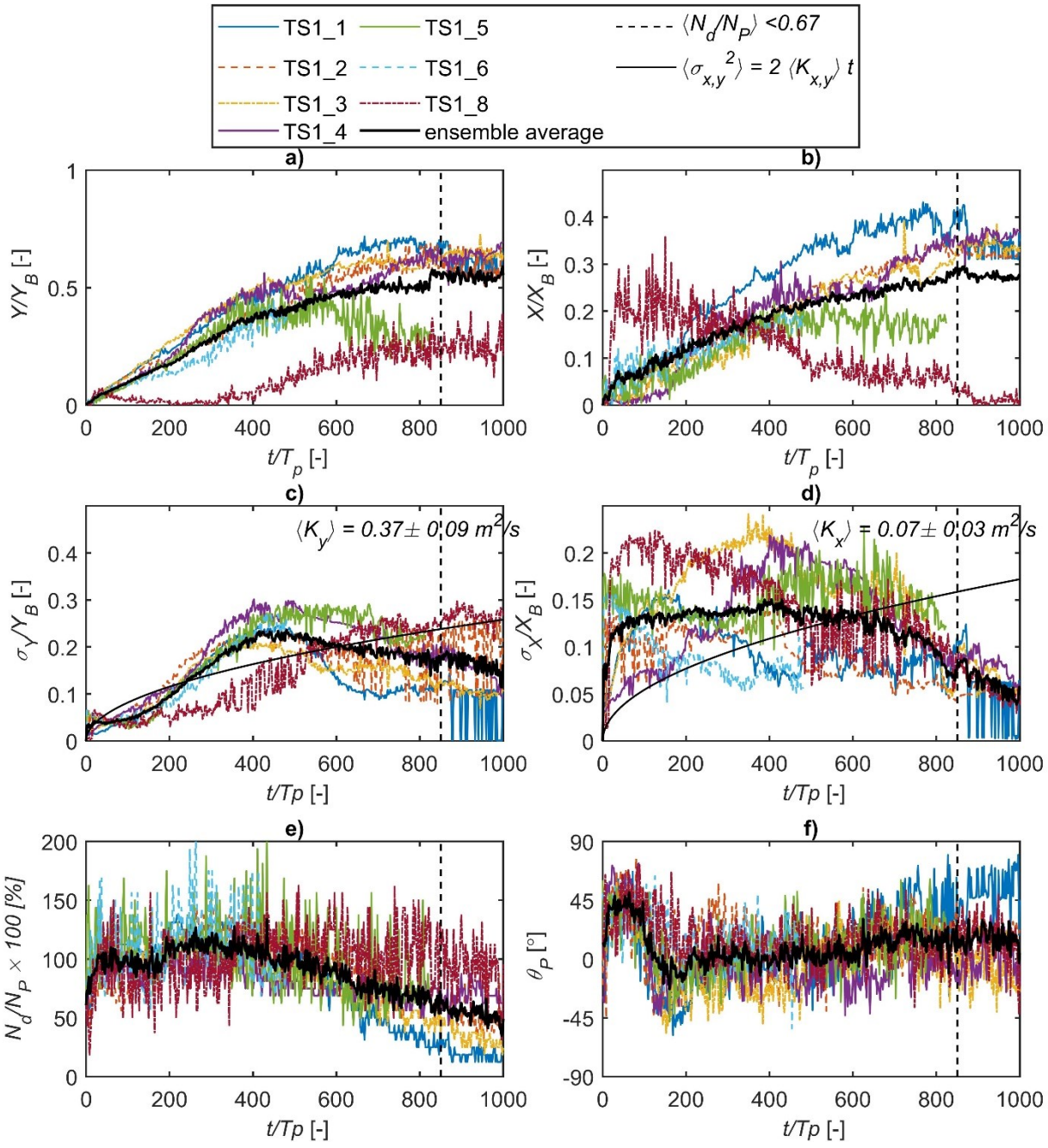

Figure A-1. a) Mean alongshore relative travel distance, b) mean cross-shore relative travel distance, c) alongshore standard deviation, d) cross-shore standard deviation, e) detection rate, and f) mean orientation versus time for smooth driftwood length class L_P = 3 m (yellow) during test series TS1 (η = 0.35 m, H_s = 0.45 m, T_p = 8 s).

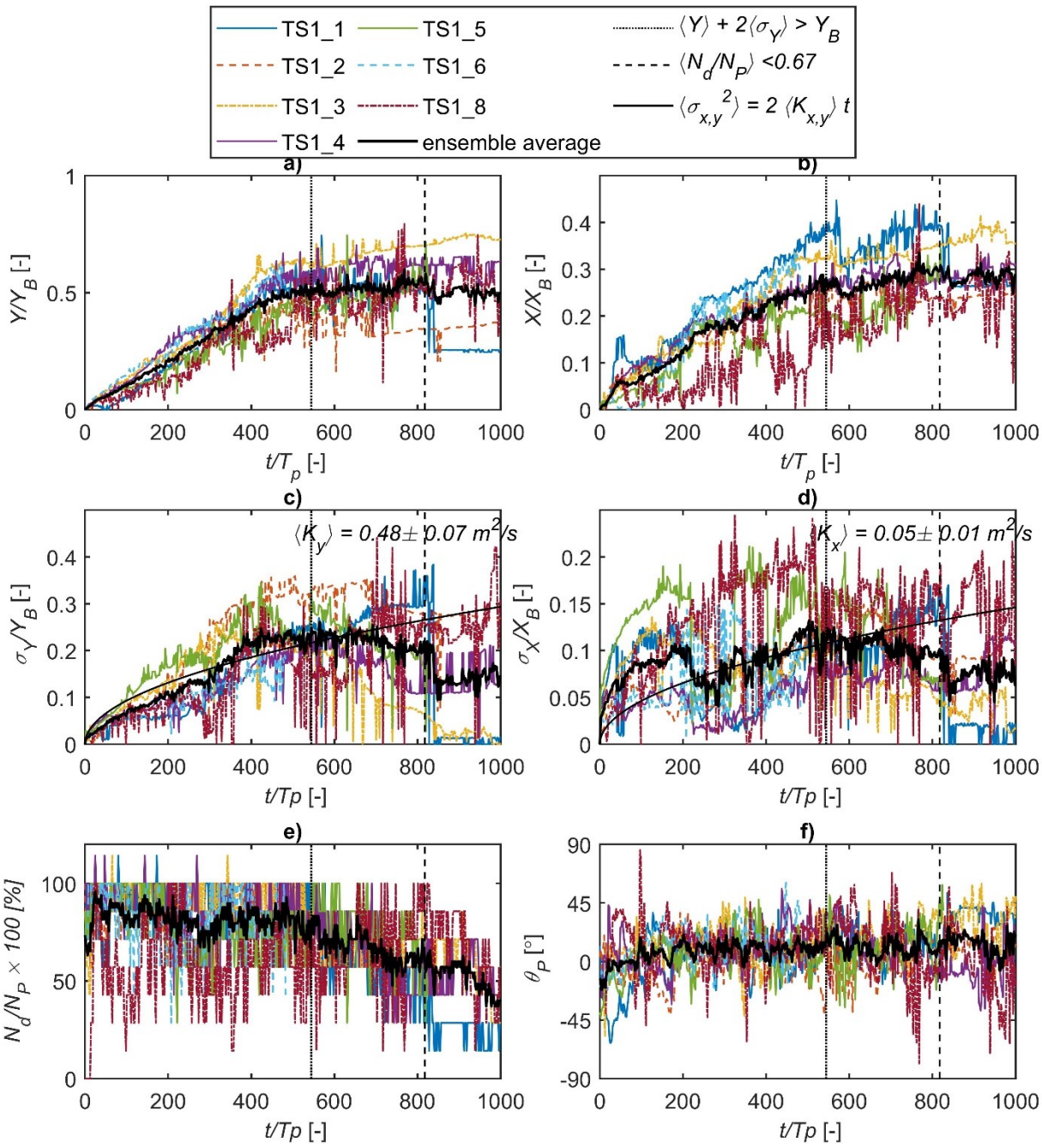

Figure A-2. a) Mean alongshore relative travel distance, b) mean cross-shore relative travel distance, c) alongshore standard deviation, d) cross-shore standard deviation, e) detection rate, and f) mean orientation versus time for smooth driftwood length class L_P = 9 m (blue) during test series TS1 (η = 0.35 m, H_s = 0.45 m, T_p = 8 s).

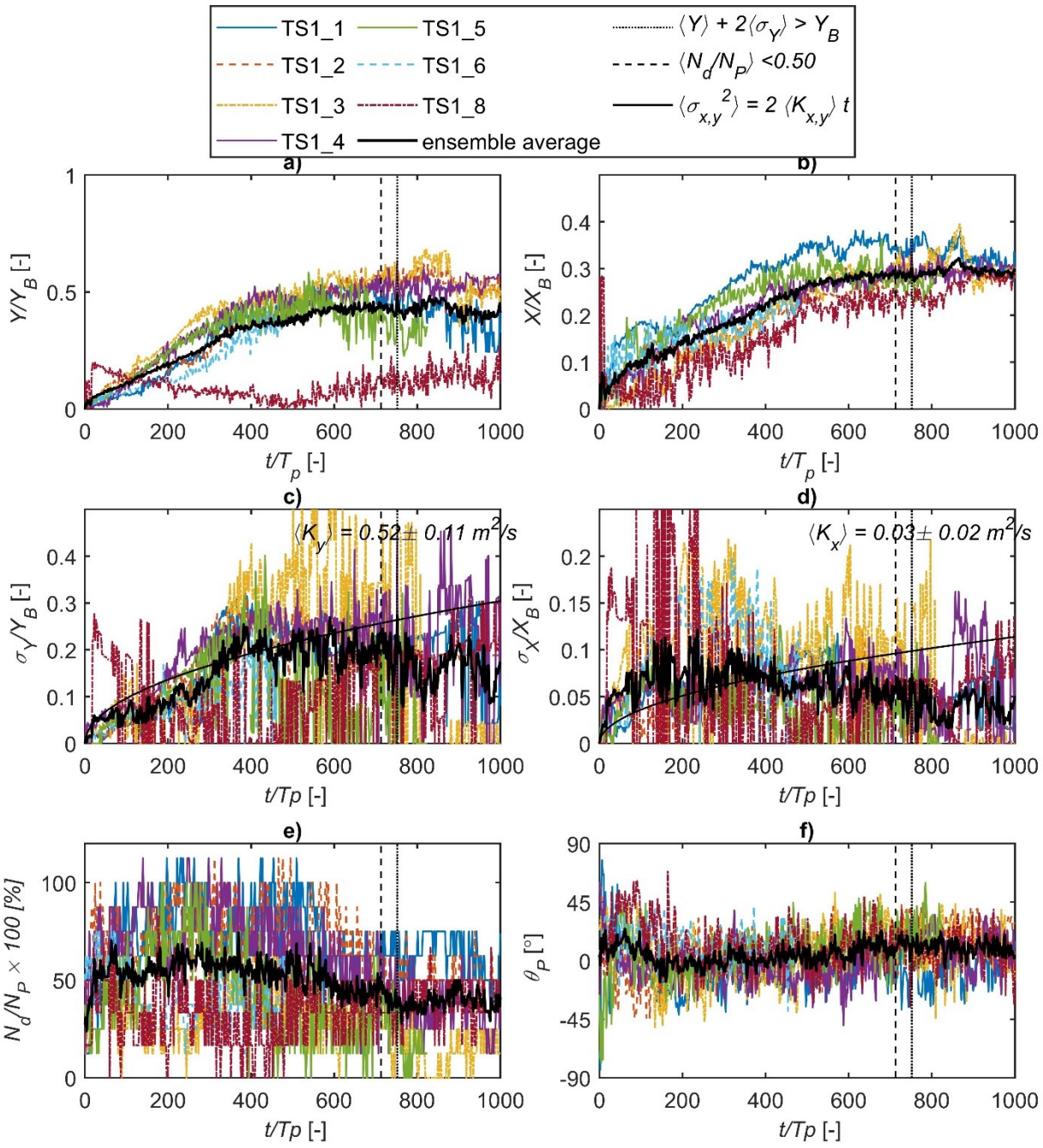

Figure A-3. a) Mean alongshore relative travel distance, b) mean cross-shore relative travel distance, c) alongshore standard deviation, d) cross-shore standard deviation, e) detection rate, and f) mean orientation versus time for smooth driftwood length class L_P = 12 m (green) during test series TS1 (η = 0.35 m, H_s = 0.45 m, T_p = 8 s).

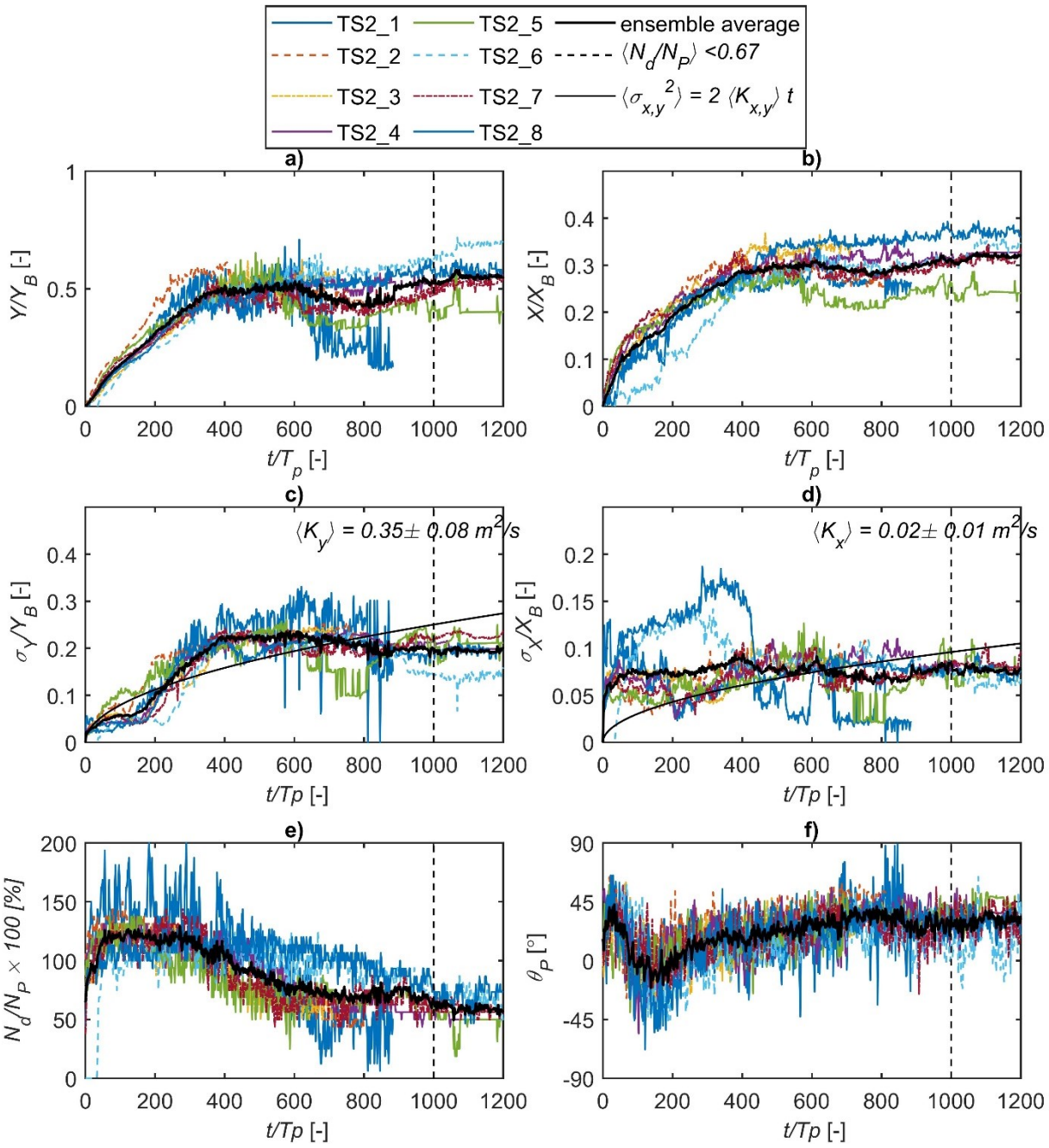

Figure A-4. a) Mean alongshore relative travel distance, b) mean cross-shore relative travel distance, c) alongshore standard deviation, d) cross-shore standard deviation, e) detection rate, and f) mean orientation versus time for smooth driftwood length class L_P = 3 m (yellow) during test series TS2 (η = 0.35 m, H_s = 0.65 m, T_p = 8 s).

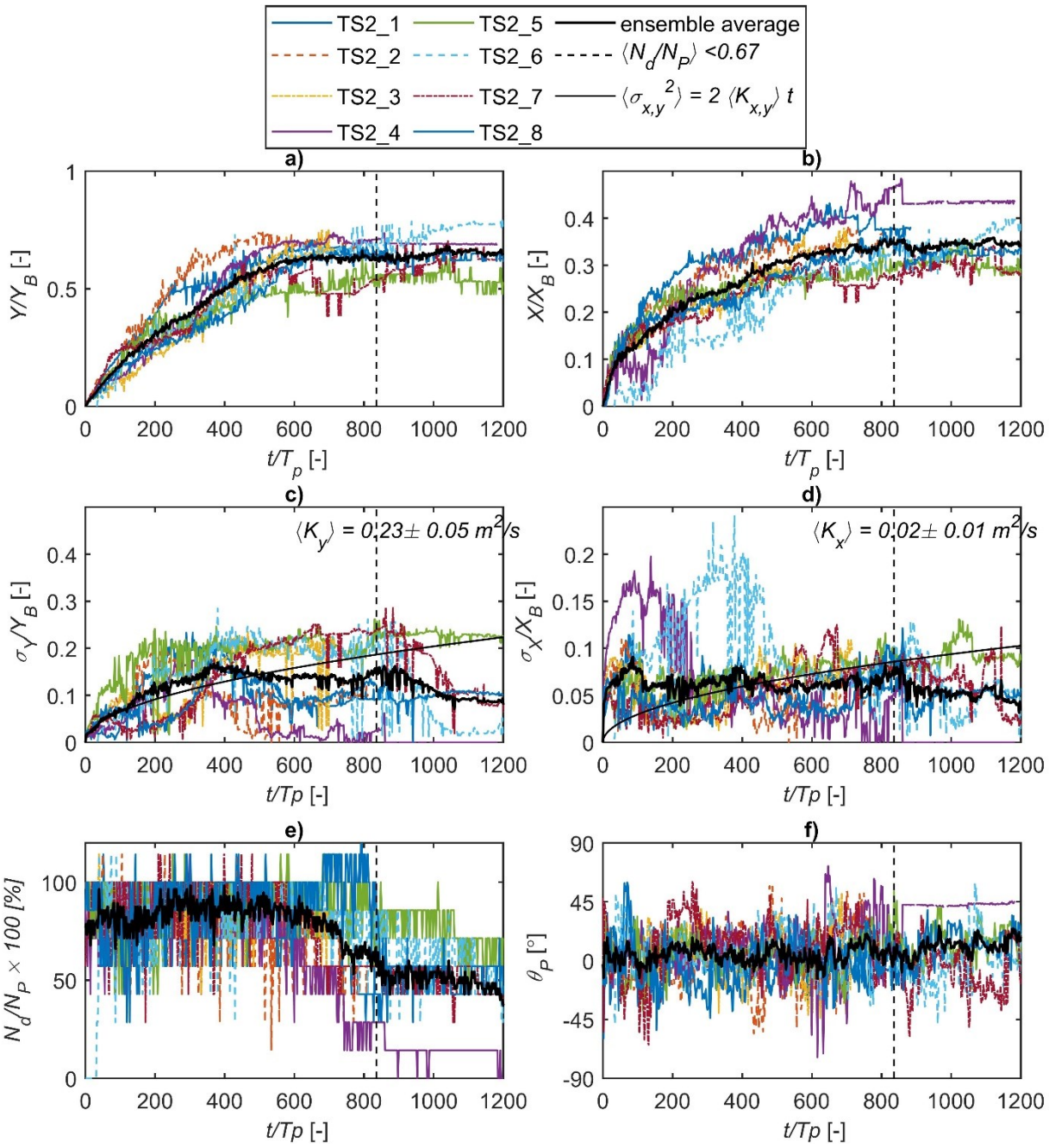

Figure A-5. a) Mean alongshore relative travel distance, b) mean cross-shore relative travel distance, c) alongshore standard deviation, d) cross-shore standard deviation, e) detection rate, and f) mean orientation versus time for smooth driftwood length class L_P = 9 m (blue) during test series TS2 (η = 0.35 m, H_s = 0.65 m, T_p = 8 s).

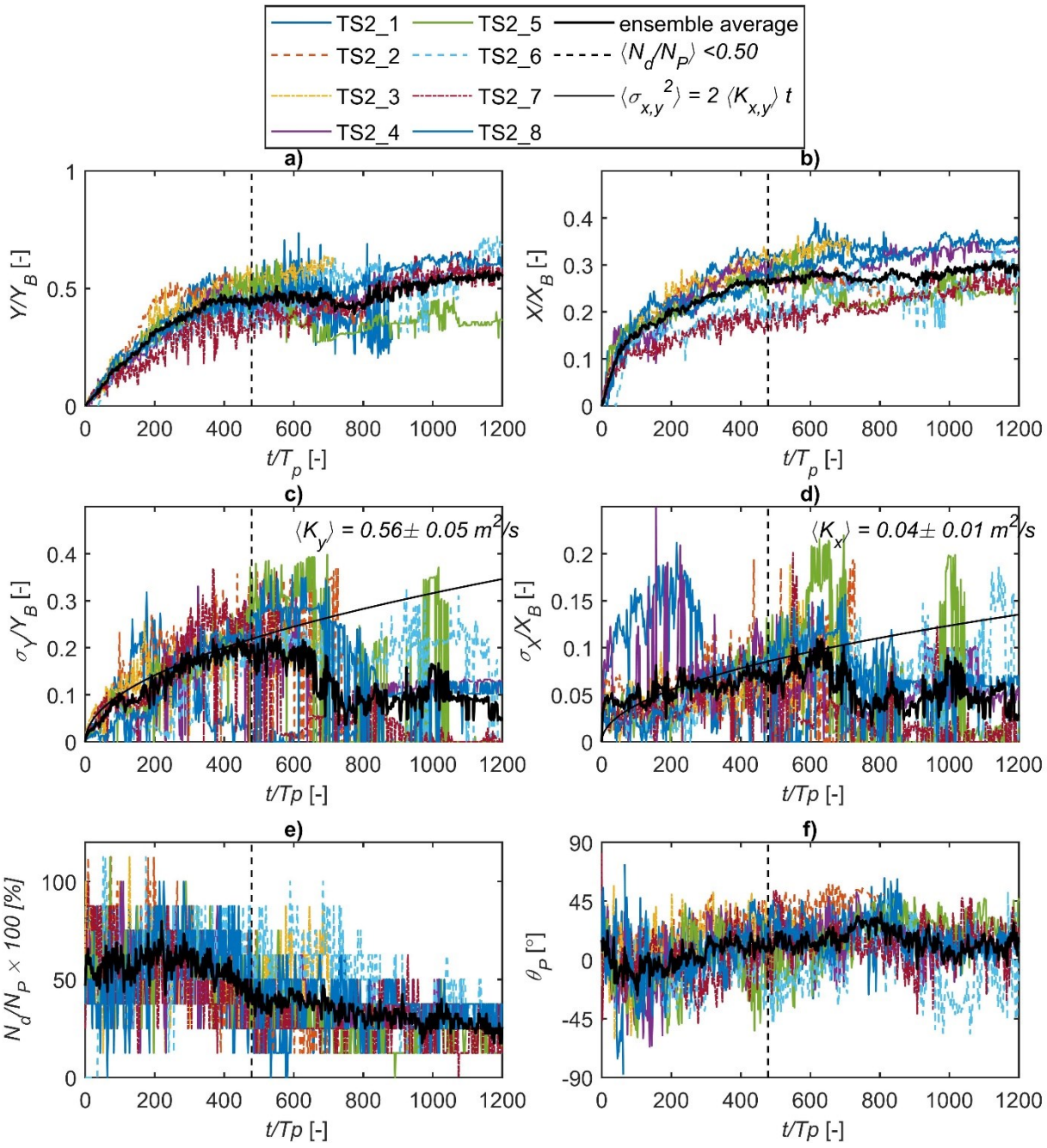

Figure A-6. a) Mean alongshore relative travel distance, b) mean cross-shore relative travel distance, c) alongshore standard deviation, d) cross-shore standard deviation, e) detection rate, and f) mean orientation versus time for smooth driftwood length class L_P = 12 m (green) during test series TS2 (η = 0.35 m, H_s = 0.65 m, T_p = 8 s).

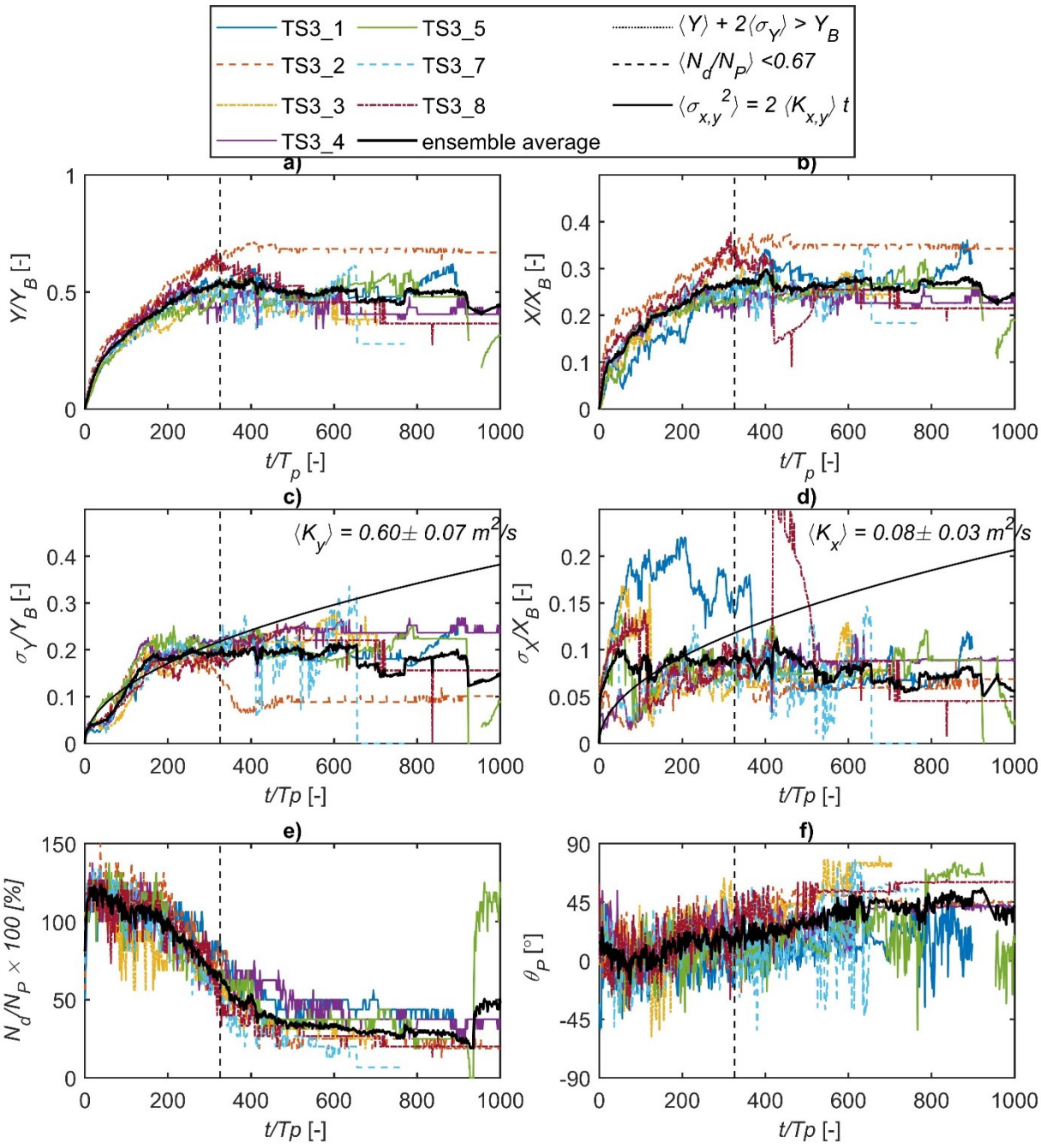

Figure A-7. a) Mean alongshore relative travel distance, b) mean cross-shore relative travel distance, c) alongshore standard deviation, d) cross-shore standard deviation, e) detection rate, and f) mean orientation versus time for smooth driftwood length class L_P = 3 m (yellow) during test series TS3 (η = 0.35 m, H_s = 0.80 m, T_p = 11 s).

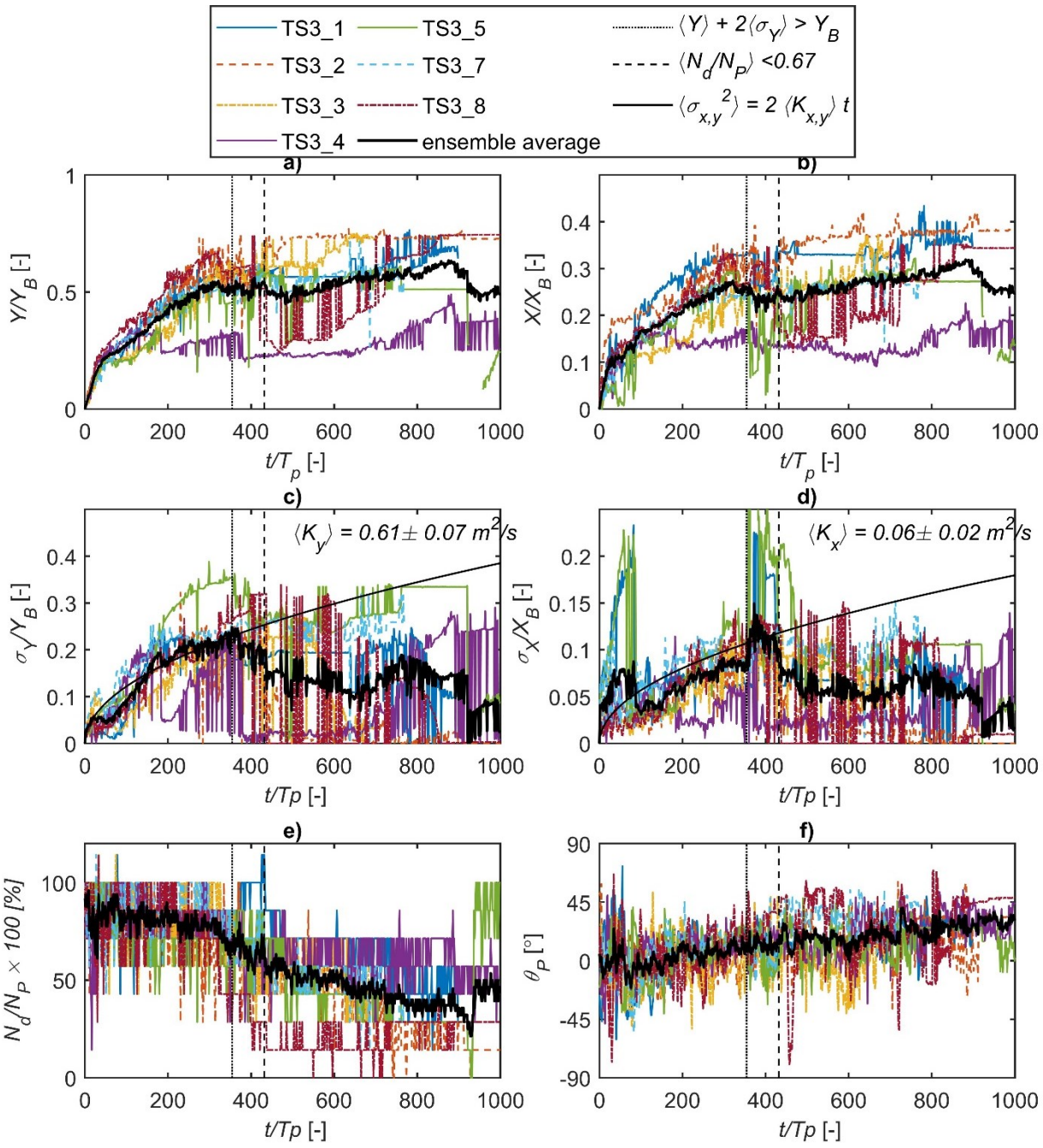

Figure A-8. a) Mean alongshore relative travel distance, b) mean cross-shore relative travel distance, c) alongshore standard deviation, d) cross-shore standard deviation, e) detection rate, and f) mean orientation versus time for smooth driftwood length class L_P = 9 m (blue) during test series TS3 (η = 0.35 m, H_s = 0.80 m, T_p = 11 s).

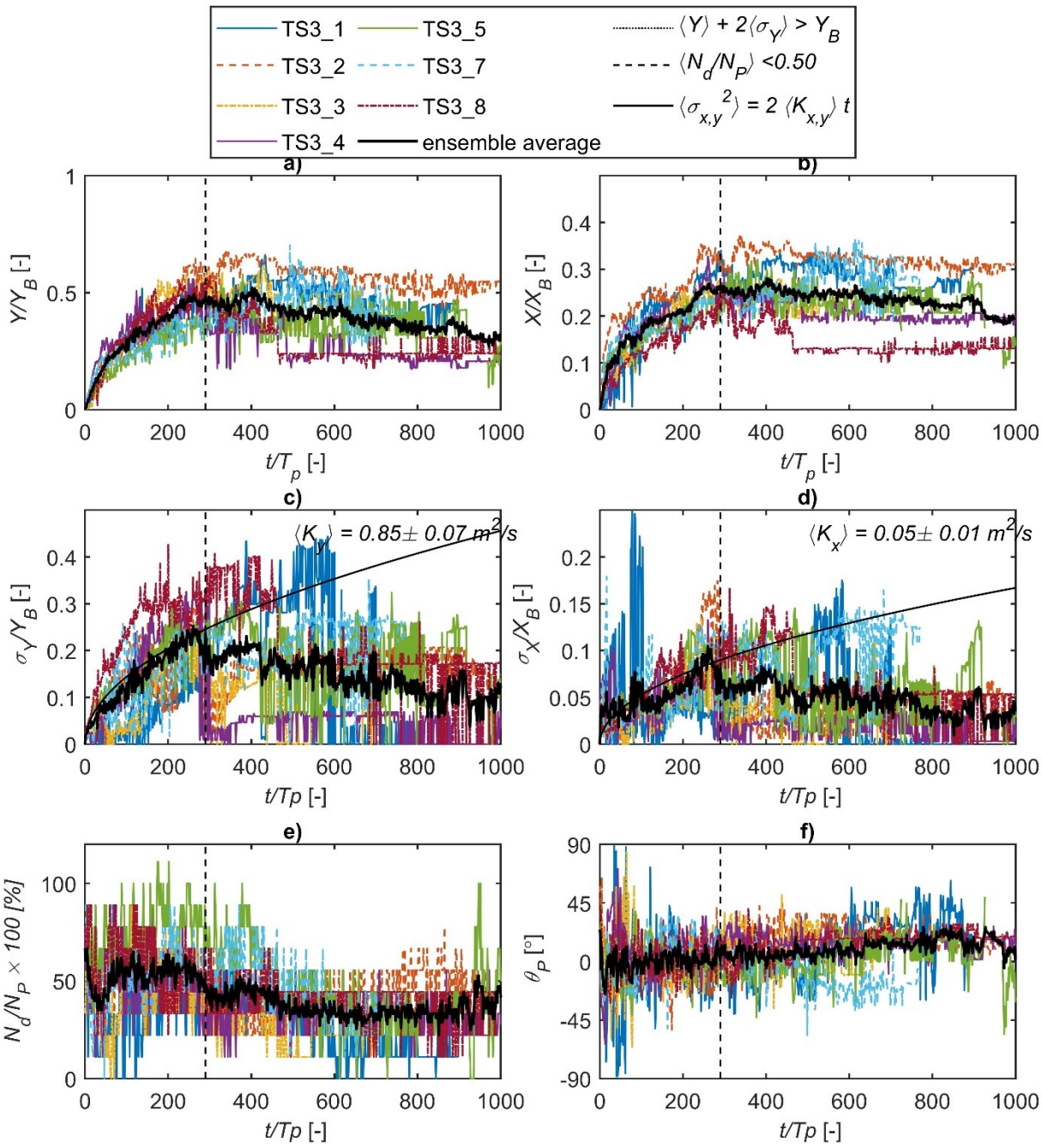

Figure A-9. a) Mean alongshore relative travel distance, b) mean cross-shore relative travel distance, c) alongshore standard deviation, d) cross-shore standard deviation, e) detection rate, and f) mean orientation versus time for smooth driftwood length class L_P = 12 m (green) during test series TS3 (η = 0.35 m, H_s = 0.80 m, T_p = 11 s).

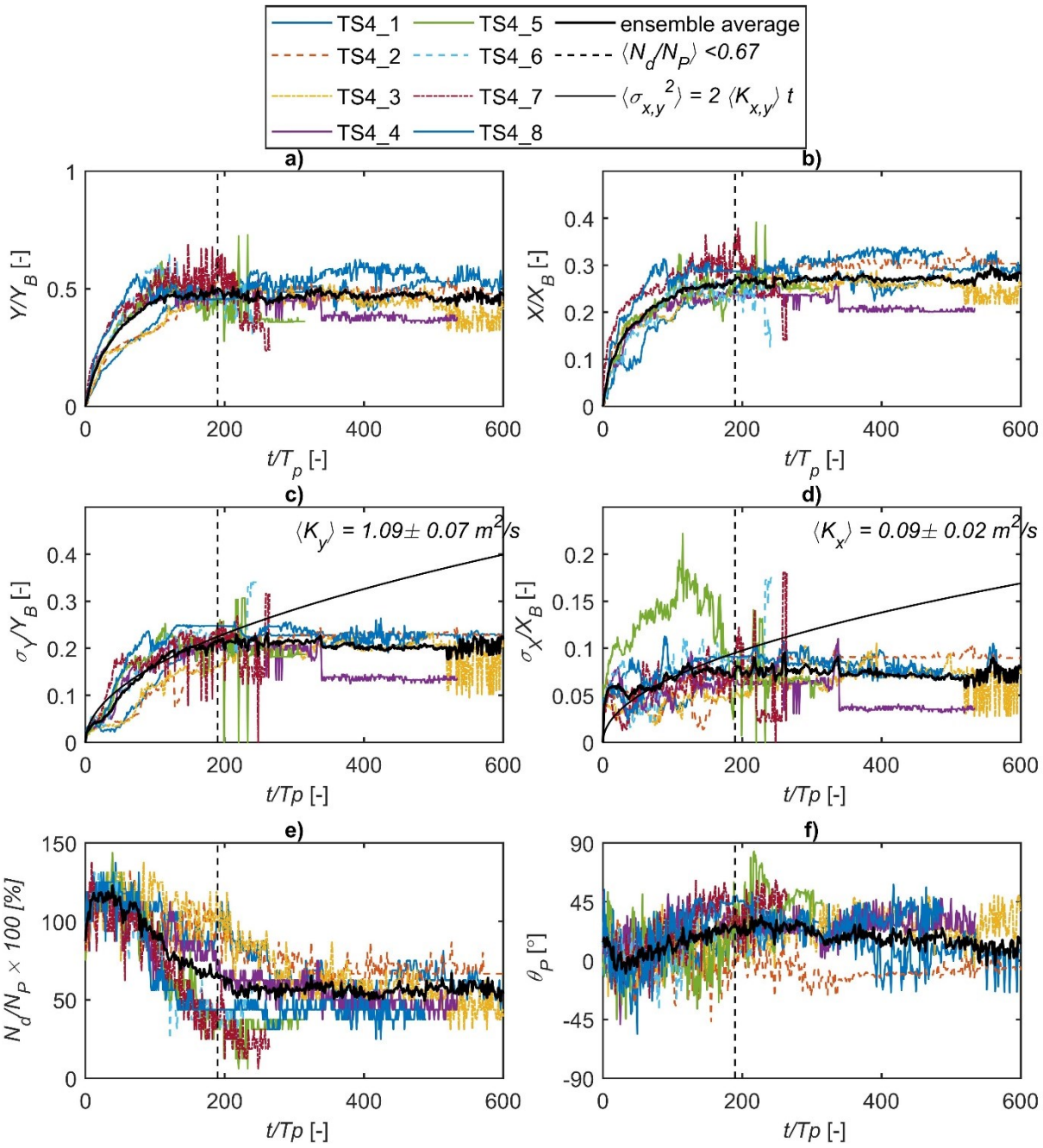

Figure A-10. a) Mean alongshore relative travel distance, b) mean cross-shore relative travel distance, c) alongshore standard deviation, d) cross-shore standard deviation, e) detection rate, and f) mean orientation versus time for smooth driftwood length class L_P = 3 m (yellow) during test series TS4 (η = 0.70 m, H_s = 0.80 m, T_p = 11 s).

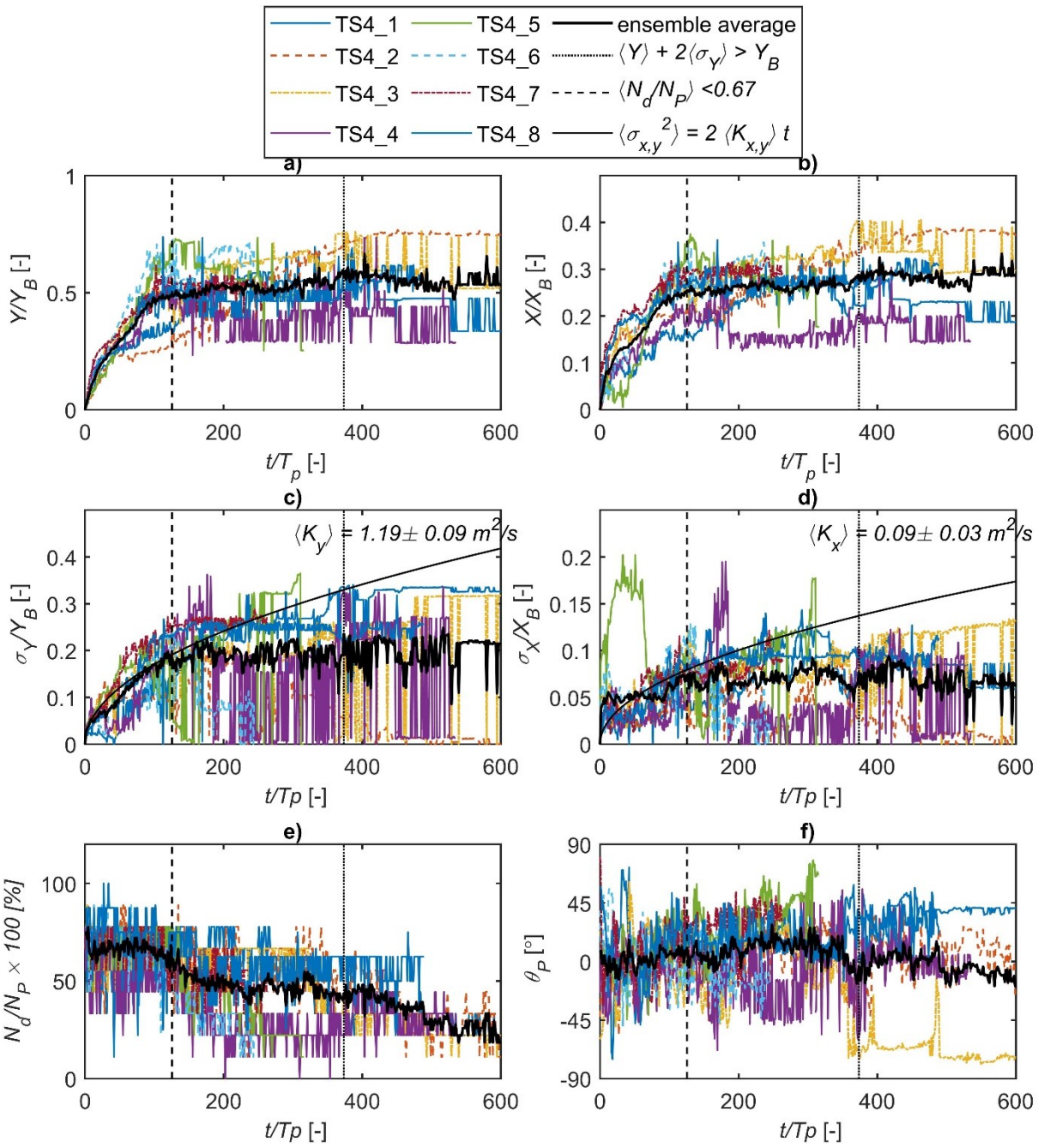

Figure A-11. a) Mean alongshore relative travel distance, b) mean cross-shore relative travel distance, c) alongshore standard deviation, d) cross-shore standard deviation, e) detection rate, and f) mean orientation versus time for smooth driftwood length class L_P = 9 m (blue) during test series TS4 (η = 0.70 m, H_s = 0.80 m, T_p = 11 s).

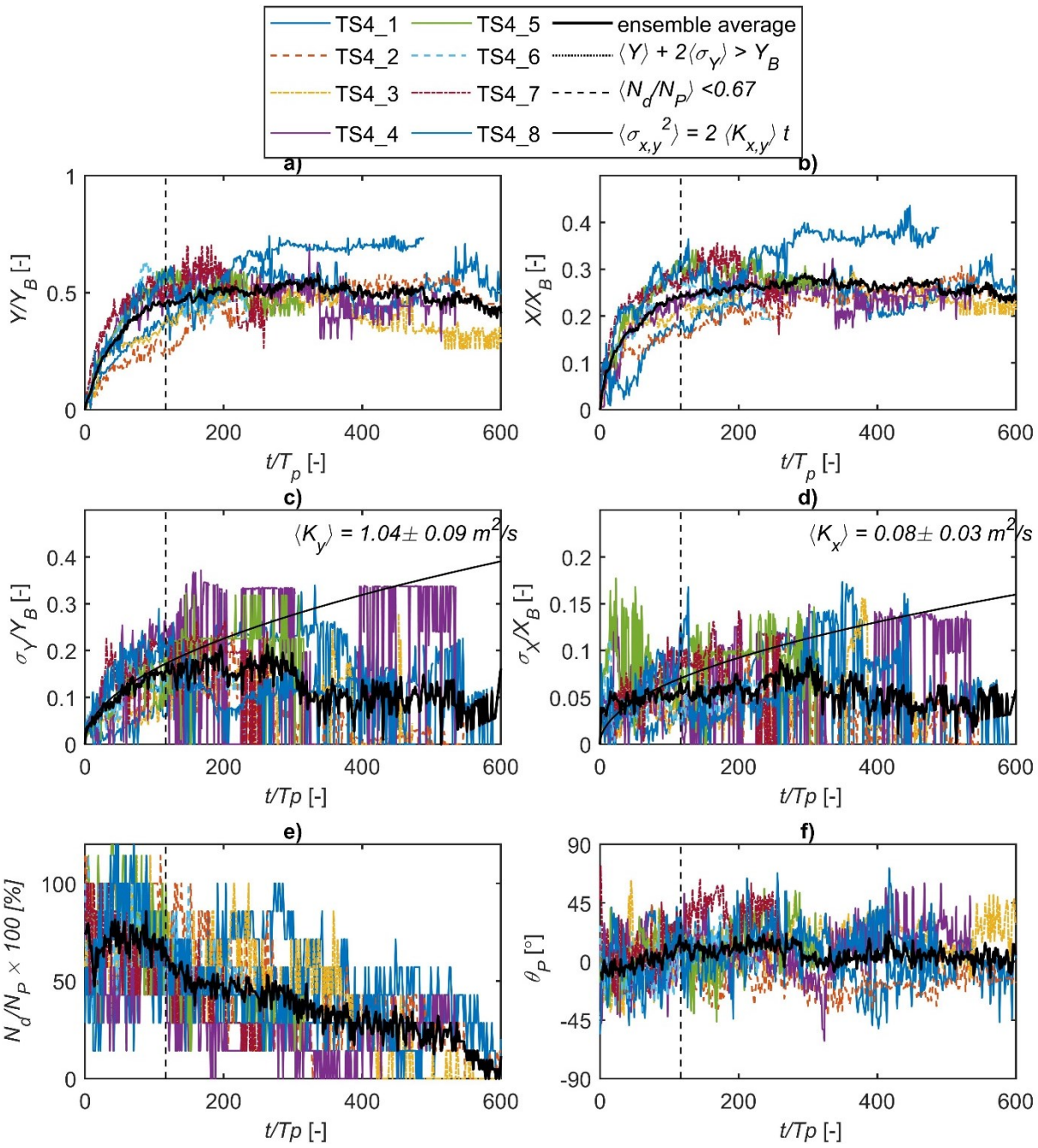

Figure A-12. a) Mean alongshore relative travel distance, b) mean cross-shore relative travel distance, c) alongshore standard deviation, d) cross-shore standard deviation, e) detection rate, and f) mean orientation versus time for smooth driftwood length class L_P = 12 m (green) during test series TS4 (η = 0.70 m, H_s = 0.80 m, T_p = 11 s).

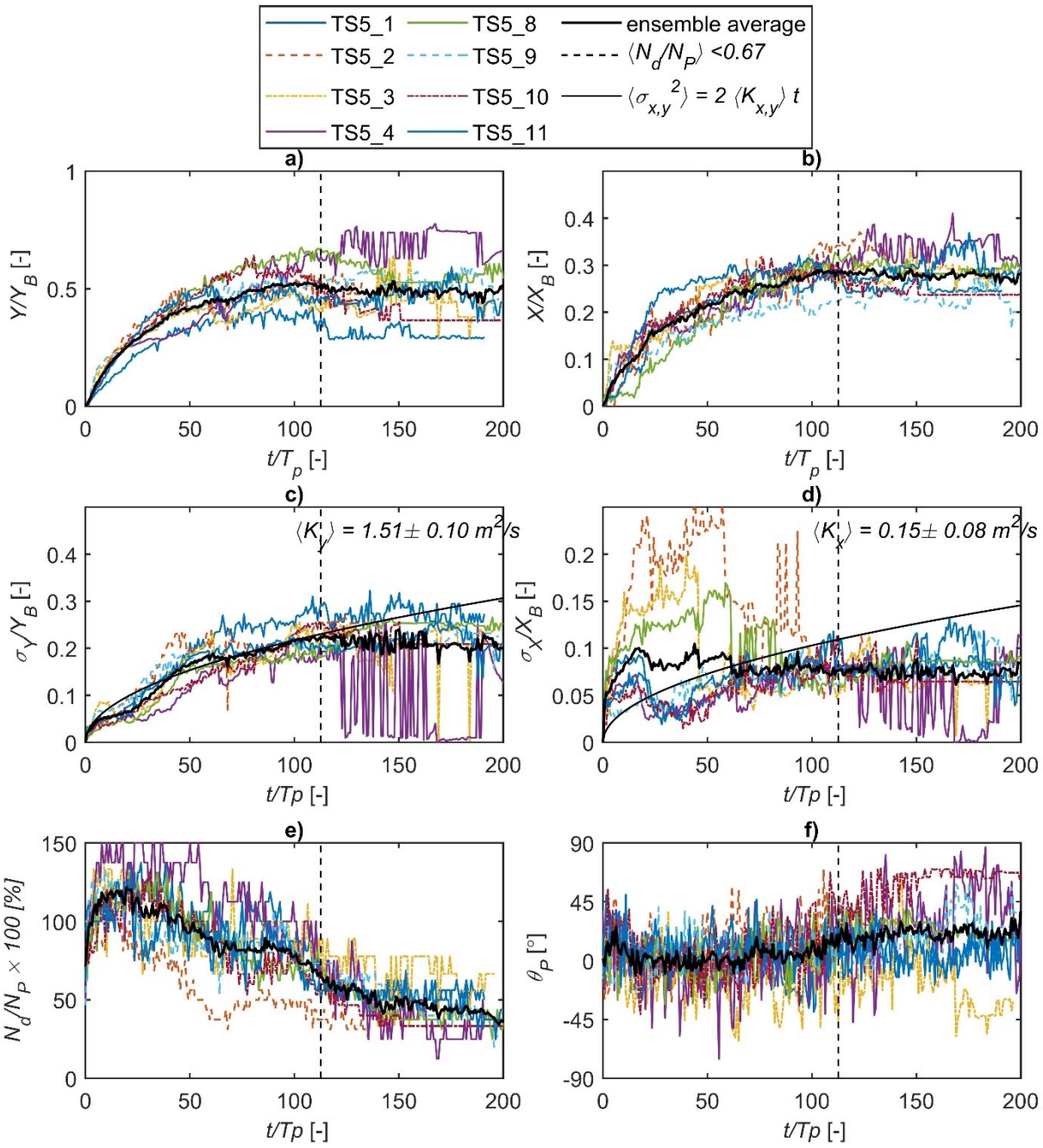

Figure A-13. a) Mean alongshore relative travel distance, b) mean cross-shore relative travel distance, c) alongshore standard deviation, d) cross-shore standard deviation, e) detection rate, and f) mean orientation versus time for smooth driftwood length class L_P = 3 m (yellow) during test series TS5 (η = 0.70 m, H_s = 0.80 m, T_p = 14 s).

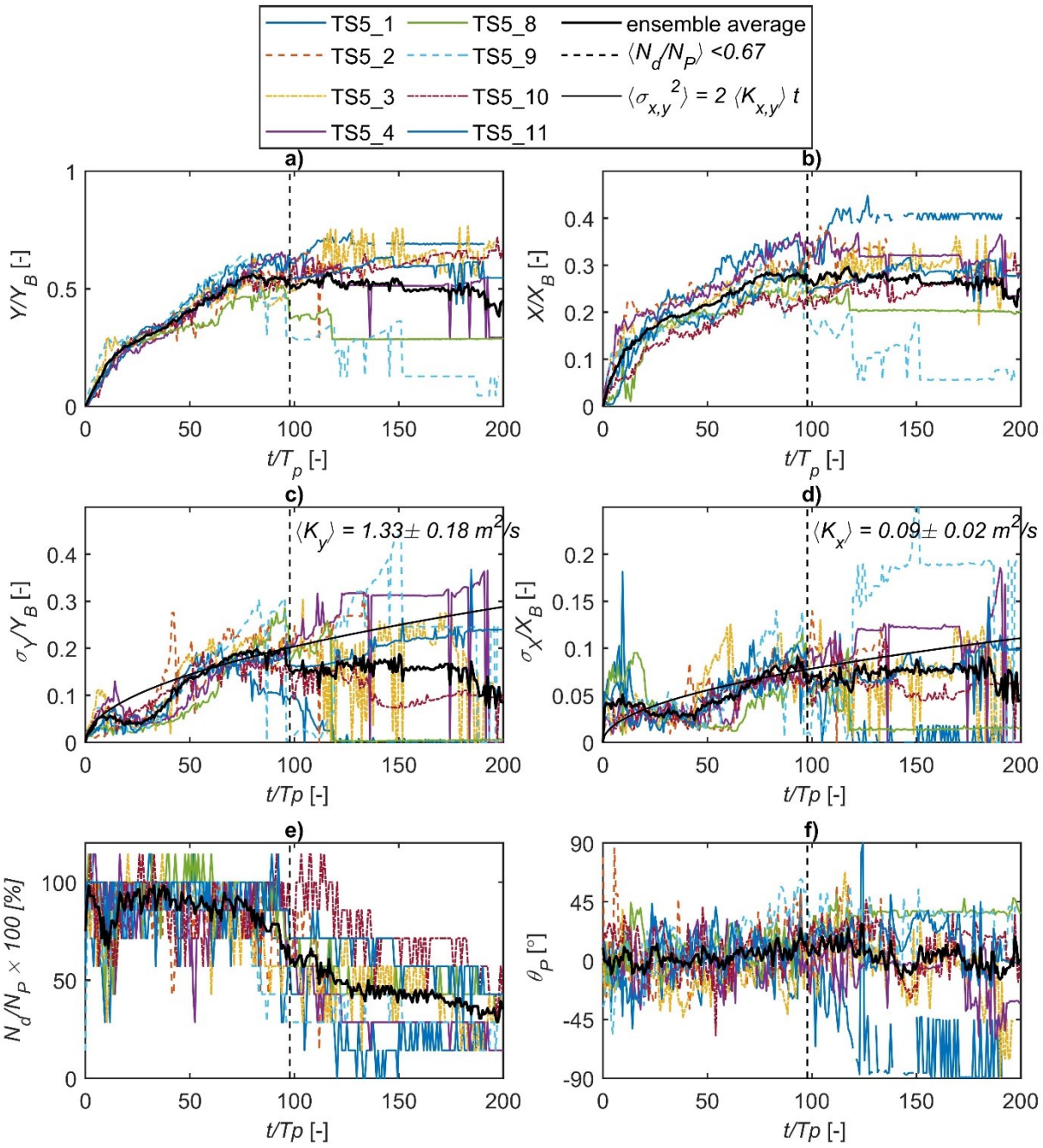

Figure A-14. a) Mean alongshore relative travel distance, b) mean cross-shore relative travel distance, c) alongshore standard deviation, d) cross-shore standard deviation, e) detection rate, and f) mean orientation versus time for smooth driftwood length class L_P = 9 m (blue) during test series TS5 (η = 0.70 m, H_s = 0.80 m, T_p = 14 s).

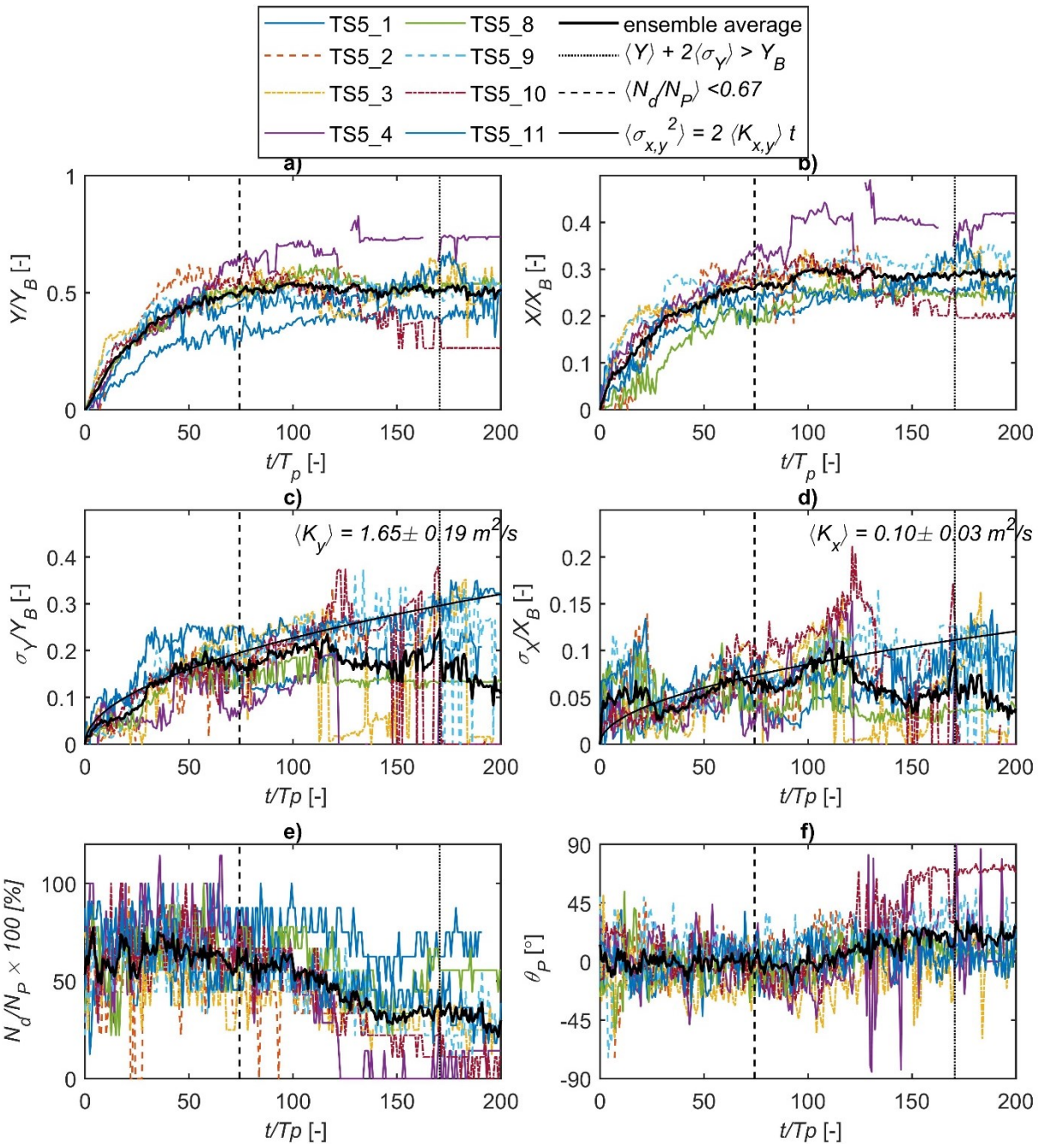

Figure A-15. a) Mean alongshore relative travel distance, b) mean cross-shore relative travel distance, c) alongshore standard deviation, d) cross-shore standard deviation, e) detection rate, and f) mean orientation versus time for smooth driftwood length class L_P = 12 m (green) during test series TS5 (η = 0.70 m, H_s = 0.80 m, T_p = 14 s).

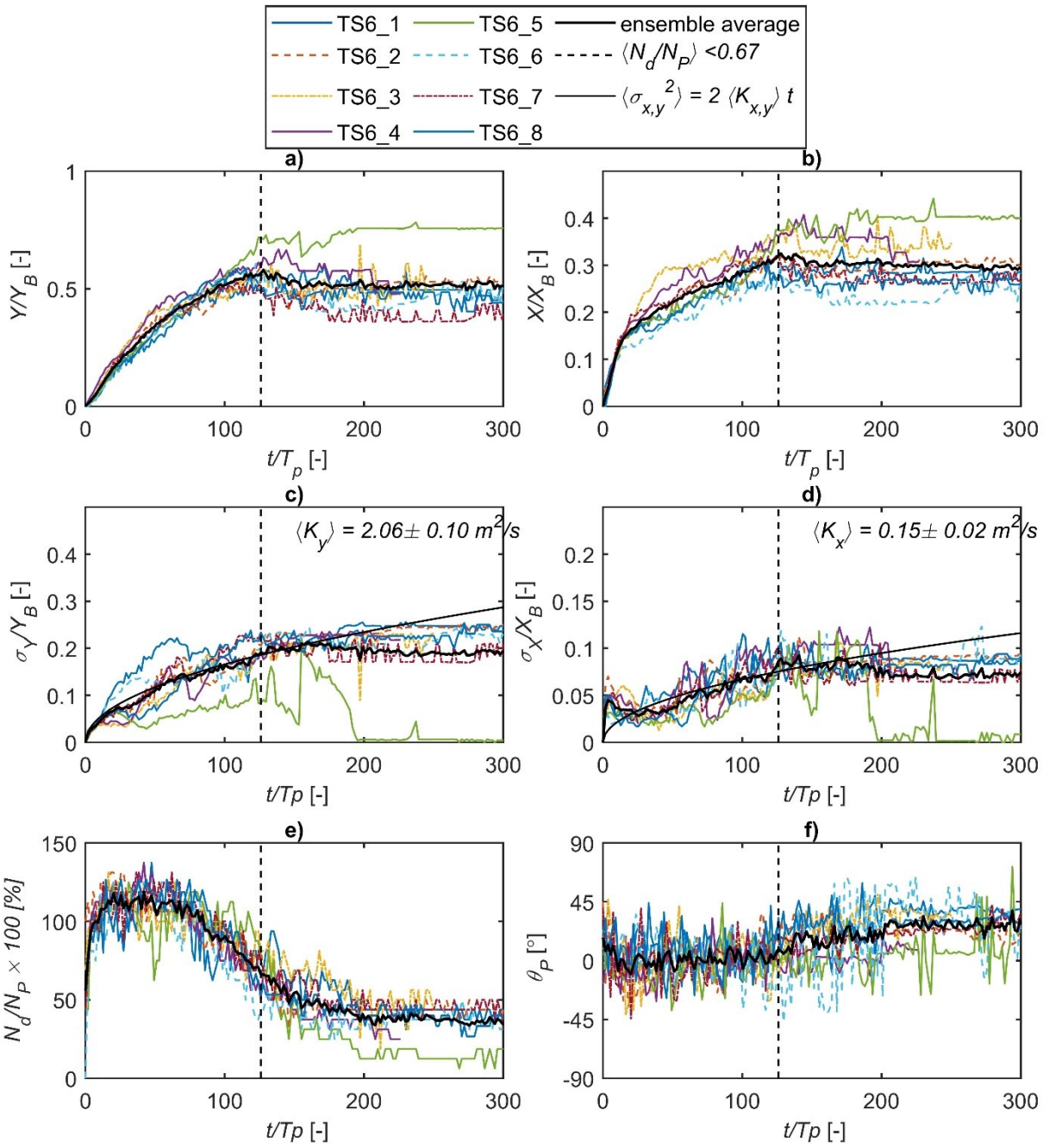

Figure A-16. a) Mean alongshore relative travel distance, b) mean cross-shore relative travel distance, c) alongshore standard deviation, d) cross-shore standard deviation, e) detection rate, and f) mean orientation versus time for smooth driftwood length class L_P = 3 m (yellow) during test series TS6 (η = 0.70 m, H_s = 1.20 m, T_p = 6 s).

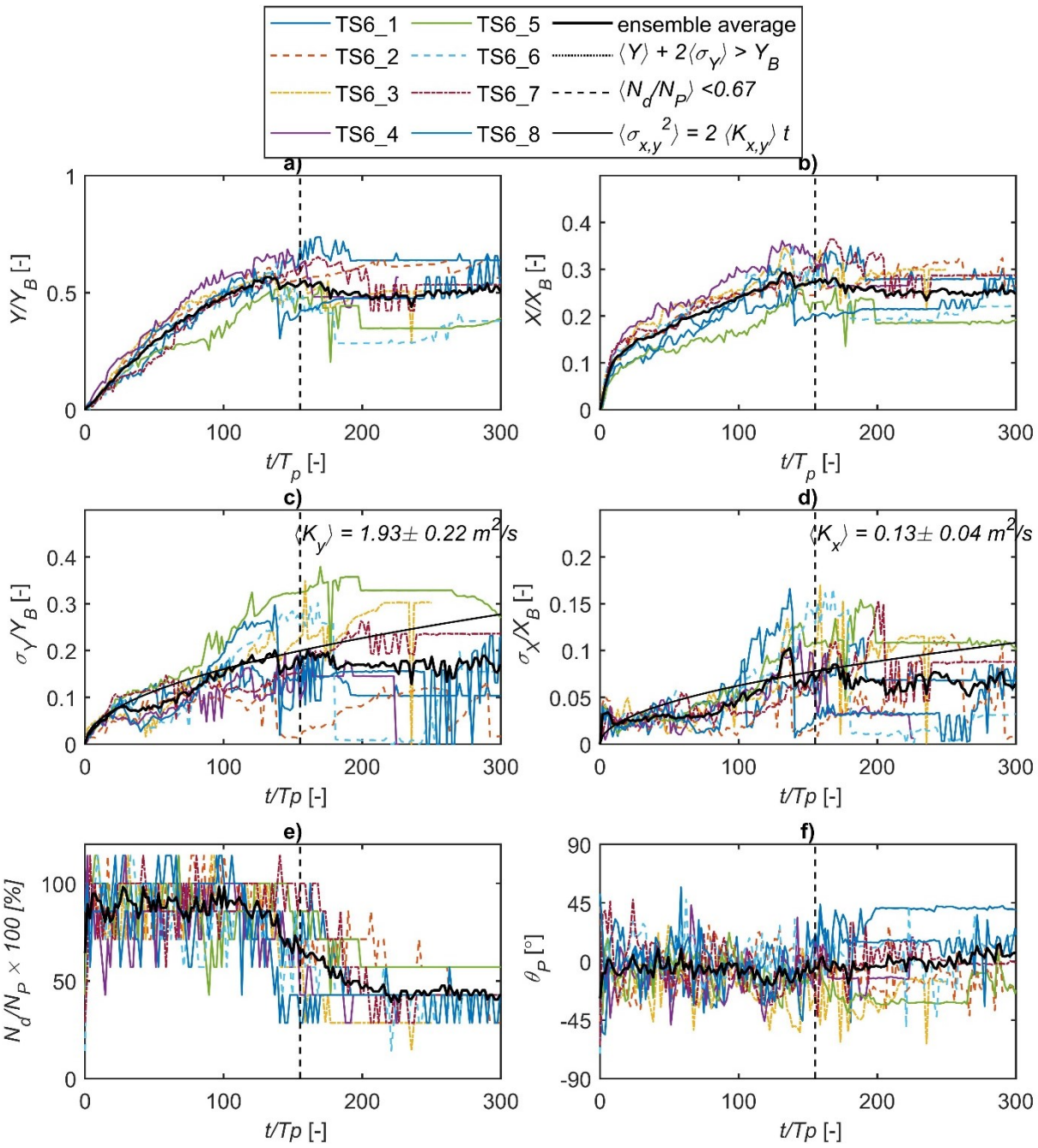

Figure A-17. a) Mean alongshore relative travel distance, b) mean cross-shore relative travel distance, c) alongshore standard deviation, d) cross-shore standard deviation, e) detection rate, and f) mean orientation versus time for smooth driftwood length class L_P = 9 m (blue) during test series TS6 (η = 0.70 m, H_s = 1.20 m, T_p = 6 s).

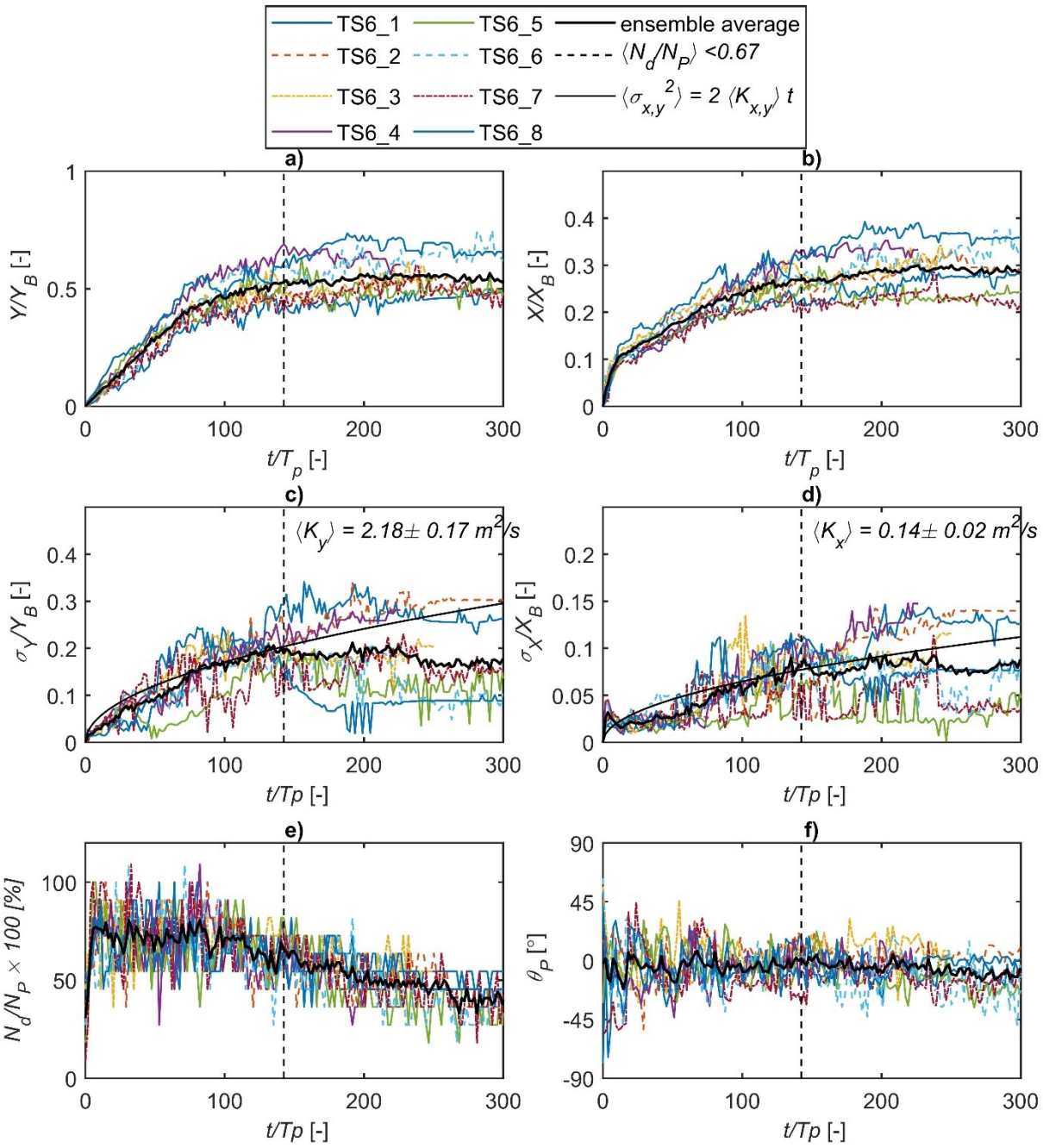

Figure A-18. a) Mean alongshore relative travel distance, b) mean cross-shore relative travel distance, c) alongshore standard deviation, d) cross-shore standard deviation, e) detection rate, and f) mean orientation versus time for smooth driftwood length class L_P = 12 m (green) during test series TS6 (η = 0.70 m, H_s = 1.20 m, T_p = 6 s).

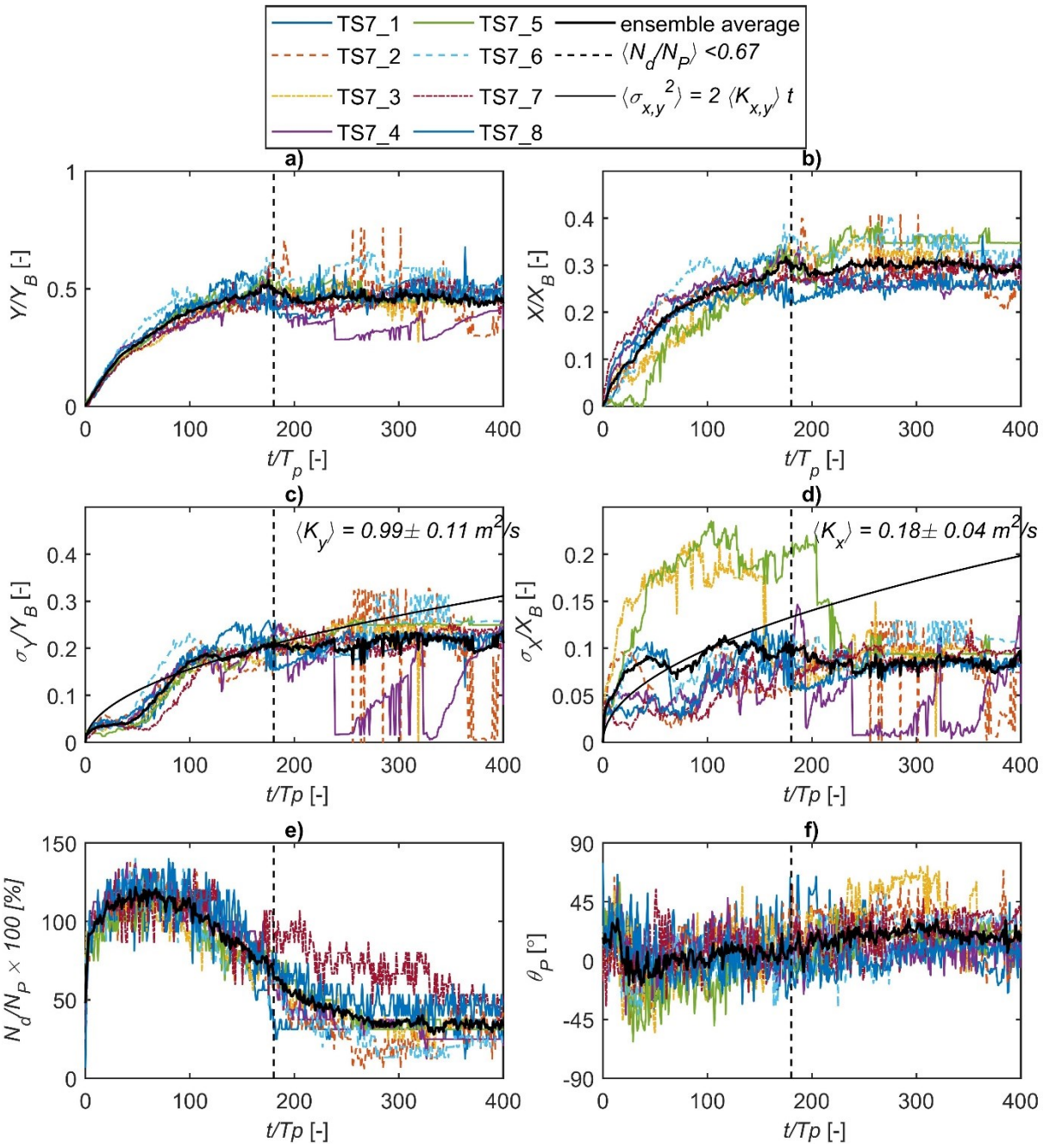

Figure A-19. a) Mean alongshore relative travel distance, b) mean cross-shore relative travel distance, c) alongshore standard deviation, d) cross-shore standard deviation, e) detection rate, and f) mean orientation versus time for smooth driftwood length class L_P = 3 m (yellow) during test series TS7 (η = 0.35 m, H_s = 0.65 m, T_p = 11 s).

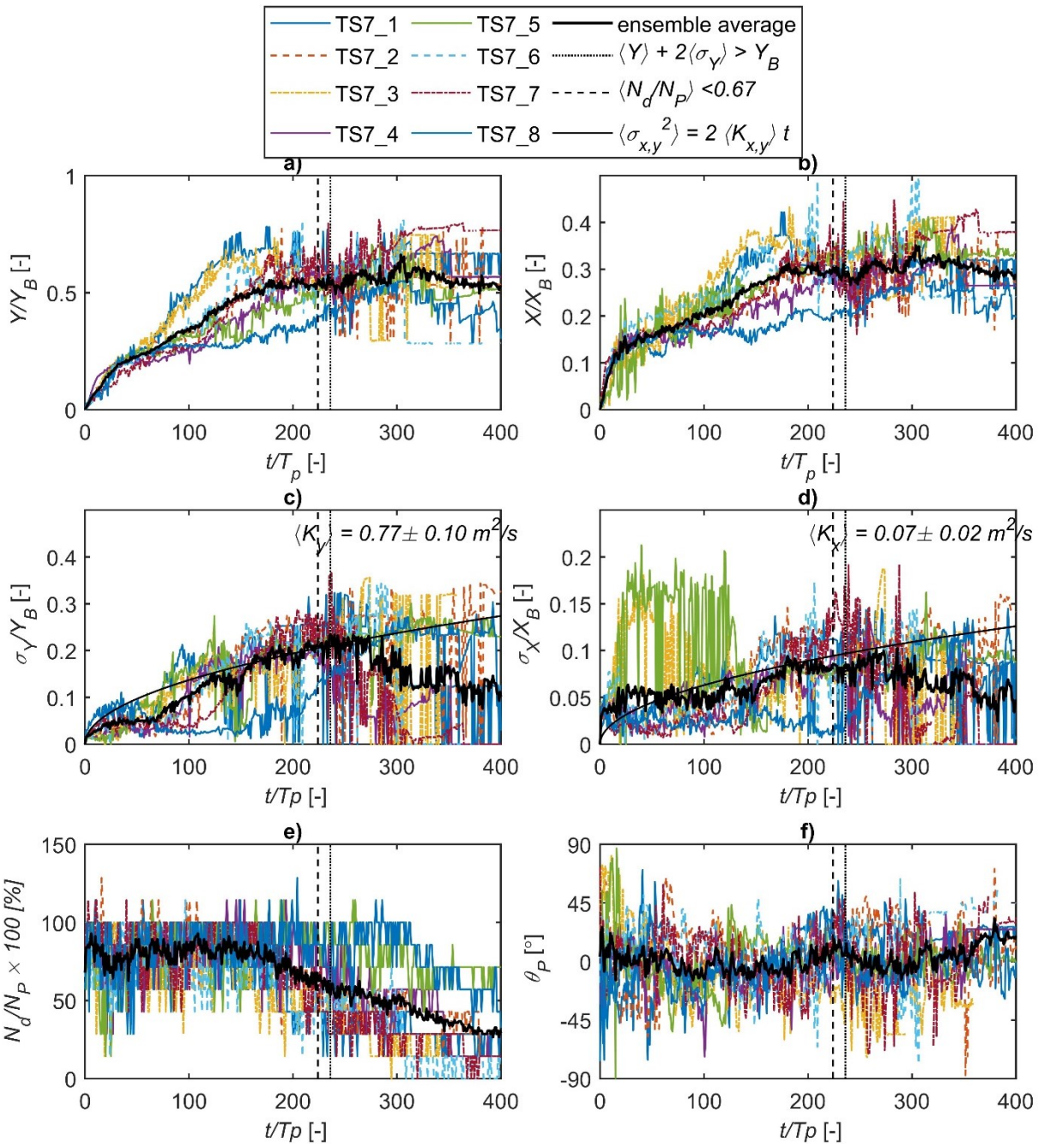

Figure A-20. a) Mean alongshore relative travel distance, b) mean cross-shore relative travel distance, c) alongshore standard deviation, d) cross-shore standard deviation, e) detection rate, and f) mean orientation versus time for smooth driftwood length class L_P = 9 m (blue) during test series TS7 (η = 0.35 m, H_s = 0.65 m, T_p = 11 s).

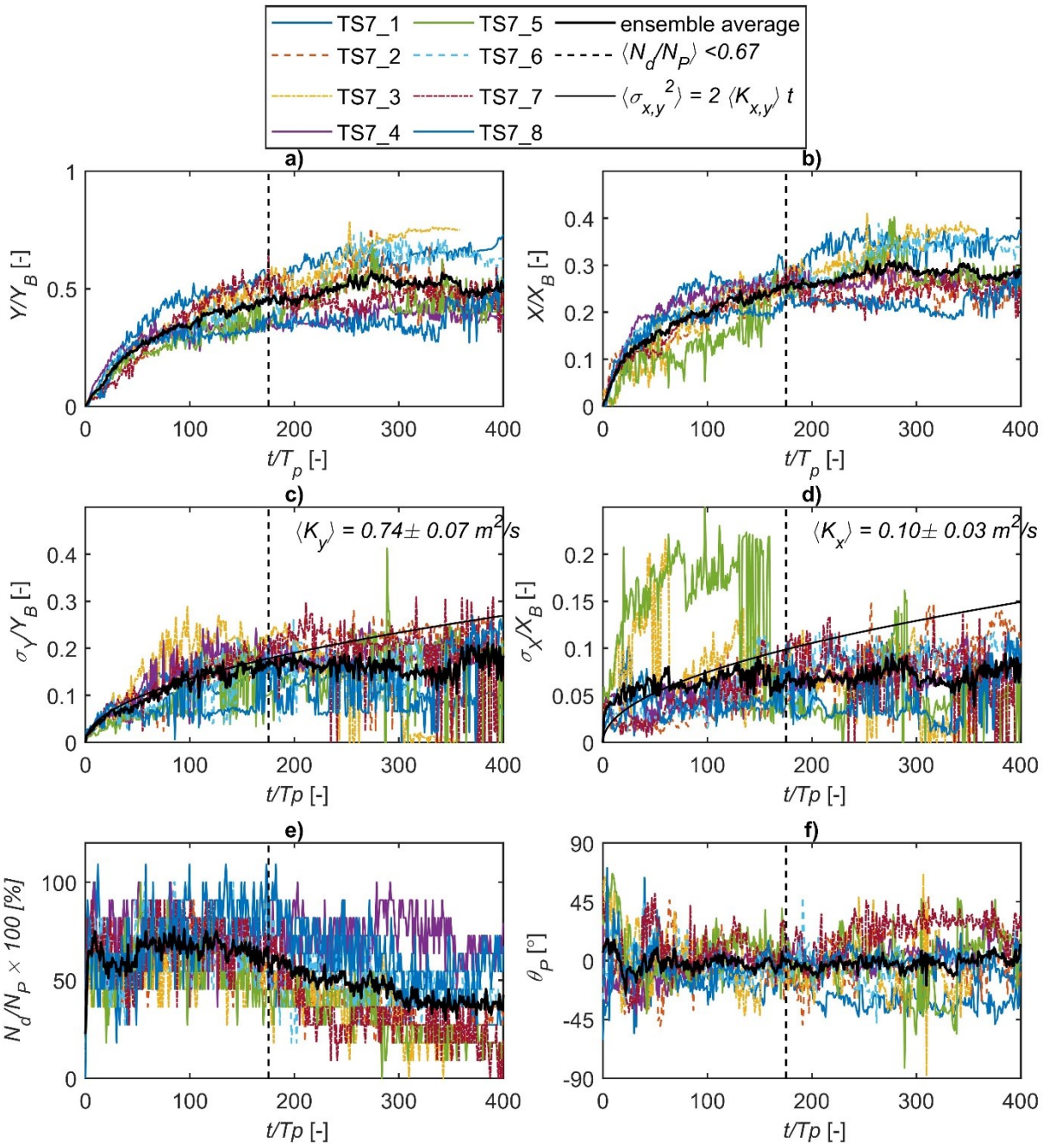

Figure A-21. a) Mean alongshore relative travel distance, b) mean cross-shore relative travel distance, c) alongshore standard deviation, d) cross-shore standard deviation, e) detection rate, and f) mean orientation versus time for smooth driftwood length class L_P = 12 m (green) during test series TS7 (η = 0.35 m, H_s = 0.65 m, T_p = 11 s).

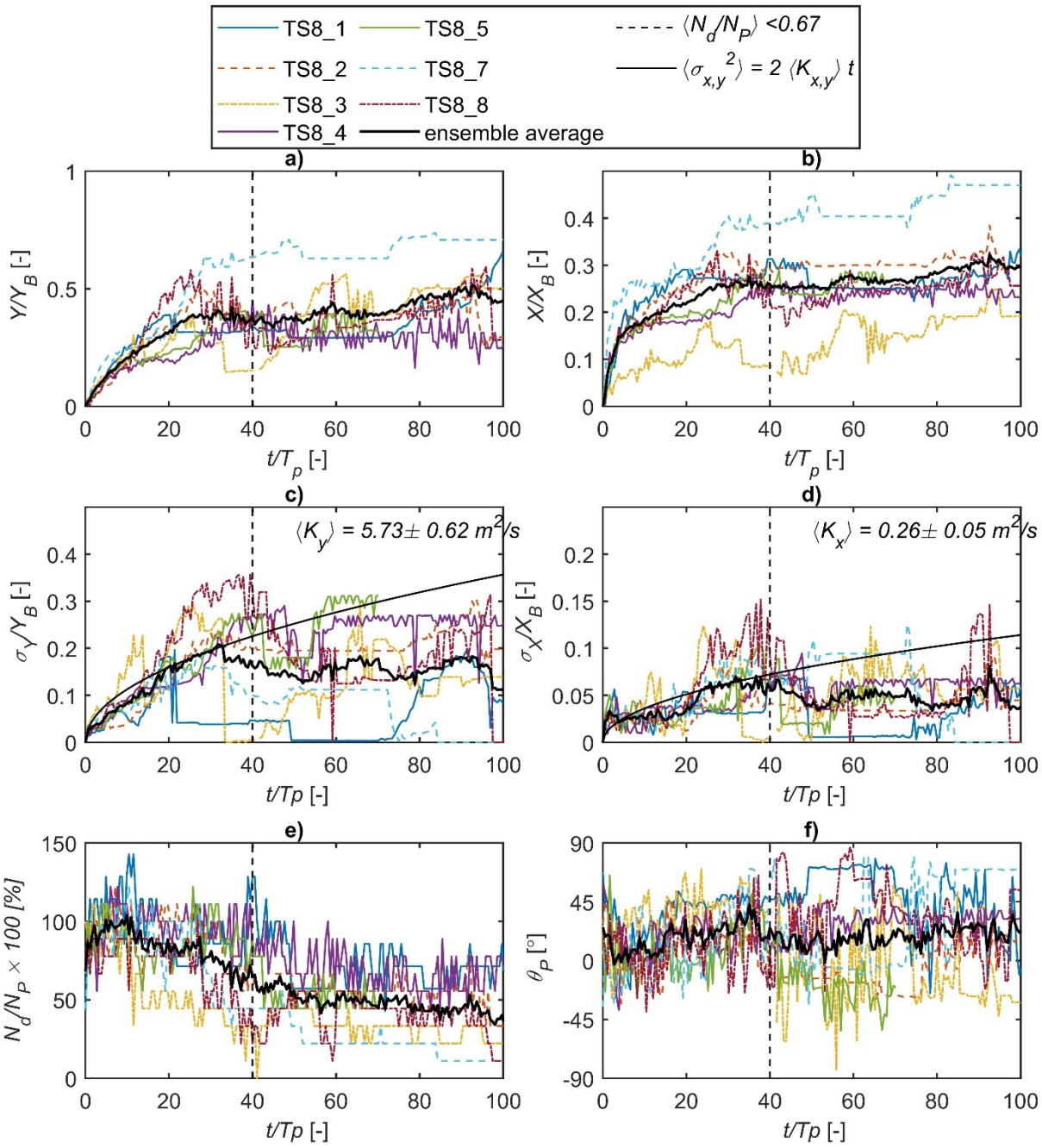

Figure A-22. a) Mean alongshore relative travel distance, b) mean cross-shore relative travel distance, c) alongshore standard deviation, d) cross-shore standard deviation, e) detection rate, and f) mean orientation versus time for smooth driftwood length class L_P = 3 m (yellow) during test series TS8 (η = 0.70 m, H_s = 3.70 m, T_p = 10 s).

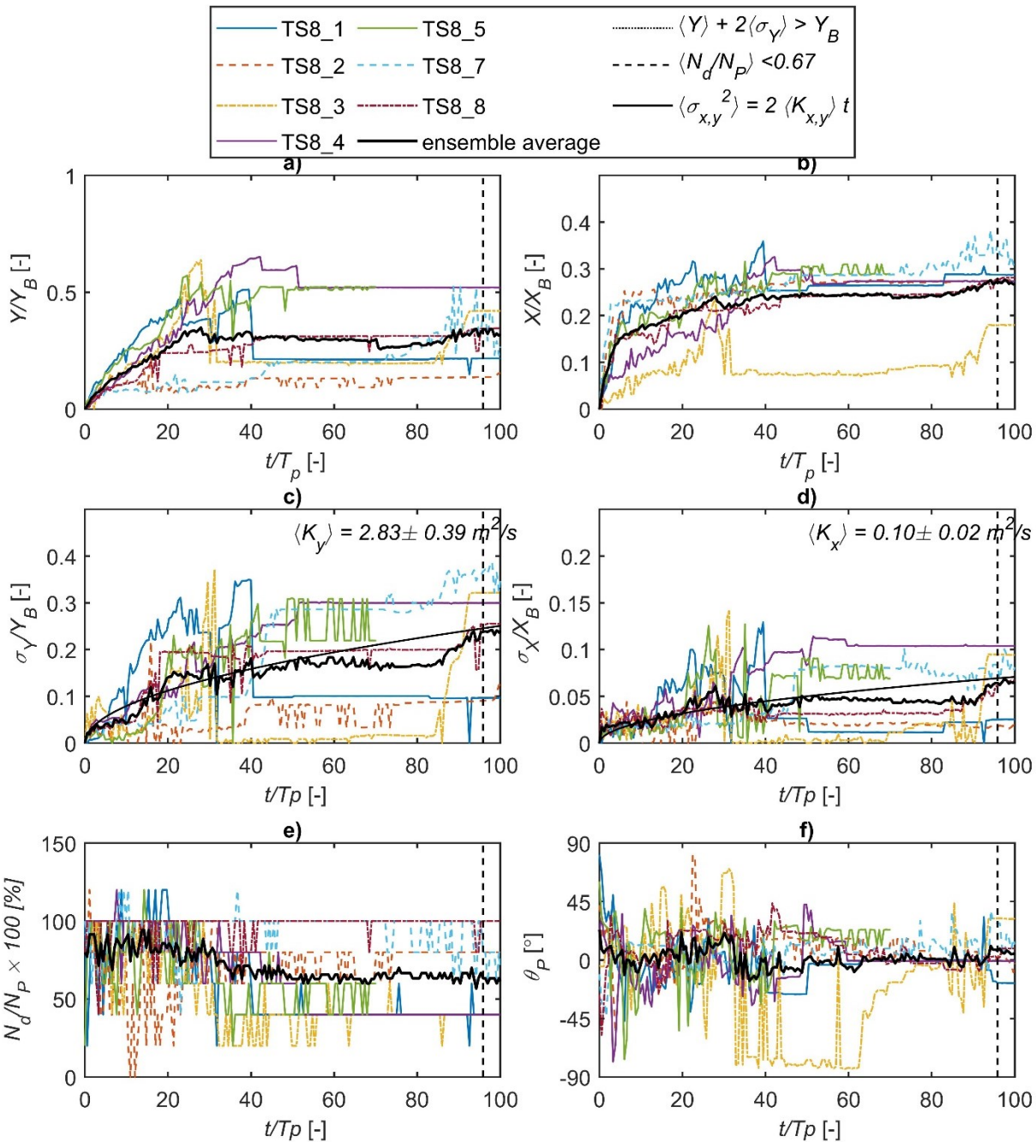

Figure A-23. a) Mean alongshore relative travel distance, b) mean cross-shore relative travel distance, c) alongshore standard deviation, d) cross-shore standard deviation, e) detection rate, and f) mean orientation versus time for smooth driftwood length class L_P = 9 m (blue) during test series TS8 (η = 0.70 m, H_s = 3.70 m, T_p = 10 s).

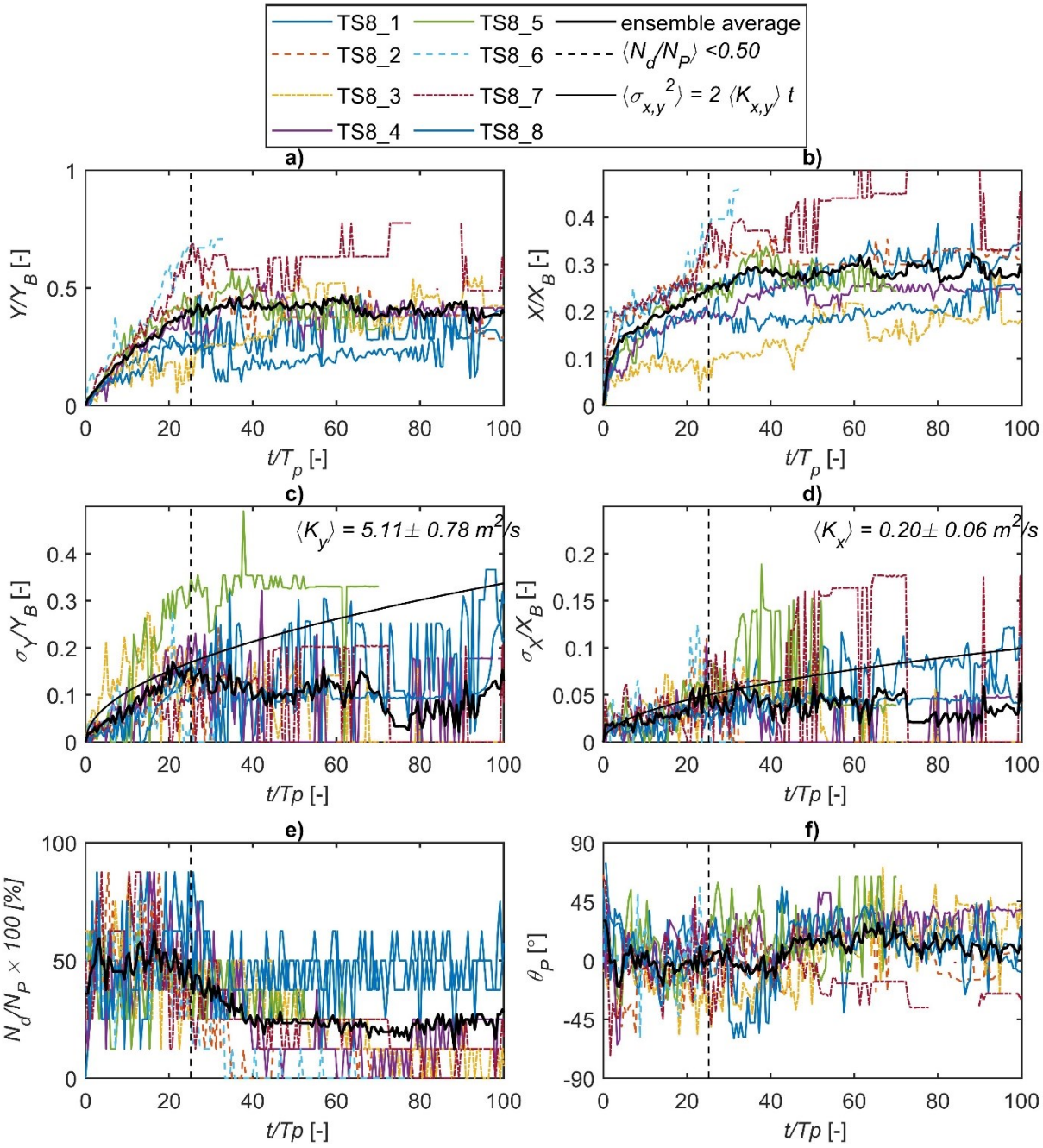

Figure A-24. a) Mean alongshore relative travel distance, b) mean cross-shore relative travel distance, c) alongshore standard deviation, d) cross-shore standard deviation, e) detection rate, and f) mean orientation versus time for smooth driftwood length class L_P = 12 m (green) during test series TS8 (η = 0.70 m, H_s = 3.70 m, T_p = 10 s).

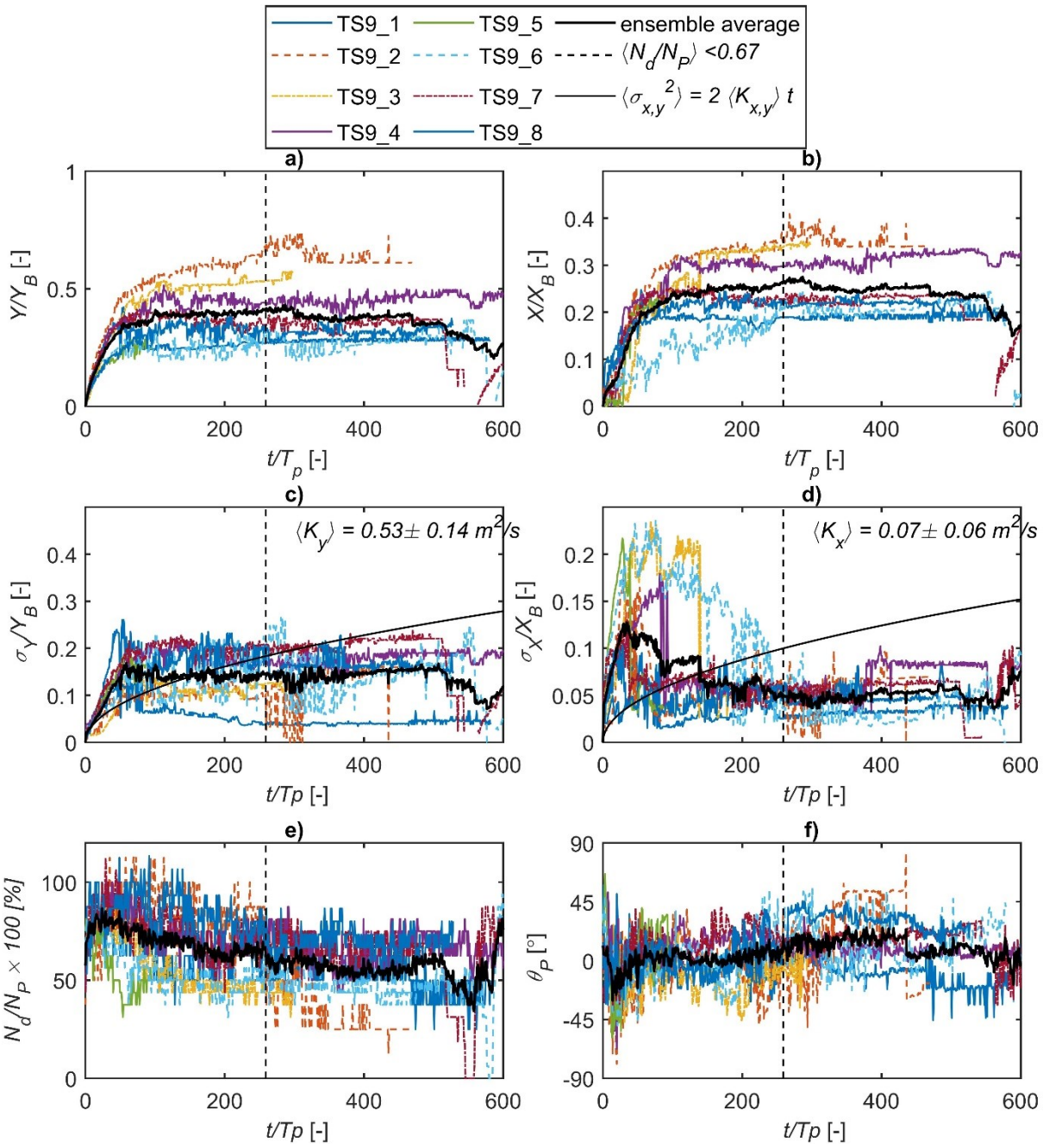

Figure A-25. a) Mean alongshore relative travel distance, b) mean cross-shore relative travel distance, c) alongshore standard deviation, d) cross-shore standard deviation, e) detection rate, and f) mean orientation versus time for rough driftwood length class L_P = 3 m (yellow) during test series TS9 (η = 0.70 m, H_s = 0.80 m, T_p = 11 s).

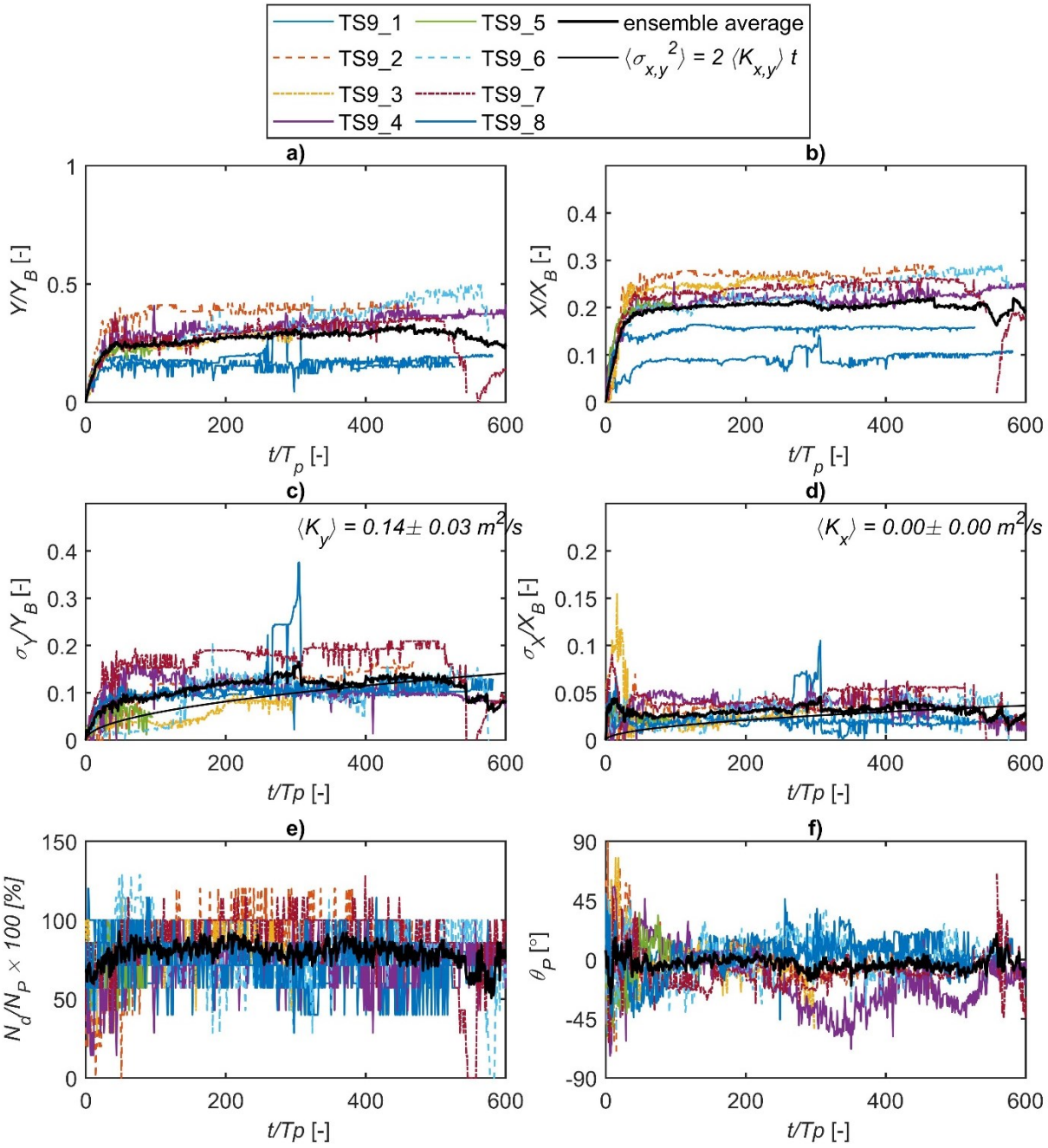

Figure A-26. a) Mean alongshore relative travel distance, b) mean cross-shore relative travel distance, c) alongshore standard deviation, d) cross-shore standard deviation, e) detection rate, and f) mean orientation versus time for rough driftwood length class L_P = 9 m (blue) during test series TS9 (η = 0.70 m, H_s = 0.80 m, T_p = 11 s).

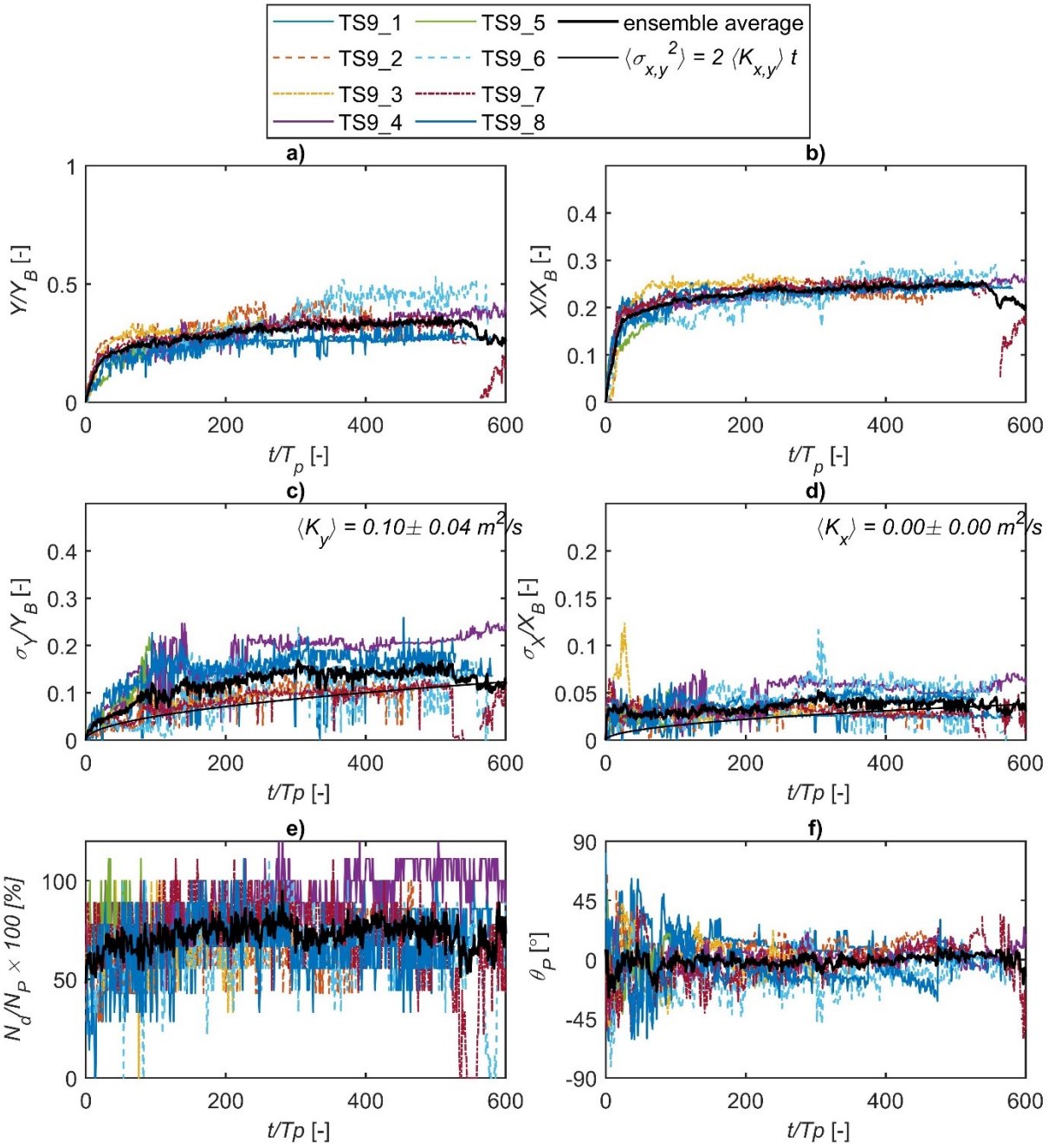

Figure A-27. a) Mean alongshore relative travel distance, b) mean cross-shore relative travel distance, c) alongshore standard deviation, d) cross-shore standard deviation, e) detection rate, and f) mean orientation versus time for rough driftwood length class L_P = 12 m (green) during test series TS9 (η = 0.70 m, H_s = 0.80 m, T_p = 11 s).

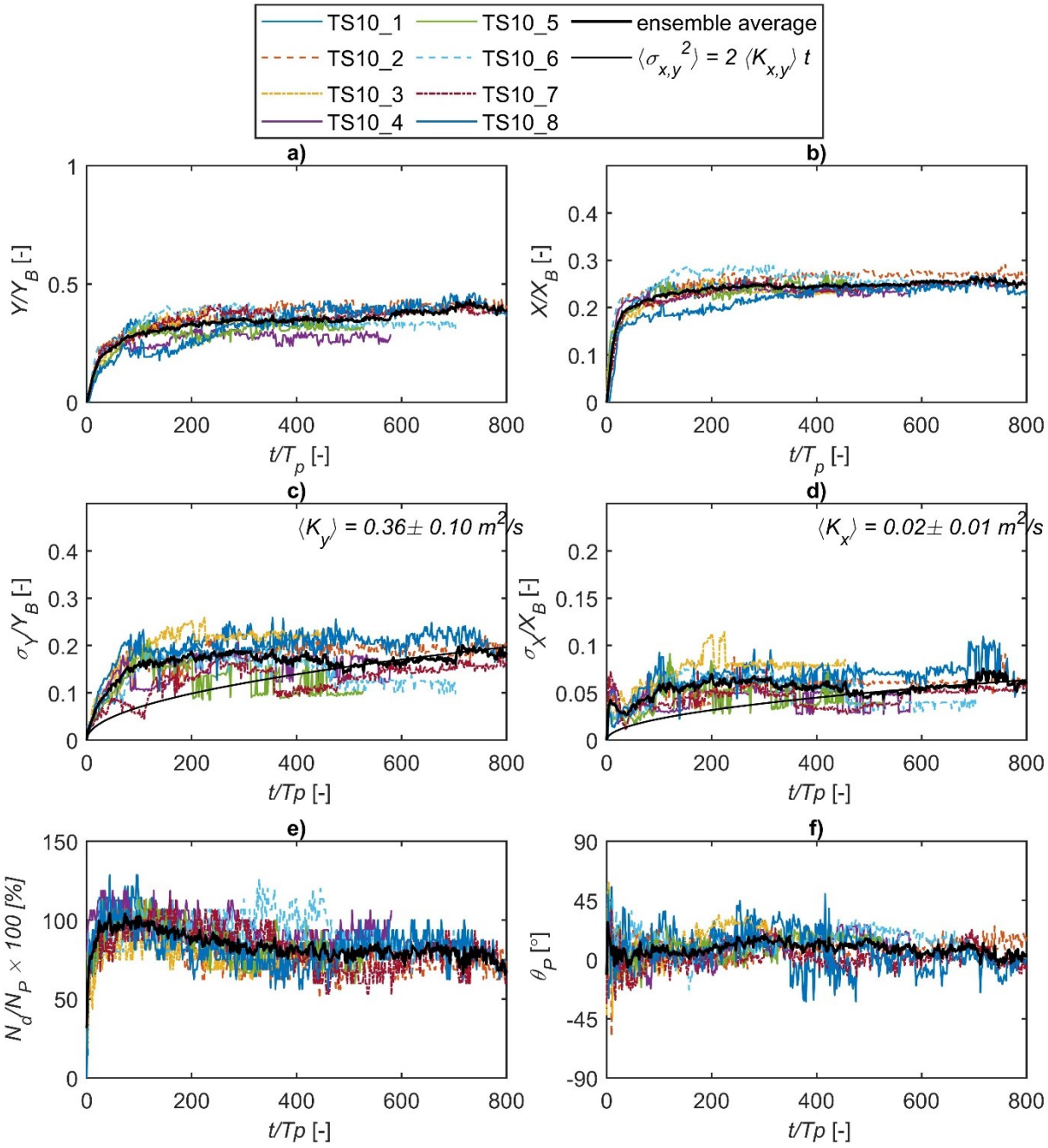

Figure A-28. a) Mean alongshore relative travel distance, b) mean cross-shore relative travel distance, c) alongshore standard deviation, d) cross-shore standard deviation, e) detection rate, and f) mean orientation versus time for rough driftwood length class L_P = 3 m (yellow) during test series TS10 (η = 0.70 m, H_s = 1.20 m, T_p = 6 s).

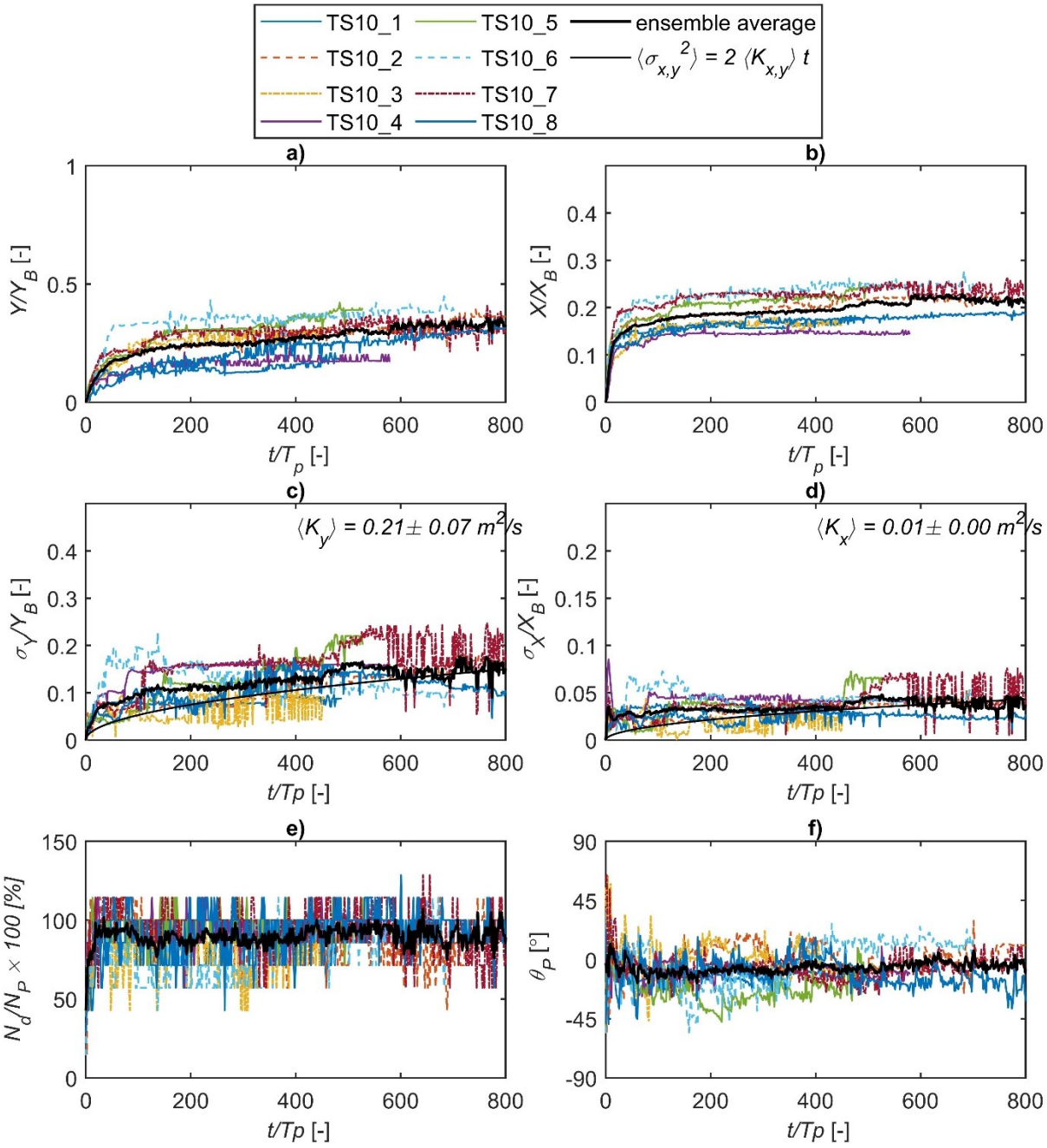

Figure A-29. a) Mean alongshore relative travel distance, b) mean cross-shore relative travel distance, c) alongshore standard deviation, d) cross-shore standard deviation, e) detection rate, and f) mean orientation versus time for rough driftwood length class L_P = 9 m (blue) during test series TS10 (η = 0.70 m, H_s = 1.20 m, T_p = 6 s).

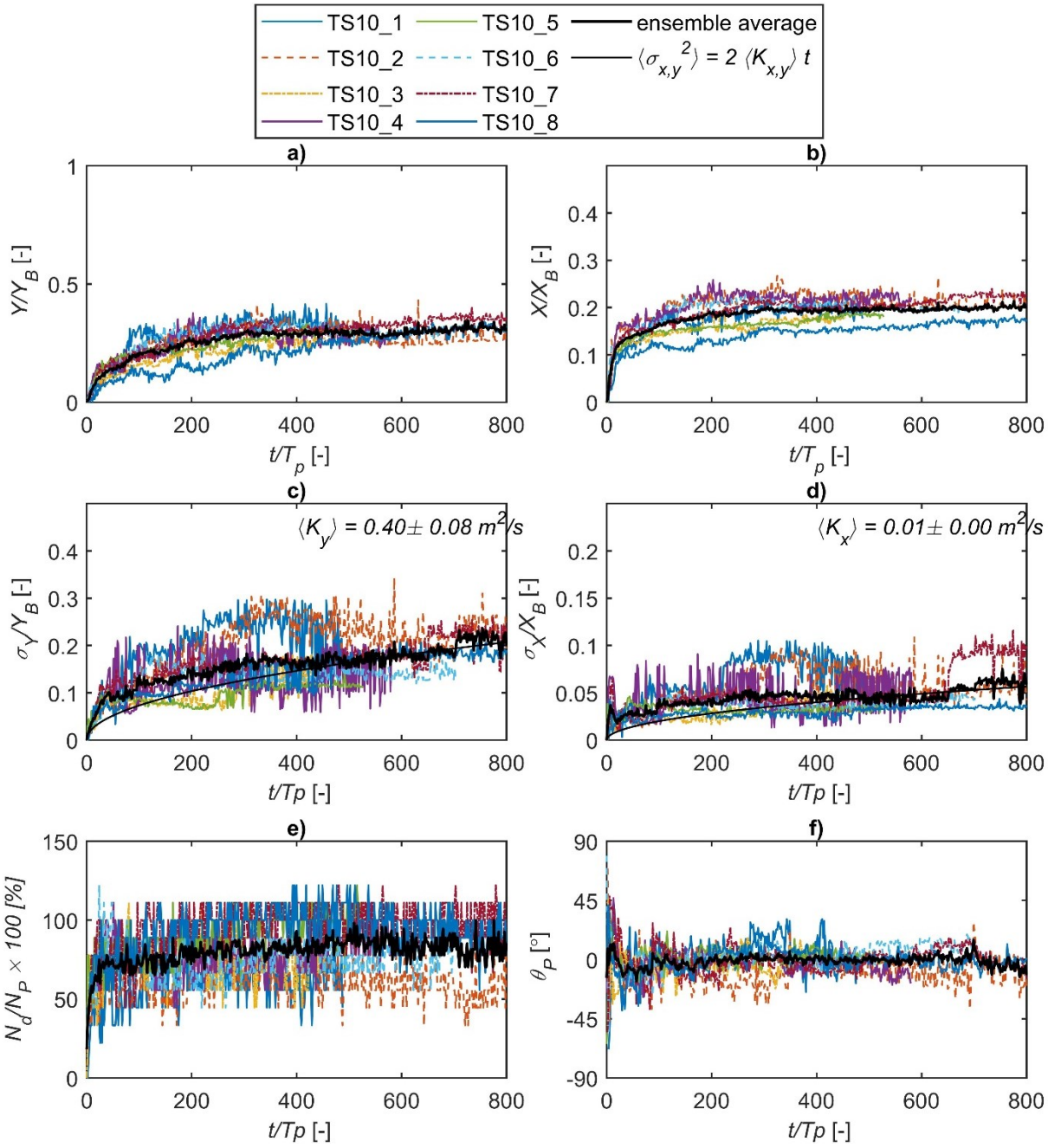

Figure A-30. a) Mean alongshore relative travel distance, b) mean cross-shore relative travel distance, c) alongshore standard deviation, d) cross-shore standard deviation, e) detection rate, and f) mean orientation versus time for rough driftwood length class L_P = 12 m (green) during test series TS10 (η = 0.70 m, H_s = 1.20 m, T_p = 6 s).

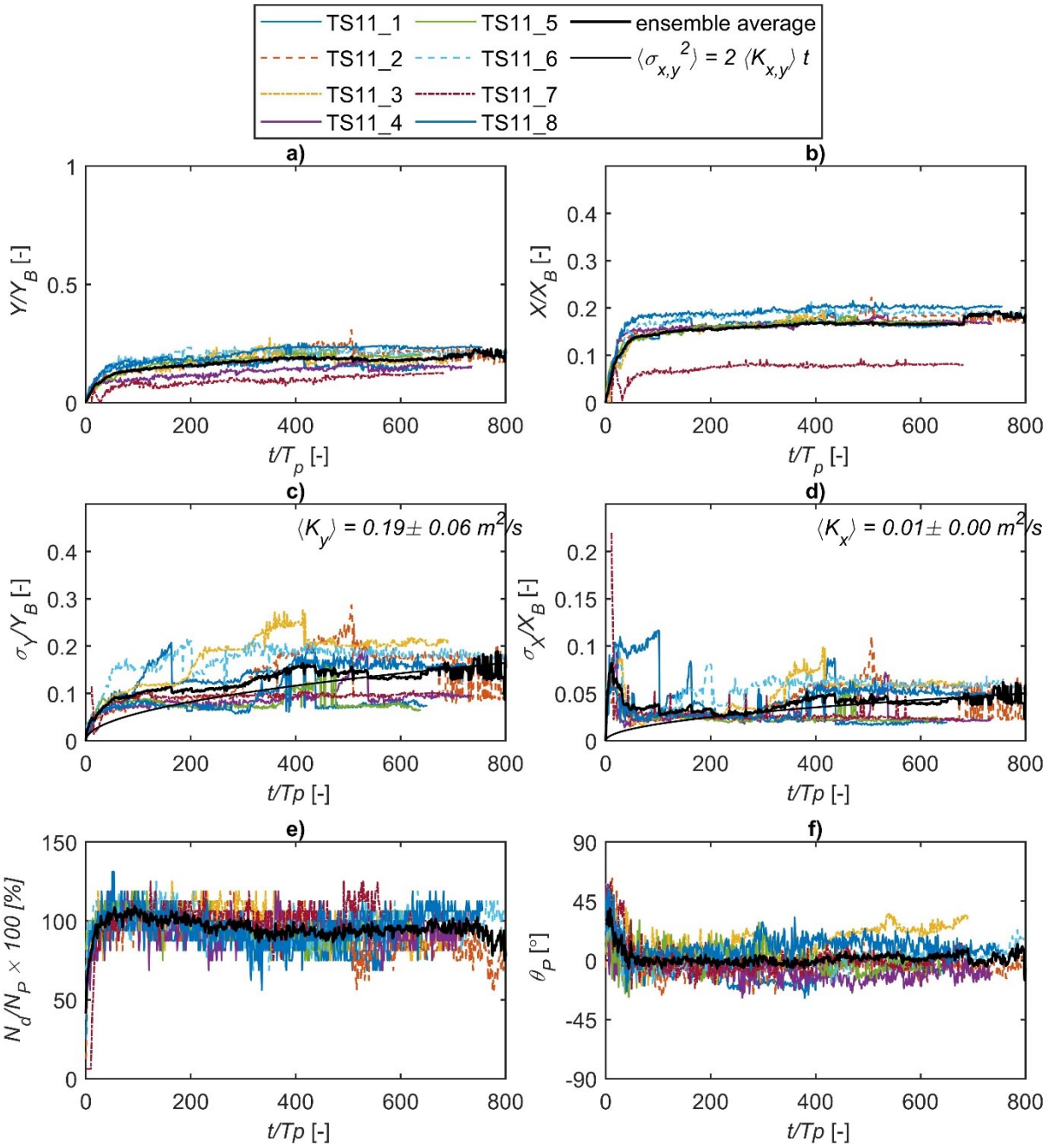

Figure A-31. a) Mean alongshore relative travel distance, b) mean cross-shore relative travel distance, c) alongshore standard deviation, d) cross-shore standard deviation, e) detection rate, and f) mean orientation versus time for rough driftwood length class L_P = 3 m (yellow) during test series TS11 (η = 0.35 m, H_s = 0.65 m, T_p = 8 s).

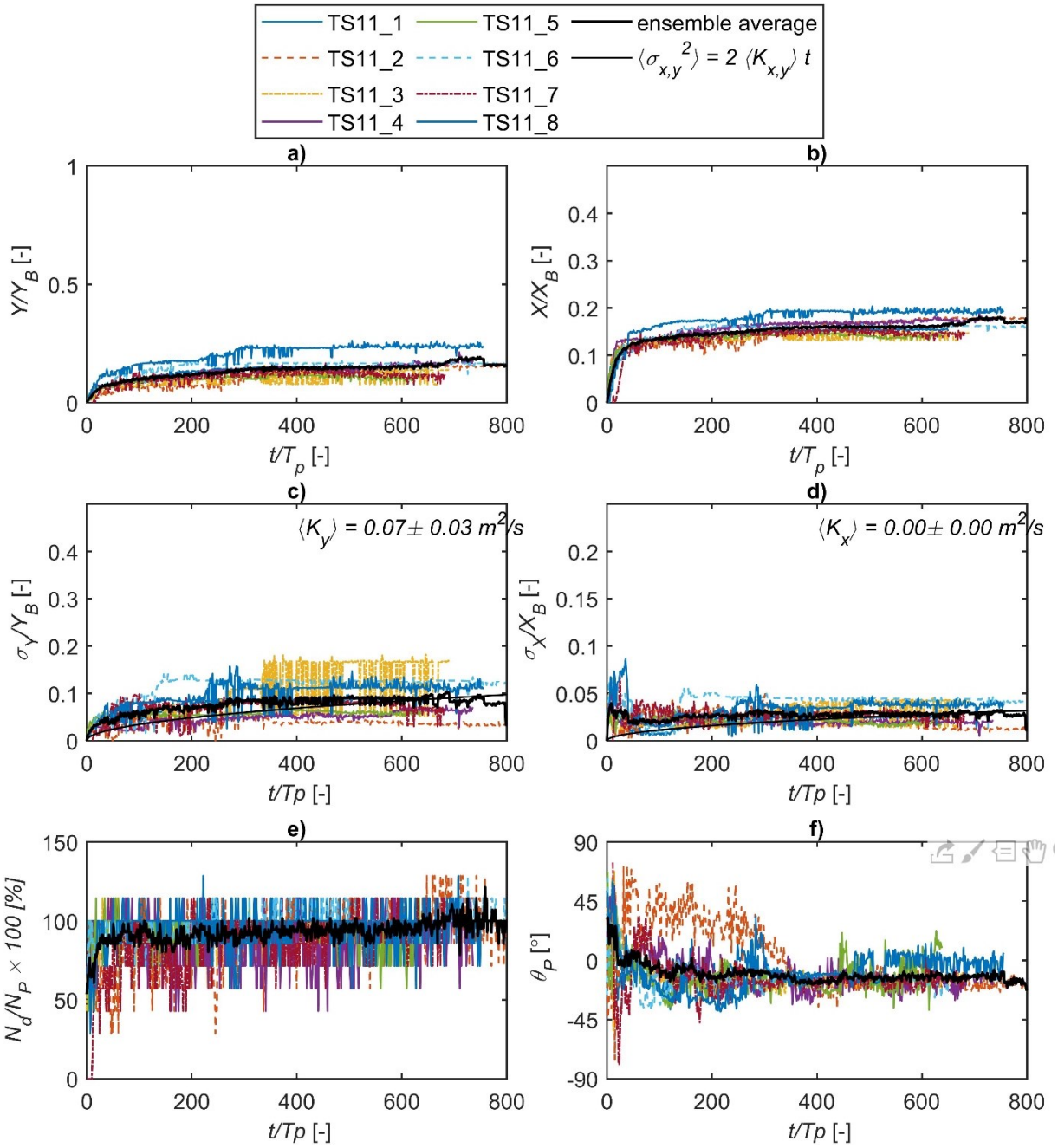

Figure A-32. a) Mean alongshore relative travel distance, b) mean cross-shore relative travel distance, c) alongshore standard deviation, d) cross-shore standard deviation, e) detection rate, and f) mean orientation versus time for rough driftwood length class L_P = 9 m (blue) during test series TS11 (η = 0.35 m, H_s = 0.65 m, T_p = 8 s).

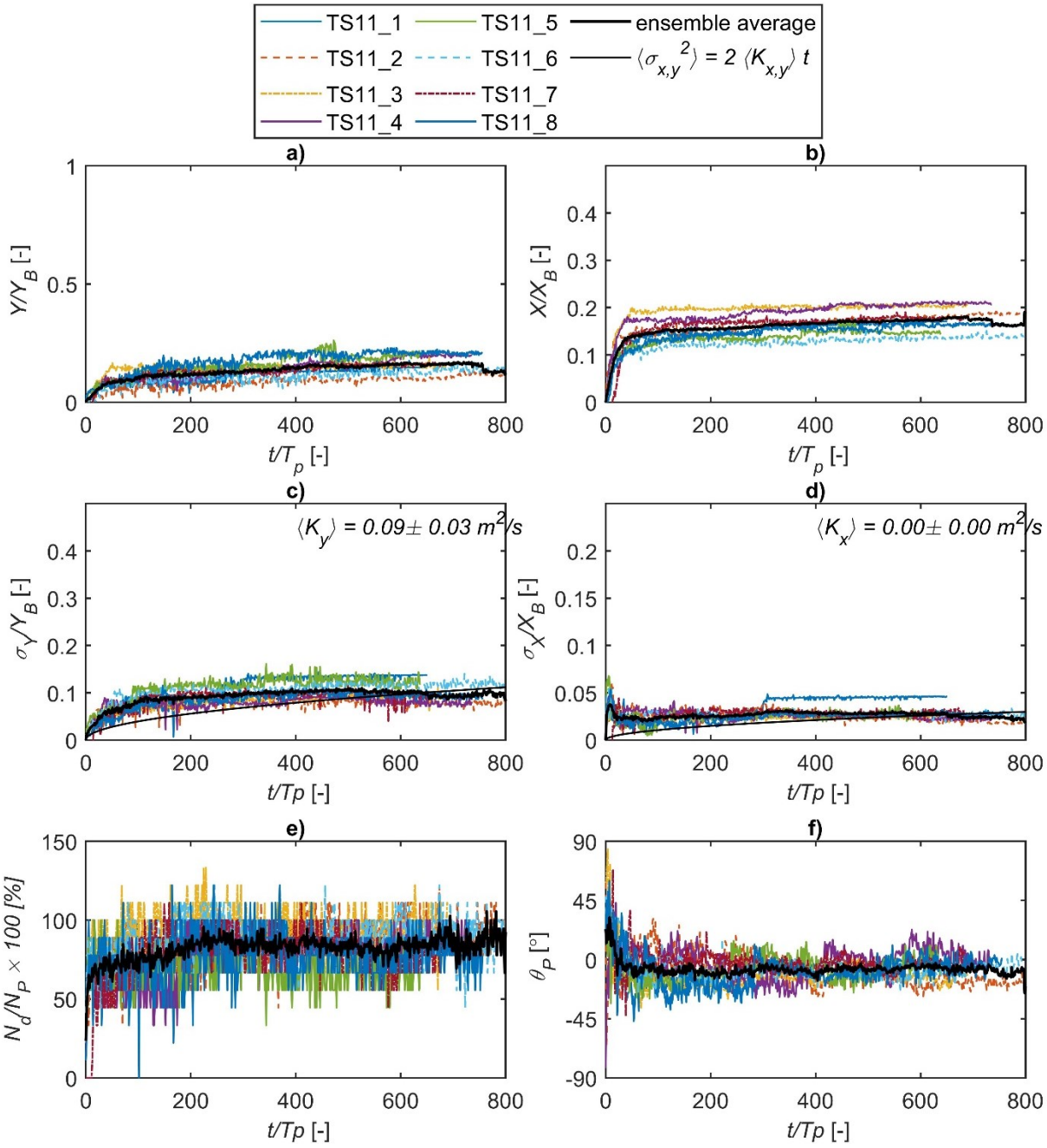

Figure A-33. a) Mean alongshore relative travel distance, b) mean cross-shore relative travel distance, c) alongshore standard deviation, d) cross-shore standard deviation, e) detection rate, and f) mean orientation versus time for rough driftwood length class L_P = 12 m (green) during test series TS11 (η = 0.35 m, H_s = 0.65 m, T_p = 8 s).

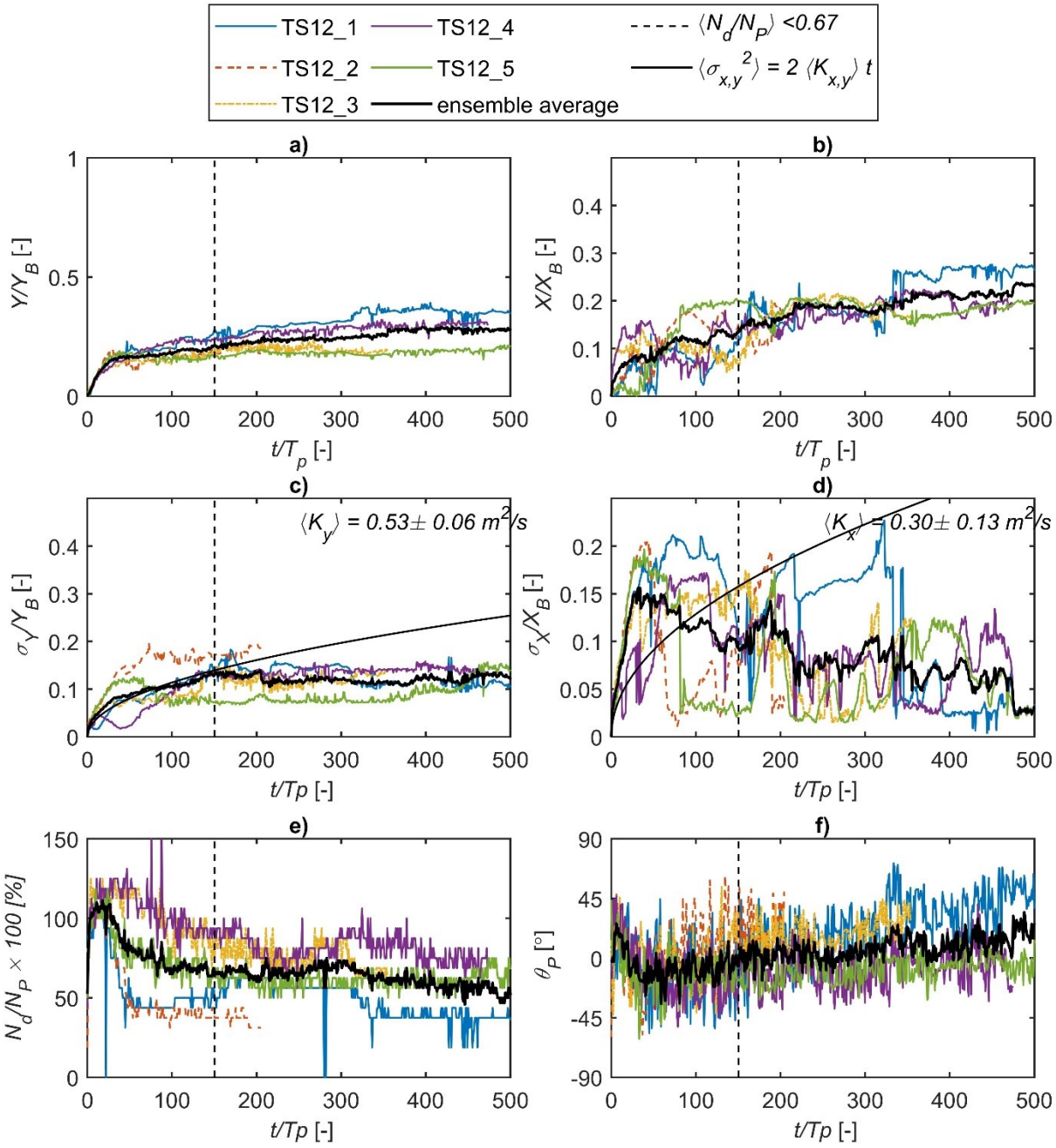

Figure A-34. a) Mean alongshore relative travel distance, b) mean cross-shore relative travel distance, c) alongshore standard deviation, d) cross-shore standard deviation, e) detection rate, and f) mean orientation versus time for rough driftwood length class L_P = 3 m (yellow) during test series TS12 (η = 0.35 m, H_s = 0.65 m, T_p = 11 s).

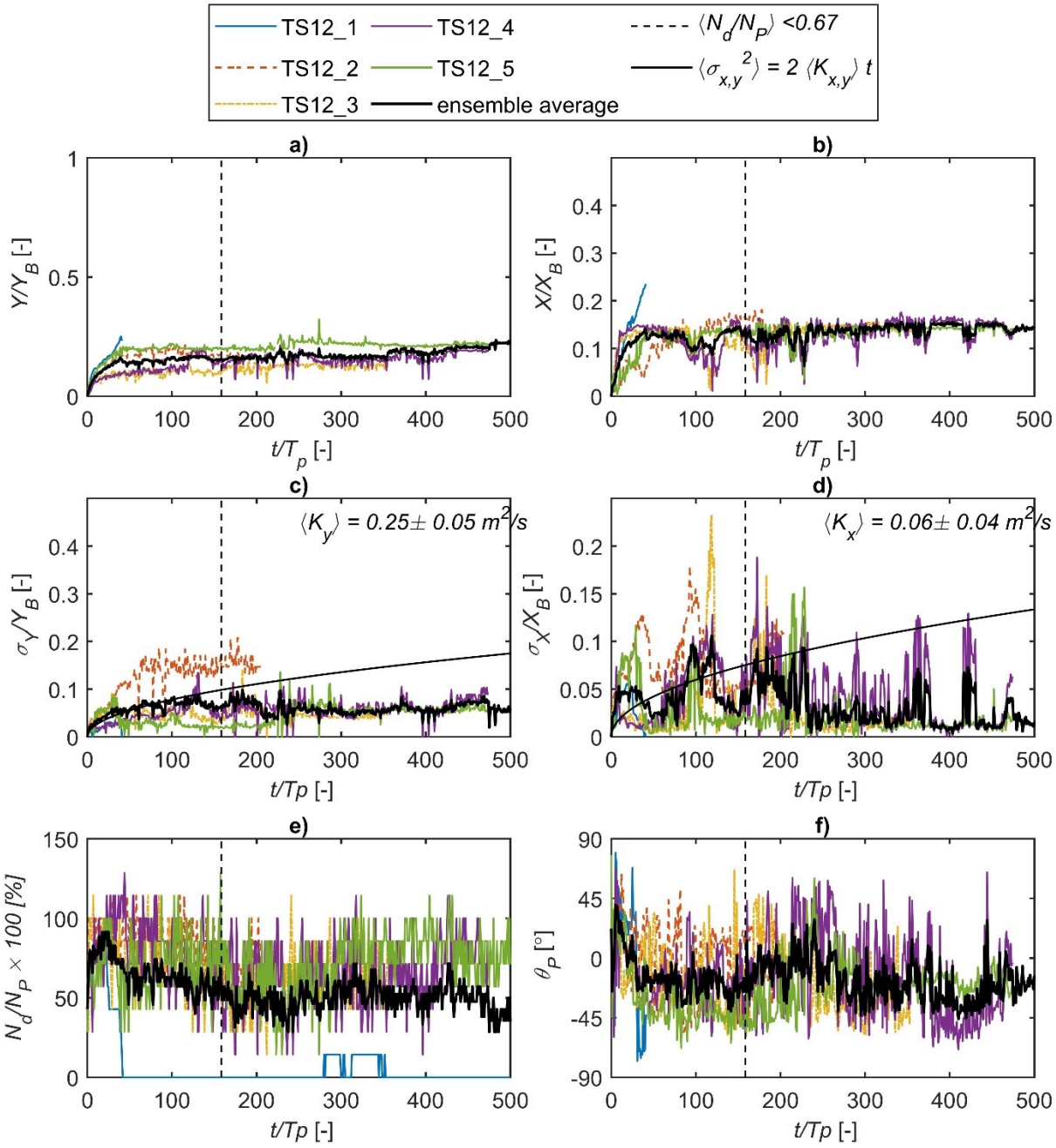

Figure A-35. a) Mean alongshore relative travel distance, b) mean cross-shore relative travel distance, c) alongshore standard deviation, d) cross-shore standard deviation, e) detection rate, and f) mean orientation versus time for rough driftwood length class L_P = 9 m (blue) during test series TS12 (η = 0.35 m, H_s = 0.65 m, T_p = 11 s).

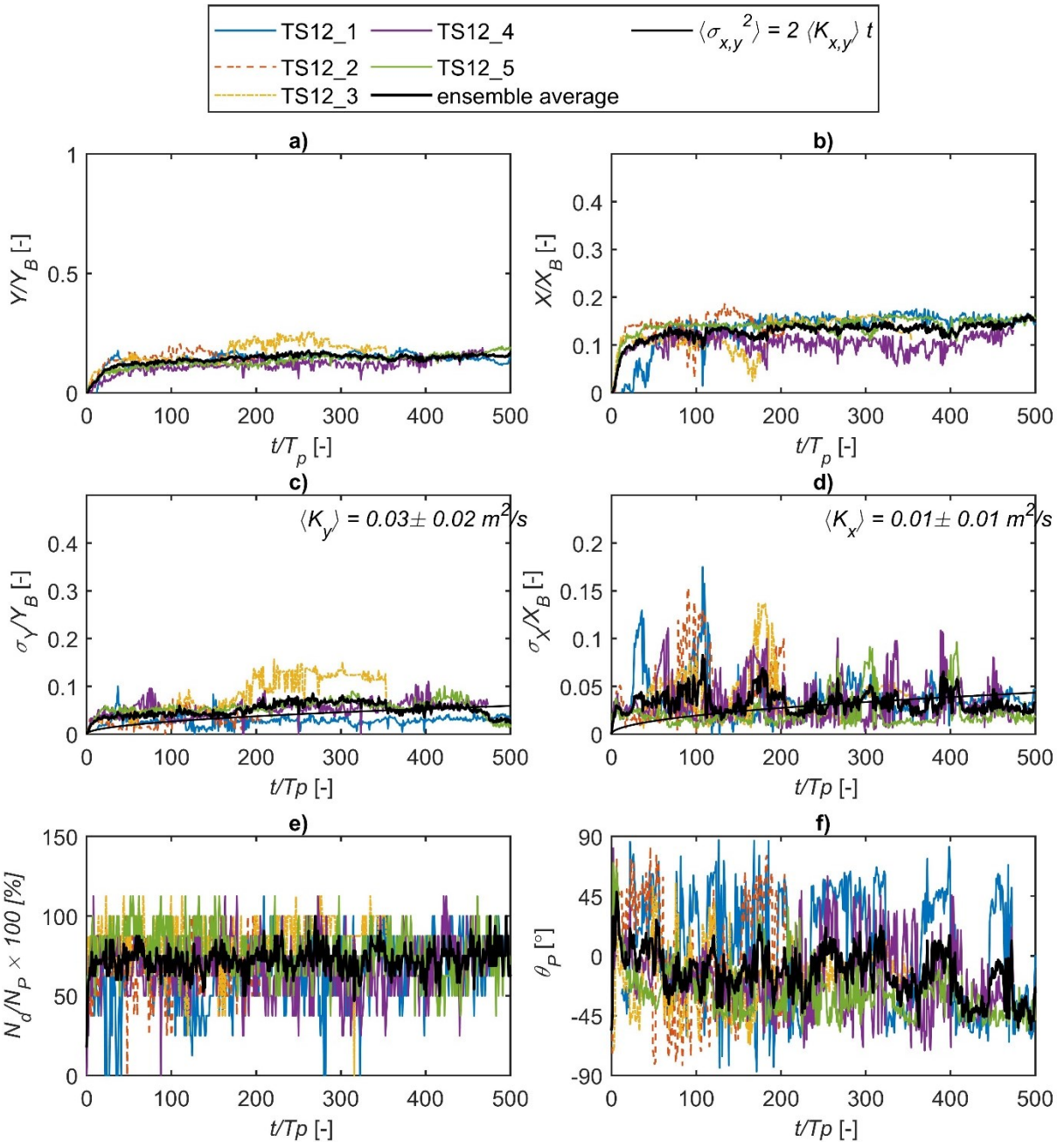

Figure A-36. a) Mean alongshore relative travel distance, b) mean cross-shore relative travel distance, c) alongshore standard deviation, d) cross-shore standard deviation, e) detection rate, and f) mean orientation versus time for rough driftwood length class L_P = 12 m (green) during test series TS12 (η = 0.35 m, H_s = 0.65 m, T_p = 11 s).

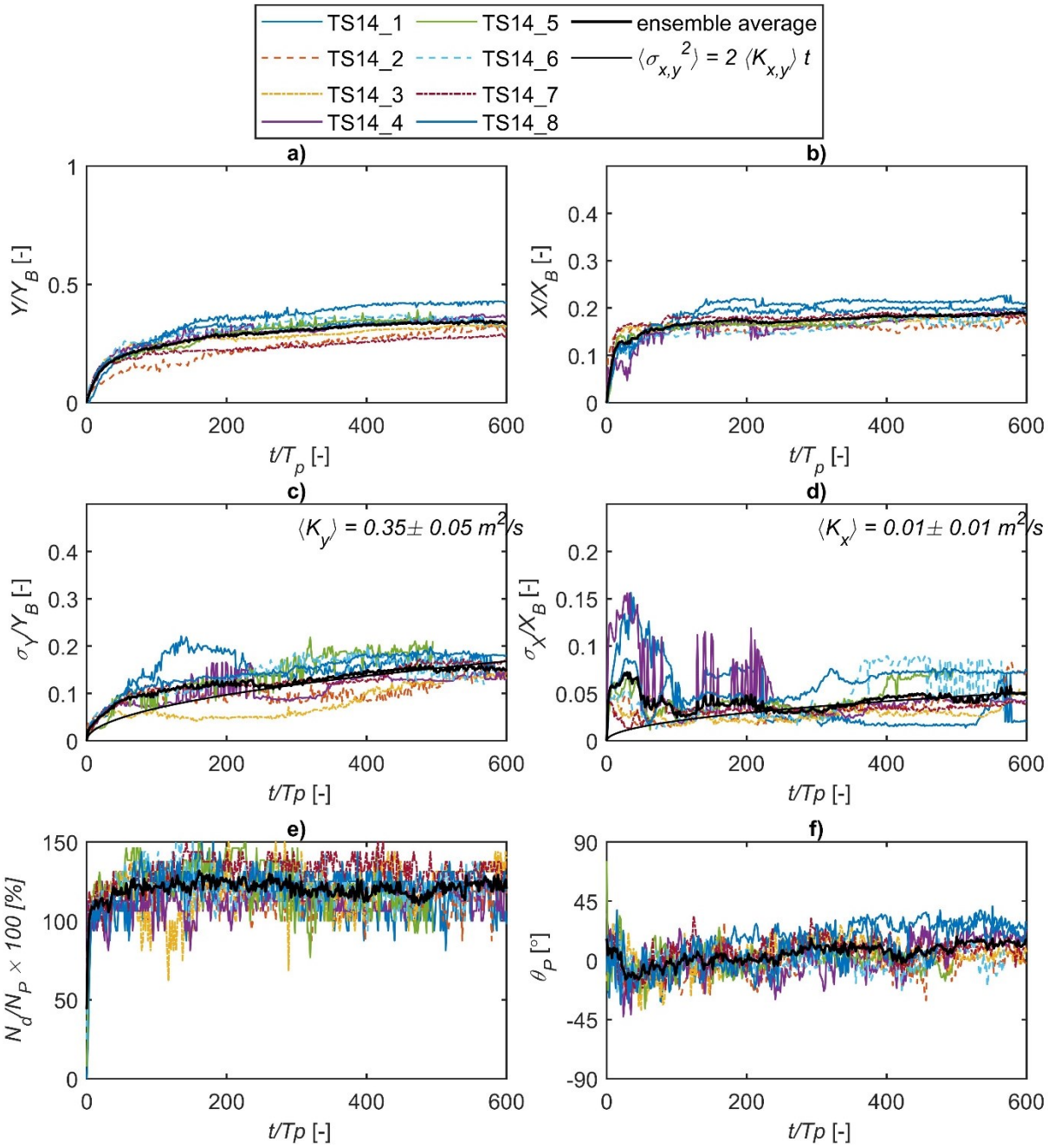

Figure A-37. a) Mean alongshore relative travel distance, b) mean cross-shore relative travel distance, c) alongshore standard deviation, d) cross-shore standard deviation, e) detection rate, and f) mean orientation versus time for rough driftwood length class L_P = 3 m (yellow) during test series TS14 (η = 0.70 m, H_s = 1.20 m, T_p = 6 s).

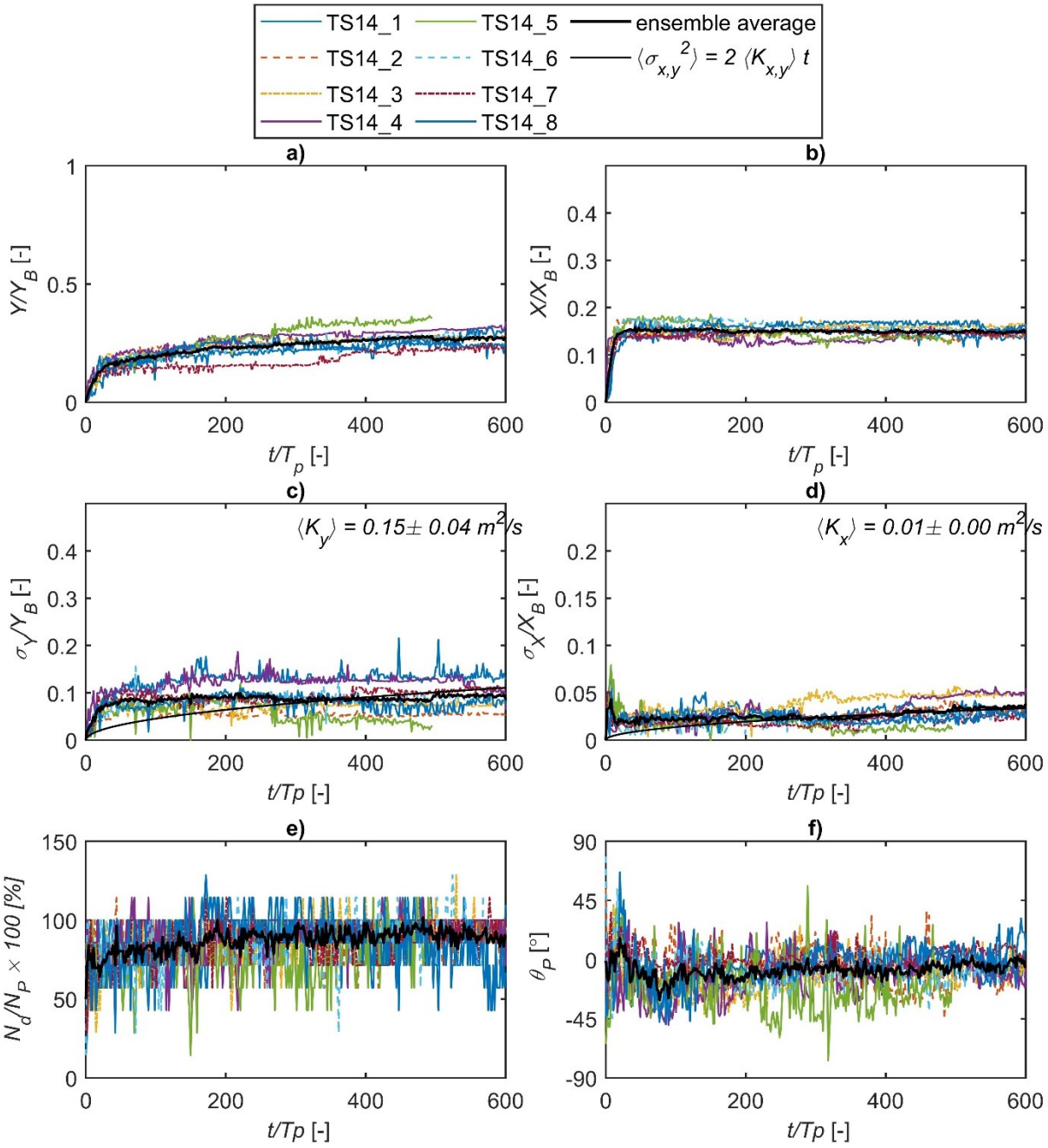

Figure A-38. a) Mean alongshore relative travel distance, b) mean cross-shore relative travel distance, c) alongshore standard deviation, d) cross-shore standard deviation, e) detection rate, and f) mean orientation versus time for rough driftwood length class L_P = 9 m (blue) during test series TS14 (η = 0.70 m, H_s = 1.20 m, T_p = 6 s).

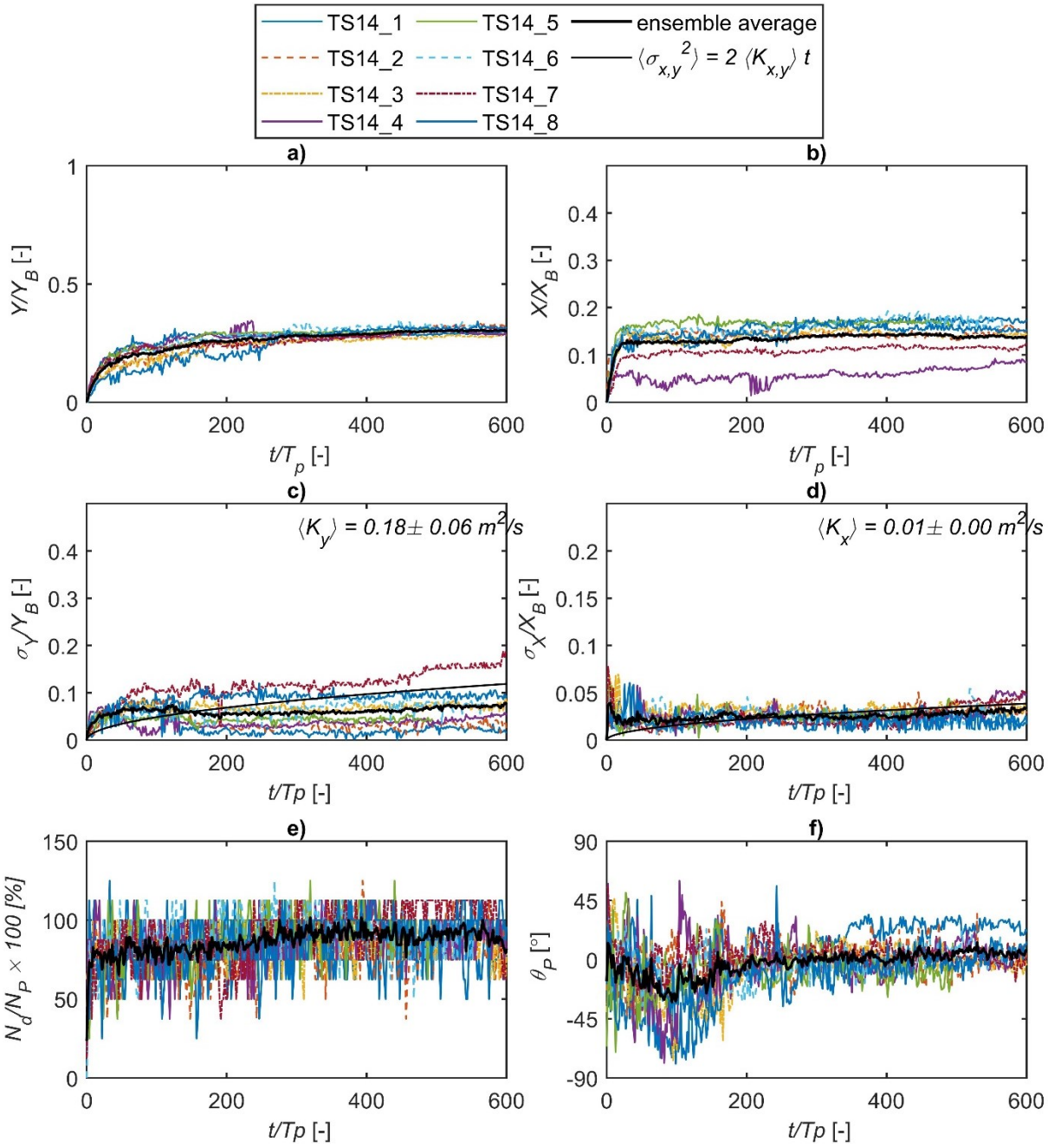

Figure A-39. a) Mean alongshore relative travel distance, b) mean cross-shore relative travel distance, c) alongshore standard deviation, d) cross-shore standard deviation, e) detection rate, and f) mean orientation versus time for rough driftwood length class L_P = 12 m (green) during test series TS14 (η = 0.70 m, H_s = 1.20 m, T_p = 6 s).

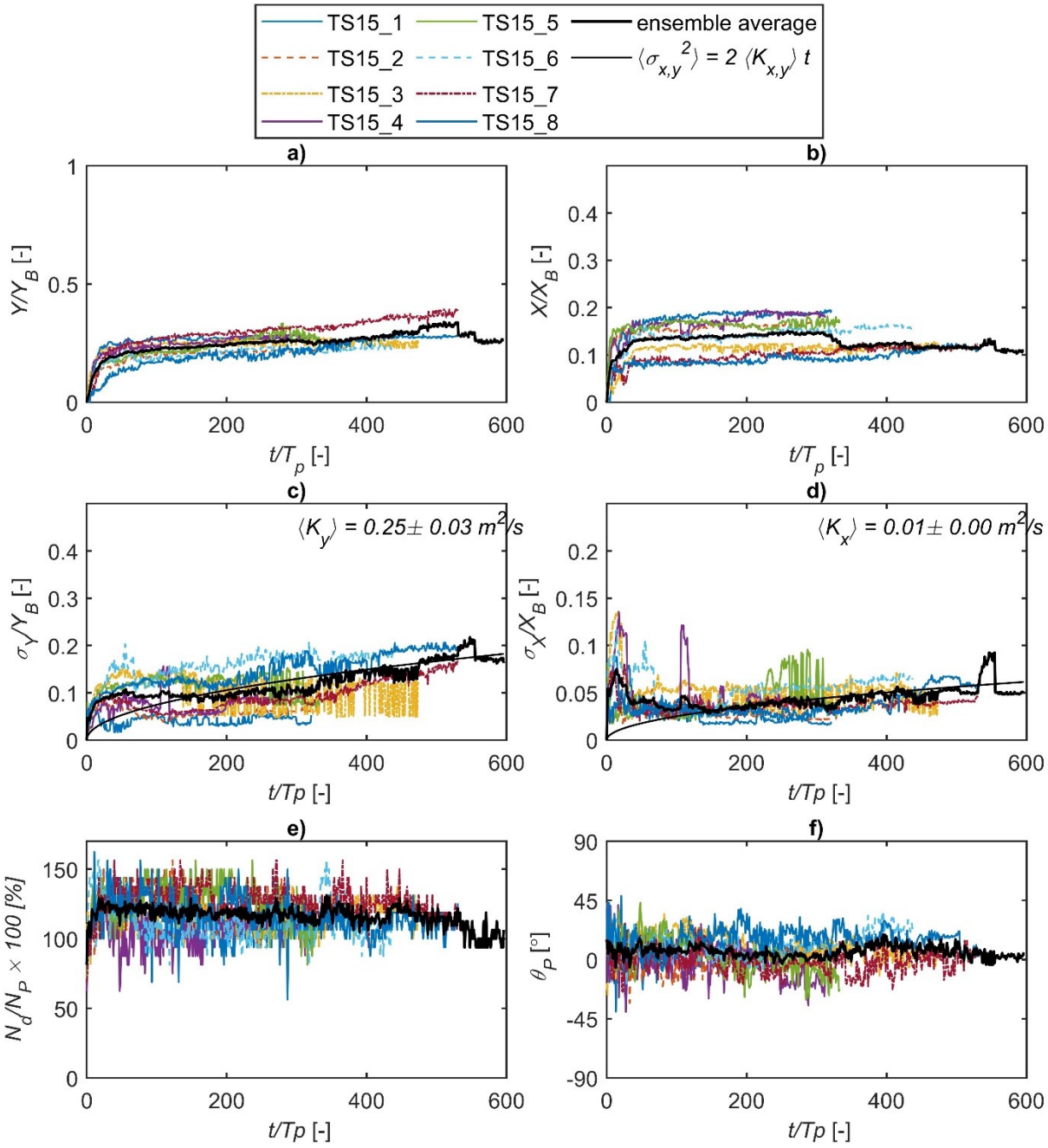

Figure A-40. a) Mean alongshore relative travel distance, b) mean cross-shore relative travel distance, c) alongshore standard deviation, d) cross-shore standard deviation, e) detection rate, and f) mean orientation versus time for rough driftwood length class L_P = 3 m (yellow) during test series TS15 (η = 0.70 m, H_s = 1.30 m, T_p = 10 s).

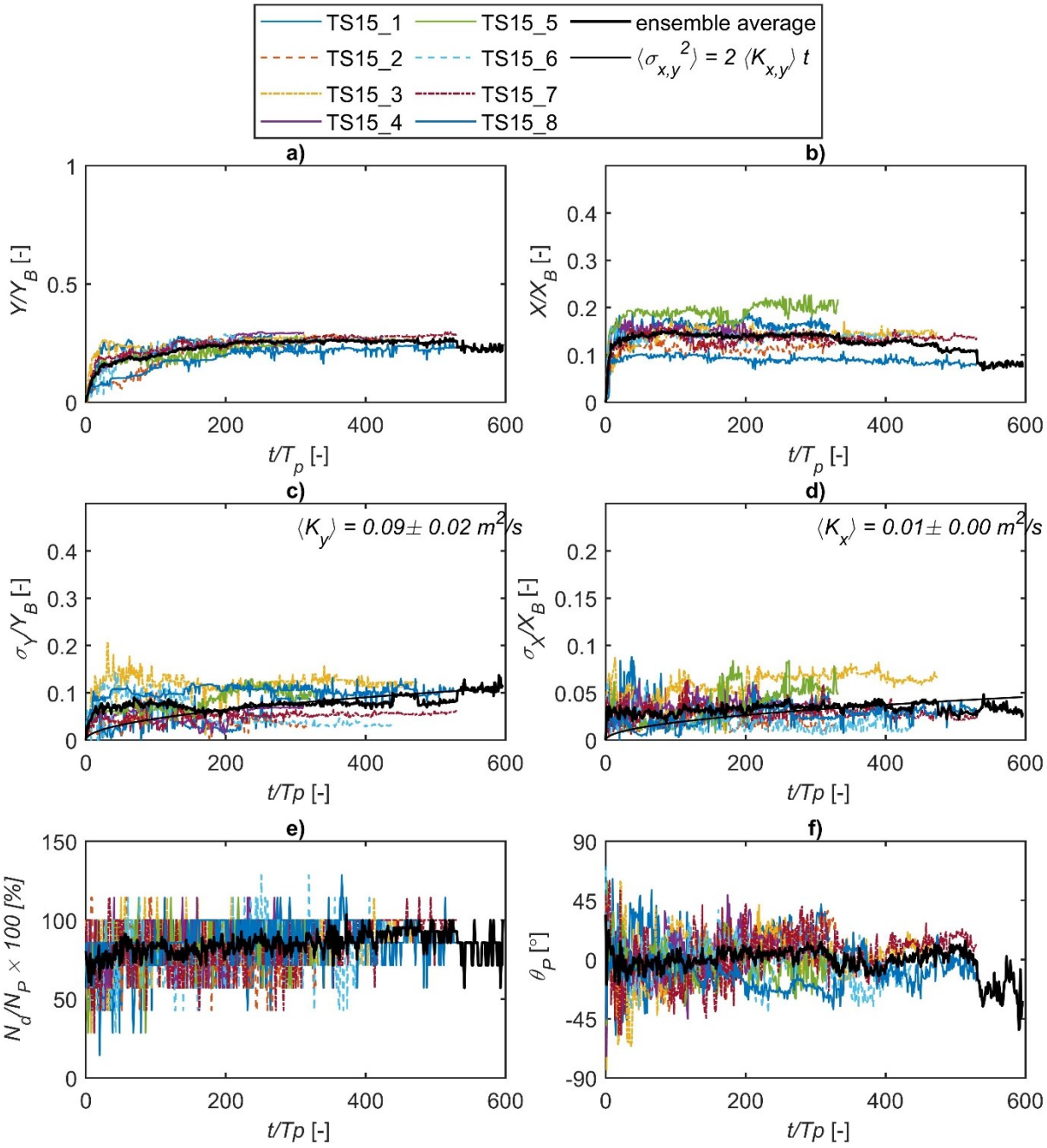

Figure A-41. a) Mean alongshore relative travel distance, b) mean cross-shore relative travel distance, c) alongshore standard deviation, d) cross-shore standard deviation, e) detection rate, and f) mean orientation versus time for rough driftwood length class L_P = 9 m (blue) during test series TS15 (η = 0.70 m, H_s = 1.30 m, T_p = 10 s).

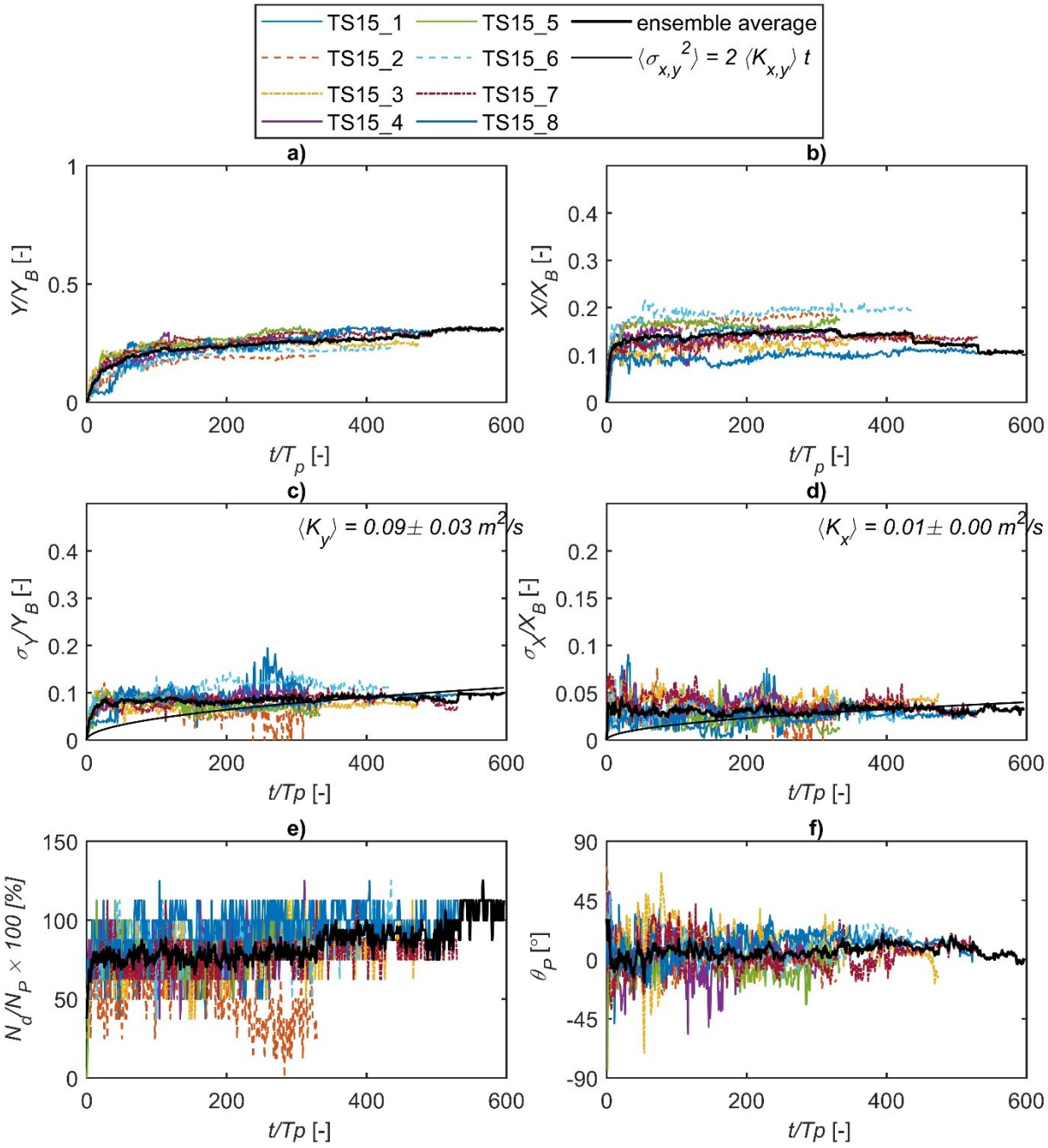

Figure A-42. a) Mean alongshore relative travel distance, b) mean cross-shore relative travel distance, c) alongshore standard deviation, d) cross-shore standard deviation, e) detection rate, and f) mean orientation versus time for rough driftwood length class L_P = 12 m (green) during test series TS15 (η = 0.70 m, H_s = 1.30 m, T_p = 10 s).

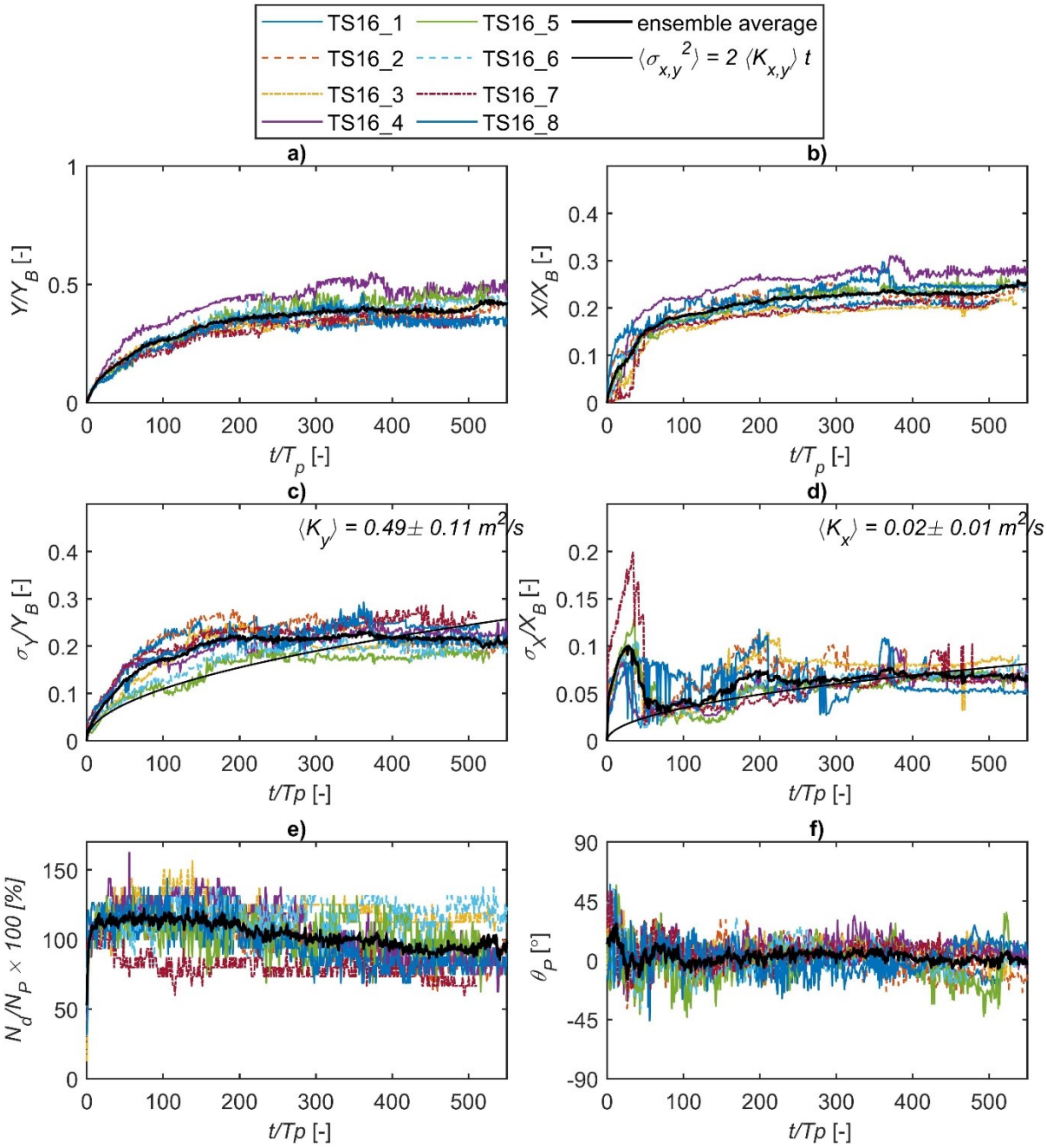

Figure A-43. a) Mean alongshore relative travel distance, b) mean cross-shore relative travel distance, c) alongshore standard deviation, d) cross-shore standard deviation, e) detection rate, and f) mean orientation versus time for rough driftwood length class L_P = 3 m (yellow) during test series TS16 (η = 0.35 m, H_s = 0.65 m, T_p = 11 s).

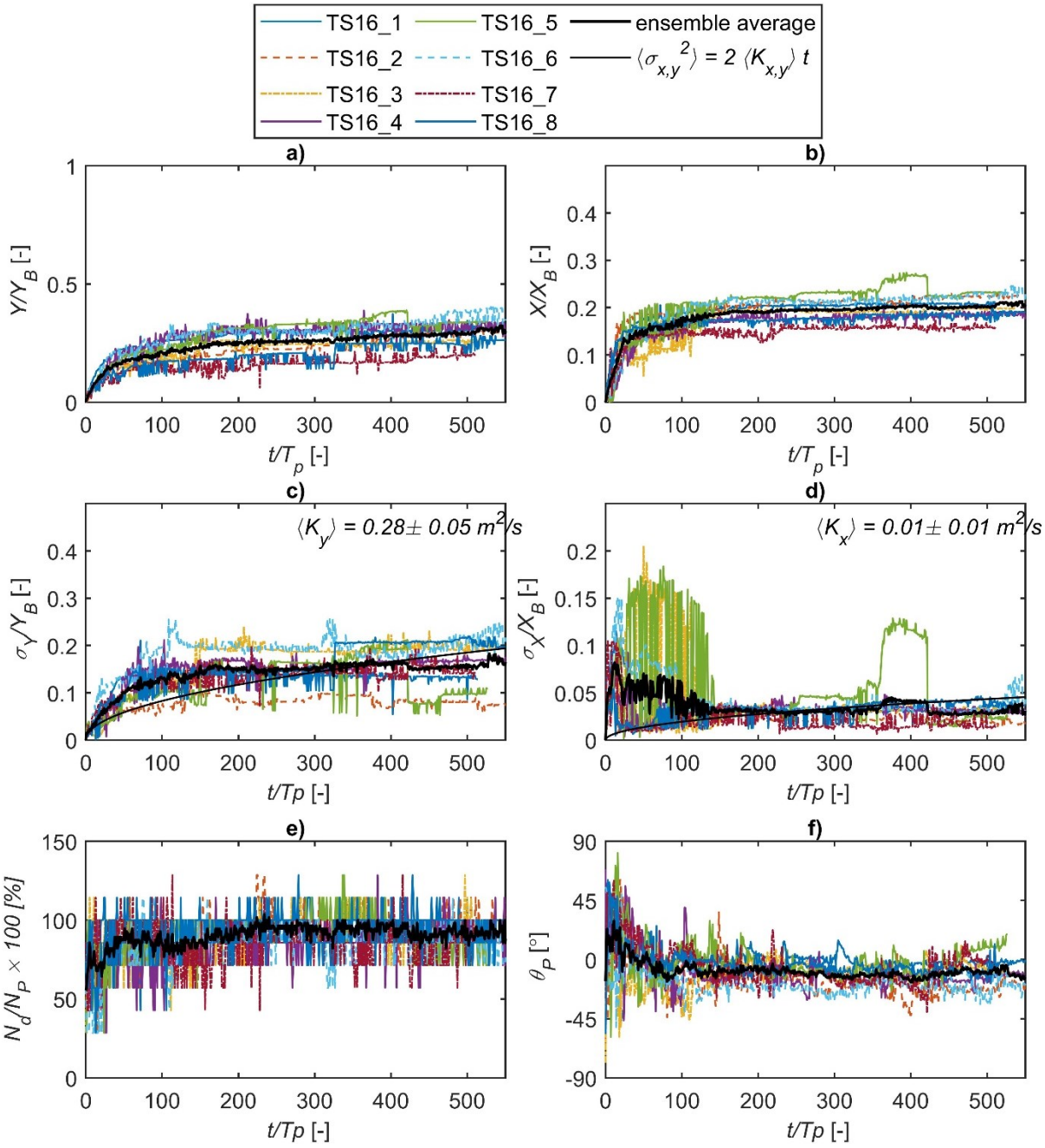

Figure A-44. a) Mean alongshore relative travel distance, b) mean cross-shore relative travel distance, c) alongshore standard deviation, d) cross-shore standard deviation, e) detection rate, and f) mean orientation versus time for rough driftwood length class L_P = 9 m (blue) during test series TS16 (η = 0.35 m, H_s = 0.65 m, T_p = 11 s).

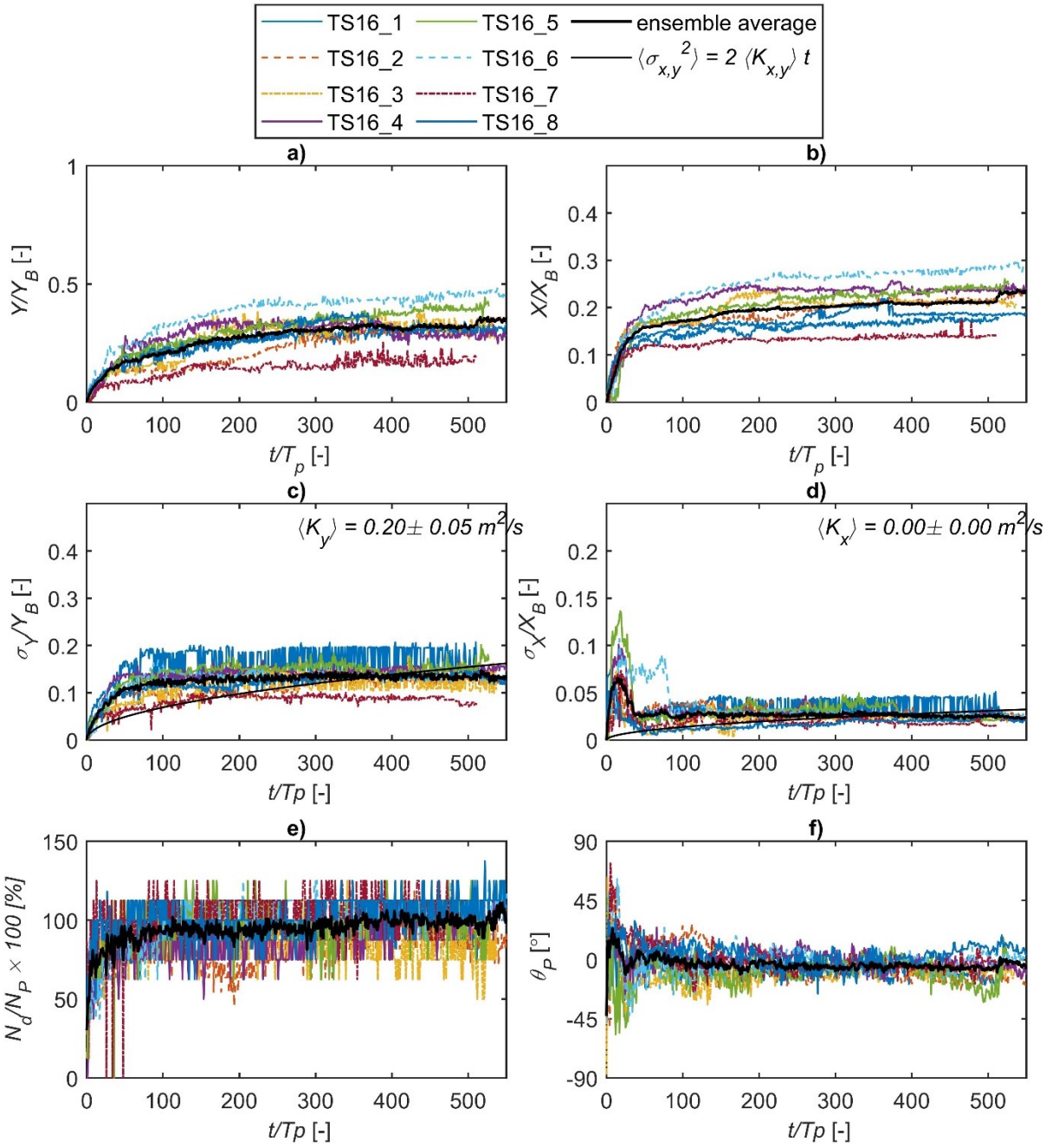

Figure A-45. a) Mean alongshore relative travel distance, b) mean cross-shore relative travel distance, c) alongshore standard deviation, d) cross-shore standard deviation, e) detection rate, and f) mean orientation versus time for rough driftwood length class L_P = 12 m (green) during test series TS16 (η = 0.35 m, H_s = 0.65 m, T_p = 11 s).

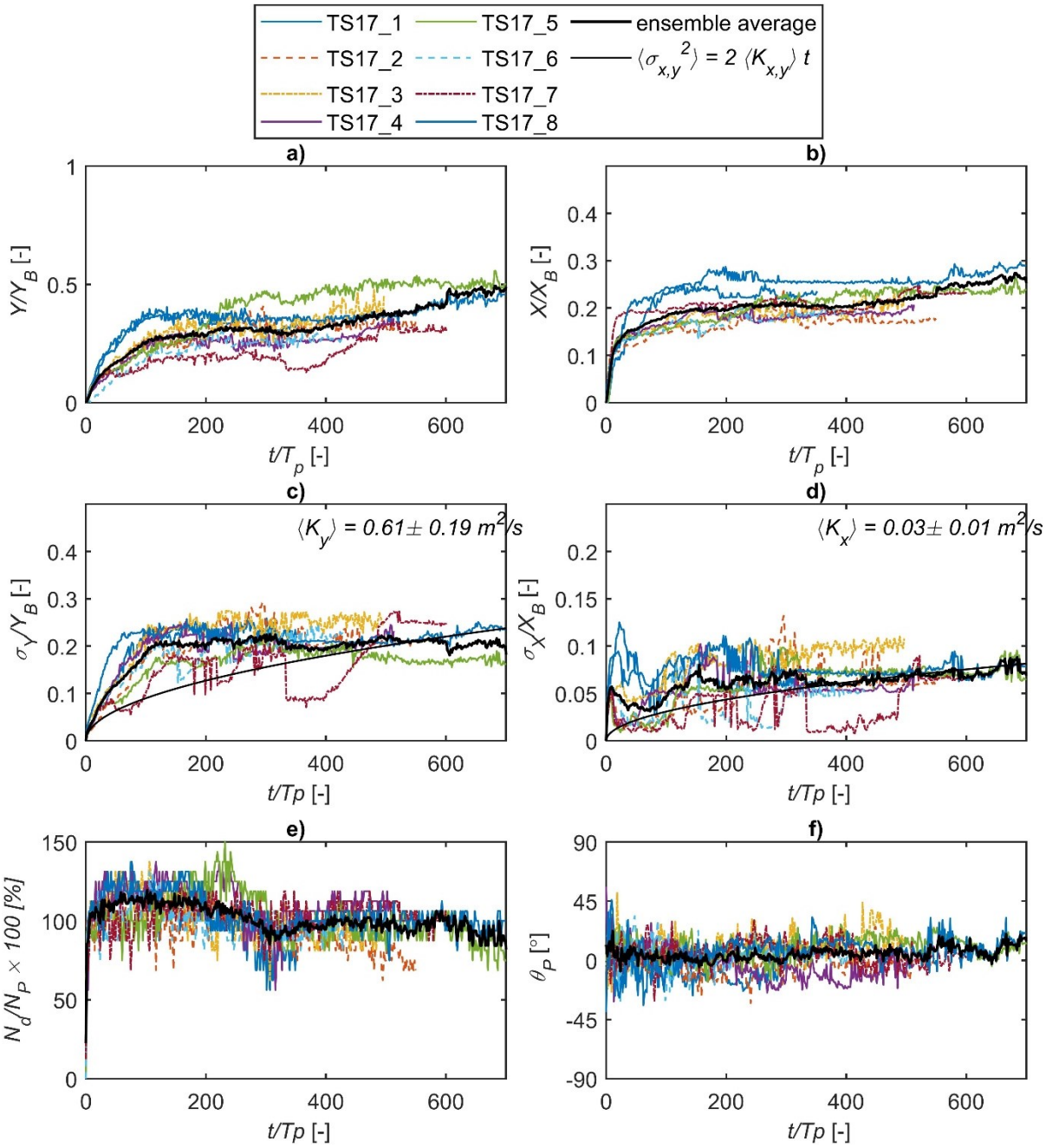

Figure A-46. a) Mean alongshore relative travel distance, b) mean cross-shore relative travel distance, c) alongshore standard deviation, d) cross-shore standard deviation, e) detection rate, and f) mean orientation versus time for rough driftwood length class L_P = 3 m (yellow) during test series TS17 (η = 0.70 m, H_s = 1.20 m, T_p = 6 s).

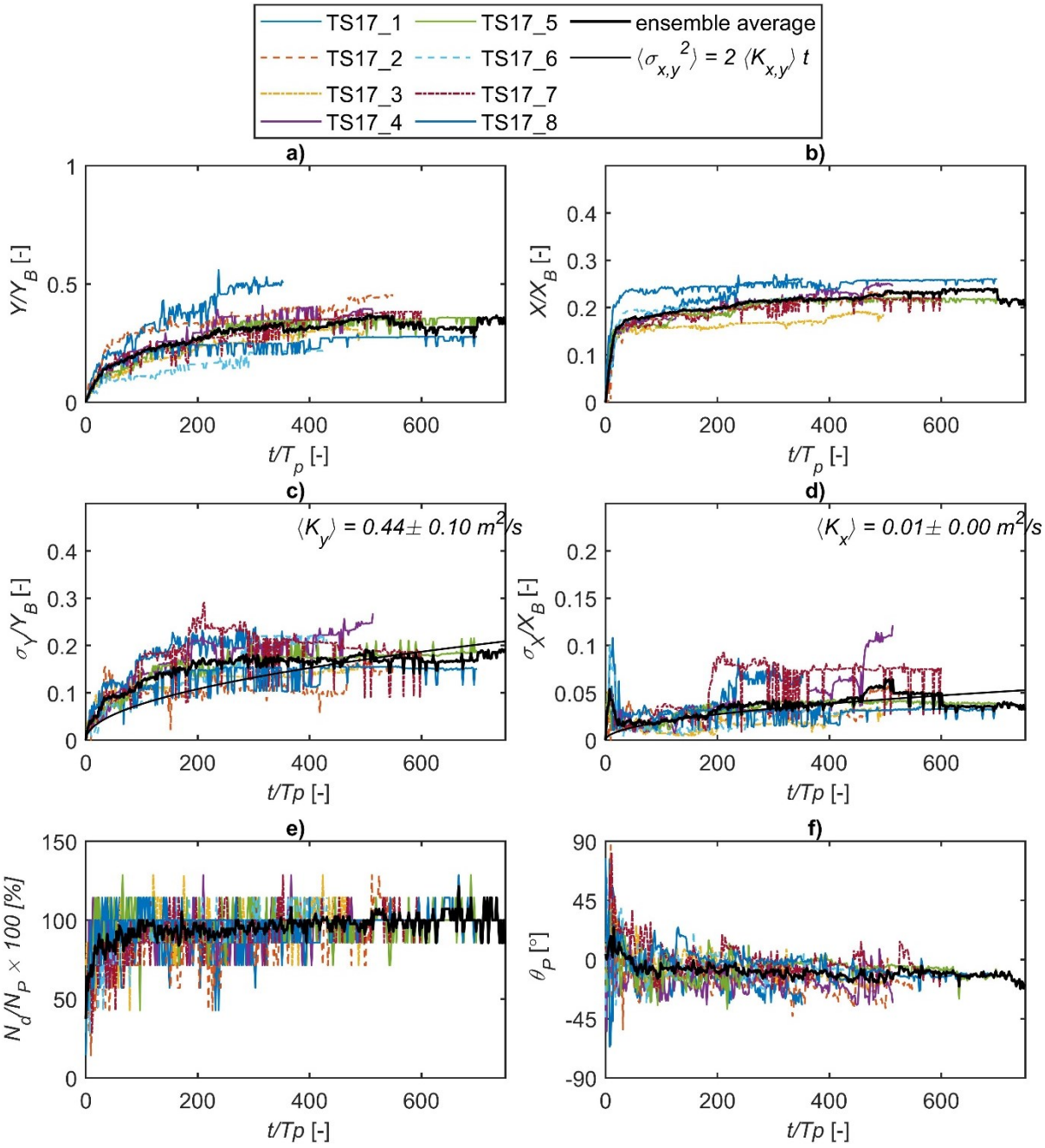

Figure A-47. a) Mean alongshore relative travel distance, b) mean cross-shore relative travel distance, c) alongshore standard deviation, d) cross-shore standard deviation, e) detection rate, and f) mean orientation versus time for rough driftwood length class L_P = 9 m (blue) during test series TS17 (η = 0.70 m, H_s = 1.20 m, T_p = 6 s).

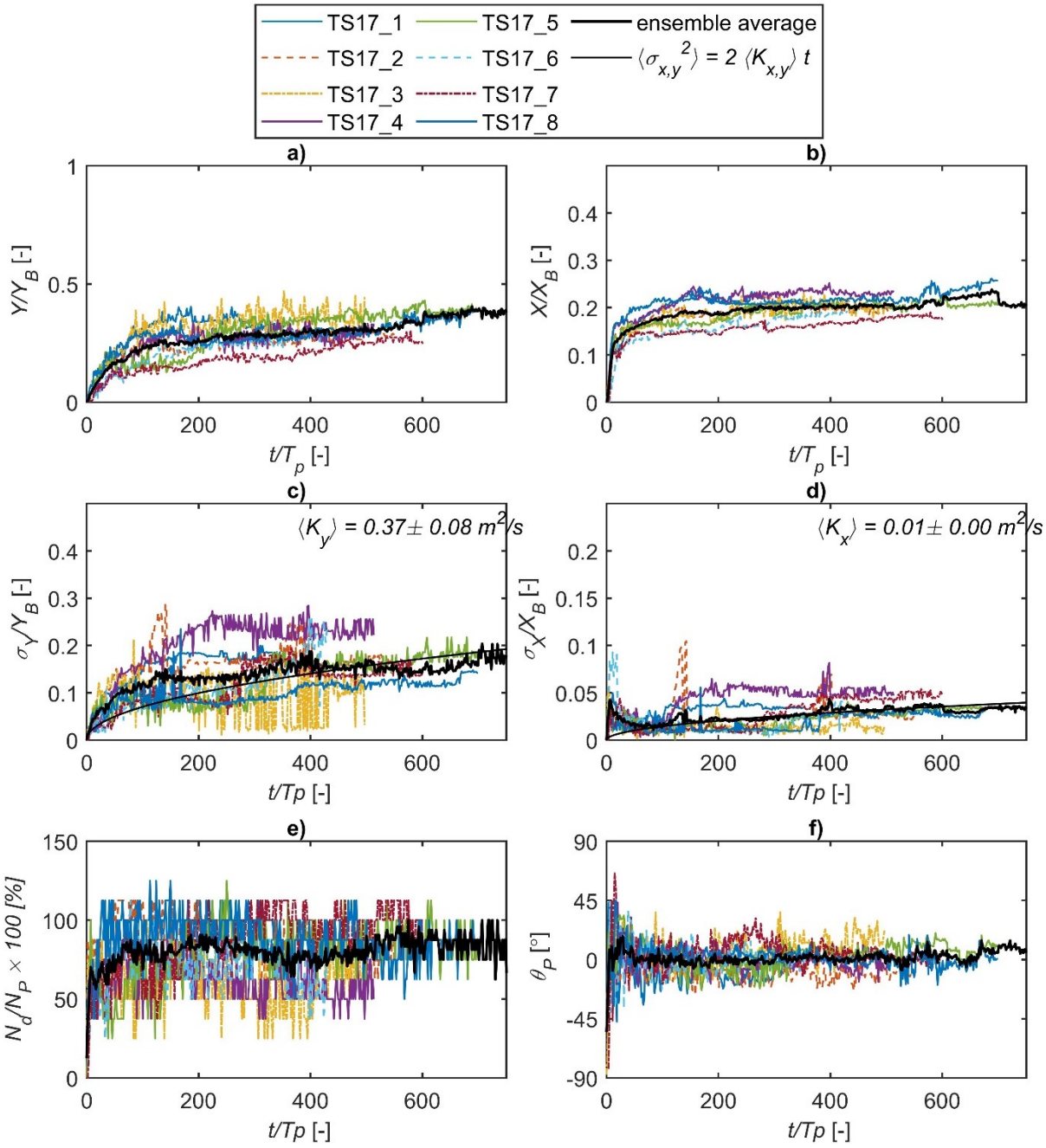

Figure A-48. a) Mean alongshore relative travel distance, b) mean cross-shore relative travel distance, c) alongshore standard deviation, d) cross-shore standard deviation, e) detection rate, and f) mean orientation versus time for rough driftwood length class L_P = 12 m (green) during test series TS17 (η = 0.70 m, H_s = 1.20 m, T_p = 6 s).

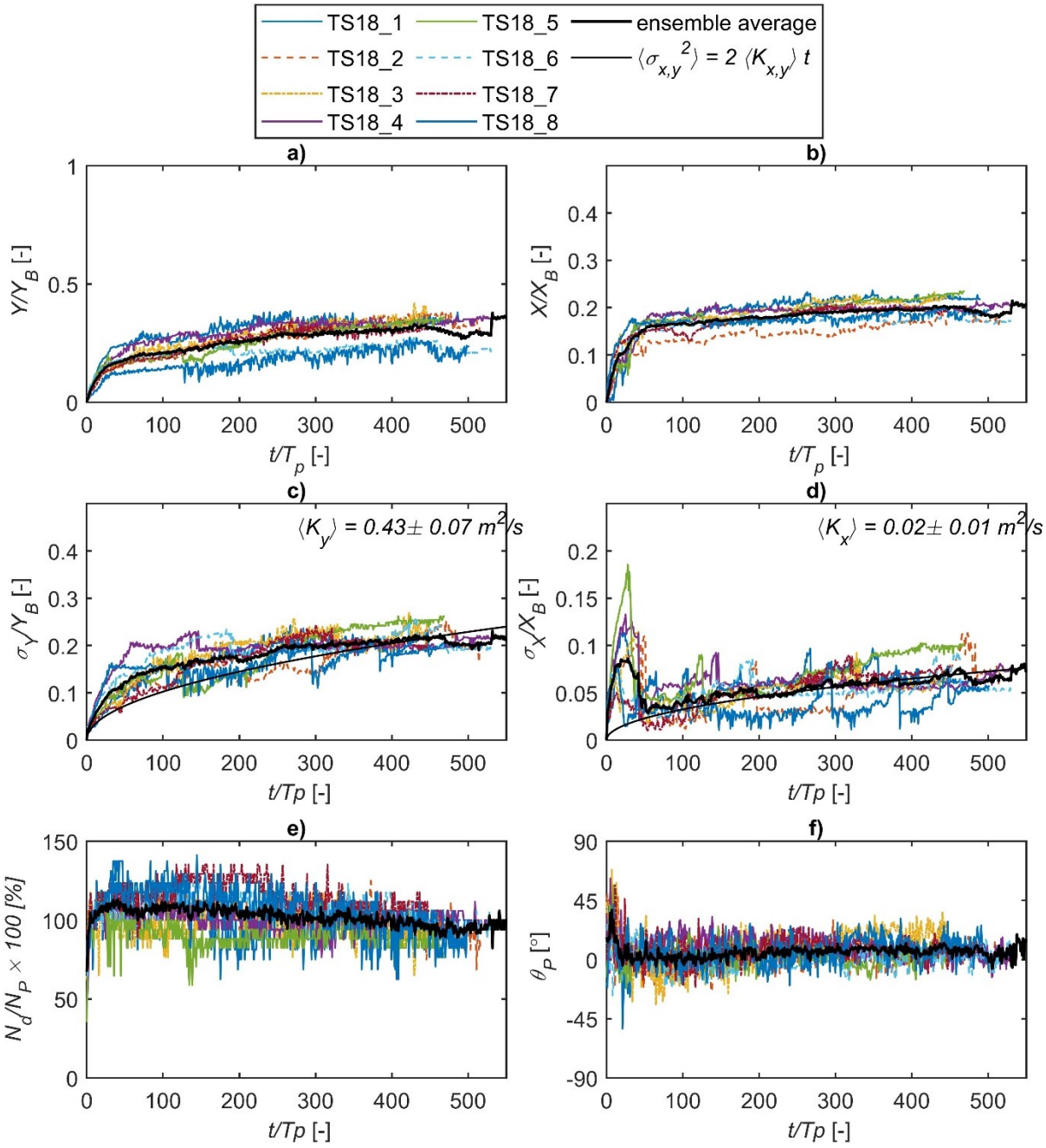

Figure A-49. a) Mean alongshore relative travel distance, b) mean cross-shore relative travel distance, c) alongshore standard deviation, d) cross-shore standard deviation, e) detection rate, and f) mean orientation versus time for rough driftwood length class L_P = 3 m (yellow) during test series TS18 (η = 0.35 m, H_s = 0.65 m, T_p = 11 s).

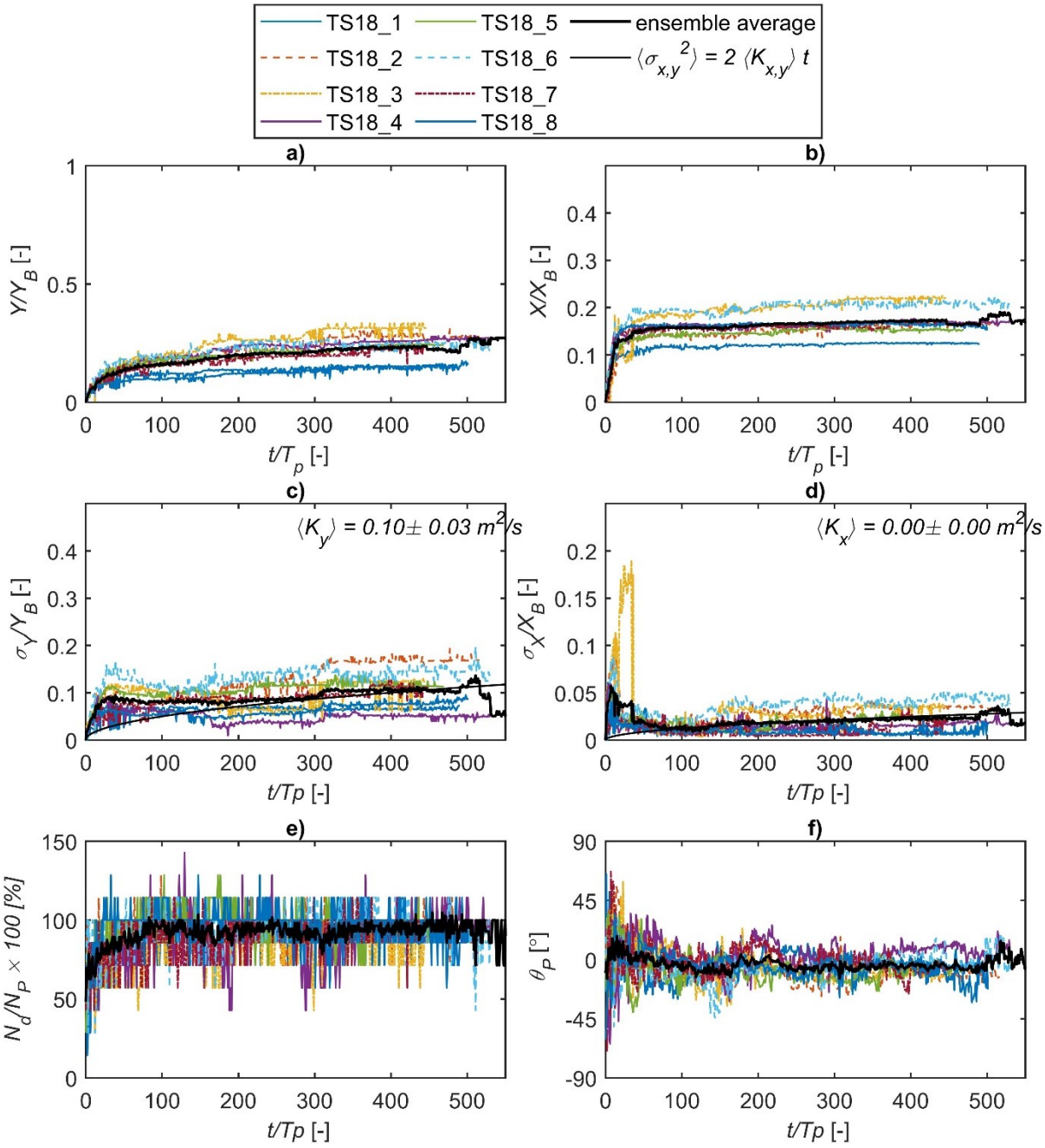

Figure A-50. a) Mean alongshore relative travel distance, b) mean cross-shore relative travel distance, c) alongshore standard deviation, d) cross-shore standard deviation, e) detection rate, and f) mean orientation versus time for rough driftwood length class L_P = 9 m (blue) during test series TS18 (η = 0.35 m, H_s = 0.65 m, T_p = 11 s).

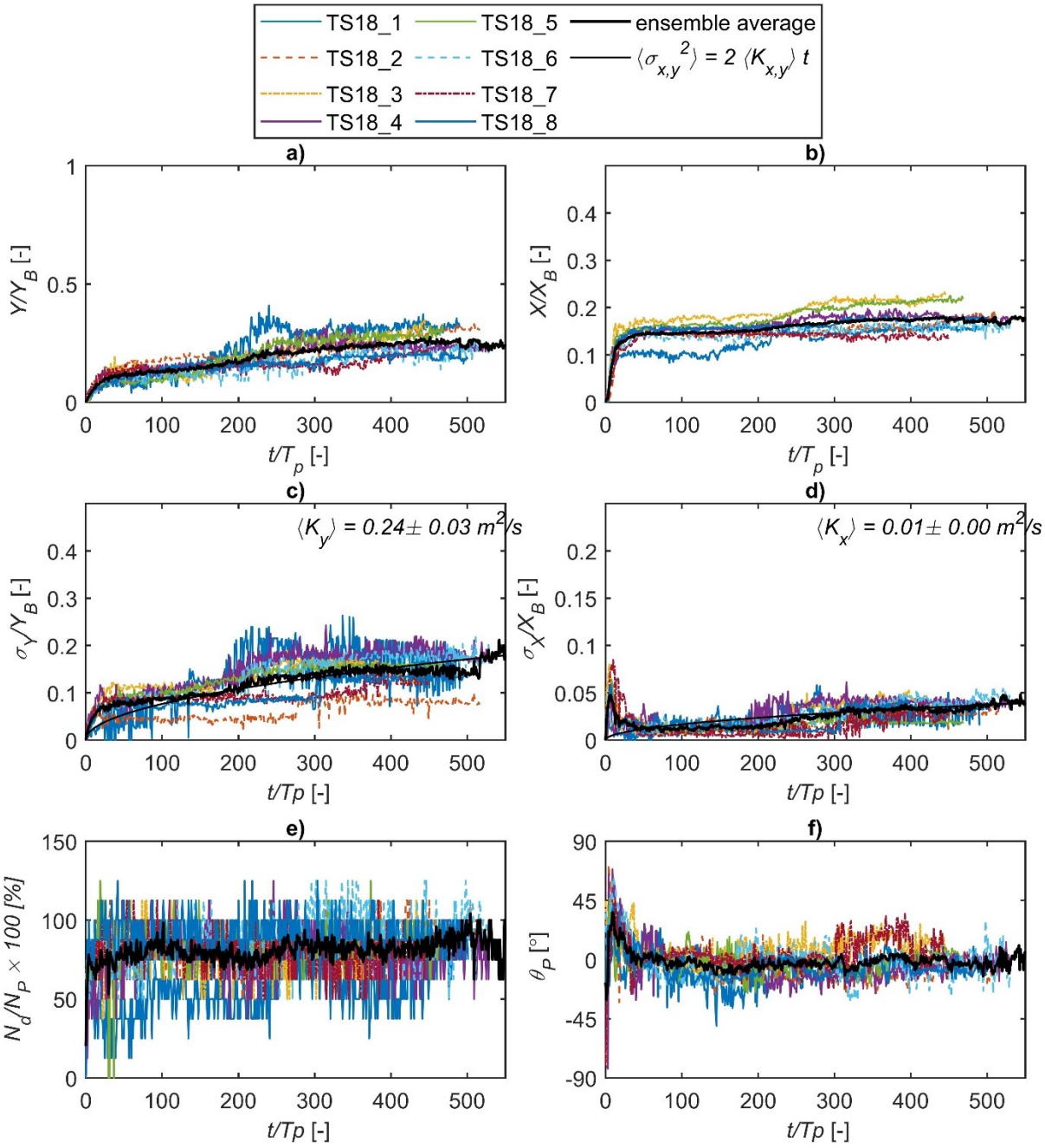

Figure A-51. a) Mean alongshore relative travel distance, b) mean cross-shore relative travel distance, c) alongshore standard deviation, d) cross-shore standard deviation, e) detection rate, and f) mean orientation versus time for rough driftwood length class L_P = 12 m (green) during test series TS18 (η = 0.35 m, H_s = 0.65 m, T_p = 11 s).

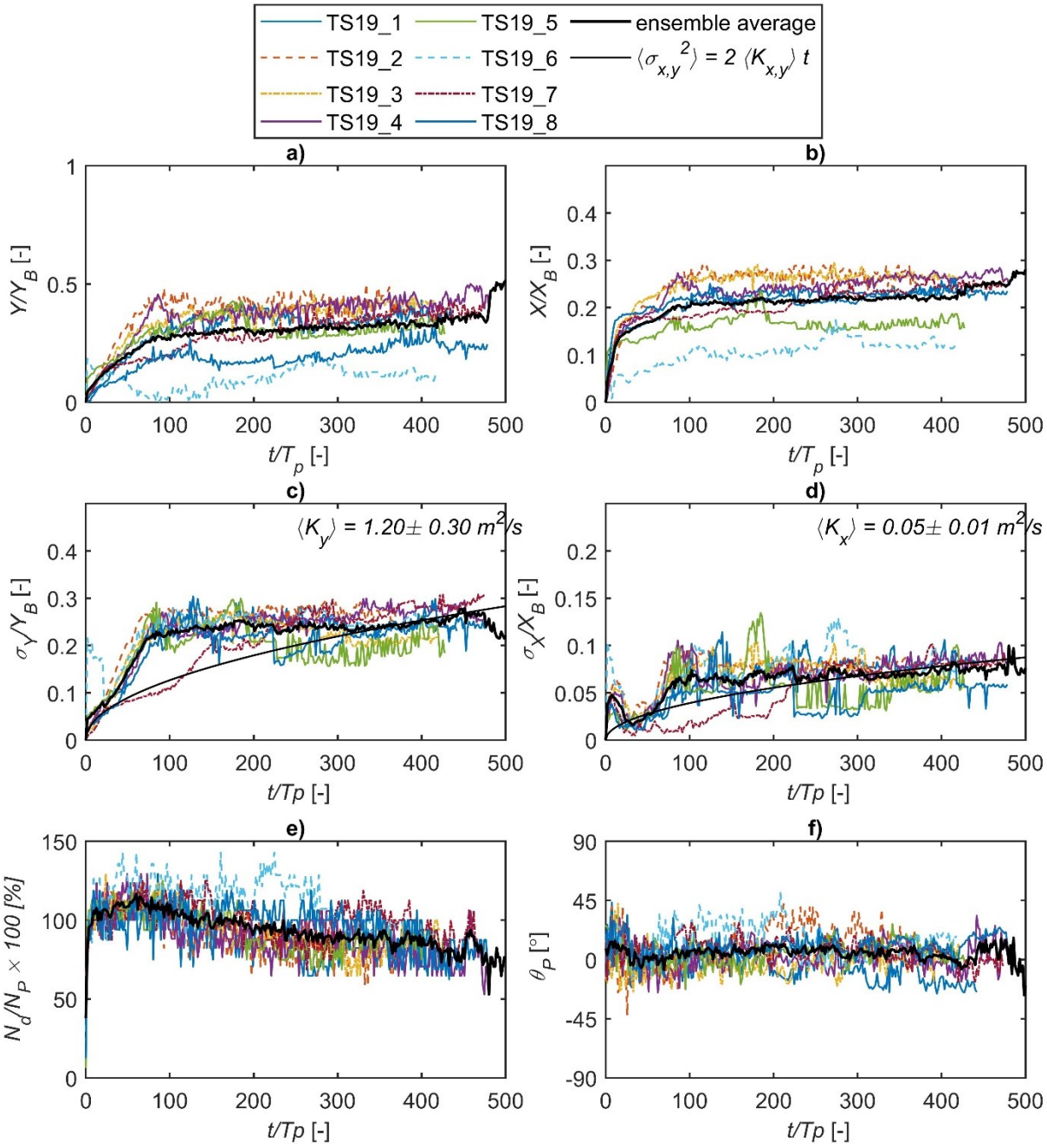

Figure A-52. a) Mean alongshore relative travel distance, b) mean cross-shore relative travel distance, c) alongshore standard deviation, d) cross-shore standard deviation, e) detection rate, and f) mean orientation versus time for rough driftwood length class L_P = 3 m (yellow) during test series TS19 (η = 0.70 m, H_s = 1.20 m, T_p = 6 s).

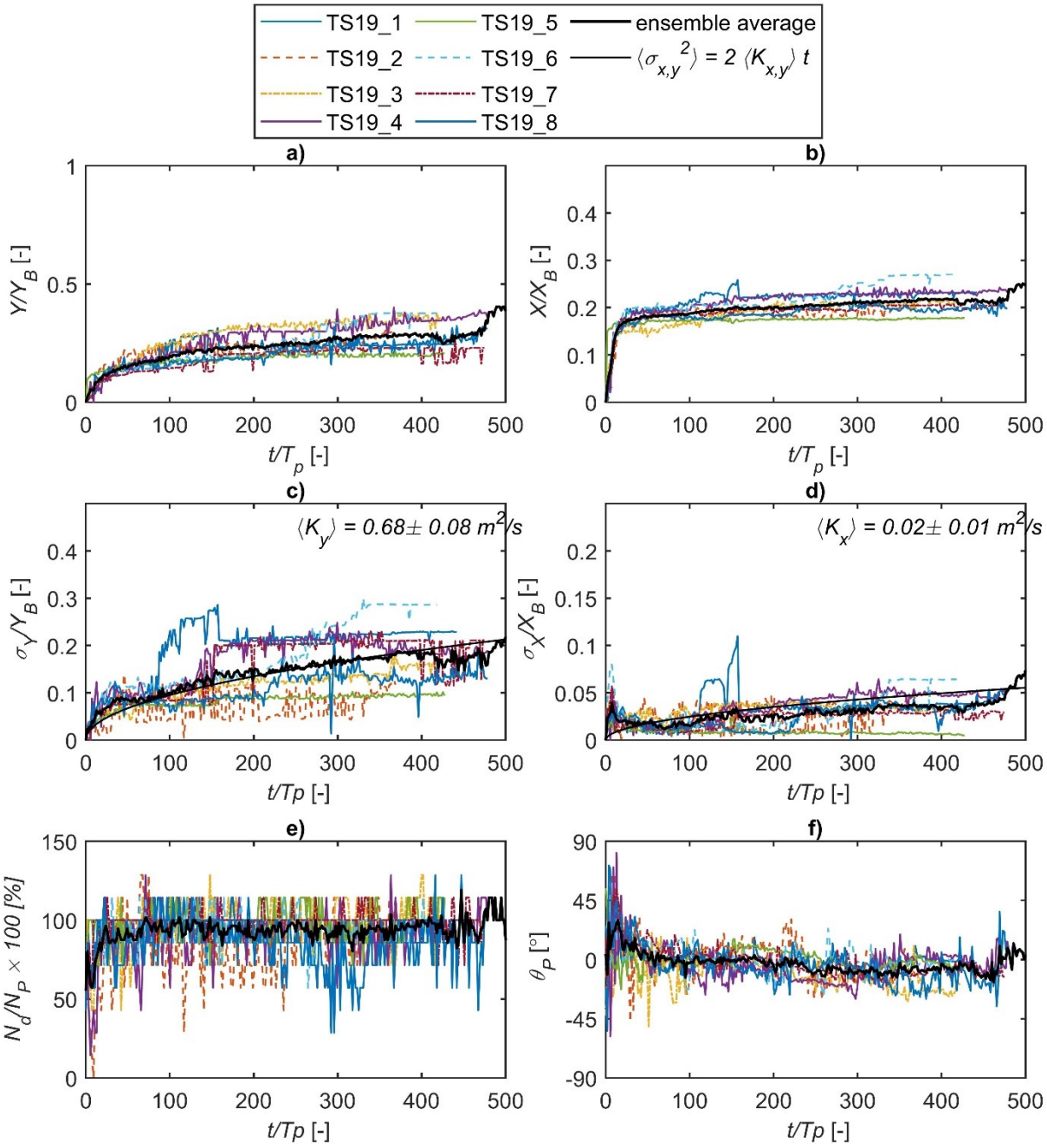

Figure A-53. a) Mean alongshore relative travel distance, b) mean cross-shore relative travel distance, c) alongshore standard deviation, d) cross-shore standard deviation, e) detection rate, and f) mean orientation versus time for rough driftwood length class L_P = 9 m (blue) during test series TS19 (η = 0.70 m, H_s = 1.20 m, T_p = 6 s).

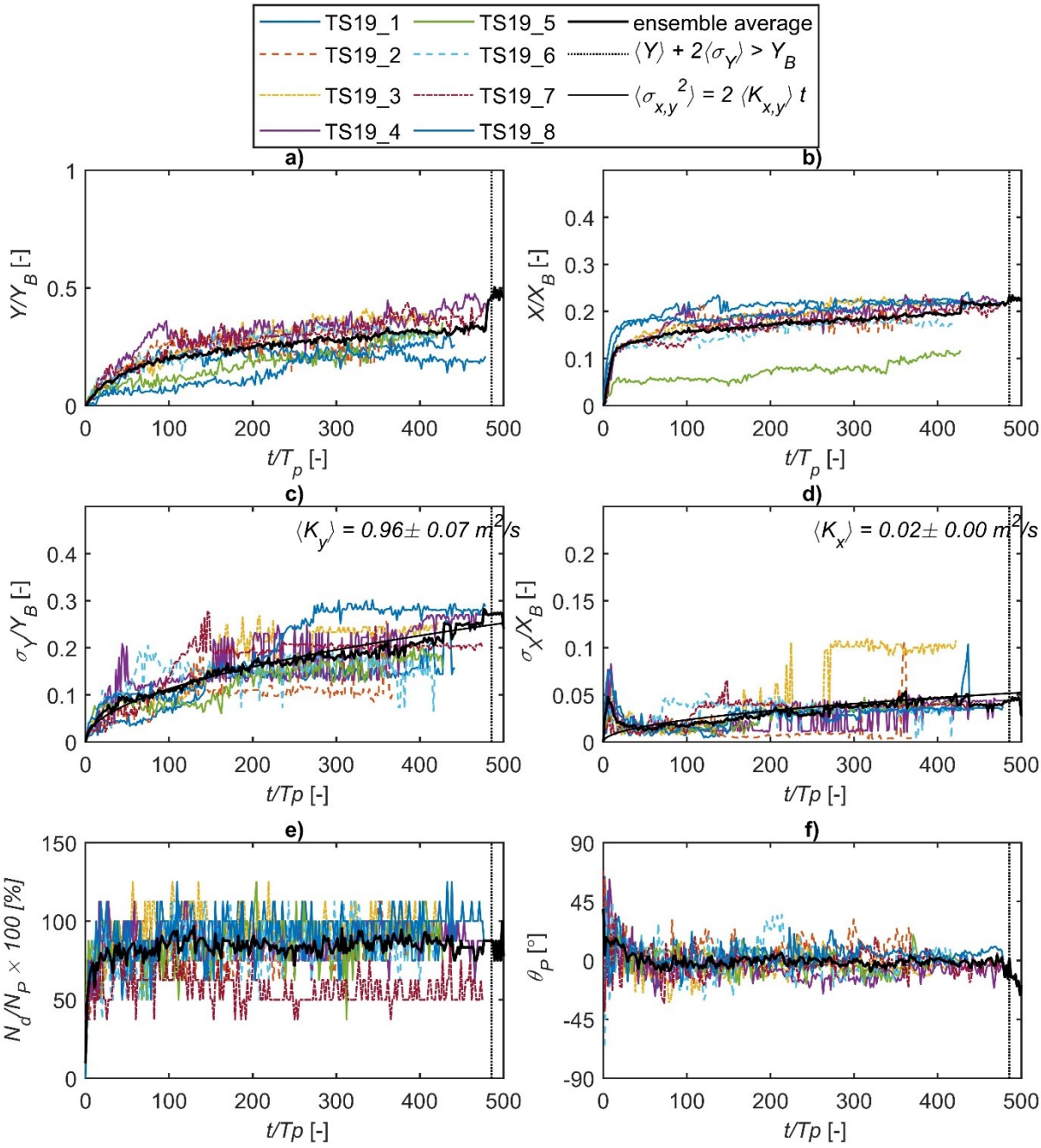

Figure A-54. a) Mean alongshore relative travel distance, b) mean cross-shore relative travel distance, c) alongshore standard deviation, d) cross-shore standard deviation, e) detection rate, and f) mean orientation versus time for rough driftwood length class L_P = 12 m (green) during test series TS19 (η = 0.70 m, H_s = 1.20 m, T_p = 6 s).

Appendix B. WOODRIFTSIM Code

```
%% MATLAB (R2023b) code

function [A,Xparthist,fBeachEver,fBeachhist,Td,thetaphist,F,...

thetapntesthist,up1testhist,vp1testhist,up2testhist,vp2testhist,distptesthist,xp1ntes
thist,...
        xp2ntesthist,yp1ntesthist,yp2ntesthist]=...
    WOODRIFTSIM_tran(suppressPlot,plotint,Nyell,Nblue,Ngreen,...
    optAdv,optBch,mur,depavg,Tp,outFile,...
    globaltime,ntsub,Kx,Ky,Kx1,Ky1,Kz,xycvec,u0vec,v0vec,dudy0vec,...
    dvdy0vec,dudx0vec,dvdx0vec,u1vec,v1vec,dudy1vec,dvdy1vec,dudx1vec,...
    dvdx1vec,zb0vec,zsvec,hvec,dzbdxvec,dzbdyvec,...
    ni,nj,zs0vec,xc,yc,nczb0,u,v,u1,v1,aviFile,plotelev,endstep,itstep)

%% Input arguments
% suppressPlot: logical option (1 or 0) to suppress animation (for batch
% runs).
% plotint: Integer number of time steps between plotting if suppressPlot
% = 0.
% Nyell: Integer number of yellow (3 m long) driftwood pieces released.
% Nblue: Integer number of blue (9 m long) driftwood pieces released.
% Ngreen: Integer number of green (12 m long) driftwood pieces released.
% optAdv: Logical option for advection scheme. 2 = second order Black &
% Gray, Euler otherwise.
% optBch: Logical option for treatment of beaching. 2 is dynamic beaching,
% 1 is permanent beaching in dry areas, 0 is no beaching.
% mur: Coeff. of (static or dynamic) friction at the driftwood-bed
% interface.
% depavg: Logical for choice of hydrodynamic input. 1 = depth average, 0 =
% specified layer.
% Tp: Peak wave period (for stop criteria and normalizing time output).
% outFile: Name of matlab output file for driftwood track data.
% globaltime: Time vector (from SWASH, XBeach or other hydrodynamic model).
% ntsub: Number of timesteps to remove from end of computation (for
% truncating or shortening simulation compared to hydrodynamic input).
% Kx,Ky: dispersion coefficient arrays (spatial and temporally varying)
% from hydrodynamic model (depth average).
% Kx1,Ky1: dispersion coefficient arrays (specified layer).
% Kz: Vertical dispersion coefficient
% xycvec: 2-column array containing coordinates of hydrodynamic model grid
% centre points.
% u0vec,v0vec: vectors of depth average velocities from hydrodynamic model.
% dudy0vec,dvdy0vec,dudx0vec,dvdx0vec: arrays containing spatial gradients
% in depth average velocity fields.
% u1vec,v1vec: vectors of specified layer velocities from hydrodynamic
% model.
% dudy1vec,dvdy1vec,dudx1vec,dvdx1vec: arrays containing spatial gradients
% in specified layer velocity fields.
% zb0vec: vector containing initial (static) bed elevations.
% zsvec: vector of free surface elevations from hydrodynamic model
% (temporally varying).
```

```
% hvec: water depth vector (i.e. zsvec-zb0vec) (temporally varying).
% dzbdxvec,dzbdyvec: bed gradient vectors.
% ni,nj: number of hydrodynamic grid cells.
% zs0vec: initial free surface elevation vector.
% xc,yc: hydrodynamic grid cell centre coordinates (array format).
% nczb0: initial (static) static bed elevation (array format).
% u,v: depth average velocity components (array format).
% u1,v1: specified layer velocity components (array format).
% aviFile: output avi file name for saving animation if suppressPlot=0.
% plotelev: addition to bottom grid elevations depending on datum used by
% hydrodynamic model (zero or initial water level elevation).
% endstep: Last time step of driftwood simulation (option to limit
% duration of simulation.
% itstep: Starting time step for driftwood release.

%% Outputs
% A: Driftwood centroid track time series statistics (mean transport
% distance, variances, etc.).
% Xparthist: Driftwood centroid coordinate time series.
% fBeachEver: Flag to identify driftwood pieces that were beached at any
% time.
% fBeachhist: Time history of driftwood beaching.
% Td: Time when 1/3 of driftwood pieces exit field of view (XB by YB).
% thetaphist: Time history of driftwood orientations
% F: frames for animation.
% thetapntesthist,up1testhist,vp1testhist,up2testhist,vp2testhist,
% distptesthist,xp1ntesthist,xp2ntesthist,yp1ntesthist,yp2ntesthist:
% optional diagnostic (debugging) outputs.

%% WOODRIFTSIM

%% Initialization
np=Nyell+Nblue+Ngreen; % total number of driftwood pieces
pt=[213365;1465160]; %center of release
asp=[20;20]; %area of release (x by y)
debrisD0(1:Nblue,1)=0.57; %diameter of blue driftwood
debrisD0(Nblue+1:Nblue+Nyell,1)=0.45; %diameter of yellow driftwood
debrisD0(Nblue+Nyell+1:np,1)=0.48; %diameter of green driftwood
debrisRho0=741.9; %density of debris

%% Additional Options
optLimit=1; %switch to activate limiting of analysis to area of interest
            % 1 = limit area; 0 = no limit

%% Additional SWASH grid parameters
dt=1; %user has to specify time step for swash output
alphagrid=330; %grid rotation in degrees

%% Other physical constants, variables, options
alphaCross=1; %multiplier for cross-shore dispersion coefficient
alphaLong=1; %multiplier for alongshore dispersion coefficient
uratio=0.1; %ratio of mean velocity to friction velocity (Eq 1.24 of
            % Fischer et al. 1979)
Kz=0.0; %vertical diffusion coefficient
rhow=1000; %water density
```

```
nuw=1E-6; %kinematic viscosity
rhoa=1.2; %air density
CL=4.0; %lift coefficient (but should be function of KC/RE - see p151
        %Sumer, p182)
CD=1.0; %drag coefficient (Sumer p. 59 figure 2.21, range 0.4-1.0 for
        %cylinder at wall; p181)
CM=3.29; %=Cm+1 (Sumer p.131), Cm=2.29 (fig 4.4 p129 Sumer; p181)
Kbuoy=0.00000001; %first order rate loss of buoyancy of wood (day^-1) due
                  % to saturation Blade et al 2016
Kdeg=0.00000001; %first order degradation rate, i.e. loss of mass (day^-1)

%clear variables from previous simulation
clear ptvec ptij xp yp zp Xpart pinds zp Xparthist xpn ypn zpn up vp Kxp;
clear Kyp zbp zsp xp1 xp2 yp1 yp2 xp1n xp2n yp1n yp2n Xpart1 Xpart2 thetap;
clear up1testhist up2testhist vp1 vp2 thetap1 thetap2;
clear A fBeachEver fBeachhist fBeachType fBeachTypehist thetaphist;

%% Driftwood release
ptvec=pt';

%For plotting release area
th = 0:pi/50:2*pi;
xunit = 0.5*asp(1) * cos(th) + pt(1);
yunit = 0.5*asp(1) * sin(th) + pt(2);

%find indices of nearest grid point to spill
ptij=dsearchn(xycvec,ptvec);
ptiind=ptij/ni;
ptiind=(ptiind-floor(ptiind))*ni;
ptjind=floor(ptiind);

%Time discretization
dt=globaltime(2)-globaltime(1);
invdt=1/dt;
ntstep=length(globaltime)-ntsub-1;
dur=ntstep*dt;

xp=(pt(1)-0.5*asp(1) + (pt(1)+0.5*asp(1) -(pt(1)-0.5*asp(1))).*rand(np,1));
yp=(pt(2)-0.5*asp(2) + (pt(2)+0.5*asp(2) -(pt(2)-0.5*asp(2))).*rand(np,1));
thetap=(360.*rand(np,1))-180;
debrisL0(1:Nblue,1)=9; %blue
debrisL0(Nblue+1:Nblue+Nyell,1)=3; %yellow
debrisL0(Nblue+Nyell+1:np,1)=12; %green

%compute debris endpoint co-ordinates
xp1=xp-(debrisL0./2).*cos(pi()/180*thetap);
xp2=xp+(debrisL0./2).*cos(pi()/180*thetap);
yp1=yp-(debrisL0./2).*sin(pi()/180*thetap);
yp2=yp+(debrisL0./2).*sin(pi()/180*thetap);

Xpart=[xp yp];
Xpart1=[xp1 yp1];
Xpart2=[xp2 yp2];

%Find particles on hydrodynamic grid and initialize
```

```
pinds=dsearchn(xycvec,Xpart);
zp=zs0vec(pinds); %initial particle elevations
umagp=zeros([np 1]);
up=zeros([np 1]);
vp=zeros([np 1]);

if depavg>0
    KxPar=sqrt(2.*Kx.*dt);
    KyPar=sqrt(2.*Ky.*dt);
    uvec=u0vec;
    vvec=v0vec;
    dudyvec=dudy0vec;
    dvdyvec=dvdy0vec;
    dudxvec=dudx0vec;
    dvdxvec=dvdx0vec;
else;
    KxPar=sqrt(2.*Kx1.*dt);
    KyPar=sqrt(2.*Ky1.*dt);
    uvec=u1vec;
    vvec=v1vec;
    dudyvec=dudy1vec;
    dvdyvec=dvdy1vec;
    dudxvec=dudx1vec;
    dvdxvec=dvdx1vec;
end;
    KzPar=sqrt(2*Kz*dt);

%beaching initial conditions
fBeach=zeros([np 1]); %flag for beached particles
fBeachEver=fBeach; %flad for how many times a particle is beached
fBeachType=fBeach;
t0Beach=fBeach; %time particle is intially beached
tBeach=t0Beach; %time elapsed since beaching
xpBeach=t0Beach; %x-coord of beached particle
ypBeach=t0Beach; %y-coord of beached particle
T50Beach=300; %half-life for debris to remain on beach (for Jalon-Rojas
                % et al approach only)

%% Initial driftwood characteristics
debrisR0=debrisD0.*0.5;

%Estimate settling velocity of cylinders(Khatmullina and Isachenko, 2017)
%Jalon-Rojas et al 2019 (negative is up)
ws=0.5*pi*(1/nuw)*9.81*((debrisRho0-rhow)/rhow)*2.*debrisL0.*...
    debrisR0./(55.238.*debrisL0+12.691);

Kbuoy=Kbuoy/(24*3600);%convert to sec^-1
Kdeg=Kdeg/(24*3600);

%% Limit mean transport and dispersion analysis to this area (e.g. camera
% FOV)
areaPolyX=[213501.052 213501.052 213297.052 213297.052 213501.052];
areaPolyY=[1464874.131 1465180.131 1465180.131 1464874.131 1464874.131];
areaPoly=[areaPolyX' areaPolyY'];
flagTd=0;
```

```
Td=0;

%% Plotting styles
style{1}='k-';
style{2}='b--';
style{3}='r--*';
style{4}='k:o';
style{5}='k-';
dim = [.15 .14 .3 .3];

%% Initialize mean travel distances
xpmeanabs=zeros(np,1);
ypmeanabs=zeros(np,1);

%% Loop over time steps
if endstep>0
    ntstep=endstep; %if limiting duration
end;
ihstep=itstep; %initialize timestep for hydrodynamics file if looping
               % hydrodynamics
ihstep0=ihstep;
maxih=size(uvec,2);

%% Diagnostics
thetapntesthist(:,1)=thetap;
up1testhist(:,1)=zeros([np 1]);
vp1testhist(:,1)=zeros([np 1]);
up2testhist(:,1)=zeros([np 1]);
vp2testhist(:,1)=zeros([np 1]);
distptesthist(:,1)=zeros([np 1]);
xp1ntesthist(:,1)=xp1;
xp2ntesthist(:,1)=xp2;
yp1ntesthist(:,1)=yp1;
yp2ntesthist(:,1)=yp2;
rotationangle=330;
Rmatrix=[cosd(rotationangle) -sind(rotationangle); sind(rotationangle)...
    cosd(rotationangle)];
dzb_dx_dy=Rmatrix*[dzbdxvec';dzbdyvec'];

%% Clear variables from previous simulation
clear time xpdist xpmeanabs ypdist ypmeanabs varpx varpy xpmeanabslim;
clear ypmeanabslim varpxlim varpylim;

%% Begin WOODRIFTSIM simulation time stepping
for istep=itstep:ntstep

time(istep-itstep+1)=(istep-itstep)*dt;
istep
if ihstep>maxih
    ihstep=ihstep0;
end;

%save variables history
Xparthist(:,:,istep-itstep+1)=[Xpart];
fBeachhist(:,istep-itstep+1)=fBeach;
```

```
fBeachTypehist(:,istep-itstep+1)=fBeachType;
thetaphist(:,istep-itstep+1)=thetap;

%compute mean travel distance and variances
if size(Xparthist,3)>1
    for i=2:size(Xparthist,3)
        xpdist(:,i)=(Xparthist(:,1,i)-Xparthist(:,1,1));
        ypdist(:,i)=(Xparthist(:,2,i)-Xparthist(:,2,1));
    end;
    %option to restrict mean transport and variance aalysis to limited area
    %(e.g. camera FOV)
    if optLimit<1
        xpmeanabs=mean(abs(xpdist));
        ypmeanabs=mean(abs(ypdist));
        varpx=var(xpdist);
        varpy=var(ypdist);
    else
        %compute this anyway for particles outside boundary
        xpmeanabs=mean(abs(xpdist));
        ypmeanabs=mean(abs(ypdist));
        varpx=var(xpdist);
        varpy=var(ypdist);
        [insideBdy,onBdy]=inpolygon(xpn,ypn,areaPolyX,areaPolyY); %logical,
                                                    % 1 if inside boundary
        NdNp=sum(insideBdy)/length(insideBdy);
        if (NdNp<0.67) && (flagTd<1)
            Td=istep./Tp;
            flagTd=1;
        end;
        indInside=find(insideBdy>0); %indices of points inside boundary
        if length(indInside)>1 %avoids averaging along time dimension if
                               % only one point inside boundary
            xpmeanabslim(1,istep-itstep+1)=mean(abs(xpdist(indInside,...
                istep-itstep+1)));
            ypmeanabslim(1,istep-itstep+1)=mean(abs(ypdist(indInside,...
                istep-itstep+1)));
            varpxlim(1,istep-itstep+1)=var(xpdist(indInside,...
                istep-itstep+1));
            varpylim(1,istep-itstep+1)=var(ypdist(indInside,...
                istep-itstep+1));
        elseif length(indInside)==1
            xpmeanabslim(1,istep-itstep+1)=abs(xpdist(indInside,...
                istep-itstep+1));
            ypmeanabslim(1,istep-itstep+1)=abs(ypdist(indInside,...
                istep-itstep+1));
            varpxlim(1,istep-itstep+1)=var(xpdist(indInside,...
                istep-itstep+1));
            varpylim(1,istep-itstep+1)=var(ypdist(indInside,...
                istep-itstep+1));
        else
            xpmeanabslim(1,istep-itstep+1)=0;
            ypmeanabslim(1,istep-itstep+1)=0;
            varpxlim(1,istep-itstep+1)=0;
            varpylim(1,istep-itstep+1)=0;
        end;
```

```
    end;
end;

    %update fall velocity with time-dependent buoyancy and degradation
    debrisRho=debrisRho0*exp(Kbuoy*time(istep-itstep+1)); %Blade et al 2016
    if debrisRho>rhow
        disp(['WARNING - debris is negatively buoyant, draft ...' ...
            'calculations not correct'])
    end;
    debrisL=debrisL0.*(1-Kdeg*time(istep-itstep+1)); %Jalon-Rojas
    debrisD=debrisD0.*(1-Kdeg*time(istep-itstep+1));
    debrisR=debrisD.*0.5;
    ws=0.5*pi*(1/nuw)*9.81*((debrisRho-rhow)/rhow)*2.*debrisL.*...
        debrisR/(55.238.*debrisL+12.691);

    %windage - Chubarenko et al 2016 as cited in Jalon-rojas
    %disabled for now
%     syms hR;
%     hRratio=double(vpasolve(((hR)^2)*(3-hR)==4*debrisRho/rhow));
%     hRratio=hRratio(find(hRratio(find(hRratio<=2))>=0));
        %find only true solution hRratio=2 is full submergence
%     alpha=2*acos(1-hRratio);
%     Sdry=(2*pi/(alpha-sin(alpha)))-1;
%     windInf=sqrt((rhoa/rhow)*Sdry);

    %Calculate driftwood draft
    myfun=@(alpha,debrisRho,rhow)alpha-(180/pi())*sind(alpha)-...
        360*debrisRho/rhow;
    fun=@(alpha)myfun(alpha,debrisRho,rhow);
    alphaflot=fzero(fun,0.1); %angle defining cord at waterline
    debrisDraft=debrisR-debrisR.*cos(0.5*alphaflot*pi()/180); %draft of
                                                    % floating cylinders
    %Calculate dry portion of cross-sectional area
    Sdry=1-(((debrisR.^2).*((pi()*alphaflot/360)-(0.5*sind(alphaflot)))-...
        ((debrisR-debrisDraft).*sqrt((debrisR.^2)-...
        (debrisR-debrisDraft).^2))./(pi().*(debrisR.^2)));
    Sdry(1:length(debrisDraft))=1-(debrisRho/rhow);

    windInf=sqrt((rhoa/rhow)*Sdry);

    [gridID,dist]=dsearchn(xycvec, Xpart); %locate driftwood centroids grid
    [gridID1,dist1]=dsearchn(xycvec, Xpart1); %locate end points
    [gridID2,dist2]=dsearchn(xycvec, Xpart2); %locate end points

    if optAdv == 2
        %2nd order advection by currents (Lebreton et al.,2012) following
        % Black & Gay (1980)
        uprime=uvec(gridID,ihstep);
        vprime=vvec(gridID,ihstep);
        upn=((uprime+((dudyvec(gridID,ihstep).*vprime-...
            dvdyvec(gridID,ihstep).*uprime)*0.5*dt))./...
            ((1-dudxvec(gridID,ihstep).*dt.*0.5).*...
            (1-dvdyvec(gridID,ihstep).*dt.*0.5)-...
            (dudyvec(gridID,ihstep).*dvdxvec(gridID,ihstep)*dt*dt*0.25)));
        vpn=((vprime+((dvdxvec(gridID,ihstep).*uprime-...
```

```
        dudxvec(gridID,ihstep).*vprime)*0.5*dt))./...
        ((1-dudxvec(gridID,ihstep).*dt.*0.5).*...
        (1-dvdyvec(gridID,ihstep).*dt.*0.5)-...
        (dudyvec(gridID,ihstep).*dvdxvec(gridID,ihstep)*dt*dt*0.25)));
else
    %First order (Euler) advection
    upn=uvec(gridID,ihstep);
    vpn=vvec(gridID,ihstep);
end;

    dudtp=(upn-up).*invdt; %acceleration x
    dvdtp=(vpn-vp).*invdt; %acceleration y

    %evaluate dispersion coefficients at driftwood centroids
    Kxp=KxPar(gridID,ihstep);
    Kyp=KyPar(gridID,ihstep);

    %velocities at endpoints, depends on grid resolution and size of
    %debris
    for ip=1:np
        if gridID(ip)==gridID1(ip)
            dudxp1(ip)=dudxvec(gridID(ip),ihstep);
            dudyp1(ip)=dudyvec(gridID(ip),ihstep);
            dvdxp1(ip)=dvdxvec(gridID(ip),ihstep);
            dvdyp1(ip)=dvdyvec(gridID(ip),ihstep);
            up1(ip,1)=upn(ip)+((xp1(ip)-xp(ip))*dudxp1(ip))+...
                ((yp1(ip)-yp(ip))*dudyp1(ip));
            vp1(ip,1)=vpn(ip)+((xp1(ip)-xp(ip))*dvdxp1(ip))+...
                ((yp1(ip)-yp(ip))*dvdyp1(ip));
         else
            up1(ip,1)=uvec(gridID1(ip),ihstep);
            vp1(ip,1)=vvec(gridID1(ip),ihstep);
        end;
        if gridID(ip)==gridID2(ip)
            dudxp2(ip)=dudxvec(gridID(ip),ihstep);
            dudyp2(ip)=dudyvec(gridID(ip),ihstep);
            dvdxp2(ip)=dvdxvec(gridID(ip),ihstep);
            dvdyp2(ip)=dvdyvec(gridID(ip),ihstep);
            up2(ip,1)=upn(ip)+((xp2(ip)-xp(ip))*dudxp2(ip))+...
                ((yp2(ip)-yp(ip))*dudyp2(ip));
            vp2(ip,1)=vpn(ip)+((xp2(ip)-xp(ip))*dvdxp2(ip))+...
                ((yp2(ip)-yp(ip))*dvdyp2(ip));
        else
            up2(ip,1)=uvec(gridID2(ip),ihstep);
            vp2(ip,1)=vvec(gridID2(ip),ihstep);
        end;
    end;

%Disabled wind influence
%         up=(uvec(gridID)+uvecWind(gridID).*windInf)./(1+windInf);
%         vp=(vvec(gridID)+vvecWind(gridID).*windInf)./(1+windInf);

%setting depths and velocities at particles to zero in areas where
%depth less than threshold
pinds=dsearchn(xycvec,[xp yp]);
```

```
    hp=hvec(pinds,ihstep); %water depth at particle locations
    zbp=zb0vec(pinds); %bed elevation at particle locations (fixed bed)
    zsp=zsvec(pinds,ihstep);
    umagpn=((upn.^2)+(vpn.^2)).^0.5; %magnitude of velocity vector

    %Advection and dispersion of centroids
    xpn=xp+(upn.*dt)+(Kxp.*randn(np,1)); %adv + disp
    ypn=yp+(vpn.*dt)+(Kyp.*randn(np,1)); %adv + disp

    %Advection of end points
    xp1n=xp1+(up1.*dt);
    yp1n=yp1+(vp1.*dt);
    xp2n=xp2+(up2.*dt);
    yp2n=yp2+(vp2.*dt);
    distp=(((xp2n-xp1n).^2)+((yp2n-yp1n).^2)).^0.5;
    thetapn=atan2d((yp2n-yp1n),(xp2n-xp1n));

    %Recompute end point locations based on angle and centroid location
    xp1n=xpn-(debrisL./2).*cos(pi()/180*thetapn);
    xp2n=xpn+(debrisL./2).*cos(pi()/180*thetapn);
    yp1n=ypn-(debrisL./2).*sin(pi()/180*thetapn);
    yp2n=ypn+(debrisL./2).*sin(pi()/180*thetapn);

    %Diagnostics
    thetapntesthist(:,istep-itstep+1)=thetapn;
    up1testhist(:,istep-itstep+1)=up1;
    vp1testhist(:,istep-itstep+1)=vp1;
    up2testhist(:,istep-itstep+1)=up2;
    vp2testhist(:,istep-itstep+1)=vp2;
    distptesthist(:,istep-itstep+1)=distp;
    xp1ntesthist(:,istep-itstep+1)=xp1n;
    xp2ntesthist(:,istep-itstep+1)=xp2n;
    yp1ntesthist(:,istep-itstep+1)=yp1n;
    yp2ntesthist(:,istep-itstep+1)=yp2n;

    %vertical position of centroid (in case of settling)
    zpn=max(min(zp+(KzPar.*randn(np,1))-ws.*dt,zsp),zbp);

%% Beaching
    %optBch=2 is dynamics-based beaching and washoff
    if optBch==2
        dzbdxp=(dzb_dx_dy(1,gridID))'; %bed gradients at debris centroid
        dzbdyp=(dzb_dx_dy(2,gridID))';
        betaxp=atand(dzbdxp); %bed gradient at centroid in degrees (pos up)
        betayp=atand(dzbdyp);
        dumagdtp=((dudtp).^2+(dvdtp).^2).^0.5; %magnitude acceler. vector
        dzbdmagp=((dzbdxp).^2+(dzbdyp).^2).^0.5; %magnitude gradient vector
        %transform all vectors to axial (ax) and perpendicular (nm) ...
        % to debris axes.
        for ip=1:np
            if umagpn(ip)<0.000001
                gammau(ip,1)=0;
            else
                gammau(ip,1)=atan2d(vpn(ip),upn(ip));
            end;
```

```
    if dumagdtp(ip)<0.00000000001
        gammaa(ip,1)=0;
    else
         gammaa(ip,1)=atan2d(dvdtp(ip),dudtp(ip)); %angle of
                        % acceleration vector in cartesian space
    end;
    if dzbdmagp(ip)<0.00000001
        gammazbrot(ip,1)=0;
        gammazb(ip,1)=0;
    else
        gammazb(ip,1)=atan2d(dzbdyp(ip),dzbdxp(ip));
        gammazbrot(ip,1)=gammazb(ip,1); %angle of bed gradient ...
        % in cartesian space, this is rotated later
    end;
end;

deltagammau=gammau-thetap; %angle between velocity vector and...
% driftwood
deltagammau=mod(deltagammau+180,360)-180; %make between -180 and...
% +180
deltagammau=deg2rad(deltagammau);
upnm=umagpn.*sin(deltagammau); %velocity component perpendicular...
% to driftwood axis
upax=umagpn.*cos(deltagammau); %velocity component along ...
% driftwood axis
deltagammaa=gammaa-thetap; %angle between acceleration vector ...
% and driftwood
deltagammaa=mod(deltagammaa+180,360)-180; %make between -180 and...
% +180
deltagammaa=deg2rad(deltagammaa);
apnm=dumagdtp.*sin(deltagammaa); %acceleration component ...
% perpendicular to debris axis
apax=dumagdtp.*cos(deltagammaa); %acceleration component...
% along debris axis
deltagammazb=gammazb-thetap; %angle between velocity vector and...
% driftwood
deltagammazb=mod(deltagammazb+180,360)-180; %make between -180...
% and +180
deltagammazb=deg2rad(deltagammazb);
dzbdnm=dzbdmagp.*sin(deltagammazb); %bed gradient perpendicular...
% to driftwood axis
dzbdax=dzbdmagp.*cos(deltagammazb); %bed gradient along...
% driftwood axis
betanm=atand(dzbdnm); %bed gradient perpendicular to ...
% axis in degrees

Fg=9.81*pi().*(debrisR.^2).*debrisRho; %self-weight
Fb=9.81*(1-Sdry).*pi().*(debrisR.^2).*rhow; %buoyancy...
% (when not touching bottom)

%following Sumer & Fredsoe p161, only consider forces normal to...
% driftwood axis
FLnm=0.5*rhow*CL.*debrisD.*(upnm.^2); %lift (need to resolve...
% along vertical)
FDnm=0.5*CD*rhow.*debrisD.*upnm.*abs(upnm); %drag
```

```
FInm=rhow*CM*0.25*pi().*(debrisD.^2).*apnm; %inertia/added mass
FInm(FDnm==0)=0; %sets inertia force to zero if no drag (avoids...
% FInm when acceleration due to rolling)
Fwaveinline=FDnm+FInm;
Fnorm=max(((Fg-Fb).*cosd(betanm))-FLnm,0);%sets to zero if...
% acting away from bed

%test vertical force balance
Fvert=Fg-Fb-FLnm.*(max(cosd(betaxp),cosd(betayp)));
Fres=Fwaveinline-((Fg-Fb).*sind(betanm)); %resultant hor. forces
FhorDir=sign(Fres); %direction of Fres (relative to driftwood axis)
Ffrnm=FhorDir.*mur.*Fnorm.*(-1);%resistance force always opposes...
% resultant of wave and gravity forces
Fhor=Fres+Ffrnm; %normal drag + inertia + gravity perp to axis

for ip=1:np
    if (debrisDraft(ip)>=hp(ip)) % does it touch bottom?...
        % this applies even in dry area

        %update draft and reevaluate forces
        debrisDraft(ip)=hp(ip); %draft reduces to water depth if...
        % theoretical (open water) draft exceeds water depth
        Asub(ip)=((2.*acos(1-((2.*hp(ip))./debrisD(ip))))-...
            sin(2.*acos(1-((2.*hp(ip))./debrisD(ip))))).*...
            (debrisD(ip).^2)./8;
        Sdry(ip)=1-(Asub(ip)./(pi.*(debrisR(ip).^2)));...
            %update dry fractional volume for this particle
        Fb(ip)=9.81*(1-Sdry(ip)).*pi().*(debrisR(ip).^2).*rhow;...
            %update buoyancy force for this particle when...
                % touching bottom
        Fnorm(ip)=max(((Fg(ip)-Fb(ip)).*cosd(betanm(ip)))-...
            FLnm(ip),0); %update normal resultant - sets to zero...
                            % if acting away from bed

        %re-assess vertical force balance
        Fvert(ip)=Fg(ip)-Fb(ip)-FLnm(ip).*...
            (max(cosd(betaxp(ip)),cosd(betayp(ip))));
        Fres(ip)=Fwaveinline(ip)-...
            ((Fg(ip)-Fb(ip)).*sind(betanm(ip)));
        FhorDir(ip)=sign(Fres(ip));
        Ffrnm(ip)=FhorDir(ip).*mur.*...
            Fnorm(ip).*(-1); %rolling frictional resistance...
                                % (Fnorm is set to zero above...
                                % if not acting towards bed)
        Fhor(ip)=Fres(ip)+Ffrnm(ip);

       if (abs(Fres(ip))-abs(Ffrnm(ip)))<=0
           %if it does touch the bottom, can horizontal forces...
           % overcome resistance? if no, beached and no movement
            fBeach(ip)=1; %beached
            fBeachEver(ip)=fBeachEver(ip)+1;
            fBeachType(ip)=1;
            t0Beach(ip)=time(istep-itstep+1); %record initial...
                        % beach time (of most recent beaching)
            tBeach(ip)=time(istep-itstep+1);
```

```
            xpBeach(ip)=xp(ip);
            ypBeach(ip)=yp(ip);
            xpn(ip)=xp(ip); %no movement
            xp1n(ip)=xp1(ip); %no movement
            xp2n(ip)=xp2(ip); %no movement
            ypn(ip)=yp(ip); %no movement
            yp1n(ip)=yp1(ip); %no movement
            yp2n(ip)=yp2(ip); %no movement
            zpn(ip)=zp(ip); %no movement
            upn(ip)=0; %no movement
            vpn(ip)=0; %no movement
            umagpn(ip)=0; %no movement
            thetapn(ip)=thetap(ip); %no rotation
            xp1n(ip)=xpn(ip)-(debrisL(ip)./2).*...
                cos(pi()/180.*thetapn(ip));
            xp2n(ip)=xpn(ip)+(debrisL(ip)./2).*...
                cos(pi()/180.*thetapn(ip));
            yp1n(ip)=ypn(ip)-(debrisL(ip)./2).*...
                sin(pi()/180.*thetapn(ip));
            yp2n(ip)=ypn(ip)+(debrisL(ip)./2).*...
                sin(pi()/180.*thetapn(ip));
            %two options if can overcome friction: ...
            % 1) in water and wave forces exist...
            % 2) dry and gravity forces dominate
        else %resistance forces are less than horizontal forces ...
            % (waves and gravity) - movement by gravity
            if (abs(Fwaveinline(ip))-abs((Fg(ip)-Fb(ip)).*...
                    sind(betanm(ip)))<=0)  %does gravity or waves...
                                           % dominate movement?
                %if gravity dominates, movement due to...
                % rolling only - still flagged as beached
                fBeach(ip)=1; %beached
                fBeachEver(ip)=fBeachEver(ip)+1;
                fBeachType(ip)=2;
                t0Beach(ip)=time(istep-itstep+1); %record...
                % initial beach time (of most recent beaching)
                tBeach(ip)=time(istep-itstep+1);
                xpBeach(ip)=xp(ip);
                ypBeach(ip)=yp(ip);
                %movement by gravity - Newton's second law
                thetarad=deg2rad(thetap(ip));
                if thetap(ip)>=0
                    upn(ip)=(Fhor(ip).*dt./((debrisRho.*...
                        (debrisR(ip).^2).*debrisL(ip)))).*...
                        cos(thetarad);
                else
                    upn(ip)=(-1).*(Fhor(ip).*dt./((debrisRho.*...
                        (debrisR(ip).^2).*debrisL(ip)))).*...
                        cos(thetarad);
                end;
                vpn(ip)=(Fhor(ip).*dt./((debrisRho.*...
                    (debrisR(ip).^2).*debrisL(ip)))).*...
                    sin(thetarad);
                if sign(upn(ip))==sign(dzbdxp(ip))
                    upn(ip)=upn(ip).*(-1);
```

```
        end;
        if sign(vpn(ip))==sign(dzbdyp(ip))
            vpn(ip)=vpn(ip).*(-1);
        end;
         umagpn(ip)=((upn(ip).^2)+...
             (vpn(ip).^2)).^0.5; %rolling speed
        dtheta=(4.*umagpn(ip).*dt./debrisL(ip)).*...
            180./pi(); %change of angle in dt assuming...
        % rotation about end

        %update centroid position due to rolling
        xpn(ip)=xp(ip)+upn(ip).*dt;
        ypn(ip)=yp(ip)+vpn(ip).*dt;
        zpn(ip)=zp(ip); %no vertical movement

        %rotation
        gammazbrot(ip,1)=90+gammazb(ip,1);
        if gammazbrot(ip,1)>180
            gammazbrot(ip,1)=gammazbrot(ip,1)-360;
        elseif gammazbrot(ip,1)<-180
            gammazbrot(ip,1)=gammazbrot(ip,1)+360;
        end;

        maxangchange=gammazbrot(ip,1)-thetap(ip); %max...
                % possible angle change to face down slope
        if maxangchange>180
            maxangchange=maxangchange-180;
        elseif maxangchange<-180
            maxangchange=(-1).*(maxangchange+180);
        end;

        if abs(dtheta)>=abs(maxangchange)
            thetapn(ip)=gammazbrot(ip); %rotate downslope
        else
            thetapn(ip)=thetap(ip)+(abs(dtheta).*...
                maxangchange./abs(maxangchange));
            %angular rotation based on force direction...
            % and assuming rotation about endpoint
            if thetapn(ip)>180
                thetapn(ip)=thetapn(ip)-360;
            elseif thetapn(ip)<-180
                thetapn(ip)=thetapn(ip)+360;
            end;
        end;
        %update end point locations after rolling rotation
        xp1n(ip)=xpn(ip)-(debrisL(ip)./2).*...
            cos(pi()/180.*thetapn(ip));
        xp2n(ip)=xpn(ip)+(debrisL(ip)./2).*...
            cos(pi()/180.*thetapn(ip));
        yp1n(ip)=ypn(ip)-(debrisL(ip)./2).*...
            sin(pi()/180.*thetapn(ip));
        yp2n(ip)=ypn(ip)+(debrisL(ip)./2).*...
            sin(pi()/180.*thetapn(ip));
    else
        %These are pieces that touch the bottom but EITHER
```

```
                    %horizontal forces exceed resistance forces ...
                    %(waves move the piece) OR
                    %inline wave forces exceed horizontal gravity...
                    %forces
                   fBeach(ip)=0; %not beached
                   fBeachType(ip)=0;
               end; %end of check if gravity or waves control motion
           end; %end of check if horizontal forces can overcome resist.
        else
            fBeach(ip)=0; %not beached
            fBeachType(ip)=0;
        end;
    end; %end loop on particles for beaching

 %optBch=1 is beaching where no water
 elseif optBch==1
    for ip=1:np
        if (hp(ip)<0.00001)
            fBeach(ip)=1; %beached
            fBeachEver(ip)=fBeachEver(ip)+1;
            fBeachType(ip)=1;
            t0Beach(ip)=time(istep-itstep+1); %record initial beach...
            % time (of most recent beaching)
            tBeach(ip)=time(istep-itstep+1);
            xpBeach(ip)=xp(ip);
            ypBeach(ip)=yp(ip);
            xpn(ip)=xp(ip); %no movement
            xp1n(ip)=xp1(ip); %no movement
            xp2n(ip)=xp2(ip); %no movement
            ypn(ip)=yp(ip); %no movement
            yp1n(ip)=yp1(ip); %no movement
            yp2n(ip)=yp2(ip); %no movement
            zpn(ip)=zp(ip); %no movement
            upn(ip)=0; %no movement
            vpn(ip)=0; %no movement
            umagpn(ip)=0; %no movement
            thetapn(ip)=thetap(ip); %no rotation
        else
            fBeach(ip)=0;
        end;
    end;%end loop over each particle

 %otpBch=0 is no beaching at all
 elseif optBch==0
    fBeach(1:np)=0; %no beaching
 else
    disp('Invalid beaching option - check optbch')
 end; %end beaching

%% update variables
 xp=xpn;
 yp=ypn;
 zp=zpn;
 xp1=xp1n;
 yp1=yp1n;
```

```
    xp2=xp2n;
    yp2=yp2n;
    thetap=thetapn;
    umagp=umagpn;
    up=upn;
    vp=vpn;
    zrecord(istep)=zp(10);
    Xpart=[xp yp];
    Xpart1=[xp1 yp1];
    Xpart2=[xp2 yp2];
    ihstep=ihstep+1;

%% plotting / animation
    if suppressPlot<1 && ~mod(istep,plotint)
        fig2=figure(2)
        hand(1)=subplot(1,2,1);
        vcol=[-20;-15;-10;-9;-8;-7;-6;-5;-4;-3;-2;-1;0;1;2];
        colormap('gray')
        contourf(xc,yc,nczb0-plotelev,vcol)
        hold on;
        ca=[-20 2];
        axis equal;
        plot([213501.052 213501.052 213297.052 213297.052 213501.052],...
            [1464874.131 1465180.131 1465180.131 1464874.131 1464874.131...
            ],'Color','k','LineWidth',3);
        scatter(xp,yp,25,'r','filled');
        caxis(ca); cb=colorbar;
        cb.Label.String = 'Bathymetry (m)';
        title(['time = ',num2str(time(istep-itstep+1)),' s']);
        xlabel('Easting (m)')
        ylabel('Northing (m)')
        hold off;

        hand(2)=subplot(1,2,2);
        vcol2=[-7;-6;-5;-4;-3;-2;-1;0;1;2;3];
        contourf(xc,yc,nczb0-plotelev,vcol2)
        hold on;
        ca=[-7 3];
        quiver(xc,yc,u(:,:,ihstep),v(:,:,ihstep),3)
        xes=[xp1'; xp2'];
        yes=[yp1'; yp2'];
        plot(xes(:,Nblue+Nyell+1:np),yes(:,Nblue+Nyell+1:np),'Color',...
            'g','LineWidth',3);
        plot(xes(:,1:Nblue),yes(:,1:Nblue),'Color','b','LineWidth',3);
        plot(xes(:,Nblue+1:Nblue+Nyell),yes(:,Nblue+1:Nblue+Nyell),...
            'Color','y','LineWidth',3);
        plot(xes(:,fBeachType==1),yes(:,fBeachType==1),'Color',...
            'r','LineWidth',3);
        plot(xes(:,fBeachType==2),yes(:,fBeachType==2),...
            'Color',[0.9290 0.6940 0.1250],'LineWidth',3);
        plot(xunit,yunit,'k--','LineWidth',1); %plot release area
        caxis(ca);
        cb=colorbar;
        cb.FontSize=12;
        cb.Label.String = 'Bathymetry (m MSL)';
```

```
        cb.Label.FontSize = 14;
        axis equal;
        axis([213297.052 213501.052 1464874.131 1465180.131])
        title(['\it{t} = ',num2str(time(istep-itstep+1)),' s'],...
            'FontSize',14);
        xlabel('Easting (m)','FontSize',14)
        ylabel('Northing (m)','FontSize',14)
        ax = gca;
        ax.FontSize = 12;
        hold off;
        drawnow;
        pause(0.01)
        F(istep-itstep+1)=getframe(gcf);
    end;
end % end of time stepping

%% Save output
if suppressPlot<1
    Fred=F(1:plotint:length(F)-mod(length(F),plotint));
    % create the video writer with 1 fps
    writerObj = VideoWriter(aviFile);
    writerObj.FrameRate = 5;
    % set the seconds per image
    % open the video writer
    open(writerObj);
    % write the frames to the video
    for i=2:length(Fred)
       % convert the image to a frame
       frame = Fred(i) ;
       writeVideo(writerObj, frame);
    end
    % close the writer object
    close(writerObj);
else
    F=[];
end;
YB=300;
XB=200;
optLimit=1; %switch for limiting analysis to area, 1 = limit; 0 = do not
A(:,1)=time'./Tp;
if optLimit<1
    stdevpx=varpx.^0.5;
    stdevpy=varpy.^0.5;
    A(:,2)=ypmeanabs'./YB;
    A(:,3)=xpmeanabs'./XB;
else
    stdevpx=varpxlim.^0.5;
    stdevpy=varpylim.^0.5;
    A(:,2)=ypmeanabslim'./YB;
    A(:,3)=xpmeanabslim'./XB;
end;
A(:,4)=stdevpy'./YB;
A(:,5)=stdevpx'./XB;
save(outFile,'A','Xparthist','fBeachEver','fBeachhist','Td','thetaphist');
end
```